L-ASPARTIC ACID BASED FUNCTIONAL POLYESTER FOR DRUG DELIVERY AND ANTIMICROBIAL APPLICATIONS

विद्या वाचस्पति की
उपाधि की अपेक्षाओं की आंशिक पूर्ति में प्रस्तुत शोध प्रबंध

A thesis submitted in partial fulfilment of the requirements of the degree of Doctor of Philosophy

द्वारा / By
मोहम्मद खुद्दूस मो इकबाल
Mohammed Khuddus Md Iqbal

पंजीकरण सं. / Registration No.
20173530

शोध प्रबंध पर्यवेक्षक / Thesis Supervisor:
Prof. M. Jayakannan

IISER PUNE
भारतीय विज्ञान शिक्षा एवं अनुसंधान संस्थान पुणे
INDIAN INSTITUTE OF SCIENCE EDUCATION AND RESEARCH PUNE

October 2023

Dedicated to

My Father

Mohammed Iqbal

भारतीय विज्ञान शिक्षा एवं अनुसंधान संस्थान पुणे
INDIAN INSTITUTE OF SCIENCE EDUCATION AND RESEARCH PUNE
(An Autonomous Institution of Ministry of Human Resource Development, Govt. of India)
Dr. Homi Bhabha Road, Pune - 411 008.

Prof. M. Jayakannan
Professor
Department of Chemistry
Indian institute of science Education and research Pune.

CERTIFICATE

This is Certified that the work incorporated in the thesis entitled ***"L-Aspartic acid Based Functional Polyesters for Drug Delivery and Antimicrobial Applications"*** Submitted by **Mr. Mohammed Khuddus Md Iqbal** was Carried out by the candidate under my supervision the work presented here or any part of it has not been included in any other thesis submitted previously or the award of any degree or diploma from any other University or Institution.

Date: 31st October 2023
Pune (MH) India

Prof. M. Jayakannan
(Thesis supervisor)
31/10/2023

Declaration

I declare that this written thesis document represents my own ideas in words and ideas that adopted from others have been adequately cited and refferenced the orginal sources. I also declare that I have obeyed to all principles of scientific honesty integraty and have been misrepresented or fabricated or falsified any idea/data/fact/source in my submission. I understand that vilation of above will be cause for disiplanary action be the institute and can also suggest penal action from the source which have doesnot been properly cited or from whom proper permission has not be taken when desired.

Khuddus
31/10/2023

Date: 31 October 2023

Pune (MH) India

Mohammed Khuddus Md Iqbal

Reg No 20173530

Acknowledgements

This is to extend my great appreciation to those who helped and supported me in completing my Ph.D. thesis.

First, I would like to express my sincere gratitude and special appreciation to my thesis supervisor, Prof. M. Jayakannan, who accepted me as a Ph.D. student and offered his mentorship. I accomplished this journey with his valuable guidance, continuous support, and motivation. I thank him for putting all his efforts into shaping my research life and encouraging me to explore my scientific potential. Working with him was a great pleasure, and I could not have imagined having a better mentor for my research study.

My sincere thanks to the present and past Directors of IISER-Pune for providing world class research facility at IISER Pune carrying out this research work.

I would like to thank Dr. Prakash Wadgaonkar and Prof H. N Gopi for being my research advisory committee (RAC) members and providing valuable comments and suggestions during RAC meetings to improve my research work.

I would like to thank Dr. Asha, S. K., as I have significantly benefited from her valuable scientific discussion and suggestions that have been helpful for this study and extending research facilities in her laboratory.

I extend my sincere thanks to faculty members in the department of chemistry, IISER Pune, for interactive scientific discussions and for teaching me various chemistry courses.

I take the opportunity to give my heartfelt thanks to my present and former lab mates for providing their support, cooperation, and stimulating environment which made my life memorable at IISER, Pune especially Dr. Sonashree, Dr. Nilesh, Dr. Bhagyashree, Dr. Dheeraj, Dr. Ruma, Utreshwar Gavhane, Mishika Virmani, Pershuram Kamble, Shahid Pathan, Sanchi, Vaishakh, Rhujhal, Aushootosh, Dr. N. Kakde, K Ganesh, Shibham pal, Akshai, Ashok, Ashwini, Megha, Yogesh and all labmates.

Special thanks to Dr. Sonashree, who has had a critical academic influence on me. She has been a wonderful colleague. I have learned a lot about how to do exciting research and overcome the difficulties in research work.

I would like to thank all instrument technicians of IISER Pune for their support: Dr Sandeep, Nitin (NMR), Prajapati (MALDI-TOF), Dr. Sandeep (HRMS), Megha

(AFM), Mahesh Jadhav, Yatish (FE-SEM). I thank the National Chemical Laboratory (NCL) Pune for HR TEM facilities.

I am indebted to many other friends for providing an inspiring and fun-filled environment in IISER Pune and NCL Pune, especially Shakeb Choudhari, Dr. Minhaj, Utreshwar, and all other friends. I also thank all the staff members in administration, finance, accounts, stores, library, and canteen, especially Mr. Mayuresh, Ms. Naina, Mr. Sandeep, Mr. Sanjay, and Mr. Tushar for their immediate help whenever I needed them. I also thank the entire cleaning depot for keeping the campus clean and clear.

I want to express my deepest gratitude to my parents for their unconditional love, affection, and support. They always encouraged me to pursue my dreams. I would not be who I am today without them. Their patience and sacrifices will always remain my inspiration throughout my life. My heartfelt thanks to my brothers Nadeem and Aqueeb and my sisters for their unwavering support, encouragement, and prayers.

I owe my deepest gratitude and appreciation to an exceptional person, my wife, Iram Tahleel, who has always been my strength. His unconditional love, patience, understanding, and eternal support made completing this journey possible. I greatly value everything she has done for me and sincerely appreciate her contribution. Financial support from UGC, IISER Pune, and my wife is greatly acknowledged.

Mohammed Khuddus Md Iqbal

Synopsis

Name of Students: Mohammed Khuddus Md Iqbal

Registration No: 20173530

Thesis Title: L-Aspartic acid Based Functional Polyesters for Drug Delivery and Antimicrobial Applications

Synthetic polymers based on L-amino acids have attracted much attention because of their excellent biocompatibility and diverse functionality which provides them improved hydrophilicity and an opportunity for further modifications with bioactive molecules. Development of synthetic strategy for synthesis of amino acid-based polymers has great research opportunity in biomedical field. In this thesis work, L-amino acid-based amide-functionalized polyester platform was designed and developed and their lysosomal enzymatic-biodegradation aspects was explored to administrate anticancer drugs in cancer cells. L-Aspartic acid was chosen and different amide-side chain functionalized diester monomers were tailor-made having aromatic, aliphatic and bio-source pendant units. Under solvent-free melt polycondensation methodology; these monomers underwent polymerization to yield high molecular weight polyesters with tuneable thermal properties. The L-aspartic acid-based polyester utilised for the construction of the nano assemblies with degradability, able to acts as carrier for drug delivery and bioimaging as well as the antibacterial applications.

Thesis is divided into the four chapters

Chapter-1 This chapter deals with the review of the literature which describe the polymer-based system for the drug delivery in cancer cells. It provides the insights for the various aspects for polymer-based drug delivery system and also discussed the natural resources-based polymer for the various biomedical application.

Chapter 2 deals with development of L-aspartic acid-based polyester, were the detailed study for the polycondensation was carried out along with the development of amphiphilic polyester. This polyester then used for design of the nanocarrier capable of encapsulation of drug and dye. The particle loaded with drug showed delivery into the cancer cells and subsequently killing it.

Chapter 3 TPE tagged hydroxyl functionalised polyester was developed for theranostic application in cancer cells. The interaction between the loaded cargo in the nanoparticle and polymer backbone was studied using FRET in nanocavity of the carrier. Further this system showed successful delivery of the cargo in Bulb C mice via live imaging of mice.

Chapter 4 L-aspartic acid based cationic polyester was developed in this chapter. The antibacterial effect of the polymer was established using different protocols. The biocompatibility of cationic polyester was studied in normal cells lines.

In Chapter 2, L-Aspartic acid served as the starting material for designing amide-side chain functionalized di-ester monomers, featuring aromatic, aliphatic, and bio-source pendant units. Through a solvent-free melt polycondensation method developed in our lab, these monomers polymerized into high molecular weight polyesters with adjustable thermal properties. A PEGylated L-aspartic monomer was engineered, leading to the creation of a thermo-responsive amphiphilic polyester. This amphiphilic polyester self-assembled into spherical nanoparticles around 140±10 nm in size in aqueous solutions. These nano-assemblies effectively encapsulated various compounds, including anticancer drug doxorubicin (DOX), anti-inflammatory drug curcumin (CUR), and biomarkers such as Rose Bengal (RB) and 8-hydroxypyrene-1,3,6-trisulfonic acid trisodium salt (HPTS). The amphiphilic polyester nanoparticles remained stable under extracellular conditions but degraded when exposed to lysosomal enzymes at 37 ºC, releasing 90% of their cargo. Cytotoxicity studies on breast cancer MCF 7 cells and normal cells lines wild-type mouse embryonic fibroblasts (WT MEFs) demonstrated that the amphiphilic polyester was non-toxic at concentrations up to 100 µg/mL, while the drug-loaded polyester nanoparticles effectively inhibited cancer cell growth.

The chapter 3 focuses on the design and development of a biodegradable polyester tagged with tetra phenyl ethylene (TPE) fluorescence from L-aspartic acid for creating polymer self-assemblies with theranostic applications in cancer cells. The synthetic process begins with the synthesis of an acetal-functionalized TPE-tagged polymer, which can be subsequently converted into the desired hydroxyl-functionalized TPE-tagged polymer. Selective deprotection of the acetal group from the polymer yields a hydroxyl-functionalized TPE-tagged polymer. This polymer with the TPE chromophore, exhibits aggregation-induced emission (AIE) properties based on the solvent composition. In solution, the polymer forms nano assemblies in water with sizes

less than 250±10nm, demonstrating the capacity to encapsulate biomarkers such as Rhodamine B (RhB), Rose Bengal (RB), or the drug doxorubicin (DOX). The photophysical properties of the nanoparticles (NPs) are characterized using absorbance, emission spectroscopy, and lifetime measurements, revealing energy transfer through the Forster resonance energy transfer (FRET) process. The FRET phenomenon is employed to demonstrate the interaction between the polymer and loaded cargo at the cellular level through bioimaging using confocal laser scanning microscopy (CSLM). These NPs are found to be biocompatible with both cancer and normal cell lines and do not exhibit cytotoxic effects on human red blood cells (RBCs). Furthermore, *in vivo* biodistribution of NPs loaded with IR780 is conducted using an IVIS imaging setup, suggesting a longer lifetime of the NPs compared to free IR780.

In Chapter 4, a cationic polyester based on L-aspartic acid is developed for antimicrobial applications. L-aspartic acid is transformed into a suitable monomer for polyester development using the melt polycondensation technique. The amine pendant of the monomer is protected with a BOC group. The polymer is synthesized through the melt polycondensation strategy using diols of different spacer lengths. Subsequently, this polyester is converted into a cationic polyester capable of self-assembly in an aqueous environment to form polymer nanoparticles. These cationic polyester nanoparticles have a diameter below 150±10 nm and exhibit a spherical morphology with a positive zeta potential value. The antimicrobial activity of the sample is assessed in both solid and solution states using various techniques, including Resazurin assays, Colony suspension method, Spread plate method, and Disc diffusion method in solution and solid state. Each technique has its unique nature in determining antibacterial activity. The biocompatibility of the polymer is assessed using the MTT assay with the normal cell line, Wild type mouse embryonic fibroblasts (WT MEF).

Overall conclusion and future direction are summarized in the end.

Table of Contents

Chapter 1

Introduction

1.1Introduction to Cancer

Cancer is a global health concern, being a major contributor to worldwide mortality, as reported by the World Health Organization in 2020[1]. Various factors, including the type of cancer, age, and geographical location, influence its prevalence and impact[2,3]. For instance, lung cancer is a leading cause of cancer-related deaths globally, while breast cancer is more prevalent among women in developed nations [1,4]. Cancer can manifest in various forms, affecting different body parts. Common types include breast cancer, lung cancer, prostate cancer, colon cancer, skin cancer (including melanoma), leukaemia (blood cancer), lymphoma, ovarian cancer, pancreatic cancer, and bladder cancer[5,6,7]. However, there are many other types of cancer, and some can be quite rare as shown in Figure 1.1 The specific type of cancer a person has can affect the course of their disease, their treatment options, and their prognosis. The advancement in cancer prevention, detection, and treatment have led to a decrease in cancer death rates in some regions, while others continue to struggle with high rates of cancer-related deaths[8].

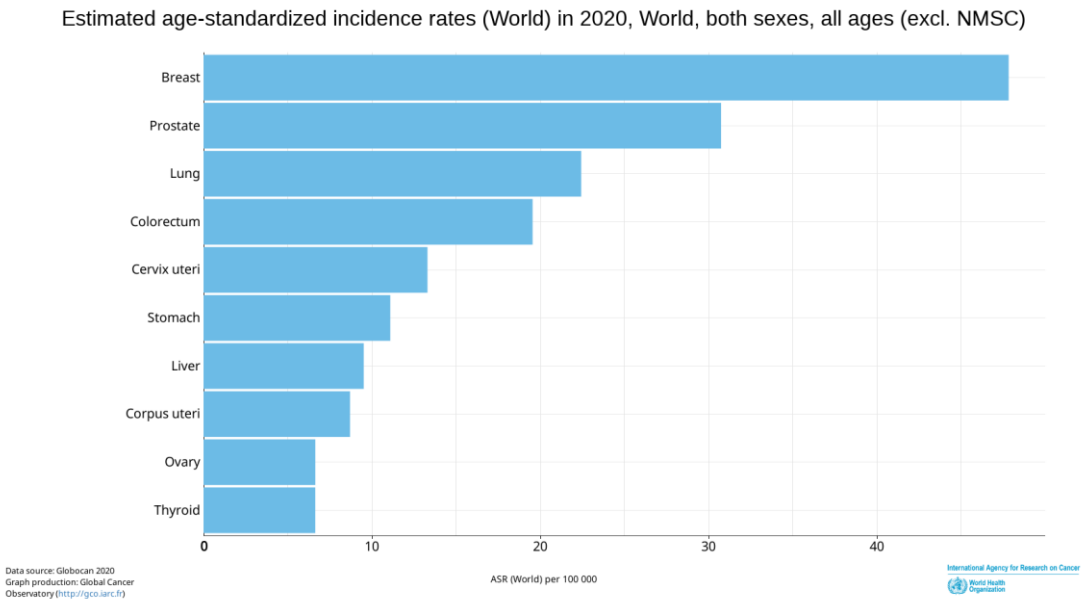

Figure 1.1 *Different types of the cancer and their ratio (Adapted from https://gco.iarc.fr/today/online-analysis-multi-bars).*

There are various treatments are involved for the cancer, which include Radiotherapy[9], Chemotherapy[10], Immunotherapy therapy[11], Surgical removal of tumours[12], Harmon therapy[13] etc.as shown in Figure 1.2.

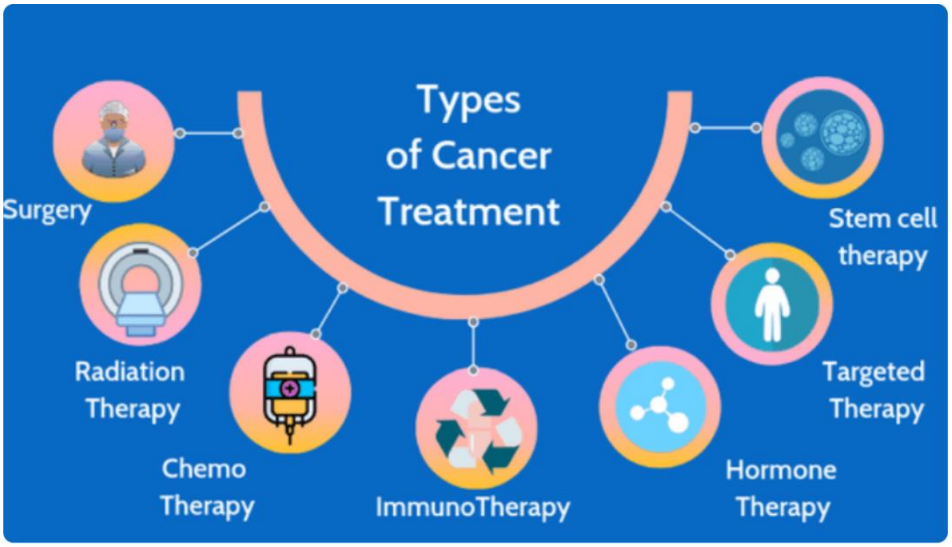

Figure 1.2 *Different types of the cancer Treatments. (Adapted from https://positivebioscience.com/types-of-cancer-treatment).*

Cancer treatment is a multifaceted endeavour, with diverse modalities tailored to cancer type, stage, and patient health. These include surgery for localized cancers, chemotherapy to combat cancer cell growth, radiation therapy to target and destroy cancer cells, immunotherapy to enhance the body's immune response, targeted therapy directed at specific molecular pathways, hormone therapy for hormone-sensitive cancers, precision medicine based on genetic analysis, stem cell transplants for damaged bone marrow, and palliative care to improve the quality of life for advanced cancer patients. The choice of treatment depends on a combination of factors, often resulting in a multifaceted approach to achieve the best possible outcome.

It is important to be noted that is no one-size-fits-all answer when it comes to determining whether which treatment is better for cancer treatment. The choice of treatment depends on various factors, including the type of cancer, its stage, the patient's overall health, and individual preferences[3]. Chemotherapy is one of several treatment options available for cancer, and its effectiveness and suitability depend on the specific situation. Chemotherapy has its advantages and disadvantages, and its appropriateness can vary based on the circumstances. In the chemotherapy the drug administered circulates throughout the body, which means it can reach cancer cells that have spread to different parts of the body[10]. This makes it effective for treating cancers that have metastasized. There is various drug commonly used which include doxorubicin, cisplatin, camptothecin, topotecan etc. which is taken up by the cancer cells at the

intracellular level and kills the cells by intercalating the DNA helix or inhibition of topoisomerase enzyme action[10]. In addition to that chemotherapy can be used in combination with other treatments like surgery or radiation therapy to improve overall treatment effectiveness and it can be used to treat a wide range of cancers, including both solid tumours and blood cancers[9]. But apart from these advantages of the chemotherapy there are limitation in this method due to their side effects including nausea, vomiting, fatigue, hair loss, immune suppression, and more[14]. These side effects can significantly impact a patient's quality of life. Due to their non-targeted nature of the drugs affecting both cancer cells and healthy cells, leading to potential damage to healthy tissues and organs. Some cancer cells can develop resistance to chemotherapy over time, reducing its effectiveness such as multidrug resistance cancer cells by the activation of p-glycoprotein influx pump[15]. It can be toxic, and the body's ability to tolerate them may vary the dosing and scheduling are critical to managing toxicity. The side effects of the chemotherapy are shown in Figure 1.3

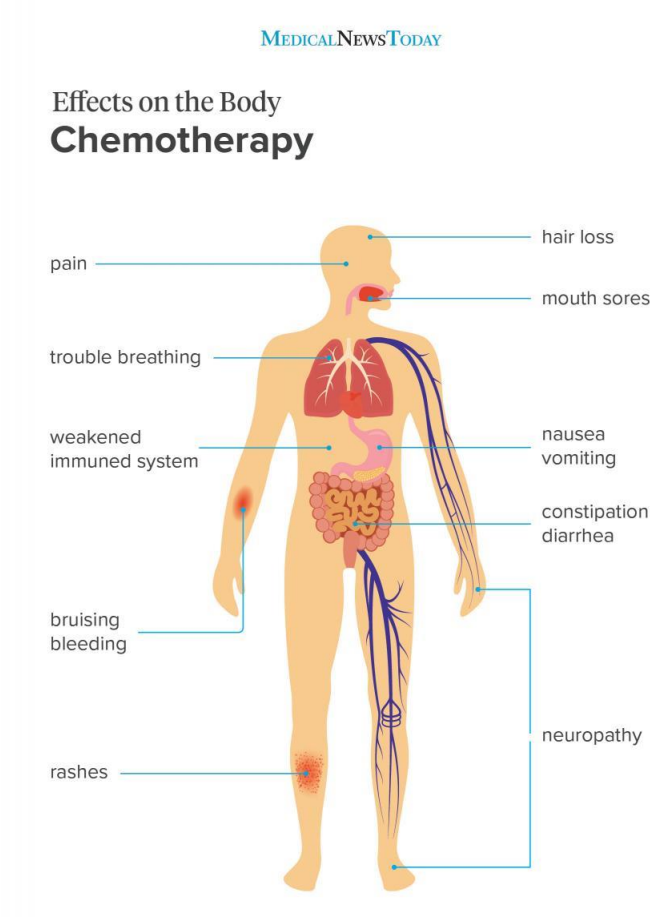

Figure 1.3 *Side effects of chemotherapy (Adapted from https://www.medicalnewstoday.com/articles/323485).*

1.2 Chemotherapy Using Nanocarriers

The new development of era of the precision medicine has started to the cancer treatment by the use of nanotechnology plate form the drug molecules are conjugated or encapsulated inside the nanoparticle so that it can be delivered at the target site cancer tissue[16]. The mechanism involves the use of nanocarriers, such as nanoparticles or liposomes, are used to encapsulate chemotherapy drugs[16]. These carriers can enhance drug solubility, stability, and targeted delivery to tumour sites, reducing off-target effects[16]. These nanocarrier can be designed to improve drug specificity by exploiting the enhanced permeability and retention (EPR) effect,[17,18,19] which allows them to accumulate preferentially in tumour tissues and by increasing drug accumulation in tumour tissues which leads reducing exposure to healthy tissues. The nanocarriers can improve the therapeutic efficacy of chemotherapy agents and has the potential to reduce side effects associated with conventional chemotherapy[16]. Targeted delivery and controlled release can minimize damage to healthy tissues. The enhanced specificity and delivery efficiency of nanocarriers can allow for lower drug doses to achieve the same therapeutic effect, potentially reducing side effects. As compare to the conventional chemotherapy the nanotechnology-based method can also modify the biodistribution of drugs, potentially overcoming limitations of poor drug solubility or rapid clearance[16]. Other advantages include nanocarriers can carry multiple drugs, enabling combination therapy by delivering different agents to the same tumour site simultaneously. This can enhance treatment effectiveness and reduce the risk of drug resistance. The challenges of developing nanocarriers with appropriate drug loading, stability, and targeting abilities requires complex engineering and formulation processes. Additionally, clearance and long-term safety of nanocarriers are areas of ongoing research[20,21]. Chemotherapy using nanocarriers offers the potential to enhance the therapeutic benefits of chemotherapy while minimizing its side effects such as by improving drug specificity, reducing off-target effects, and enabling combination therapy, nanocarriers hold promise for advancing cancer treatment strategies. For example, the nanotechnology-based platform is shown in Figure 1.4.

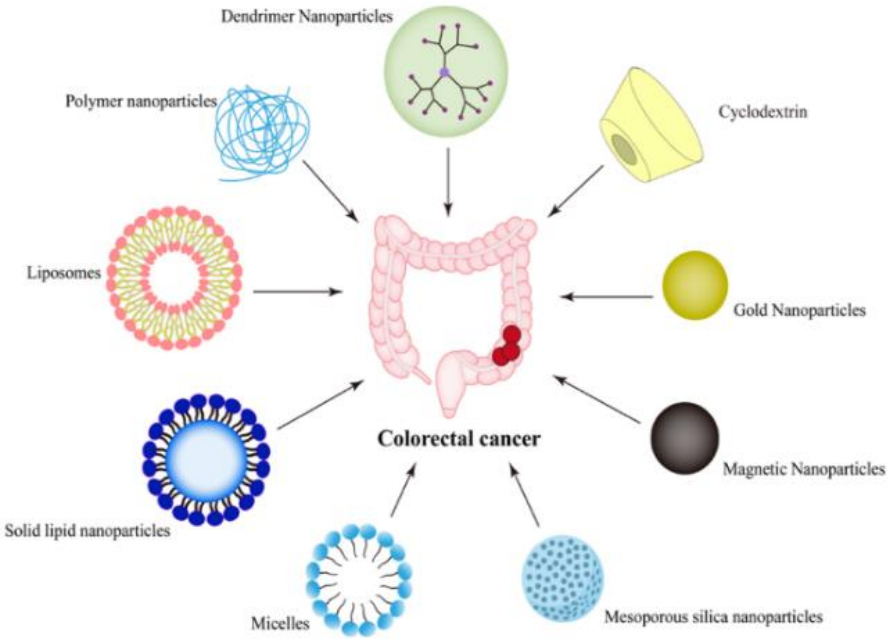

Figure 1.4 *Nanotechnology based platform for drug delivery system in colorectal cancer. (Adapted from Molecules* ***2022****, 27(9), 2981).*

When nano-formulations are administered intravenously into the body, they undergo a complex process known as the CAPIR mechanism[22,23]. The CAPIR mechanism comprises five distinct steps, each playing a pivotal role in determining the overall efficiency of drug delivery. These steps are: circulation, accumulation, permeation, internalization, and release, as illustrated in **Figure 1.5.**

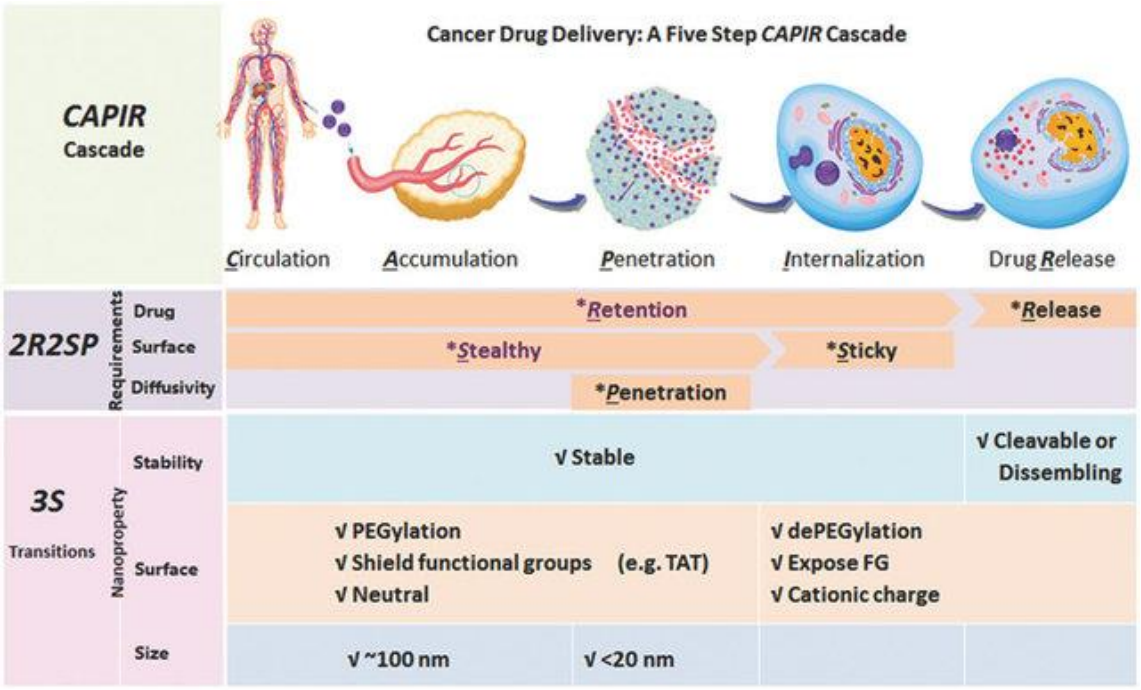

Figure 1.5 *CAPIR cascades for cancer drug delivery (Adapted from Adv. Mater. 2017, 29, 1606628).*

Circulation: The first step in the CAPIR cascade involves the circulation of nano-formulations within the bloodstream. For successful drug delivery, these nanomedicines must remain stable and intact while navigating the circulatory system[22].

Accumulation: Nanomedicines must accumulate within the tumour site, taking advantage of the leaky and rapidly formed vasculature in the tumour tissue. This accumulation is a critical step in ensuring that a sufficient concentration of therapeutic agents reaches the target[22].

Permeation: Subsequent to accumulation, nano-formulations need to deeply penetrate the tumour tissue to access the tumour cells effectively. Efficient permeation is essential to reach the intended target cells within the tumour[22].

Internalization: Once within the tumour tissue, the nano-formulations must be internalized by the tumour cells. This step allows the therapeutic agents to exert their pharmacological effects directly within the cancer cells[22].

Release: The final step in the CAPIR mechanism involves the release of the drug within the interior of the target cell. This ensures that the drug molecules are in their unbound, active form, ready to carry out their intended function[22].

Efficiency Considerations: Ultimate goal of cancer drug delivery is to maximize the delivery of therapeutic agents into cancer cells in their active form. Achieving this goal depends on optimizing each of the five steps in the CAPIR cascade, denoted as QC (Circulation Efficiency), QA (Accumulation Efficiency), QP (Permeation Efficiency), QI (Internalization Efficiency), and QR (Release Efficiency). The overall delivery efficiency (Q) is a measure of the proportion of drug molecules existing freely within the targeted cells relative to the total quantity injected. It is crucial to emphasize that the success of the drug delivery cascade relies on the efficiencies of all five steps, and none of these efficiencies should approach zero[22,23].

1.3. Enhance Permeability and Retention (EPR) Effect

EPR stands for enhance permeability and retention effect refers to the permeability of the nanoparticle to the cancer tissue as compare to normal tissue[24,25,26]. Maeda et al showed the phenomena of EPR, the nanoparticle of size less than 500nm can go inside the tumour tissue and retain there at the intercellular level. Due to enhanced cell growth of the cancer cells as compare to normal cells, there is no proper

arrangement of the cells due to which cells were grown with large intracellular space[26]. Due to fast growth rate of the cells the tumour develops the poor vasculature and lymphatic drainage. Using this characteristic of the cancer cells, the nanoparticle with encapsulated drug can get permeated inside the tumour and retained due to poor lymphatic drainage system which is further internalise by endocytosis process as shown in Figure 1.6.

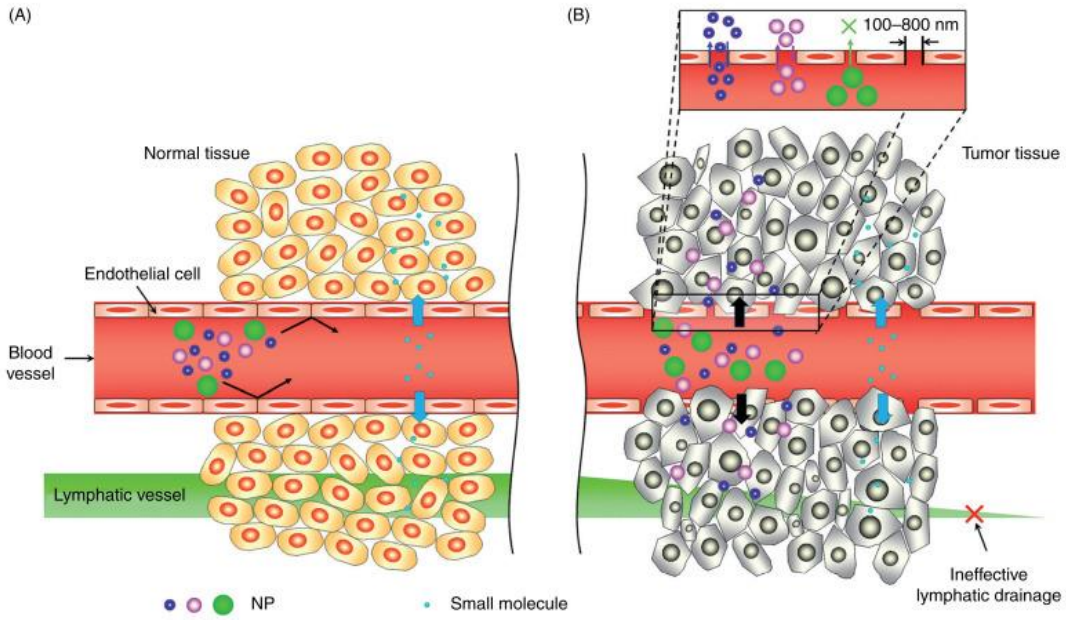

Figure 1.6 *EPR Effect comparison of the normal vs cancer tissue for treatment using nanoparticle-based chemotherapy. (Adapted from Multifunctional Systems for Combined Delivery, Biosensing and Diagnostics 2017, Pages 245-259.)*

When the nano-formulations administered in the blood circulation, during the circulation in the blood stream it can passively accumulate at the target site or tumour site due to EPR effect of the cancer tissue[26]. Based on the how the nano-formulation reaches the target site it has divided into two types active targeting and passive targeting. Passive targeting approach in cancer treatments utilises the EPR effect, when the nanoparticle injected in the blood stream it can selectively accumulate inside the cancer tissue as compare to the normal tissue due to EPR effect. As compare to active targeting where nanoparticle does not contain any specific targeting ligand attached to it[27,28]. In case of active targeting refers to the development of the nanoparticle decorated with target ligand or target stimuli[27,28]. Christine E. Wang eta synthesized the sunflower type polymer outer layer decorated with the folate ligand while inner core having DOX. They demonstrate use of sun flower polymers for targeted drug delivery. In this system

they attached the DOX to the polymer with hydrazone linkage to achieve pH responsive release.[29] (See Figure 1.7). Mingyang Li et al developed active targeting silicon nanoparticles (Si NPs) for targeting HER2-positive breast cancer cells. These nanoparticles specifically targeted HER2-positive breast cancer cells, and their targeting effectiveness was improved by increasing the Fab density. The targeting efficacy and nanoparticle dosage directly impacted cytotoxicity. Additionally, the rapid response of cancer cells to the nanoparticles correlated with the Fab density and HER2 expression level.[30]

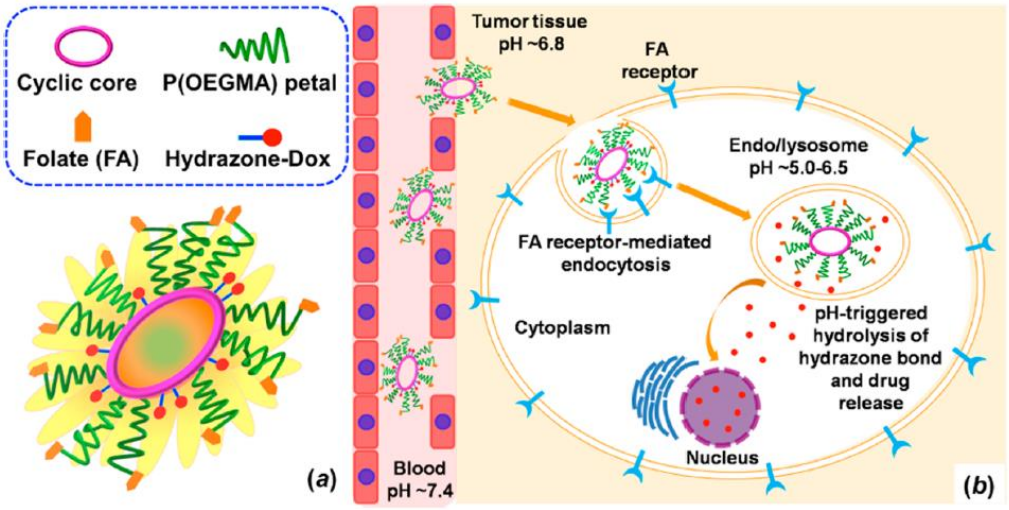

Figure 1.7 *Sun flower type polymer for active targeting for the folate receptor (Adapted from Biomacromolecules 2016, 17, 69−75).*

Arpan Satsangi et al synthesized and characterized paclitaxel (PTX) conjugate using a PAMAM dendrimer linked with a cathepsin B cleavable GFLG peptide spacer (PGD). When delivered via this conjugate, PTX exhibited enhanced cytotoxicity, reducing the metabolic activity of various cancer cells compared to PTX alone. This effect was particularly pronounced in cells expressing moderate-to-high levels of cathepsin B activity[31]. Simon A. Costa and colleagues introduce an innovative approach for concurrent genetic encoding of a drug conjugation site and a structured bioactive domain within a biopolymer-based nanoparticle. This method utilizes an unnatural amino acid for drug attachment, capable of incorporating a nanobody as a targeting element, which relies on a disulfide bond for stability. Their study showcases successful active targeting at the cellular level, as illustrated in Figure 1.8. [32]

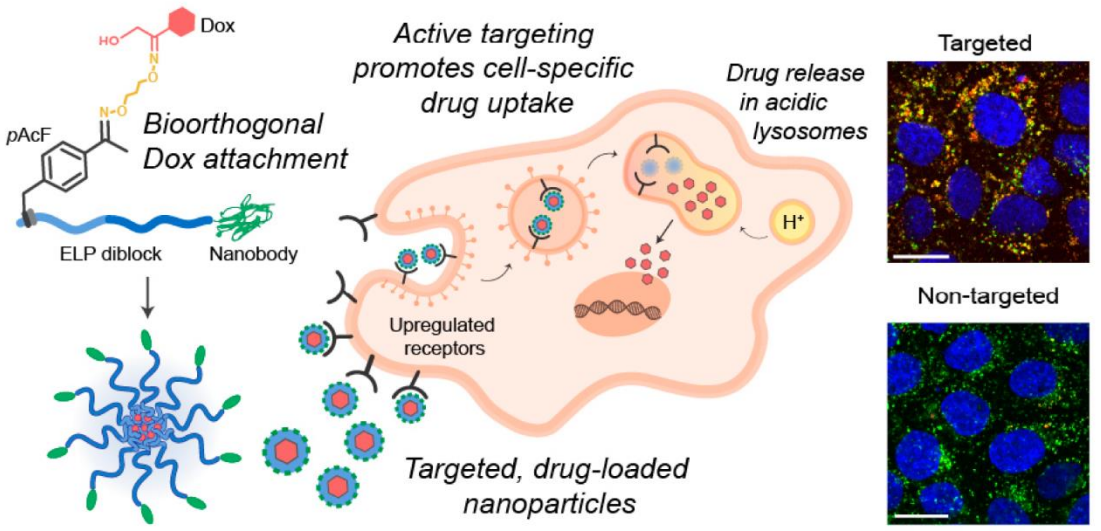

Figure 1.8 *Active targeting of the nanoparticle to cancer cells using DOX conjugated nanoparticles. (Adapted from Nano Lett. 2019, 19, 247−254).*

1.4 Polymeric nanoparticles for cancer therapy

There is various type of the nanoparticles are developed depending upon the type of material used for the development, such as lipid-based nanoparticles[33,34], polymer nanoparticles[35,36], inorganic nanoparticle[37,38] and more for the chemotherapy. In this chapter we will be focused only on the polymeric material used for drug delivery. Helmut Ringsdorf's is a German chemist who is known for his pioneering work in the field of polymers and materials science. The applications of polymers that Ringsdorf's work has contributed to include drug delivery systems, where the dendritic structure can encapsulate and release drugs in a controlled manner, and nanotechnology, where polymers serve as scaffolds for building nanoscale structures with specific properties[39,40,41]. The Ringsdorf's model dealt with the development of polymer for the drug delivery system, it talks about conjugating the drug molecules to the water-soluble polymers to enhance the uptake of the hydrophobic drug. Figure 1.9 shows that polymer with active drug covalently attached, the polymer can be further attached with active targeting molecules to specifically attacking the target site and minimising off target effects.

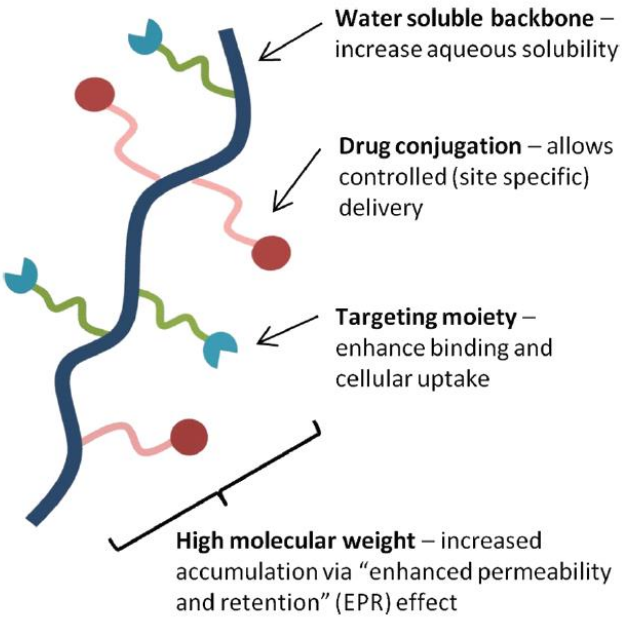

Figure 1.9 *Helmut Ringsdorf's Model for drug delivery (Adapted from Chem. Mater. 2012, 24, 840−853).*

Based on the Ringdrof's model various there are various successful attempts were made for the development of pharmacological polymer, these include the drug molecule attached with the polymer or polymeric assembly by the covalent or non-covalent interaction. The class of polymer drug conjugates include the attachment of the drug or pharmacologically active compound with the polymer backbone by the susceptible linkage such as ester, hydrazone, imine etc.[42,43,44] Here are some examples shown below, Alexandra A. P. Mansur et al studied the carboxyl methyl cellulose-DOX conjugates, these polymer drug conjugates decorated with RGD and arginine for specific targeting and killing the cells by chemotherapy. DOX and polysaccharides were linked together by cleavable amide covalent bond, the cellular uptake of the polymer-drug conjugate assisted by RGD peptides. The polymer taken up by the cells DOX gets released under lysosome ultimately kill the cells.[45] Pedro R. Figueiredo et al studied for various different polymeric models, 30 polymer-drug conjugates which undergoes enzymatic degradation using Hce2. By Docking and simulation methods they evaluated hCE2 capacity for recognizing the polymer-drug conjugates. They further argued that features of the drugs such as flat core and small size are important for the binding confirmation, for enzymatic hydrolysis.[46]Other approach of the drug delivery involves encapsulation of the drug inside the polymeric nanoparticle. The drug loaded inside the polymeric nanoparticles due non covalent interaction such as Wan der

Val's interactions, hydrogen bonding interaction, ionic interaction of the drug with the polymers is also responsible for the high drug loading content (DLC) in the polymeric nanoparticles[47, 48].

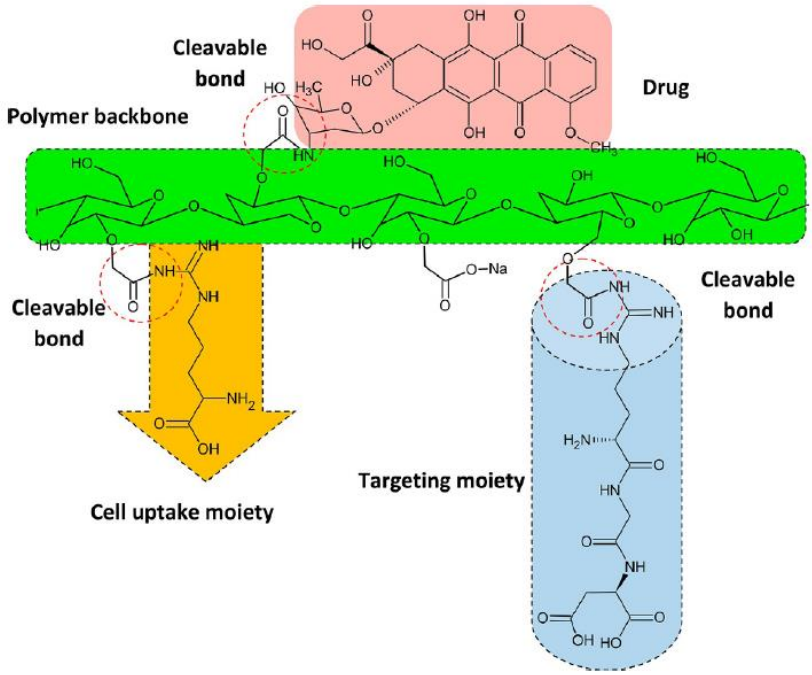

Figure 1.10 *Polymer-Drug conjugates employed for the cancer treatments (Adapted from Mol. Pharmaceutics 2021, 18, 1196−1207).*

Vahid Ahmadi and the team developed a one-step method to synthesize urethane-activated monomers and used them to create block-copoly-peptides, particularly P(Glu-b-NADA), with variable hydrophobic/hydrophilic ratios. Among these, a moderately hydrophobic copolymer displayed excellent stability, high drug loading (4 wt%), and formed 200 nm spherical nanoparticles. Loaded with m-THPP, it exhibited controlled drug release at skin-like pH (5.5-6.5), making it a promising option for dermal drug delivery. Cytotoxicity studies showed no harm to HaCa T and HeLa cells up to 1 mg/mL, highlighting its potential as a safe drug carrier.[49]

.

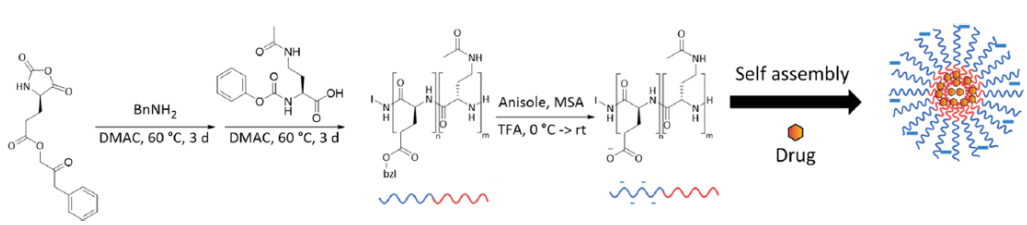

Figure 1.11 *Synthesis of Drug loaded polypeptides nanocarrier for drug delivery in chemotherapy. (Adapted from ACS Appl. Nano Mater. 2021, 4, 6709−6721).*

Min Qiu and the team created a nanoplatform using PEG-b-poly(α-aminopalmitic acid) block copolymers for precise anticancer drug delivery. These copolymers, synthesized from α-aminopalmitic acid N-carboxyanhydride (APA-NCA), self-assembled into stable polylipopeptide micelles (Lipep-Ms). These micelles effectively loaded and released potent anticancer drugs like DTX within cancer cells, showcasing their potential as drug delivery vehicles[50]. Polymeric nanocarriers are a promising approach for drug delivery applications. These nanoscale systems are designed to encapsulate and deliver therapeutic agents, such as drugs, proteins, or nucleic acids, to target sites in a controlled and efficient manner. They can enhance drug solubility, improve bioavailability, prolong circulation time, and provide targeted delivery, thereby reducing side effects and increasing therapeutic efficacy. Here are some common types of polymeric nanocarriers used for drug delivery[51,52]. Polymeric nanoparticles, typically sized between 10 nm to 500 nm, offer versatile drug delivery options and are composed of polymers like PLGA, PEG, and chitosan. They can encapsulate both hydrophobic and hydrophilic drugs, ensuring controlled release and drug protection. Polymeric micelles, formed by self-assembling amphiphilic polymers in aqueous solutions, possess a core-shell structure that can encapsulate poorly water-soluble drugs in the hydrophobic core while maintaining stability with a hydrophilic shell.

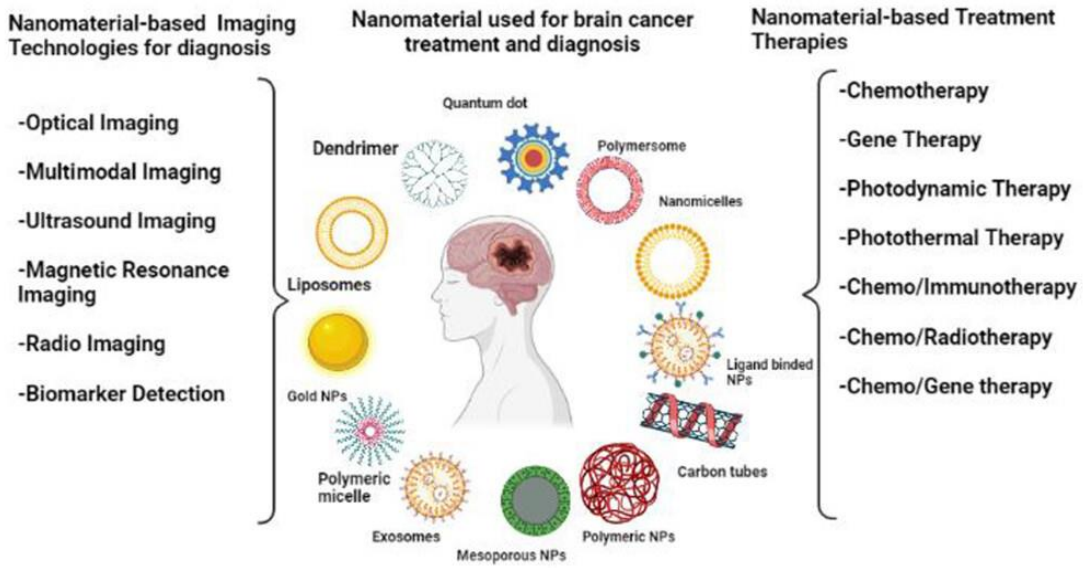

Figure 1.12 *Polymer-based nanoparticle for drug delivery in cancer cells. (Adapted from Mol. Pharmaceutics 2023, 20, 10, 4893–4921).*

The properties of nanocarriers play a crucial role in determining the effectiveness, safety, and performance of a drug delivery system. The design and optimization of

nanocarrier properties are essential to ensure targeted and controlled drug delivery. Herein, we elucidate the critical properties of nanocarriers and their consequential effects on drug delivery systems. The size and surface area of polymeric nanocarriers are pivotal determinants of their functionality. Nanoparticles possess impressive surface area-to-volume ratios, thereby augmenting their drug loading capacity and their ability to interact with target cells. Smaller nanocarriers have been found to achieve higher drug loading, enhance drug release kinetics, and facilitate cellular uptake due to their expanded surface area. Nevertheless, exceedingly diminutive sizes may lead to rapid clearance from the body.[53,54] The charge of nanoparticles is primarily characterized by the presence of charged functional groups on their outer shell. Nanoparticles can bear positive, negative, or neutral charges, each bestowing unique interactions with cell surfaces. The negatively charged outer layer of cell plasma membranes results in distinct interactions with cationic and anionic nanoparticles. Surface charge significantly influences how nanocarriers interact with biological components, including cells and proteins. Positively charged nanocarriers may enhance cellular uptake through electrostatic interactions, while negatively charged ones might evade immune clearance and exhibit distinct biodistribution patterns. [55,56] Functional groups on the nanocarrier's surface offer the potential for facile conjugation of targeting ligands, therapeutic agents, or stimuli-responsive molecules. Functionalization empowers targeted delivery to specific cells or tissues, controlled release, and responsiveness to environmental cues. The incorporation of targeting ligands further augments specificity, allowing for precision in drug delivery. [57,58]The drug loading capacity (DLC) of a nanoparticle refers to its ability to encapsulate drug molecules within its core. A higher DLC translates to greater efficacy in drug delivery to the target site. Optimizing DLC is critical for maximizing therapeutic outcomes.[59,60] Efficient drug release kinetics are essential for successful drug delivery. Nanoparticles must release their loaded drugs at the target site, either through external stimuli or triggers. This nanotechnology-based approach ensures that the drug reaches its destination with minimal off-target effects. Controlled release kinetics govern the duration and intensity of drug exposure, which, in turn, affects therapeutic efficacy, minimizes side effects, and maintains therapeutic levels over time.[61,62] The stability of nanocarriers is a critical factor that impacts their shelf life, storage conditions, and performance in biological environments. Stable nanocarriers must endure both storage conditions and circulation in the bloodstream. Stability is paramount for preserving drug integrity during storage

and ensuring effective drug release at the target site. Instability can result in premature drug release or carrier degradation.[63,64] The properties of nanocarriers wield a profound influence on the performance of drug delivery systems. These properties encompass drug release, targeting, stability, and safety. A comprehensive understanding of how these properties interact with biological systems and with each other is paramount for designing effective and safe nanocarrier-based drug delivery systems.

1.5 Stimuli responsive polymer Nano-carrier

Stimuli-responsive polymers, often referred to as "smart" or "intelligent" polymers, constitute a category of polymers capable of modifying their physical or chemical characteristics in reaction to external stimuli. These polymers hold great promise in drug delivery as they can be tailored to release drugs in a precise and controlled manner in response to specific environmental triggers. Notably, Figure 1.13 presents examples of such stimuli-responsive polymers designed for advanced drug delivery applications.

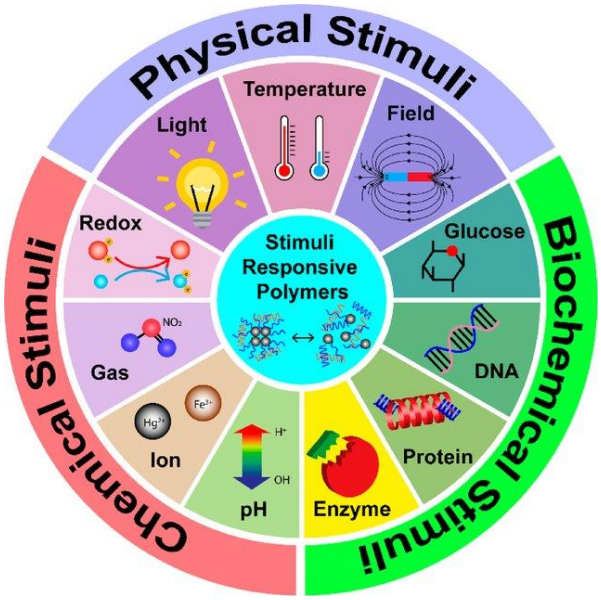

Figure 1.13 *Stimuli responsive drug release. (Adapted from ACS Appl. Bio Mater. 2021, 4, 1, 140–162).*

pH-sensitive polymers can change conformation or undergo degradation in response to variations in pH levels. In the context of cancer drug delivery, these polymers can take advantage of the lower pH environment of tumor tissues compared to healthy tissues. Dalin Wu and colleagues have developed two types of nanoparticles (NPs) with a strong pH-responsive capability. The first type, based on the polymer PDEAEMA, transitions from solid to soft states across a wide pH range (pH 2.0 to 10.0). The second type,

PDMAEMA-grafted PS NPs, exhibits pH-dependent interfacial behaviour, reducing interfacial tension under acidic (pH < 6.0) or basic (pH > 7.0) conditions. Both NPs efficiently serve as emulsifiers for toluene and water, enabling dynamic control of emulsion phases by adjusting pH, promising applications in drug encapsulation and triggered release, highlighting the significance of Pickering emulsions for stability and the role of particle surface properties in their formation.[65]

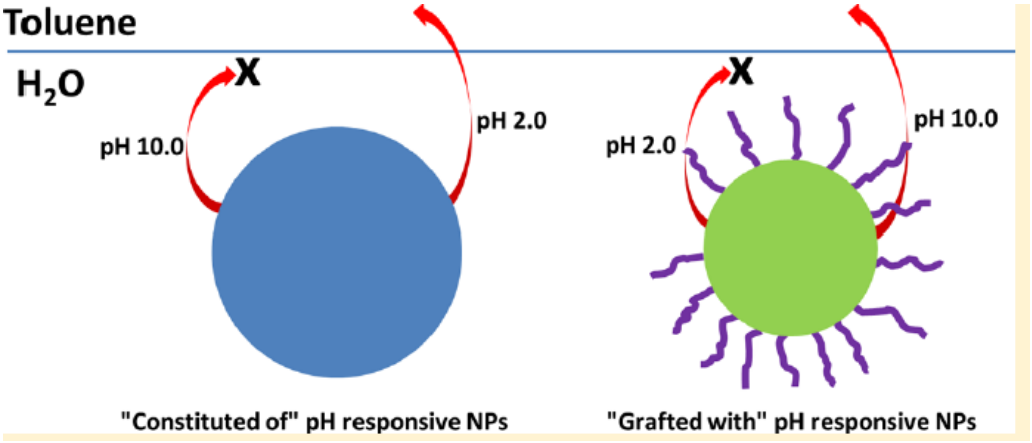

Figure 1.14 *pH responsive polyester. (Adapted from Langmuir 2018, 34, 6170−6182).*

Kajal Kumbhakar et al studied the interaction of solute C153 with pH-responsive polymers in aqueous solutions differs from its interaction with neat water. The primary factor influencing spectral characteristics and fluorescence anisotropy decays is the preferential interaction of C153 with the hydrophobic regions of these polymers at the polymer-water interface. Dielectric relaxation measurements reveal water-like properties in the MHz to GHz range within these pH-responsive polymer solutions, and no abrupt changes were observed in static and dynamic properties with varying pH. The blue shift in C153 fluorescence emission suggests its preferential localization at the polymer-water interface, with restricted solute rotation leading to unique rotational behaviour. This finding supports the idea that the interface is formed through the coiling of individual polymer chains rather than polymer aggregation, offering potential applications in targeted drug delivery. Further investigation via THz dielectric relaxation measurements is warranted to confirm the "bulk-like" nature of water molecules around the surface.[66]In the investigation, a team led by Yongjun Luo devised Gold Nanorod (GNR) - DPArPEGMA nanocomposites, featured pH-responsive adhesive properties for bacterial targeting and efficient bacterial eradication using near-infrared (NIR) technology. GNR-DPArPEGMA displayed a negative charge within physiological conditions but transitioned to a positive charge in sub-acidic

microenvironments, thereby minimizing harm to surrounding tissues while enhancing adherence to bacterial targets[67].

Temperature-sensitive polymers can undergo reversible phase transitions in response to changes in temperature. These transitions can result in changes in polymer solubility, swelling, or drug release. Polymers like poly(N-isopropylacrylamide) (PNIPAAm) exhibit a lower critical solution temperature (LCST) behavior, causing them to collapse and expel encapsulated drugs when the temperature exceeds their LCST. Thermo-responsive polymers are similar to temperature-responsive polymers but respond to temperature changes within a specific range. They can be designed to release drugs when exposed to localized hyperthermic conditions, such as those induced by external heat sources like laser irradiation. Bin Wang Synthesized hyperbranched polymer with thermo-responsive properties, they varied the spatial distribution in the form of two layer in the form of two layers with different amide group. The resultant hyperbranched polymer showed different behaviour when two amide groups that is butyramide and acetamide planted in the different layers of the hyperbranched polymer. Molecular transition was monitored using NMR studies. As the two amide groups are present in two different layers which resulted into different packing of the polymer, the change in the phase of the polymer was driven the hydration and dehydration of the polymer.[68]

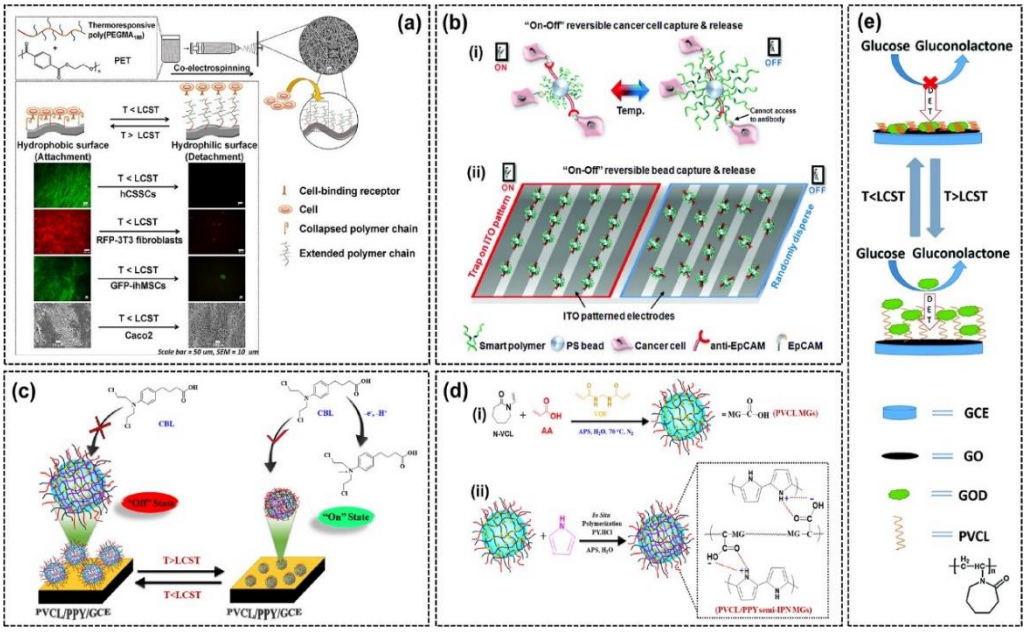

Figure 1.15 *Different types of the thermo-responsive polymer. (Adapted from ACS Appl. Polym. Mater. 2023, 5, 3181−3200).*

Wenxin Fu et al developed polyalphaolefin with UCST type thermo-responsive type behavior polymers. The polymer was prepared from alkyl methacrylate by employing raft polymerization, it was found that PAO with appropriate side chain exhibit the property of thermo-responsiveness. They further demonstrated that triblock copolymer with appropriate composition and concentration undergo thermally induced reversible sol gel transition and the transition temperature of sol gel can be varied with change in the composition of the polymer.[69] Juan L Paris et al developed ultra sound responsive polymers that utilizes microporous silica nanoparticle as a Drug carrier for drug delivery system. The polymer below LCST can be grafted to MPS NPs on the pore of MSN to avoid premature drug release. When the Ultra sound was irradiated the there is a detachment (tetrahydropyranyl) of hydrophobic and hydrophilic segment of the polymer chain which leads to reduction in LCST of the polymer and ultimately causes release of the loaded drug. In this case polymer acts as the nanogates. The cellular uptake study further confirms the US responsive release of the DOX which led to killing of the cells.[70]

Photo-responsive polymers can change their properties when exposed to light of specific wavelengths. Ultraviolet (UV) or near-infrared (NIR) light can trigger changes in polymer conformation, degradation, or drug release. This approach can allow for on-demand drug release at specific sites using external light sources. Mathieu L. Viger et al studied the release of the loaded payload from the polymeric nanoparticle due to the thermally induced a phase change. The water confined in the polymer matrix was excited with the help of IR laser of 980nm which resulted in the increase in the temperature which subsequently causes phase change of the polymer which ultimately release the loaded cargo. They further demonstrated proof of concept at both *in vitro* or *in vivo* conditions.[71]

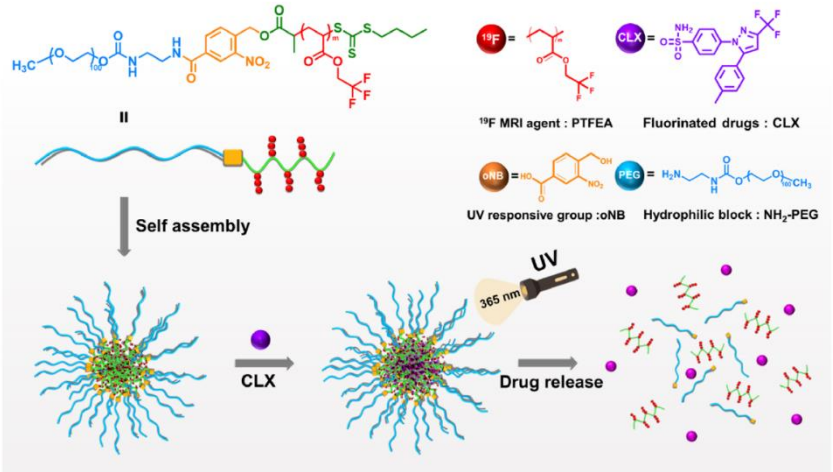

Figure 1.16 *Photo-responsive polymer. (Adapted from ACS Nano 2014, 8, 5, 4815–4826).*

Chenlong Li et al developed photo-responsive amphiphilic polymer with photo-responsive linker for the 19F MRI theranostic. The polymer self-assembled to form nanoparticle in aqueous environment these nanoparticles were labelled for 19F to improve the thernostic efficacy of the NPs by MRI imaging. The photo-triggered release of the loaded cargo was monitored by the action of UV light.[72] Sebastian Inacker et al developed coumarin based the photo-responsive polymer, which undergoes intramolecular dimerization. The polyurethanes were prepared from the coumarin based diol; this polymer film was prepared by spin coating technique which can be utilized for cyclo-reversion reaction induce by light. The pendant dimer can be converted into monomer by light intense laser utilizing two photon absorption spectra[73]. Redox-responsive polymers undergo changes in response to changes in the redox environment. For example, they can be designed to release drugs in the presence of high concentrations of reducing agents, such as glutathione, which is abundant in certain tumour cells. Johannes Elbert et al developed poly(vinylferrocene)s with redox switchable properties. The ROMP was carried out on surface modified silica nanoparticle, the pendant ferrocene group of the polymer showed the redox switchable behavior. The nanoparticle with Polyvinylferrocene-grafted exhibited response after chemical oxidization, deactivating surface-attached Grubbs catalysts. This system has the potential application in the drug delivery, catalysis and sensor applications.[74]
Christina M. Geiselhart et al synthesized TMBQ redox responsive multifunctional polymer using step growth polymerization. The polymer showed both redox responsive and self-emulative behavior. This system can be further utilized for development of the implant or nanocarrier which can show amplified release under hypoxia condition[75].

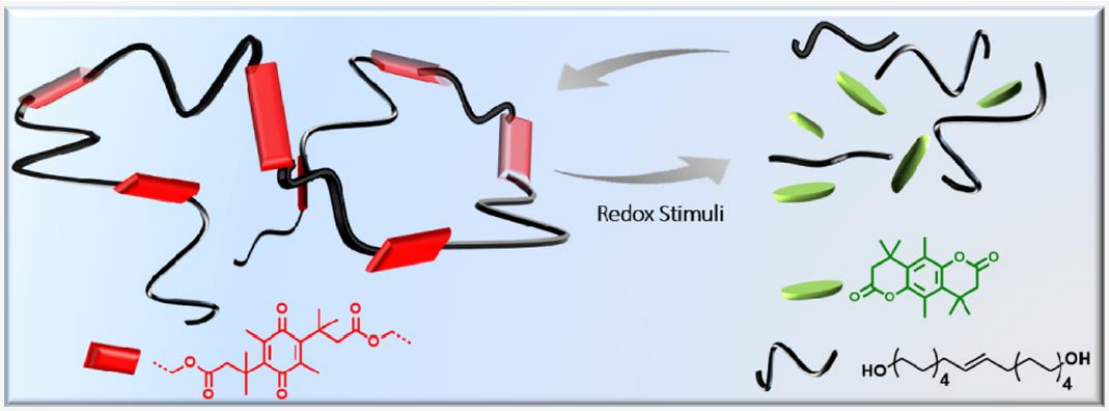

Figure 1.17 *Redox-responsive polymer. (Adapted from Macromolecules 2021, 54, 1775−1782).*

Enzyme sensitive polymers can be designed to degrade or undergo conformational changes in response to the presence of specific enzymes. This can be particularly useful for drug release in disease-specific environments where certain enzymes are overexpressed. Assaf J. Harnoy and the team have developed six enzyme-responsive PEG-dendron hybrids that self-assemble into micelles in water and disassemble in the presence of specific enzymes. These micelles can encapsulate and release hydrophobic molecules, demonstrated using Nile Red dye.

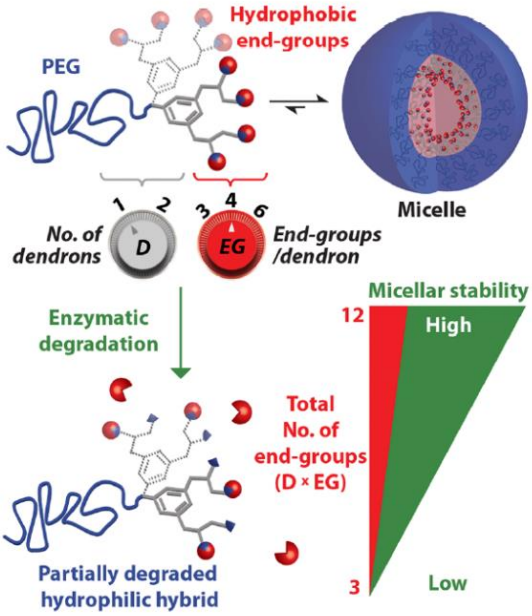

Figure 1.18 *Enzyme-responsive polymer. (Adapted from Biomacromolecules 2017, 18, 1218−1228).*

Importantly, dendritic scaffolds play a pivotal role in this approach, controlling enzyme activation through hydrophobicity. The research underscores how even minor changes in the hydrophobic block can impact the stability of these structures against enzymatic degradation[76]. Yun Yu and colleagues have developed a method for the synthesis of alkyne and allyl-functionalized Poly (Lactic Acid) (PLA) without requiring a deprotection step. These functionalized PLAs are then employed in highly efficient azide-alkyne or thiol-ene click reactions to create innovative PLA-based conjugates and nanostructures. These materials hold promise for applications in drug and gene delivery, with a particular emphasis on enzyme responsiveness. They designed PLA-g-DOX-based nanoparticles with controlled high drug loading, tailored for pH and

enzyme-triggered drug release. This research endeavours to advance drug delivery systems, leveraging PLA-based conjugates and nanoparticles with improved performance and targeting capabilities through the incorporation of acid-sensitive linkages and biocompatible surfactants, ultimately enhancing their enzyme-triggered responsiveness.[77] Xibo Xang and team have created an enzyme-responsive polymeric supra-amphiphile by combining poly(ethylene glycol)-block-poly(acrylic acid) (PEG-b-PAA) with myristoylcholine chloride (MCC). These polymers can self-assemble into spherical aggregates (40-150 nm) and disassemble when exposed to acetylcholinesterase (AChE), a natural human enzyme. This innovative material could serve as a drug carrier, particularly for drugs regulating AChE, with potential applications in treating neurological diseases.[78] Yuetong Kang et al have utilized natural polymer chitosan and ATP for development of the enzyme responsive self-assembly. The ATP molecules loads in the polymeric micelle due to the electrostatic interaction between the positive charge on the polymer and negative charge on the ATP molecules. This kind of the structure can be utilized for the drug delivery in chemotherapy.[79]Magnetic nanoparticles can be incorporated into polymers, allowing for triggered drug release using external magnetic fields. By applying a magnetic field, the polymer can be heated, causing drug release or changes in its structure. [80,81]Reimen Jauregu and colleagues developed magnetic nanoparticles (mNPs) via in-situ co-precipitation, concurrently functionalizing them with temperature-responsive polymers. They utilized a diblock copolymer, poly(acrylic acid)-block-poly(N-isopropylacrylamide) (pAAc-b-pNIPAAm), where the pAAc block coordinated with iron cations. This approach allowed for magnetic nanoparticle synthesis at room temperature, ensuring stability and scalability. The mNPs were employed in a temperature-responsive system for protein biomarker separation and the isolation of extracellular vesicle subpopulations.[82] Manuel Perinea Leal and team devised a method to create magnetic thermo-responsive nanocarriers featuring multiple iron oxide nanoparticles (IONPs) within a dual-shell structure. This design includes an inner shell using poly(maleic anhydride-alt-1-octadecene) and an outer shell with thermo-responsive polymers. They fine-tuned the composition to achieve adjustable phase transition temperatures (26 to 47°C) under physiological conditions. Importantly, these nanocarriers exhibit magnetic responsiveness, allowing for manipulation within a microfluidic chip through thermal actuation.[83]

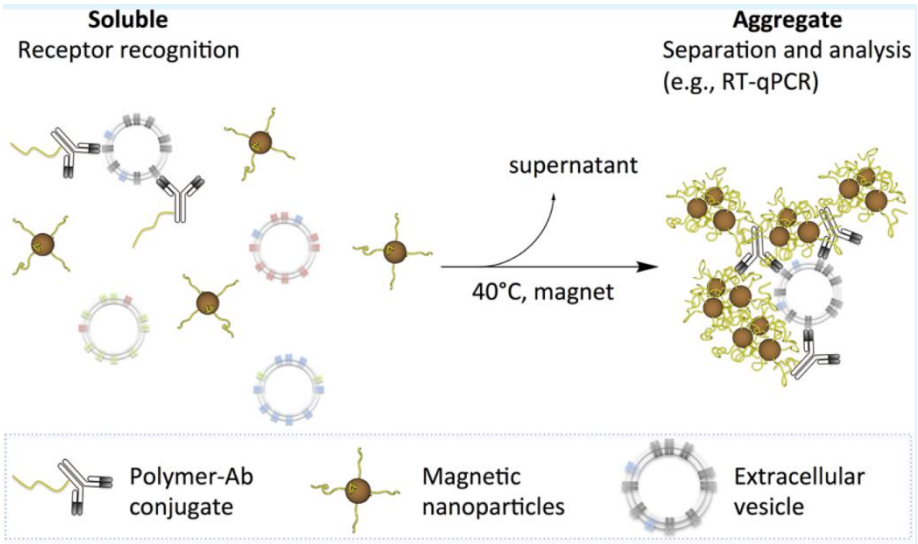

Figure 1.19 *Magnetic-responsive polymer. (Adapted from ACS Appl. Mater. Interfaces 2018, 10, 33847−33856).*

Polymers can be engineered to release drugs in response to ultrasound stimulation. The mechanical effects of ultrasound waves can trigger drug release from polymer carriers[84,85,86] Pengying Wu et al synthesized Ultra sound responsive polymeric micelle for the chemotherapy capable nan-invasive killing of the cancer cells. The cells where incubated with micelle loaded CUR and then it was immediately exposed to sonication for 5 min. Which resulted into increase in the vascular permeability followed by increases in accumulation. They further studied the localized injection of the nano-formulation followed by US treatment resulted in suppression of the tumour in xenograft mice[87].Julein H Arrizabalaga et al developed ultra sound responsive hydrogel for protein delivery, in this case they utilized chemistry of Diels alder reversible reaction. The loaded bovine albumin labeled with fluorescein only can be delivered on application of ultra sound. The chitosan biocompatible polymer was utilized for the construction of US responsive hydrogel[88].Jing Xia et al developed modified natural polysaccharide pullulan with ultra sound responsive linker with hydrophobic stearic segment. This amphiphilic polymer was able to load DOX payload undergo ultra sound triggered release which help to develop on demand therapeutics at the target site.

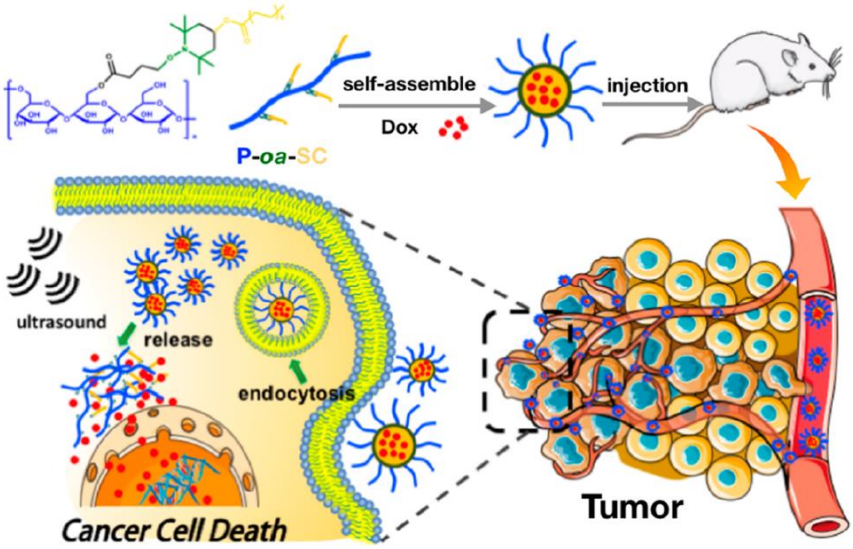

Figure 1.20 *Ultrasound-responsive polymer. (Adapted from ACS Appl. Mater. Interfaces 2018, 10, 33847−33856).*

In this case P-oa-SC/DOX nanoparticle supplemented with localized ultra sound which exhibited anti-tumour efficacy in in vivo model with minimized possibility of non-specific target interaction[89]. These examples highlight the versatility of stimuli-responsive polymers in designing drug delivery systems that respond to specific cues, leading to improved therapeutic outcomes and reduced side effects. However, it's important to carefully design and characterize these polymers to ensure their effectiveness and safety in clinical applications.

1.6 Polymer from Natural resources L-Amino acid

L-amino acid-based polymers are an intriguing class of materials that hold great potential for various biomedical applications, including drug delivery. These polymers are derived from natural L-amino acids, which are the building blocks of proteins. They offer biocompatibility, biodegradability, and the ability to be modified for specific drug delivery requirements. These L amino acid based synthetic polymers were utilized by drug delivery applications, these includes synthetic peptides and polypeptides. L amino

acid first converted into polymerizable monomer unit which is referred as NCA. The units undergo ROP using initiator to produce polypeptides as shown in scheme.

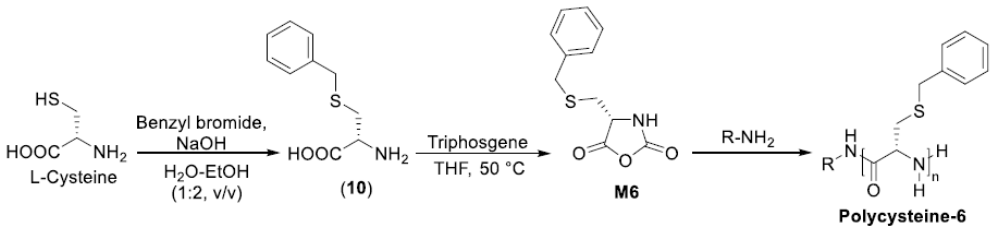

Figure 1.21 *Synthesis of poly L-Cysteine (Adapted from Biomacromolecules 2022, 23, 6, 2667–2684).*

The utilization of ring-opening polymerization techniques involving NCA monomers derived from L-amino acids is a well-established route for fabricating precisely defined di- and triblock synthetic polypeptides. These polypeptides have demonstrated a remarkable propensity for self-assembly into an array of nanostructures, including fibrillar networks, micelles, and vesicles, which, in turn, have garnered substantial attention in both material science and biomedical domains [90-92]. Ifat Cohen Erez and colleagues introduce a NP platform involving oppositely charged components: γ-PGA and cationic PFK peptides. These PoP-NPs can deliver charged molecules, exemplified with LND. They studied core-to-shell assembly and cellular internalization by endocytosis. They mPoP-NPs may exit endosomes and colocalize near mitochondria, facilitating drug release. LND-loaded mPoP-NPs exhibit enhanced toxicity.[92]

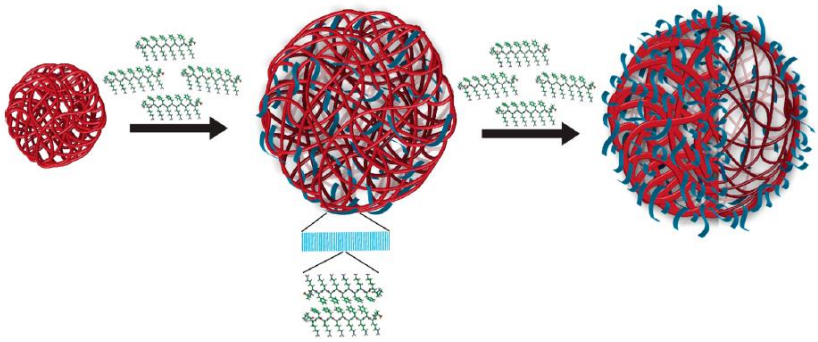

Figure 1.22 *Polypeptides based self-assembly (Adapted from Biomacromolecules 2015, 16, 3827−3835).*

Notwithstanding their exceptional biocompatibility, concerns linger regarding the intracellular enzymatic biodegradation of high molecular weight polypeptides, posing challenges for their enduring utility in biomedical contexts. Over the past decade, significant endeavors have been dedicated to formulating alternative strategies

for generating biodegradable polymeric nanomaterials using amino acids through diverse polymerization methodologies. This pursuit has given rise to an array of nonpeptide polymers hailing from amino acids, encompassing Poly (α-hydroxy acids)[93-94], poly (ester amide) s [95-97], polyurethanes[98], poly(disulfide-urea-urethane)[99] and more. These versatile materials have discovered manifold applications within the expansive realm of biomedical engineering's of the polymer with good biocompatibility and mechanical properties.

The poly(α-hydroxy acids) category, consists of a group of biocompatible and biodegradable polymers, which includes poly(lactide), poly(glycolide), and poly(lactide-coglycolide). These versatile materials have found extensive applications in the realms of biomedicine and pharmaceuticals, encompassing resorbable sutures, implantable devices, drug delivery systems, and tissue engineering scaffolds. [93,94] Functional polyesters are often synthesized from α-amino acids through processes such as polycondensation or ring opening polymerization. In the polycondensation approach, the amino group of α-amino acids undergoes diazotization to convert it into a hydroxyl group, facilitating the formation of polyesters. Nonetheless, direct polycondensation typically results in polymers with low molecular weights and poor dispersity. [93]

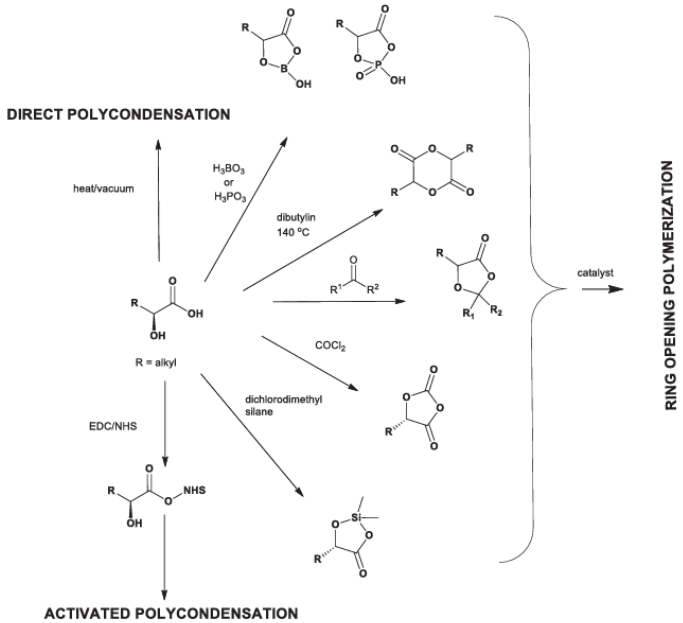

Figure 1.23 *Synthesis of Poly (α-hydroxy acid) s from L amino acid (Adapted from A.Basuetal./Advanced Drug Delivery Reviews 107 (2016) 82–96).*

In response to these challenges, Abraham J Domb and colleagues embarked on the synthesis of a range of polyesters using hydroxy acids derived from amino acids, such as isoleucine, leucine, phenylalanine, valine, methionine, arginine, histidine, asparagine, and glutamine. Their methodology involved the use of p-toluenesulfonic acid as a catalyst. Additionally, alternative approaches have been developed to produce poly(α-hydroxy acids) with improved control and under milder reaction conditions. These approaches encompass the cyclic dimerization of α-hydroxy acids, followed by ring opening polymerization, resulting in poly(α-hydroxy acids) with predictable molecular weights and well-defined chain structures.[100]

Scheme 1. Synthesis of the α-Hydroxy Acids

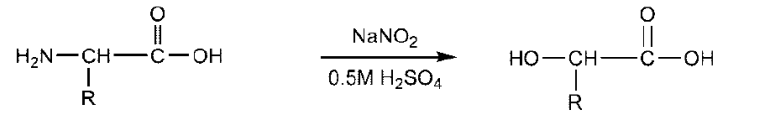

R= CH_2CONH_2, CH_2COOH, CH_2SH, $CH_2CH(CH_3)_2$, $(CH_2)_4OH$, $CH_2C_6H_5$, CH_2OH...

Scheme 2. Direct Condensation of the α-Hydroxy Acids

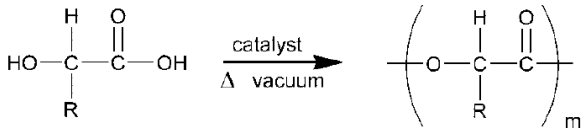

R= CH_2CONH_2, CH_2COOH, CH_2SH, $CH_2CH(CH_3)_2$, $(CH_2)_4OH$, $CH_2C_6H_5$, CH_2OH...

Figure 1.24 *Polyhydroxyl acid from l amino acid Adapted from Macromolecules, Vol. 41, No. 20, 2008).*

Poly (ester amide) s represents an emerging class of polymers characterized by their exceptional mechanical attributes, complemented by favorable biocompatibility and biodegradability profiles. This unique amalgamation of properties positions them as highly sought-after materials, finding applications in biodegradable plastics for both consumable products and the medical field alike. The synthesis of poly(ester amides) derived from amino acids can be accomplished through two distinct methodologies: (1) Ring-opening polymerization and (2) the polycondensation approach.

Ring-opening polymerization serves as a crucial pathway for crafting poly(depsipeptide)s (PDPs), which are characterized as alternating copolymers comprising an α-amino acid and an α-OH acid.

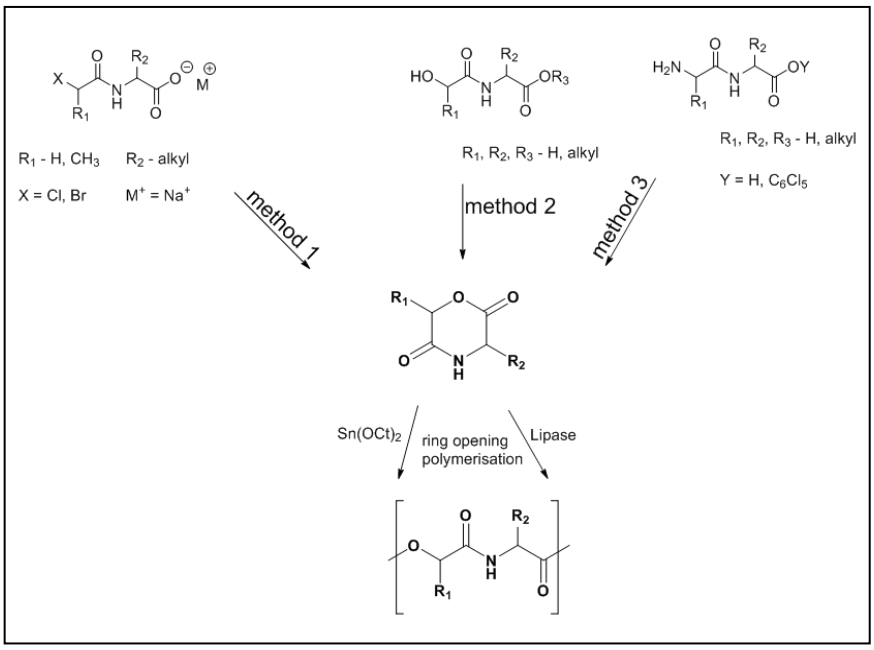

Figure 1.25 *Synthesis of Polyester amide from amino acid. (Adapted from Biomacromolecules 2015, 16, 597−605).*

In 1985, Helder and colleagues pioneered the synthesis of poly(depsipeptide)s (PDPs) through the ring-opening polymerization of morpholine-2,5-dione (MDs). Formation of 6-membered MDs derivatives can be achieved using three distinct methods: (i) intramolecular transesterification of N-(α-hydroxyacyl)-α-amino acid esters, (ii) cyclization of N-(α-haloacyl)-α-amino acid salts, and (iii) O-(α-aminoacyl)-α-hydroxycarboxylic acids. Typically, the ring-opening polymerization of MDs is conducted at elevated temperatures under melt conditions, employing a tin-based catalyst known as stannous octoate (Sn(Oct)2). An alternative and effective method for producing PDPs is the lipase-catalyzed ring opening of MDs. Chang-Xia Shi and their research group have successfully synthesized various MDs from amino acids such as glycine, phenylalanine, and leucine. The ring-opening polymerization of these MDs yielded PDPs that exhibited acid-catalyzed degradation, resulting in the formation of monomers. Moreover, copolymerization of MDs with caprolactone, glycolide, and lactide has been explored, enabling the fine-tuning of polymer properties by adjusting the monomer ratios[101].

The synthesis of polyester amides via solution polycondensation was initially reported by Katasarawa et al in the 1980s. This technique remains the most commonly employed method for polyester amide synthesis due to its rapid polymerization rate and gentle reaction conditions. The synthetic process entails polycondensation between di-

toluene sulfonic acid salts of bis-α-(L-amino acid)-α,ω alkylene diesters and an activated carboxylic acid. Ruano et al. synthesized an unsaturated polyester amide comprising phenylalanine, butenediol, and fumarate, which was subsequently photo-crosslinked to form hydrogels. These hydrogels were utilized in cell proliferation assays, demonstrating a substantial enhancement in cellular colonization after seven days.[102] Sun et al. introduced amino acid-based poly(ester amides) via solution polycondensation, employing di-p-toluenesulfonic acid salts of bis-L-phenylalanine diesters (SS-Phe-2TsOH) in conjunction with di-p-nitrophenyl adipate. These poly(ester amides) were enzymatically and reductively degradable. SS-PEA films exhibited exceptional adhesion and proliferation properties in preliminary cell culture studies, signifying remarkable cell compatibility. Degradation investigations of SS-PEA films revealed swift surface degradation mediated by α-chymotrypsin and bulk degradation in a reductive environment. Furthermore, the cytotoxicity of DOX-loaded SS-PEA nanoparticles was evaluated in both drug-sensitive and drug-resistant MCF-7 cells, highlighting the potent cytotoxicity of these nanoparticles[103]

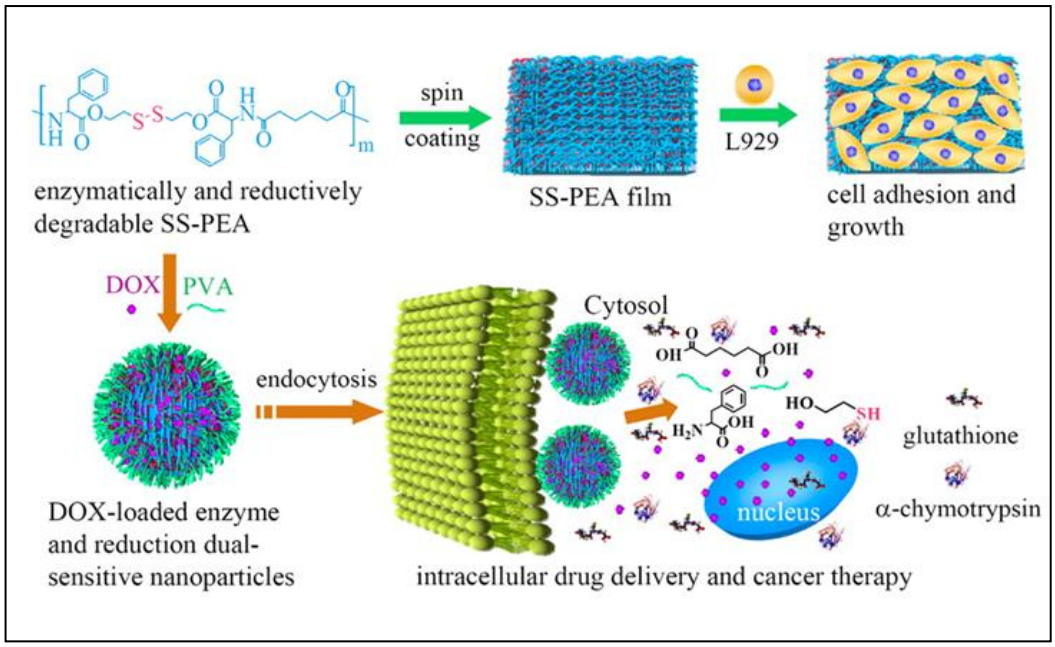

Figure 1.26 *Polyester amide containing disulphide from tyrosine used for stimuli responsive drug release for drug delivery application Adapted from Biomacromolecules 2015, 16, 597−605).*

Polydisulphide urethanes are another class of the polymer, which are having two acetal and polyurethanes as repeating units. This class of the polymer showed degradability at two different stimuli such as enzymes and acidic pH. Poly(disulfide-urethane) s Redox stimuli responsive polymer reported by Zhiyuan Zhong et al. Synthetic method

of the polymer involve the development of Lysine based isocyanate monomer followed by the polymerization with redox responsive diol under solution rout to produce desired polymer. This class of the polymer showed formation of the nano micelle for the drug delivery application.[99]

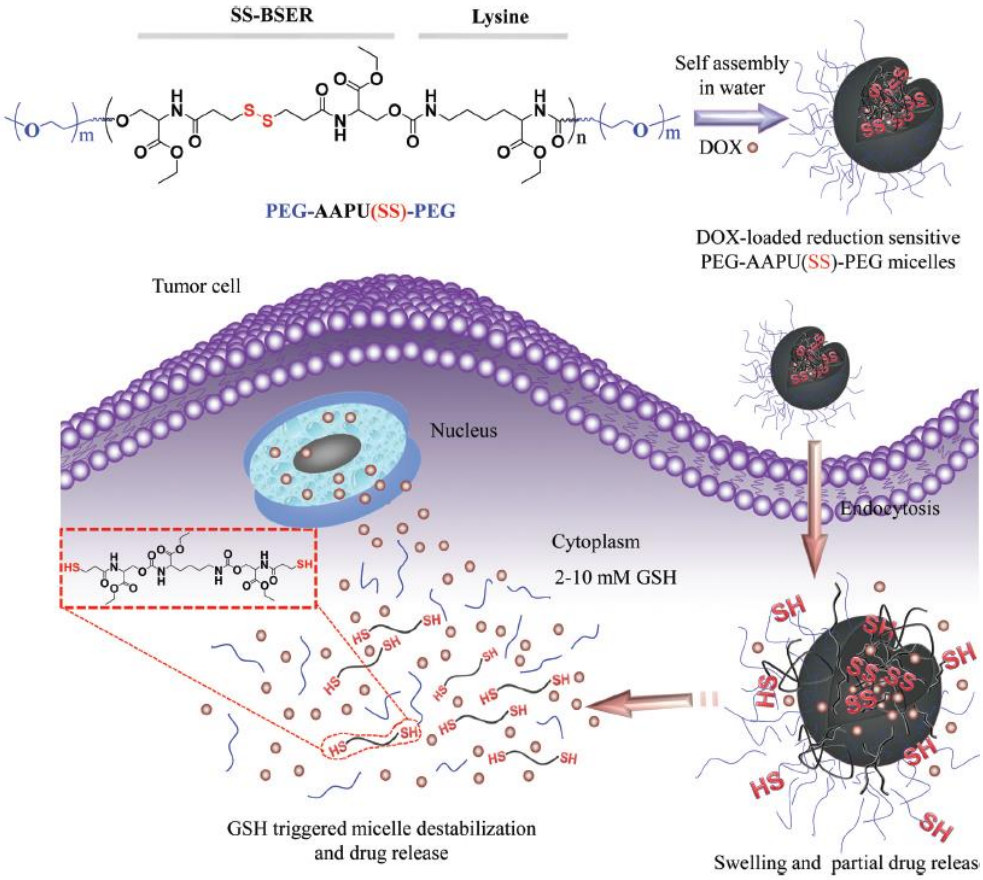

Figure 1.27 *Poly-disulphide urethane from lysine Adapted from Polym. Chem., 2015, 6, 6001–6010).*

Among the stimuli responsive polymer this another class amide repeating unit synthesized from the cystine amino acid, where the amino acid was first converted into dimethyl ester amine part was then coupled with acid to produce polyamides with disulphide from amino acid precursor. Polycarbonates Tyrosine based polycarbonates are reported by Mathew L Backer et. al, They have reported it the impact of iodinated surfaces on osteoblastcell morphological response was investigated using 2D thin films of poly(desaminotyrosyl tyrosine ethyl ester carbonate), poly-(DTE carbonate) its iodinated form, poly(I2-DTE carbonate),and several discrete blends.[104]

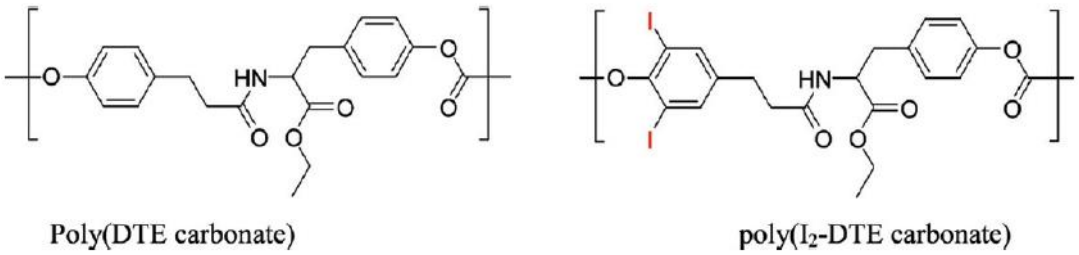

Figure 1.28 *Structure of polycarbonates for tyrosine Adapted from Biomacromolecules, Vol. 10, No. 9, 2009).*

In this class of the polymers shown by Chih-Chang Chu et al, they have successfully demonstrated that these class of the polymer are biocompatible and can be utilised for drug delivery in cancer treatments.Enzyme-catalyzed strategy was also reported for the synthesis of polyesters and very recently the process was improved to make high molecular weight helical chiral polyesters. [105]

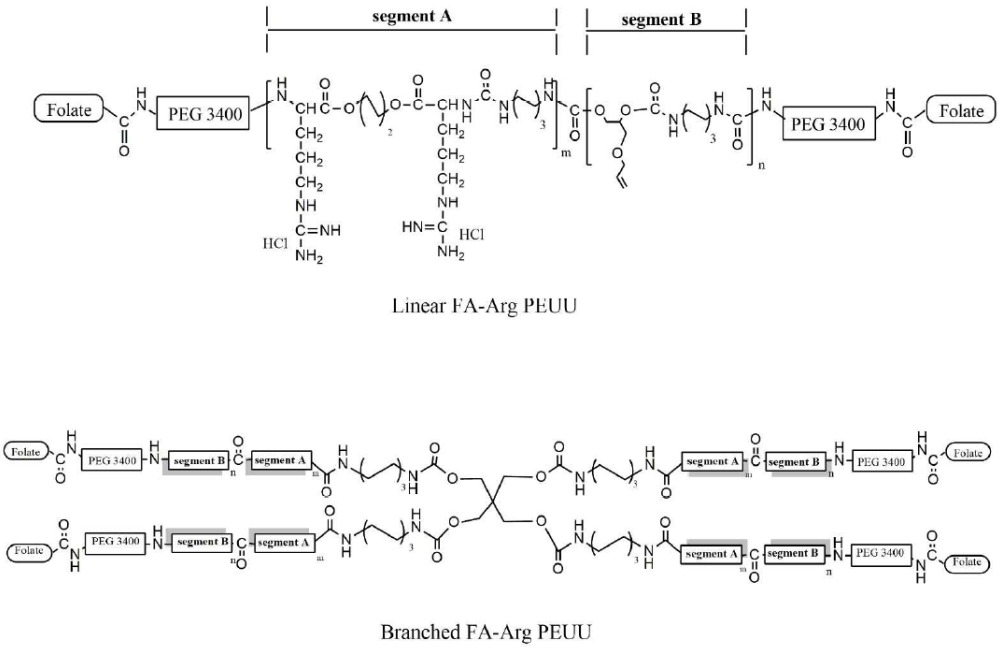

Figure 1.29 *Structure of linear and branched poly (ester urea urethane) Adapted from J. Biomed. Mater. Res. Part A 2017, 105, 475–490. https://doi.org/https://doi.org/10.1002/jbm.a.35924).*

Melt Polycondensation from Our lab

The solvent-free, non-isocyanate, melt trans-urethane polycondensation method for the synthesis of aliphatic polyurethanes has been pioneered in our laboratory led by Deepa et al in our lab. This approach involves the conversion of diamines into dicarbamate monomers, which are subsequently utilized in a melt polymerization process with various diols. This process is facilitated by a titanium catalyst, resulting in the production of high molecular weight polyurethanes[106-108]. An extension of this polycondensation technique was accomplished by Ananthraj et al., who adapted it for amino acids, enabling the synthesis of poly(ester urethane)s. In this modified process, amino acids are converted into monomers with ester and urethane functional groups. To achieve this, amino acids undergo initial reactions with thionyl chloride and methanol, yielding amino acid methyl ester hydrochloride salt. Subsequently, this salt is reacted with methyl chloroformate to generate amino acid-based dual ester urethane monomers, as depicted in Figure 1.30 [108].

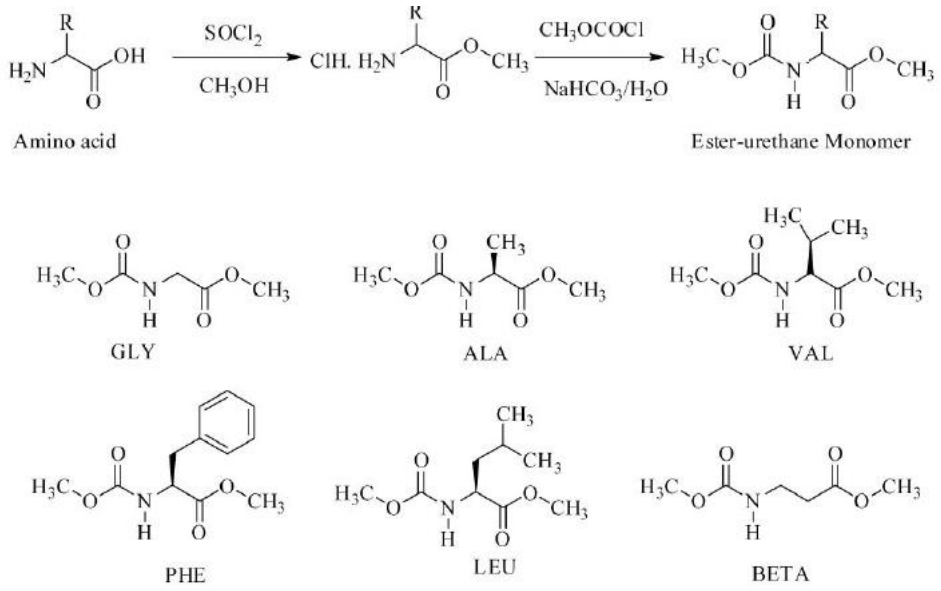

Figure 1.30 *Synthesis of the dual ester urethanes monomer from L amino acid for melt polycondensation route (Adapted from Biomacromolecules 2012, 13, 2446−2455)*

The melt polymerization of equimolar quantities of amino acid monomer and commercially available diol is carried out in a two-step process. Initially, the monomers undergo a reaction at 150°C under nitrogen conditions, using a 1 mol % catalyst. In the final step, the oligomeric melt is subjected to high vacuum treatment (0.01 mm Hg) to

produce polyester urethanes. Further purification of the polymers involves precipitation in methanol, resulting in the isolation of white fibrous poly(esterurethane)s.

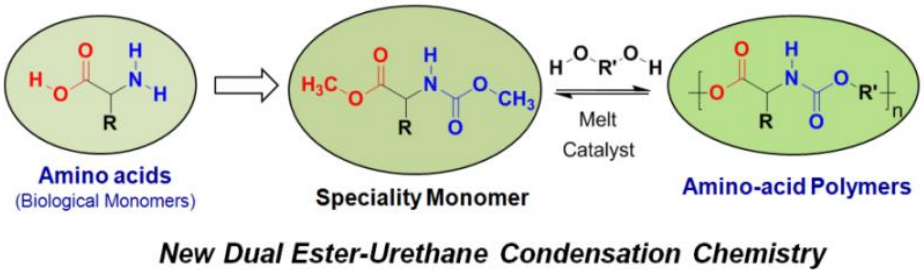

Figure 1.31 *Synthesis of poly(ester-urethane) s from L amino acid using melt polycondensation.*

The confirmation of the polycondensation reaction is established through NMR analysis, involving a comparison of the integration of end groups with the newly formed ester and urethane peaks in relation to the end group of the polymer chains. To explore the reactivity of the amino acid monomer, variations are made at the carbonyl carbon, including methyl, ethyl, and t-butyl groups. It is observed that increased steric hindrance at the carbonyl carbon leads to decreased reactivity, resulting in the production of low molecular weight polymers[109]. The reactivity of the two distinct carbonyl carbons within the amino acid monomer, specifically the ester and urethane functionalities, is investigated to understand the temperature-dependent selectivity during polycondensation. Experimental results demonstrate that at 120°C, the ester linkage undergoes an exchange reaction while the urethane linkage remains unreactive at this temperature. However, at 150°C, both the ester and urethane bonds exhibit exchange reactions. Figure 1.32 provides a visual representation of the mechanism underlying this thermo-selective reaction.

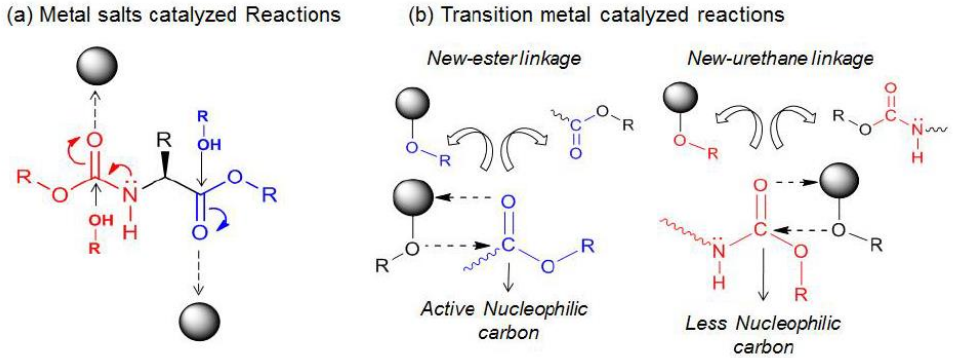

Figure 1.32 *Mechanism of the melt polycondensation by transition metal catalyst. (Adapted from JOURNAL OF POLYMER SCIENCE, PART A: POLYMER CHEMISTRY 2016, 54, 1065–1077)*

In a molten state, the hydroxyl group (R-OH) interacts with $Ti(OBu)_4$, forming an active complex denoted as Ti-OR. This complex then initiates the attack on the carbonyl carbon via a four-membered transition state during the exchange reaction. In the case of the urethane linkage, the lone pair situated on the nitrogen atom interacts more effectively with the π* orbital of the carbonyl carbon, making it less electrophilic. DFT calculations support this observation, revealing a higher electron density on the carbonyl carbon of the urethane compared to the ester. At higher temperatures, active rotation within the N-C=O bond hinders the efficient interaction between the filled p orbital and the vacant π* orbital, leading to increased reactivity and facilitating exchange reactions at elevated temperatures[110]. The influence of catalysts on the polycondensation reaction is assessed by thoroughly examining a wide range of catalysts. These catalysts represent diverse categories, including metal catalysts like alkali and alkali-earth metals, transition metals, as well as various lanthanide compounds [110]. The exploration of melt polycondensation chemistry further extends to the development of redox-responsive polyesters utilizing L-cystine as a precursor. In this process, the acid functional groups in the cystine amino acid are transformed into methyl esters, while the amine group is protected as a Boc urethane. Exploiting the distinct thermo-sensitivity of ester and urethane groups, this property is harnessed to create linear polyesters. At a temperature of 120°C, only the ester functionality undergoes an exchange reaction, leaving the Boc urethane group unaffected. This selective reactivity leads to the formation of a streamlined polyester containing disulfide linkages[111].

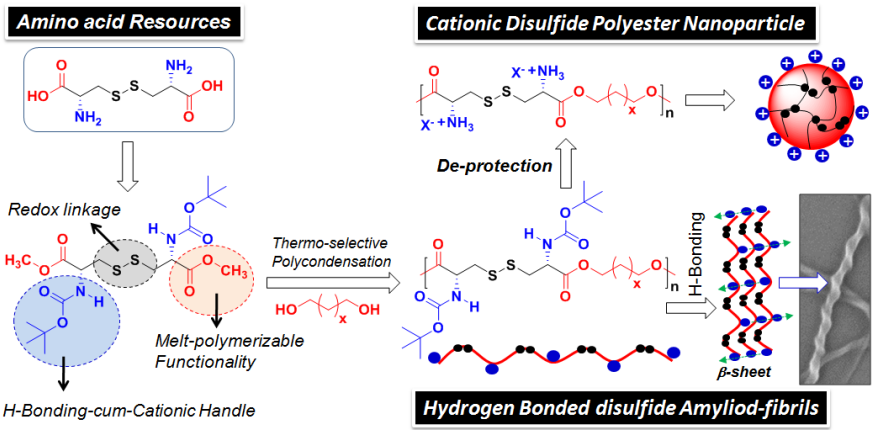

Figure 1.33 *development of the L-Cystine based redox responsive polyester by melt polycondensation (Adapted from JOURNAL OF POLYMER SCIENCE, PART A: POLYMER CHEMISTRY 2016, 54, 2864–2875).*

Subsequent post-polymerization deprotection of the Boc urethane moiety results in a cationic polymer that self-assembles in aqueous solvents, forming charged nanoparticles. To evaluate its responsiveness to reduction, polymer degradation studies are conducted in the presence of DTT (dithiothreitol). Samples are collected at various time intervals and subjected to both SEC (Size Exclusion chromatography) and NMR (nuclear magnetic resonance) analyses. The results from GPC and NMR analyses confirm the complete cleavage of the disulfide bond within the polymer, leading to the formation of monomeric units[111]. Dr. Rajendra expanded the application of melt polycondensation to multifunctional amino acids, including D and L-Serine, L-Threonine, and L-Tyrosine, to facilitate the synthesis of diverse linear and hyperbranched polyester and poly(esterurethane)s[112].

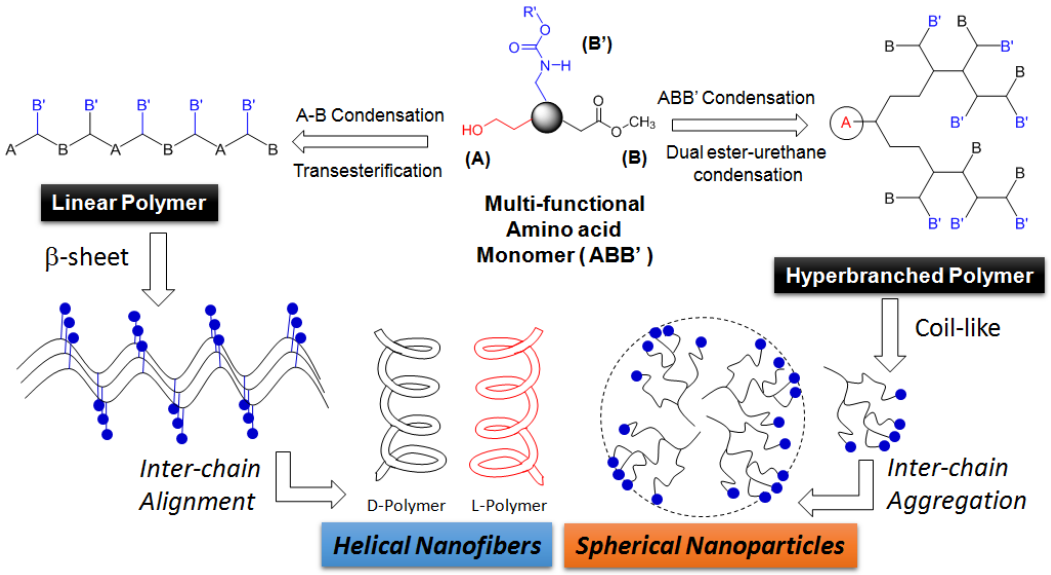

Figure 1.34 *Synthesis of linear or hyperbranched polymer from serine amino acid by melt polycondensation (Adapted from Biomacromolecules 2017, 18, 189−200.)*

To achieve this, a novel strategy is employed that takes advantage of the varying reactivity of ester and urethane groups. This approach allows for the production of both linear and hyperbranched polymers from serine and threonine within a single reaction vessel based on temperature. In this process, serine and threonine are converted into specialized ABB'-type ester urethane monomers, where A represents the hydroxy group, B denotes the ester group, and B' signifies the urethane group. Subsequent melt polymerization at 120°C ensures that the ester group exclusively reacts with the –OH group, resulting in the formation of linear polyesters. With a further increase in

temperature, no significant difference in reactivity between the ester and urethane groups emerge, leading to the creation of hyperbranched polyester urethanes[112].

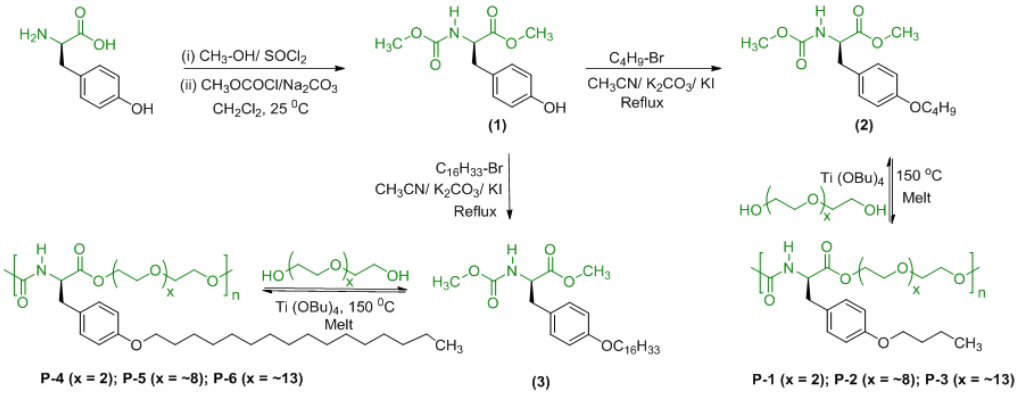

Figure 1.35 *Synthetic scheme of the poly(ester-urethane)s from L Tyrosine by melt condensation approach (Adapted from Biomacromolecules 2017, 18, 189−200.)*

Novel enzyme-responsive amphiphilic poly(ester-urethane) nanocarriers based on L-tyrosine are meticulously engineered to serve as versatile drug delivery vehicles targeting cancer cells. The strategy involves the conjugation of the phenolic –OH group of L-tyrosine ester urethane monomers with alkyl halides of varying chain lengths. These modified monomers are subsequently subjected to polymerization alongside polyethylene glycol diols (PEG 400, PEG 600), resulting in the creation of L-tyrosine-derived amphiphilic polyester urethanes[113]. In these structures, the aliphatic side chain serves as the hydrophobic component, while the primary chain composed of polyethylene glycol exhibits hydrophilic properties. The synthetic pathway for both monomer and polymer synthesis is illustrated in Figure 1.35. Depending on the length of the alkyl chain, polymers incorporating a C16 alkyl side chain and PEG 400 as the main chain display well-defined amphiphilicity. These polymers are capable of self-assembly in aqueous solvents, forming core-shell nanoparticles with an approximate size of 200 nm [113]. In another system, multifunctional amphiphilic poly(ester-urethane) nanoassemblies are meticulously designed for drug delivery applications in cancer cells. This approach hinges on anchoring the phenolic –OH group of L-tyrosine polyester urethane to PEG 350 monomethyl ether, followed by polymerization with various aliphatic and cyclic aliphatic diols. The diols encompass a spectrum ranging from 1,4-cyclohexanedimethanol and 1,6-hexanediol, 1,8-octanediol, 1,10-decanediol,

and 1,12-dodecanediol, thus facilitating the modulation of the hydrophilic and hydrophobic balance.

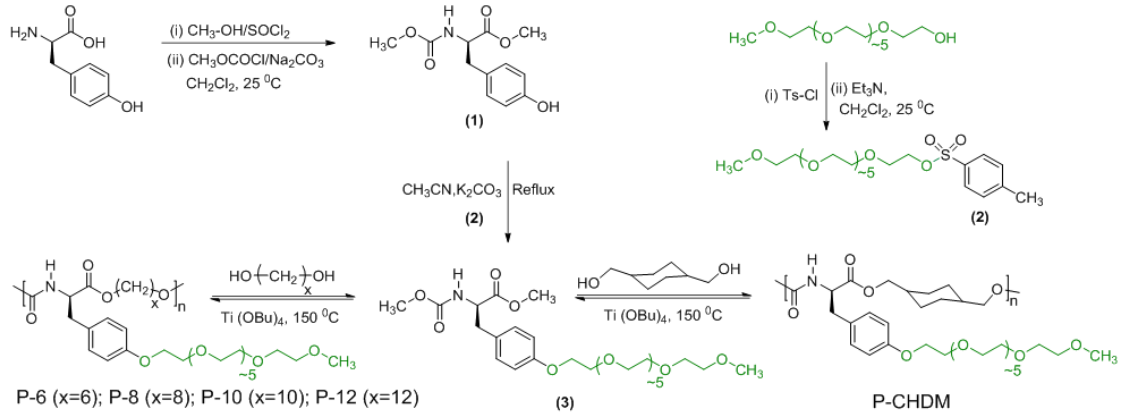

Figure 1.36 *Synthetic scheme of the poly(ester-urethane) s from L Tyrosine by melt condensation approach (Adapted from Biomacromolecules 2018, 19, 2166−2181)*

Notably, polymers derived from 1,12-dodecanediol exhibit the desired amphiphilicity, further demonstrating thermoresponsive behavior at a concentration of 3 mg/ml. The investigation into the lower solution critical temperature (LCST) involves transmittance studies, revealing LCST temperatures spanning from 32°C to 50°C, contingent upon the specific diol length [114]. The development of multifunctional L-tyrosine-based nanocarriers, responsive to a spectrum of stimuli, is meticulously orchestrated through the optimization of their amphiphilic properties. These innovatively designed poly(ester urethane) structures exhibit a remarkable capacity for self-assembly in aqueous solutions, yielding nanoparticles with a diameter of approximately 200 nm. These nanoparticles possess the unique capability to encapsulate two distinct anticancer drugs, namely doxorubicin and camptothecin. To assess their thermoresponsive attributes, an extensive examination is conducted, involving variable-temperature transmittance studies[114]. In later studies by Sonashree et al., innovative enzyme and pH-responsive polyester nanocarriers are developed, leveraging the principles of melt polycondensation chemistry and utilizing L-aspartic acid as the foundational building block. To engineer multifunctionality, L-aspartic acid undergoes a transformative process, converting its acid and amine groups into methyl ester and Boc urethane functionalities, respectively. The resulting multifunctional monomer is then subjected to thermoselective copolymerization, alongside triethylene glycol and dodecanediol, leading to the synthesis of a diverse array of amphiphilic copolymers[115].

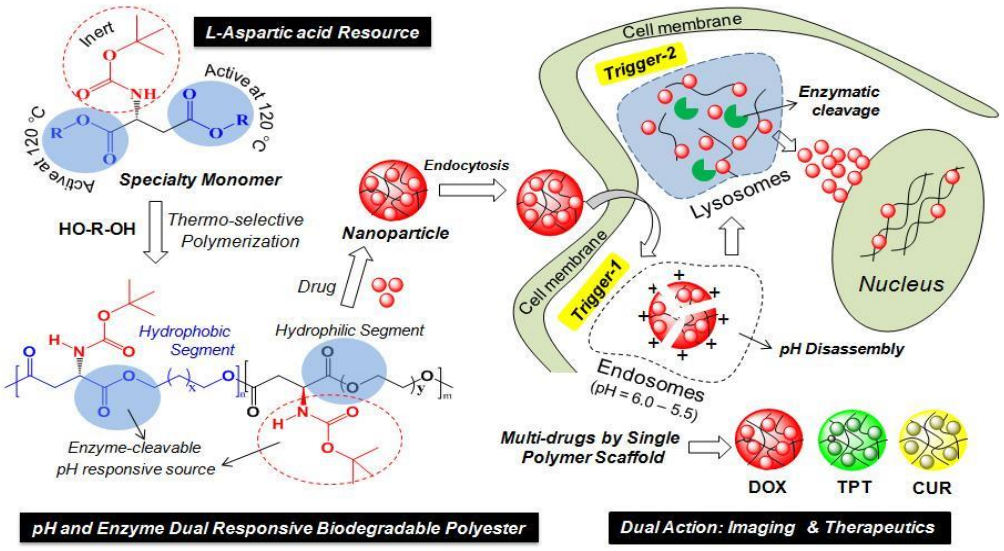

Figure 1.37 *pH responsive polymer for drug delivery and anticancer applications (Adapted from JOURNAL OF POLYMER SCIENCE, PART A: POLYMER CHEMISTRY 2016, 54, 3279–3293).*

These amphiphilic polymers exhibit a propensity to self-assemble into core-shell-type nanoparticles upon introduction to aqueous environments. Remarkably, these nanoparticles display the capacity to encapsulate multiple anticancer drugs, including Topotecan, Doxorubicin, and Curcumin. The innate enzymatic and pH-dependent biodegradability of these polymer nanoparticles is attributed to their polyester backbone and the presence of Boc urethane pendant groups. Furthermore, thorough investigations are conducted to evaluate the cellular uptake and cytotoxicity of these polymer nanoparticles, employing cervical cancer cell lines (HeLa) and breast cancer cell lines (MCF-7). The findings underscore the nanoparticles' remarkable ability to deliver drugs intracellularly, resulting in a pronounced cytotoxic effect[115]. The L-aspartic acid-based monomer is subjected to copolymerization with triethylene glycol, dodecane diol, and oligo-phenylenevinylene (OPV) diol via melt polymerization, yielding a class of amphiphilic polymers tagged with a fluorophore. These amphiphilic polymers exhibit self-assembly behavior facilitated by π-π stacking interactions in aqueous solvents, resulting in the formation of blue luminescent nanoparticles with a size of approximately 200 nm. Within these OPV-tagged nanoparticles, a fluorescent drug, nile red, is physically encapsulated, establishing a FRET pair where OPV fluorophores serve as FRET donors and nile red acts as FRET acceptors[116].

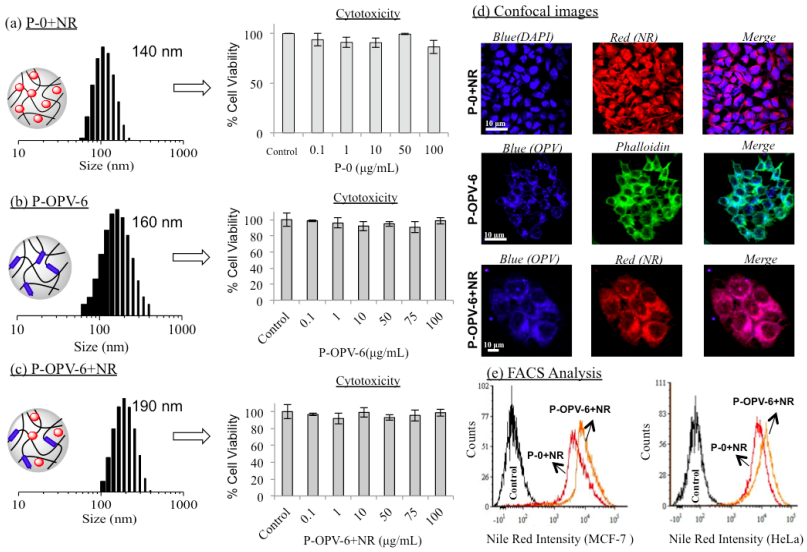

Figure 1.38 *Fluorescent polyester for bioimaging in cancer cells (Adapted from Biomacromolecules 2017, 18, 2594−2609.)*

The synthesis of hydroxyl-functionalized polyesters is accomplished utilizing L-aspartic acid as the precursor. A novel multifunctional monomer derived from L-aspartic acid is engineered, incorporating an acetal protecting group and dicarboxylic esters within its structure. This aspartic acid-based monomer undergoes transesterification with various commercially available aliphatic diols, resulting in the production of acetal-functionalized polyesters, all conducted under melt conditions. Subsequent to synthesis, acid-catalyzed deprotection procedures are executed on the acetal polymer, yielding hydroxyl-functionalized polymers characterized by a dihydroxyl functionality in each repeat unit[117]. These novel hydroxyls functionalized polyester was used for nano-assemblies which were utilized for drug delivery in cancer cells. The melt polycondensation strategy adopted

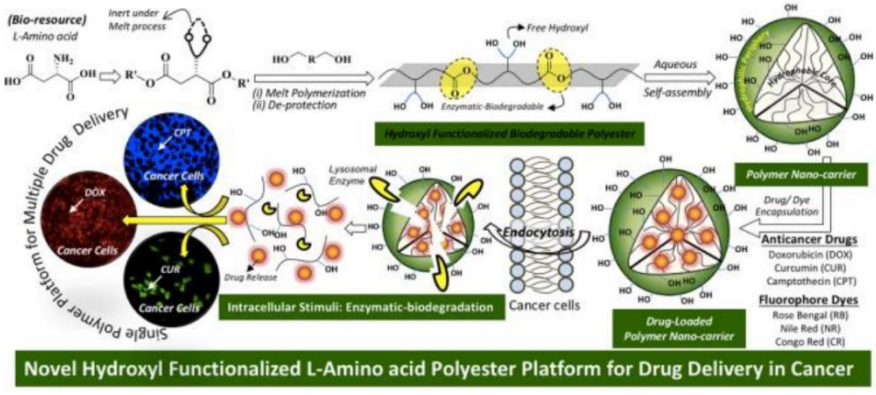

Figure 1.39 *Hydroxyl functionalized polyester for drug delivery in cancer therapy. (Adapted from Biomacromolecules 2020, 21, 171−187).*

Dheeraj et al and developed polyurethanes from L- Lysine. Were the L-Lysine basing Di urethane monomer was designed the two-amine group was converted to urethanes and acid part was converted into amide. These monomers were polymerized by melt polycondensation strategy at 150 C to produce new class of the polyurethanes[118].

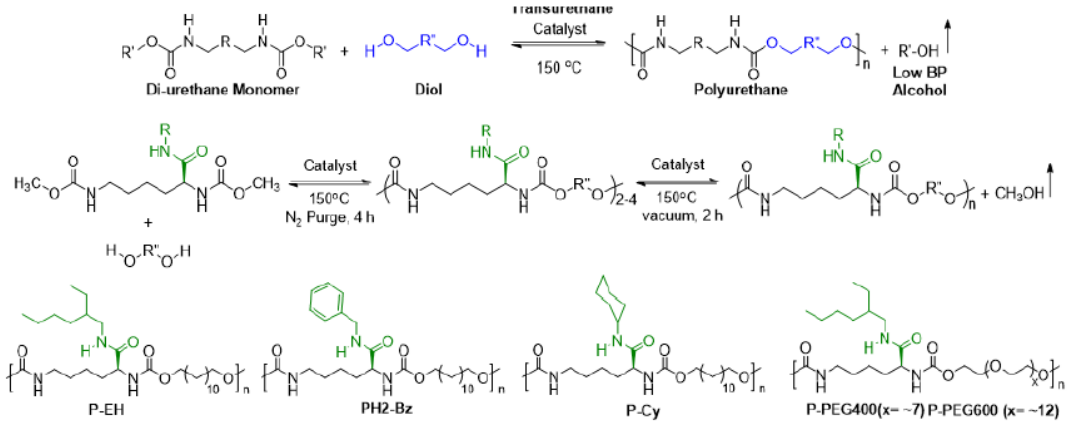

Figure 1.40 *Synthesis of L-Lysin based polyurethane using melt polycondensation strategy. (Adapted from ACS Appl. Polym. Mater. 2019, 1, 1866−1880)*

Using this approach, they synthesized the amphiphilic polyurethanes which are capable to form polymeric nanoparticle in aqueous environment and loaded DOX drug. The polymer found to be thermo-responsive to assess their thermo-responsive attributes, an extensive examination was conducted, involving variable-temperature transmittance studies. The results unveiled a transformative behavior within the polymer's aqueous solutions, transitioning from transparency to turbidity at a critical temperature, denoted as LCST (Lower Critical Solution Temperature), specifically at 40−42 °C[98].The amphiphilic polyurethanes found to be biocompatible with both normal and cancerous cell lines with nanoparticle capable of delivery of the drug in the cancer cells. Thermo-responsive ness of the polymer nano-assemblies loaded with DOX was studied to study

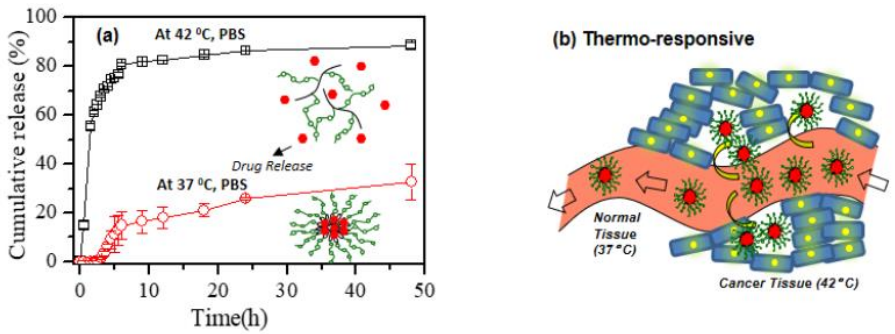

Figure 1.41 *Thermo-responsive release of DOX from the nanoparticle. (Adapted from ACS Appl. Polym. Mater. 2019, 1, 1866−1880).*

the drug release kinetics of the polymer at or above LCST by dialysis method as shown in the Figure 1.41. In another paper Dheeraj et al developed Phenol and catechol functionalized poly(ester urethane)s using Tyrosine and L-Dopa amino acid. In this work they have clearly demonstrate the role of the pi-pi stacking and hydrogen bonding in stabilization of the loaded cargo inside the polymeric nanoparticle.[118]

1.10. Aim of the thesis:

This thesis work aimed to design and develop an amide-functionalized polyester platform based on L-amino acids, with a specific focus on L-aspartic acid. The goal was to explore the lysosomal enzymatic biodegradation aspects of these polymers for the targeted delivery of anticancer drugs in cancer cells. The approach involved the careful design and synthesis of diester monomers with different amide-side chain functionalization, encompassing aromatic, aliphatic, and bio-source pendant units. These tailor-made monomers were then subjected to solvent-free melt polycondensation, resulting in high molecular weight polyesters with tunable thermal properties. The resulting amphiphilic polyester exhibited self-assembly capabilities, forming spherical nanoparticles with an average size of 140±10 nm in aqueous media. Notably, these nanoparticles displayed a lower critical solution temperature (LCST) at 40-42ºC. The amphiphilic polyester nanoparticles demonstrated exceptional encapsulation properties, accommodating a range of compounds, including the anticancer drug doxorubicin (DOX), the anti-inflammatory drug curcumin (CUR), as well as biomarkers like Rose Bengal (RB) and 8-hydroxypyrene-1,3,6-trisulfonic acid trisodium salt (HPTS). Importantly, the polyester nanoparticles exhibited stability under extracellular conditions but underwent enzymatic degradation when exposed to horse liver esterase enzyme in phosphate-buffered saline (PBS). Temperature-dependent cellular uptake studies provided further insights, confirming the energy-dependent endocytosis of polymer nanoparticles across cellular membranes. This was directly evidenced by time-dependent cellular uptake analysis using confocal laser scanning microscopy (CLSM), which demonstrated the endocytosis of DOX-loaded polymer nanoparticles and their subsequent internalization for biodegradation. Furthermore, the thesis work involved the development of hydroxyl-functionalized polyesters tagged with a TPE fluorophore to investigate real-time drug delivery aspects. These polyesters were designed with the fluorophore both as the main chain and as a side chain to explore the impact of polymer topology on drug loading and delivery

capabilities. Photophysical characterizations of the nanoparticles were carried out using absorbance and emission spectroscopy, as well as time-correlated single-photon counting (TCSPC) to establish a Förster resonance energy transfer (FRET) probe. The research demonstrated efficient energy transfer from the TPE molecule to RB/RhB/DOX within the hydrophobic nanocavities of the nanoparticles, confirmed by various parameters such as donor-acceptor distance and FRET efficiency. The polyester-based FRET probes exhibited enzyme-responsive behaviour, supported by the enzyme-triggered release of DOX. The study extended to the development of L-aspartic acid-based cationic polyesters with potential applications in antibacterial contexts. These cationic polyesters were designed through a thermo-selective melt polycondensation approach, employing a protection-deprotection strategy. They were characterized for their structural and thermal properties. Upon becoming cationic, these polymers became water-soluble and formed polymer nanoparticles. Zeta potential studies revealed positive zeta potential values, a desirable characteristic for antibacterial polymers. Antibacterial assessments were conducted through colony suspension and disc diffusion methods, indicating that the polymers exhibited antibacterial activity against gram-negative E. Coli cells at a concentration of 0.8 mg/mL. In summary, this work underscores the importance of biodegradable polymers in the field of biomedicine, with a specific focus on the contributions of L-aspartic acid-based polymer systems. The work presented here demonstrates the versatility and potential applications of these innovative polymers, ranging from drug delivery to antibacterial agents, and highlights the opportunities they offer in the realm of biomedical research.

1.11 Reference

(1) Kamaly, N.; Yameen, B.; Wu, J.; Farokhzad, O. C. Degradable Controlled-Release Polymers and Polymeric Nanoparticles: Mechanisms of Controlling Drug Release. *Chemical Reviews*. American Chemical Society February 24, 2016, pp 2602–2663. https://doi.org/10.1021/acs.chemrev.5b00346.

(2) Silberschmidt, G. The World Health Organization and Global Health. In *Handbook of Global Health*; Springer International Publishing, 2021; pp 1–47. https://doi.org/10.1007/978-3-030-05325-3_125-1.

(3) White, M. C.; Holman, D. M.; Boehm, J. E.; Peipins, L. A.; Grossman, M.; Jane Henley, S. Age and Cancer Risk: A Potentially Modifiable Relationship. *Am J Prev Med* **2014**, *46* (3 SUPPL. 1). https://doi.org/10.1016/j.amepre.2013.10.029.

(4) Mathur, P.; Krishnan Sathishkumar, ; Chaturvedi, M.; Das, B-Level, P.; Kondalli, ; Sudarshan, L.; Santhappan, S.; Nallasamy, V.; John, A.; Narasimhan, S.; Roselind, F. S. *Cancer Statistics, 2020: Report From National Cancer Registry Programme, India*; 2020; Vol. 6. https://ascopubs.org/go/authors/open-access.

(5) Bray, F.; McCarron, P.; Parkin, D. M. The Changing Global Patterns of Female Breast Cancer Incidence and Mortality. *Breast Cancer Research*. November 2004, pp 229–239. https://doi.org/10.1186/bcr932.

(6) Hassanpour, S. H.; Dehghani, M. Review of Cancer from Perspective of Molecular. *Journal of Cancer Research and Practice* **2017**, *4* (4), 127–129. https://doi.org/10.1016/j.jcrpr.2017.07.001.

(7) Chhikara, B. S.; Parang, K. Global Cancer Statistics 2022: The Trends Projection Analysis. *Chemical Biology Letters* **2023**, *10* (1), 451.

(8) Sabarwal, A.; Kumar, K.; Singh, R. P. Hazardous Effects of Chemical Pesticides on Human Health–Cancer and Other Associated Disorders. *Environmental Toxicology and Pharmacology*. Elsevier B.V. October 1, 2018, pp 103–114. https://doi.org/10.1016/j.etap.2018.08.018.

(9) Ma, J.; Jemal, A. Breast Cancer Statistics. In *Breast Cancer Metastasis and Drug Resistance: Progress and Prospects*; Springer New York, 2013; Vol. 9781461456476, pp 1–18. https://doi.org/10.1007/978-1-4614-5647-6_1.

(10) Wang, K.; Tepper, J. E. Radiation Therapy-associated Toxicity: Etiology, Management, and Prevention. *CA Cancer J Clin* **2021**, *71* (5), 437–454. https://doi.org/10.3322/caac.21689.

(11) Yan, M.; Wu, S.; Wang, Y.; Liang, M.; Wang, M.; Hu, W.; Yu, G.; Mao, Z.; Huang, F.; Zhou, J. Recent Progress of Supramolecular Chemotherapy Based on Host–Guest Interactions. *Advanced Materials* **2023**. https://doi.org/10.1002/adma.202304249.

(12) Zugazagoitia, J.; Guedes, C.; Ponce, S.; Ferrer, I.; Molina-Pinelo, S.; Paz-Ares, L. Current Challenges in Cancer Treatment. *Clinical Therapeutics*. Excerpta Medica Inc. July 1, 2016, pp 1551–1566. https://doi.org/10.1016/j.clinthera.2016.03.026.

(13) *Personal View Excisional Surgery*. http://oncology.thelancet.com.

(14) Dougan, M.; Dranoff, G. Immune Therapy for Cancer. *Annual Review of Immunology*. 2009, pp 83–117. https://doi.org/10.1146/annurev.immunol.021908.132544.

(15) Brianna; Lee, S. H. Chemotherapy: How to Reduce Its Adverse Effects While Maintaining the Potency? *Medical Oncology*. Springer March 1, 2023. https://doi.org/10.1007/s12032-023-01954-6.

(16) Cerqueira, B. B. S.; Lasham, A.; Shelling, A. N.; Al-Kassas, R. Nanoparticle Therapeutics: Technologies and Methods for Overcoming Cancer. *European Journal of Pharmaceutics and Biopharmaceutics*. Elsevier B.V. November 1, 2015, pp 140–151. https://doi.org/10.1016/j.ejpb.2015.10.007.

(17) Riehemann, K.; Schneider, S. W.; Luger, T. A.; Godin, B.; Ferrari, M.; Fuchs, H. Nanomedicine - Challenge and Perspectives. *Angewandte Chemie - International Edition*. January 19, 2009, pp 872–897. https://doi.org/10.1002/anie.200802585.

(18) Chen, J.; Zhang, W. J.; Guo, Z.; Wang, H. B.; Wang, D. D.; Zhou, J. J.; Chen, Q. W. PH-Responsive Iron Manganese Silicate Nanoparticles as T 1- T 2∗ Dual-Modal Imaging Probes for Tumor Diagnosis. *ACS Appl Mater Interfaces* **2015**, *7* (9), 5373–5383. https://doi.org/10.1021/acsami.5b00727.

(19) Lang, J.; Zhao, X.; Wang, X.; Zhao, Y.; Li, Y.; Zhao, R.; Cheng, K.; Li, Y.; Han, X.; Zheng, X.; Qin, H.; Geranpayehvaghei, M.; Shi, J.; Anderson, G. J.; Hao, J.; Ren, H.; Nie, G. Targeted Co-Delivery of the Iron Chelator Deferoxamine and a HIF1α Inhibitor Impairs Pancreatic Tumor Growth. *ACS Nano* **2019**, *13* (2), 2176–2189. https://doi.org/10.1021/acsnano.8b08823.

(20) Xie, Y.; Hang, Y.; Wang, Y.; Sleightholm, R.; Prajapati, D. R.; Bader, J.; Yu, A.; Tang, W.; Jaramillo, L.; Li, J.; Singh, R. K.; Oupický, D. Stromal Modulation and Treatment of Metastatic Pancreatic Cancer with Local Intraperitoneal Triple MiRNA/SiRNA Nanotherapy. *ACS Nano* **2020**, *14* (1), 255–271. https://doi.org/10.1021/acsnano.9b03978.

(21) Kolhar, P.; Anselmo, A. C.; Gupta, V.; Pant, K.; Prabhakarpandian, B.; Ruoslahti, E.; Mitragotri, S. Using Shape Effects to Target Antibody-Coated Nanoparticles to Lung and Brain Endothelium. *Proc Natl Acad Sci U S A* **2013**, *110* (26), 10753–10758. https://doi.org/10.1073/pnas.1308345110.

(22) Anselmo, A. C.; Mitragotri, S. Nanoparticles in the Clinic: An Update. *Bioeng Transl Med* **2019**, *4* (3). https://doi.org/10.1002/btm2.10143.

(23) Sun, Q.; Zhou, Z.; Qiu, N.; Shen, Y. Rational Design of Cancer Nanomedicine: Nanoproperty Integration and Synchronization. *Advanced Materials*. Wiley-VCH Verlag April 11, 2017. https://doi.org/10.1002/adma.201606628.

(24) Xu, C.; Sun, Y.; Yu, Y.; Hu, M.; Yang, C.; Zhang, Z. A Sequentially Responsive and Structure-Transformable Nanoparticle with a Comprehensively Improved "CAPIR Cascade" for Enhanced Antitumor Effect. *Nanoscale* **2019**, *11* (3), 1177–1194. https://doi.org/10.1039/c8nr08781d.

(25) Nakamura, Y.; Mochida, A.; Choyke, P. L.; Kobayashi, H. Nanodrug Delivery: Is the Enhanced Permeability and Retention Effect Sufficient for Curing Cancer?

Bioconjugate Chemistry. American Chemical Society October 19, 2016, pp 2225–2238. https://doi.org/10.1021/acs.bioconjchem.6b00437.

(26) Wan, D.; Li, C.; Pan, J. Polymeric Micelles with Reduction-Responsive Function for Targeted Cancer Chemotherapy. *ACS Appl Bio Mater* **2020**, *3* (2), 1139–1146. https://doi.org/10.1021/acsabm.9b01070.

(27) Miller, T.; Hill, A.; Uezguen, S.; Weigandt, M.; Goepferich, A. Analysis of Immediate Stress Mechanisms upon Injection of Polymeric Micelles and Related Colloidal Drug Carriers: Implications on Drug Targeting. *Biomacromolecules*. June 11, 2012, pp 1707–1718. https://doi.org/10.1021/bm3002045.

(28) Cabral, H.; Kataoka, K. Progress of Drug-Loaded Polymeric Micelles into Clinical Studies. *Journal of Controlled Release*. Elsevier B.V. September 28, 2014, pp 465–476. https://doi.org/10.1016/j.jconrel.2014.06.042.

(29) Clemons, T. D.; Singh, R.; Sorolla, A.; Chaudhari, N.; Hubbard, A.; Iyer, K. S. Distinction between Active and Passive Targeting of Nanoparticles Dictate Their Overall Therapeutic Efficacy. *Langmuir* **2018**, *34* (50), 15343–15349. https://doi.org/10.1021/acs.langmuir.8b02946.

(30) Wang, C. E.; Wei, H.; Tan, N.; Boydston, A. J.; Pun, S. H. Sunflower Polymers for Folate-Mediated Drug Delivery. *Biomacromolecules* **2016**, *17* (1), 69–75. https://doi.org/10.1021/acs.biomac.5b01176.

(31) Li, M.; Dong, J.; Cheng, F.; Li, C.; Wang, H.; Sun, T.; He, W.; Wang, Q. Controlling Conjugated Antibodies at the Molecular Level for Active Targeting Nanoparticles toward HER2-Positive Cancer Cells. *Mol Pharm* **2021**, *18* (3), 1196–1207. https://doi.org/10.1021/acs.molpharmaceut.0c01090.

(32) Satsangi, A.; Roy, S. S.; Satsangi, R. K.; Vadlamudi, R. K.; Ong, J. L. Design of a Paclitaxel Prodrug Conjugate for Active Targeting of an Enzyme Upregulated in Breast Cancer Cells. *Mol Pharm* **2014**, *11* (6), 1906–1918. https://doi.org/10.1021/mp500128k.

(33) Costa, S. A.; Mozhdehi, D.; Dzuricky, M. J.; Isaacs, F. J.; Brustad, E. M.; Chilkoti, A. Active Targeting of Cancer Cells by Nanobody Decorated Polypeptide Micelle with Bio-Orthogonally Conjugated Drug. *Nano Lett* **2019**, *19* (1), 247–254. https://doi.org/10.1021/acs.nanolett.8b03837.

(34) Mitchell, M. J.; Billingsley, M. M.; Haley, R. M.; Wechsler, M. E.; Peppas, N. A.; Langer, R. Engineering Precision Nanoparticles for Drug Delivery. *Nature Reviews Drug Discovery*. Nature Research February 1, 2021, pp 101–124. https://doi.org/10.1038/s41573-020-0090-8.

(35) Davis, M. E.; Chen, Z.; Shin, D. M. Nanoparticle Therapeutics: An Emerging Treatment Modality for Cancer. *Nature Reviews Drug Discovery*. 2008, pp 771–782. https://doi.org/10.1038/nrd2614.

(36) Xu, M.; Zhang, C.; Zeng, Z.; Pu, K. Semiconducting Polymer Nanoparticles as Activatable Nanomedicines for Combinational Phototherapy. *ACS Applied Polymer Materials*. American Chemical Society September 10, 2021, pp 4375–4389. https://doi.org/10.1021/acsapm.1c00695.

(37) Liu, Y.; Wang, J.; Zhang, M.; Li, H.; Lin, Z. Polymer-Ligated Nanocrystals Enabled by Nonlinear Block Copolymer Nanoreactors: Synthesis, Properties, and Applications. *ACS Nano* **2020**, *14* (10), 12491–12521. https://doi.org/10.1021/acsnano.0c06936.

(38) Vines, J. B.; Yoon, J. H.; Ryu, N. E.; Lim, D. J.; Park, H. Gold Nanoparticles for Photothermal Cancer Therapy. *Frontiers in Chemistry*. Frontiers Media S.A. 2019. https://doi.org/10.3389/fchem.2019.00167.

(39) Wang, J.; Potocny, A. M.; Rosenthal, J.; Day, E. S. Gold Nanoshell-Linear Tetrapyrrole Conjugates for near Infrared-Activated Dual Photodynamic and Photothermal Therapies. *ACS Omega* **2020**, *5* (1), 926–940. https://doi.org/10.1021/acsomega.9b04150.

(40) Larson, N.; Ghandehari, H. Polymeric Conjugates for Drug Delivery. *Chemistry of Materials*. March 13, 2012, pp 840–853. https://doi.org/10.1021/cm2031569.

(41) Ringsdorf, H. *STRUCTURE AND PROPERTIES OF PHARMACOLOGICALLY ACTIVE POLYMERS*; 1975.

(42) Duncan, R. *Designing Polymer Conjugates as Lysosomotropic Nanomedicines*; 2007; Vol. 35. http://www.esf.org/.

(43) Yu, Y.; Chen, C. K.; Law, W. C.; Weinheimer, E.; Sengupta, S.; Prasad, P. N.; Cheng, C. Polylactide-Graft-Doxorubicin Nanoparticles with Precisely Controlled Drug Loading for PH-Triggered Drug Delivery. *Biomacromolecules* **2014**, *15* (2), 524–532. https://doi.org/10.1021/bm401471p.

(44) Deshpande, N. U.; Jayakannan, M. Cisplatin-Stitched Polysaccharide Vesicles for Synergistic Cancer Therapy of Triple Antagonistic Drugs. *Biomacromolecules* **2017**, *18* (1), 113–126. https://doi.org/10.1021/acs.biomac.6b01411.

(45) Abdullah, C. S.; Ray, P.; Alam, S.; Kale, N.; Aishwarya, R.; Morshed, M.; Dutta, D.; Hudziak, C.; Banerjee, S. K.; Mallik, S.; Banerjee, S.; Bhuiyan, M. S.; Quadir, M. Chemical Architecture of Block Copolymers Differentially Abrogate Cardiotoxicity and Maintain the Anticancer Efficacy of Doxorubicin. *Mol Pharm* **2020**, *17* (12), 4676–4690. https://doi.org/10.1021/acs.molpharmaceut.0c00963.

(46) Mansur, A. A. P.; Carvalho, S. M.; Lobato, Z. I. P.; Leite, M. D. F.; Cunha, A. D. S.; Mansur, H. S. Design and Development of Polysaccharide-Doxorubicin-Peptide Bioconjugates for Dual Synergistic Effects of Integrin-Targeted and Cell-Penetrating Peptides for Cancer Chemotherapy. *Bioconjug Chem* **2018**, *29* (6), 1973–2000. https://doi.org/10.1021/acs.bioconjchem.8b00208.

(47) Figueiredo, P. R.; González, R. D.; Carvalho, A. T. P. Insights into the Degradation of Polymer-Drug Conjugates by an Overexpressed Enzyme in Cancer Cells. *J Med Chem* **2023**, *66* (4), 2761–2772. https://doi.org/10.1021/acs.jmedchem.2c01781.

(48) Liu, Y.; Yang, G.; Zou, D.; Hui, Y.; Nigam, K.; Middelberg, A. P. J.; Zhao, C. X. Formulation of Nanoparticles Using Mixing-Induced Nanoprecipitation for Drug Delivery. *Industrial and Engineering Chemistry Research*. American Chemical Society March 4, 2020, pp 4134–4149. https://doi.org/10.1021/acs.iecr.9b04747.

(49) Ediriwickrema, A.; Saltzman, W. M. Nanotherapy for Cancer: Targeting and Multifunctionality in the Future of Cancer Therapies. *ACS Biomaterials Science and Engineering*. American Chemical Society February 9, 2015, pp 64–78. https://doi.org/10.1021/ab500084g.

(50) Ahmadi, V.; Zabihi, F.; Rancan, F.; Staszak, A. A.; Nie, C.; Dimde, M.; Achazi, K.; Wiehe, A.; Vogt, A.; Haag, R. Amphiphilic Co-Polypeptides Self-Assembled into Spherical Nanoparticles for Dermal Drug Delivery. *ACS Appl Nano Mater* **2021**, *4* (7), 6709–6721. https://doi.org/10.1021/acsanm.1c00693.

(51) Qiu, M.; Ouyang, J.; Sun, H.; Meng, F.; Cheng, R.; Zhang, J.; Cheng, L.; Lan, Q.; Deng, C.; Zhong, Z. Biodegradable Micelles Based on Poly(Ethylene Glycol)-b-Polylipopeptide Copolymer: A Robust and Versatile Nanoplatform for Anticancer Drug Delivery. *ACS Appl Mater Interfaces* **2017**, *9* (33), 27587–27595. https://doi.org/10.1021/acsami.7b10533.

(52) Sun, T.; Zhang, Y. S.; Pang, B.; Hyun, D. C.; Yang, M.; Xia, Y. Engineered Nanoparticles for Drug Delivery in Cancer Therapy. *Angewandte Chemie - International Edition*. Wiley-VCH Verlag November 10, 2014, pp 12320–12364. https://doi.org/10.1002/anie.201403036.

(53) Shi, J.; Votruba, A. R.; Farokhzad, O. C.; Langer, R. Nanotechnology in Drug Delivery and Tissue Engineering: From Discovery to Applications. *Nano Letters*. September 8, 2010, pp 3223–3230. https://doi.org/10.1021/nl102184c.

(54) Banerjee, A.; Qi, J.; Gogoi, R.; Wong, J.; Mitragotri, S. *Role of Nanoparticle Size, Shape and Surface Chemistry in Oral Drug Delivery*; 2016.

(55) Zielinska, A.; Carreiró, F.; Oliveira, A. M.; Neves, A.; Pires, B.; Nagasamy Venkatesh, D.; Durazzo, A.; Lucarini, M.; Eder, P.; Silva, A. M.; Santini, A.; Souto, E. B. Polymeric Nanoparticles: Production, Characterization, Toxicology and Ecotoxicology. *Molecules*. MDPI AG August 1, 2020. https://doi.org/10.3390/molecules25163731.

(56) Jo, D. H.; Kim, J. H.; Lee, T. G.; Kim, J. H. Size, Surface Charge, and Shape Determine Therapeutic Effects of Nanoparticles on Brain and Retinal Diseases. *Nanomedicine: Nanotechnology, Biology, and Medicine*. Elsevier Inc. October 1, 2015, pp 1603–1611. https://doi.org/10.1016/j.nano.2015.04.015.

(57) Rasmussen, M. K.; Pedersen, J. N.; Marie, R. Size and Surface Charge Characterization of Nanoparticles with a Salt Gradient. *Nat Commun* **2020**, *11* (1). https://doi.org/10.1038/s41467-020-15889-3.

(58) Zhou, J.; Kroll, A. V.; Holay, M.; Fang, R. H.; Zhang, L. Biomimetic Nanotechnology toward Personalized Vaccines. *Advanced Materials*. Wiley-VCH Verlag April 1, 2020. https://doi.org/10.1002/adma.201901255.

(59) Asem, H.; Zheng, W.; Nilsson, F.; Zhang, Y.; Hedenqvist, M. S.; Hassan, M.; Malmström, E. Functional Nanocarriers for Drug Delivery by Surface Engineering of Polymeric Nanoparticle Post-Polymerization-Induced Self-Assembly. *ACS Appl Bio Mater* **2021**, *4* (1), 1045–1056. https://doi.org/10.1021/acsabm.0c01552.

(60) Rosenblatt, K. M.; Bunjes, H. Evaluation of the Drug Loading Capacity of Different Lipid Nanoparticle Dispersions by Passive Drug Loading. *European Journal of Pharmaceutics and Biopharmaceutics* **2017**, *117*, 49–59. https://doi.org/10.1016/j.ejpb.2017.03.010.

(61) Shen, S.; Wu, Y.; Liu, Y.; Wu, D. High Drug-Loading Nanomedicines: Progress, Current Status, and Prospects. *International Journal of Nanomedicine*. Dove Medical Press Ltd. May 31, 2017, pp 4085–4109. https://doi.org/10.2147/IJN.S132780.

(62) Morgulchik, N.; Kamaly, N. Meta-Analysis of in Vitro Drug-Release Parameters Reveals Predictable and Robust Kinetics for Redox-Responsive Drug-Conjugated Therapeutic Nanogels. *ACS Appl Nano Mater* **2021**, *4* (5), 4256–4268. https://doi.org/10.1021/acsanm.1c00170.

(63) Moore, T.; Chen, H.; Morrison, R.; Wang, F.; Anker, J. N.; Alexis, F. Nanotechnologies for Noninvasive Measurement of Drug Release. *Molecular Pharmaceutics*. January 6, 2014, pp 24–39. https://doi.org/10.1021/mp400419k.

(64) Dolai, J.; Mandal, K.; Jana, N. R. Nanoparticle Size Effects in Biomedical Applications. *ACS Applied Nano Materials*. American Chemical Society July 23, 2021, pp 6471–6496. https://doi.org/10.1021/acsanm.1c00987.

(65) Xu, L.; Liang, H. W.; Yang, Y.; Yu, S. H. Stability and Reactivity: Positive and Negative Aspects for Nanoparticle Processing. *Chemical Reviews*. American Chemical Society April 11, 2018, pp 3209–3250. https://doi.org/10.1021/acs.chemrev.7b00208.

(66) Kumbhakar, K.; Dey, A.; Mondal, A.; De, P.; Biswas, R. Interactions and Dynamics in Aqueous Solutions of PH-Responsive Polymers: A Combined Fluorescence and Dielectric Relaxation Study. *Journal of Physical Chemistry B* **2021**, *125* (22), 6023–6035. https://doi.org/10.1021/acs.jpcb.1c03435.

(67) Luo, Y.; Zhu, X.; Qian, J.; Yu, Y.; Li, J.; He, Z.; Duan, S.; Guo, H.; Shen, X.; Guo, Q. Au Nanorods Coated with PH-Responsive Polymers for Photothermal Therapy Against Multidrug-Resistant Bacteria. *ACS Appl Nano Mater* **2022**, *5* (11), 16884–16895. https://doi.org/10.1021/acsanm.2c03739.

(68) Wang, B.; Xiao, T.; Fu, X. Bin; Jiang, T. T.; Chen, Y.; Yao, Y. F. Thermoresponsive Hyperbranched Polymers with Spatially Isomerized Groups: NMR Implication to Their Thermoresponsive Behaviors. *Macromolecules* **2017**, *50* (24), 9647–9655. https://doi.org/10.1021/acs.macromol.7b01887.

(69) Fu, W.; Bai, W.; Jiang, S.; Seymour, B. T.; Zhao, B. UCST-Type Thermoresponsive Polymers in Synthetic Lubricating Oil Polyalphaolefin (PAO). *Macromolecules* **2018**, *51* (5), 1674–1680. https://doi.org/10.1021/acs.macromol.7b02755.

(70) Paris, J. L.; Cabanas, M. V.; Manzano, M.; Vallet-Regí, M. Polymer-Grafted Mesoporous Silica Nanoparticles as Ultrasound-Responsive Drug Carriers. *ACS Nano* **2015**, *9* (11), 11023–11033. https://doi.org/10.1021/acsnano.5b04378.

(71) Viger, M. L.; Sheng, W.; Doré, K.; Alhasan, A. H.; Carling, C. J.; Lux, J.; De Gracia Lux, C.; Grossman, M.; Malinow, R.; Almutairi, A. Near-Infrared-Induced Heating of Confined Water in Polymeric Particles for Efficient Payload Release. *ACS Nano* **2014**, *8* (5), 4815–4826. https://doi.org/10.1021/nn500702g.

(72) Li, C.; Zhou, H.; Sun, J.; Wang, D.; Chang, J.; Wang, Q.; Li, Y.; Zhao, W. Photo-Responsive Self-Assembled Polymeric Nanoparticle Probes for 19F MRI Theranostics. *Biomacromolecules* **2023**, *24* (6), 2777–2789. https://doi.org/10.1021/acs.biomac.3c00179.

(73) Inacker, S.; Fanelli, J.; Ivlev, S. I.; Hampp, N. A. Intramolecular Coumarin-Dimer Containing Polyurethanes: Optical Tuning via Single- and Two-Photon Absorption Processes. *Macromolecules* **2022**, *55* (19), 8461–8471. https://doi.org/10.1021/acs.macromol.2c01374.

(74) Elbert, J.; Mersini, J.; Vilbrandt, N.; Lederle, C.; Kraska, M.; Gallei, M.; Stühn, B.; Plenio, H.; Rehahn, M. Reversible Activity Modulation of Surface-Attached Grubbs Second Generation Type Catalysts Using Redox-Responsive Polymers. *Macromolecules* **2013**, *46* (11), 4255–4267. https://doi.org/10.1021/ma4007126.

(75) Geiselhart, C. M.; Xue, W.; Barner-Kowollik, C.; Mutlu, H. Degradable Redox-Responsive Polyolefins. *Macromolecules* **2021**, *54* (4), 1775–1782. https://doi.org/10.1021/acs.macromol.1c00010.

(76) Harnoy, A. J.; Buzhor, M.; Tirosh, E.; Shaharabani, R.; Beck, R.; Amir, R. J. Modular Synthetic Approach for Adjusting the Disassembly Rates of Enzyme-Responsive Polymeric Micelles. *Biomacromolecules* **2017**, *18* (4), 1218–1228. https://doi.org/10.1021/acs.biomac.6b01906.

(77) Gao, T.; Zhao, S. J.; Bao, R. Y.; Zhong, G. J.; Li, Z. M.; Yang, M. B.; Yang, W. Constructing Sandwich-Architectured Poly(l -Lactide)/High-Melting-Point Poly(l -Lactide) Nonwoven Fabrics: Toward Heat-Resistant Poly(l -Lactide) Barrier Biocomposites with Full Biodegradability. *ACS Appl Bio Mater* **2019**, *2* (3), 1357–1367. https://doi.org/10.1021/acsabm.9b00056.

(78) Xing, Y.; Wang, C.; Han, P.; Wang, Z.; Zhang, X. Acetylcholinesterase Responsive Polymeric Supra-Amphiphiles for Controlled Self-Assembly and Disassembly. *Langmuir*. April 10, 2012, pp 6032–6036. https://doi.org/10.1021/la300612k.

(79) Kang, Y.; Wang, C.; Liu, K.; Wang, Z.; Zhang, X. Enzyme-Responsive Polymeric Supra-Amphiphiles Formed by the Complexation of Chitosan and ATP. *Langmuir* **2012**, *28* (41), 14562–14566. https://doi.org/10.1021/la303271f.

(80) Mai, B. T.; Fernandes, S.; Balakrishnan, P. B.; Pellegrino, T. Nanosystems Based on Magnetic Nanoparticles and Thermo- or PH-Responsive Polymers: An Update and Future Perspectives. *Acc Chem Res* **2018**, *51* (5), 999–1013. https://doi.org/10.1021/acs.accounts.7b00549.

(81) Liu, Y.; Lin, G.; Medina-Sánchez, M.; Guix, M.; Makarov, D.; Jin, D. Responsive Magnetic Nanocomposites for Intelligent Shape-Morphing Microrobots. *ACS Nano*. American Chemical Society May 23, 2023, pp 8899–8917. https://doi.org/10.1021/acsnano.3c01609.

(82) Jauregui, R.; Srinivasan, S.; Vojtech, L. N.; Gammill, H. S.; Chiu, D. T.; Hladik, F.; Stayton, P. S.; Lai, J. J. Temperature-Responsive Magnetic Nanoparticles for Enabling Affinity Separation of Extracellular Vesicles. *ACS Appl Mater Interfaces* **2018**, *10* (40), 33847–33856. https://doi.org/10.1021/acsami.8b09751.

(83) Pernia Leal, M.; Torti, A.; Riedinger, A.; La Fleur, R.; Petti, D.; Cingolani, R.; Bertacco, R.; Pellegrino, T. Controlled Release of Doxorubicin Loaded within Magnetic Thermo-Responsive Nanocarriers under Magnetic and Thermal Actuation in a Microfluidic Channel. *ACS Nano* **2012**, *6* (12), 10535–10545. https://doi.org/10.1021/nn3028425.

(84) Awad, N. S.; Paul, V.; Alsawaftah, N. M.; Ter Haar, G.; Allen, T. M.; Pitt, W. G.; Husseini, G. A. Ultrasound-Responsive Nanocarriers in Cancer Treatment: A Review. *ACS Pharmacology and Translational Science*. American Chemical Society April 9, 2021, pp 589–612. https://doi.org/10.1021/acsptsci.0c00212.

(85) Chandan, R.; Mehta, S.; Banerjee, R. Ultrasound-Responsive Carriers for Therapeutic Applications. *ACS Biomater Sci Eng* **2020**, *6* (9), 4731–4747. https://doi.org/10.1021/acsbiomaterials.9b01979.

(86) Athanassiadis, A. G.; Ma, Z.; Moreno-Gomez, N.; Melde, K.; Choi, E.; Goyal, R.; Fischer, P. Ultrasound-Responsive Systems as Components for Smart Materials. *Chemical Reviews*. American Chemical Society March 9, 2022, pp 5165–5208. https://doi.org/10.1021/acs.chemrev.1c00622.

(87) Wu, P.; Jia, Y.; Qu, F.; Sun, Y.; Wang, P.; Zhang, K.; Xu, C.; Liu, Q.; Wang, X. Ultrasound-Responsive Polymeric Micelles for Sonoporation-Assisted Site-Specific Therapeutic Action. *ACS Appl Mater Interfaces* **2017**, *9* (31), 25706–25716. https://doi.org/10.1021/acsami.7b05469.

(88) Arrizabalaga, J. H.; Smallcomb, M.; Abu-Laban, M.; Liu, Y.; Yeingst, T. J.; Dhawan, A.; Simon, J. C.; Hayes, D. J. Ultrasound-Responsive Hydrogels for On-Demand Protein Release. *ACS Appl Bio Mater* **2022**, *5* (7), 3212–3218. https://doi.org/10.1021/acsabm.2c00192.

(89) Xia, J.; Wang, J.; Wang, X.; Qian, M.; Zhang, L.; Chen, Q. Ultrasound-Responsive Nanoparticulate for Selective Amplification of Chemotherapeutic Potency for Ablation of Solid Tumors. *Bioconjug Chem* **2018**, *29* (10), 3467–3475. https://doi.org/10.1021/acs.bioconjchem.8b00626.

(90) Song, Z.; Tan, Z.; Cheng, J. Recent Advances and Future Perspectives of Synthetic Polypeptides from N-Carboxyanhydrides. *Macromolecules*. American Chemical Society November 26, 2019, pp 8521–8539. https://doi.org/10.1021/acs.macromol.9b01450.

(91) Park, S. E.; Sajid, M. I.; Parang, K.; Tiwari, R. K. Cyclic Cell-Penetrating Peptides as Efficient Intracellular Drug Delivery Tools. *Molecular Pharmaceutics*. American Chemical Society September 3, 2019, pp 3727–3743. https://doi.org/10.1021/acs.molpharmaceut.9b00633.

(92) Cohen-Erez, I.; Rapaport, H. Coassemblies of the Anionic Polypeptide γ-PGA and Cationic β-Sheet Peptides for Drug Delivery to Mitochondria. *Biomacromolecules* **2015**, *16* (12), 3827–3835. https://doi.org/10.1021/acs.biomac.5b01140.

(93) Basu, A.; Kunduru, K. R.; Katzhendler, J.; Domb, A. J. Poly(α-Hydroxy Acid)s and Poly(α-Hydroxy Acid-Co-α-Amino Acid)s Derived from Amino Acid. *Advanced Drug Delivery Reviews*. Elsevier B.V. December 15, 2016, pp 82–96. https://doi.org/10.1016/j.addr.2016.08.003.

(94) Yin, Q.; Yin, L.; Wang, H.; Cheng, J. Synthesis and Biomedical Applications of Functional Poly(α-Hydroxy Acids) via Ring-Opening Polymerization of O-Carboxyanhydrides. *Acc Chem Res* **2015**, *48* (7), 1777–1787. https://doi.org/10.1021/ar500455z.

(95) Fonseca, A. C.; Gil, M. H.; Simões, P. N. Biodegradable Poly(Ester Amide)s - A Remarkable Opportunity for the Biomedical Area: Review on the Synthesis, Characterization and Applications. *Progress in Polymer Science*. Elsevier Ltd 2014, pp 1291–1311. https://doi.org/10.1016/j.progpolymsci.2013.11.007.

(96) Wu, J.; Wu, D.; Mutschler, M. A.; Chu, C. C. Cationic Hybrid Hydrogels from Amino-Acid-Based Poly(Ester Amide): Fabrication, Characterization, and Biological Properties. *Adv Funct Mater* **2012**, *22* (18), 3815–3823. https://doi.org/10.1002/adfm.201103147.

(97) Sheihet, L.; Piotrowska, K.; Dubin, R. A.; Kohn, J.; Devore, D. Effect of Tyrosine-Derived Triblock Copolymer Compositions on Nanosphere Self-Assembly and Drug Delivery. *Biomacromolecules* **2007**, *8* (3), 998–1003. https://doi.org/10.1021/bm060860t.

(98) Joshi, D. C.; Saxena, S.; Jayakannan, M. Development of l -Lysine Based Biodegradable Polyurethanes and Their Dual-Responsive Amphiphilic Nanocarriers for Drug Delivery to Cancer Cells. *ACS Appl Polym Mater* **2019**, *1* (7), 1866–1880. https://doi.org/10.1021/acsapm.9b00413.

(99) Lu, W.; Wang, X.; Cheng, R.; Deng, C.; Meng, F.; Zhong, Z. Biocompatible and Bioreducible Micelles Fabricated from Novel α-Amino Acid-Based Poly(Disulfide Urethane)s: Design, Synthesis and Triggered Doxorubicin Release. *Polym Chem* **2015**, *6* (33), 6001–6010. https://doi.org/10.1039/c5py00828j.

(100) Cohen-Arazi, N.; Katzhendler, J.; Kolitz, M.; Domb, A. J. Preparation of New α-Hydroxy Acids Derived from Amino Acids and Their Corresponding Polyesters. *Macromolecules* **2008**, *41* (20), 7259–7263. https://doi.org/10.1021/ma8012477.

(101) Shi, C. X.; Guo, Y. T.; Wu, Y. H.; Li, Z. Y.; Wang, Y. Z.; Du, F. S.; Li, Z. C. Synthesis and Controlled Organobase-Catalyzed Ring-Opening Polymerization of Morpholine-2,5-Dione Derivatives and Monomer Recovery by Acid-Catalyzed Degradation of the Polymers. *Macromolecules* **2019**, *52* (11), 4260–4269. https://doi.org/10.1021/acs.macromol.8b02498.

(102) Ruano, G.; Iribarren, J. I.; Pérez-Madrigal, M. M.; Torras, J.; Alemán, C. Electrical and Capacitive Response of Hydrogel Solid-like Electrolytes for Supercapacitors. *Polymers (Basel)* **2021**, *13* (8). https://doi.org/10.3390/polym13081337.

(103) Sun, H.; Cheng, R.; Deng, C.; Meng, F.; Dias, A. A.; Hendriks, M.; Feijen, J.; Zhong, Z. Enzymatically and Reductively Degradable α-Amino Acid-Based Poly(Ester Amide)s: Synthesis, Cell Compatibility, and Intracellular Anticancer Drug Delivery. *Biomacromolecules* **2015**, *16* (2), 597–605. https://doi.org/10.1021/bm501652d.

(104) Aamer, K. A.; Genson, K. L.; Kohn, J.; Becker, M. L. Impact of Polymer-Bound Iodine on Fibronectin Adsorption and Osteoblast Cell Morphology in Radiopaque Medical Polymers: Tyrosine-Derived Polycarbonate Blends as a Model System. *Biomacromolecules* **2009**, *10* (9), 2418–2426. https://doi.org/10.1021/bm900327b.

(105) He, M.; Ro, L.; Liu, J.; Chu, C. C. Folate-Decorated Arginine-Based Poly(Ester Urea Urethane) Nanoparticles as Carriers for Gambogic Acid and Effect on Cancer Cells. *J Biomed Mater Res A* **2017**, *105* (2), 475–490. https://doi.org/10.1002/jbm.a.35924.

(106) Deepa, P.; Jayakannan, M. Solvent-Free and Nonisocyanate Melt Transurethane Reaction for Aliphatic Polyurethanes and Mechanistic Aspects. *J Polym Sci A Polym Chem* **2008**, *46* (7), 2445–2458. https://doi.org/10.1002/pola.22578.

(107) Deepa, P.; Jayakannan, M. Polyurethane-Oligo(Phenylenevinylene) Random Copolymers: π-Conjugated Pores, Vesicles, and Nanospheres via Solvent-Induced Self-Organization. *J Polym Sci A Polym Chem* **2008**, *46* (17), 5897–5915. https://doi.org/10.1002/pola.22907.

(108) Deepa, P.; Jayakannan, M. Solvent-Induced Self-Organization Approach for Polymeric Architectures of Micropores, Hexagons and Spheres Based on Polyurethanes Prepared via Novel Melt Transurethane Methodology. *J Polym Sci A Polym Chem* **2007**, *45* (12), 2351–2366. https://doi.org/10.1002/pola.22058.

(109) Anantharaj, S.; Jayakannan, M. Polymers from Amino Acids: Development of Dual Ester-Urethane Melt Condensation Approach and Mechanistic Aspects. *Biomacromolecules* **2012**, *13* (8), 2446–2455. https://doi.org/10.1021/bm300697h.

(110) Anantharaj, S.; Jayakannan, M. Catalysts and Temperature Driven Melt Polycondensation Reaction for Helical Poly(Ester-Urethane)s Based on Natural L-Amino Acids. *J Polym Sci A Polym Chem* **2016**, *54* (8), 1065–1077. https://doi.org/10.1002/pola.27970.

(111) Anantharaj, S.; Jayakannan, M. Melt Polycondensation Approach for Reduction Degradable Helical Polyester Based on L-Cystine. *J Polym Sci A Polym Chem* **2016**, *54* (18), 2864–2875. https://doi.org/10.1002/pola.28172.

(112) Aluri, R.; Jayakannan, M. One-Pot Two Polymers: ABB′ Melt Polycondensation for Linear Polyesters and Hyperbranched Poly(Ester-Urethane)s Based on Natural l-Amino Acids. *Polym Chem* **2015**, *6* (25), 4641–4649. https://doi.org/10.1039/c5py00602c.

(113) Aluri, R.; Saxena, S.; Joshi, D. C.; Jayakannan, M. Multistimuli-Responsive Amphiphilic Poly(Ester-Urethane) Nanoassemblies Based on l -Tyrosine for Intracellular Drug Delivery to Cancer Cells. *Biomacromolecules* **2018**, *19* (6), 2166–2181. https://doi.org/10.1021/acs.biomac.8b00334.

(114) Aluri, R.; Jayakannan, M. Development of L-Tyrosine-Based Enzyme-Responsive Amphiphilic Poly(Ester-Urethane) Nanocarriers for Multiple Drug Delivery to Cancer Cells. *Biomacromolecules* **2017**, *18* (1), 189–200. https://doi.org/10.1021/acs.biomac.6b01476.

(115) Saxena, S.; Jayakannan, M. Enzyme and PH Dual Responsive L-Amino Acid Based Biodegradable Polymer Nanocarrier for Multidrug Delivery to Cancer Cells. *J Polym Sci A Polym Chem* **2016**, *54* (20), 3279–3293. https://doi.org/10.1002/pola.28216.

(116) Saxena, S.; Jayakannan, M. π-Conjugate Fluorophore-Tagged and Enzyme-Responsive l -Amino Acid Polymer Nanocarrier and Their Color-Tunable Intracellular FRET Probe in Cancer Cells. *Biomacromolecules* **2017**, *18* (8), 2594–2609. https://doi.org/10.1021/acs.biomac.7b00710.

(117) Saxena, S.; Jayakannan, M. Development of L-Amino-Acid-Based Hydroxyl Functionalized Biodegradable Amphiphilic Polyesters and Their Drug Delivery Capabilities to Cancer Cells. *Biomacromolecules* **2020**, *21* (1), 171–187. https://doi.org/10.1021/acs.biomac.9b01124.

(118) Chandra Joshi, D.; Ashokan, A.; Jayakannan, M. L -Amino Acid Based Phenol- and Catechol-Functionalized Poly(Ester-Urethane)s for Aromatic π-Interaction Driven Drug Stabilization and Their Enzyme-Responsive Delivery in Cancer Cells. *ACS Appl Bio Mater* **2022**, *5* (11), 5432–5444. https://doi.org/10.1021/acsabm.2c00775.

Chapter 2

Melt Polycondensation Strategy for Amide Functionalized L-Aspartic acid Amphiphilic Polyester Nano-assemblies

Abstract

Aliphatic polyesters are intrinsically enzymatic-biodegradable and they have found ever-increasing demand for safe and smart next generation biomaterial application including drug delivery nano-vectors in cancer research. Bioresources based biodegradable polyesters is one of the elegant strategies to cater this requirement; here, we report L-amino acid-based amide-functionalized polyester platform and explore their lysosomal enzymatic-biodegradation aspects to administrate anticancer drugs in cancer cells. L-Aspartic acid was chosen and different amide-side chain functionalized di-ester monomers were tailor-made having aromatic, aliphatic and bio-source pendant units. Under solvent-free melt polycondensation methodology developed from our laboratory; these new monomers underwent polymerization to yield high molecular weight polyesters with tuneable thermal properties. PEGlated L-aspartic monomer was designed and thermo-responsive amphiphilic polyester was synthesized. This amphiphilic polyester was self-assembled into 140 ± 10 nm sized spherical nanoparticle in aqueous medium which exhibited lower critical solution temperature (LCST) at 40-42 °C. The polyester nano-assemblies showed excellent encapsulation capabilities for anticancer drug doxorubicin (DOX), anti-inflammatory drug curcumin (CUR), biomarkers such as Rose Bengal (RB), and 8-hydroxypyrene-1,3,6-trisulfonic acid trisodium salt (HPTS), etc. The amphiphilic polyester NP was found to be very stable under extracellular conditions and underwent degradation upon exposure to lysosomal enzyme-horse liver esterase in PBS at 37 °C to release 90 % of the loaded cargoes. Cytotoxicity studies in breast cancer MCF 7 and wild-type mouse embryonic fibroblasts (WT MEFs) cell lines revealed that the amphiphilic polyester was non-toxic cell lines up to 100 µg/mL while their drug loaded polyester nanoparticle were able to inhibit the cancerous cell growth. Temperature dependent-cellular uptake studies further confirmed the energy dependent endocytosis of polymer nanoparticles across the cellular membranes. Confocal laser scanning microscopy (CSLM) assisted time-dependent cellular uptake analysis directly evident for the of DOX loaded polymer NP endocytosis and their internalization for biodegradation. In a nut shell, the present investigation opens up new avenue for the L-amino acid based biodegradable polyesters from L-aspartic acids, and the proof-of-concept is demonstrated for drug delivery in cancer cell line.

2.1 Introduction

Biodegradable polymers are emerging as important components in the construction of nano-scaffolds for tissue engineering[1], bone-repair[2], delivery vehicles for therapeutics drugs and genes in cancer treatment[3,4] and many other diverse biomedical applications.[5] Among various chemical linkages that are readily susceptible to biodegradation under physiological conditions, aliphatic polyesters are very special due to their unique ability to degrade by lysosomal enzyme-stimuli at the intracellular compartments[6,7,8]. Aliphatic polyesters are typically synthesized either by ring opening polymerization (ROP) of cyclic monomers[9,10] or direct polycondensation of dicarboxylic acids and diols[11,12]. ROP strategy has been used industrially for the production of polycaprolactone (PCL)[13,14,15], poly(L-lactic acid) and poly($_{D,L}$-lactic-co-glycolic acid), and for the synthesis of di- and tri-block copolymers in the laboratory scale[16,17].

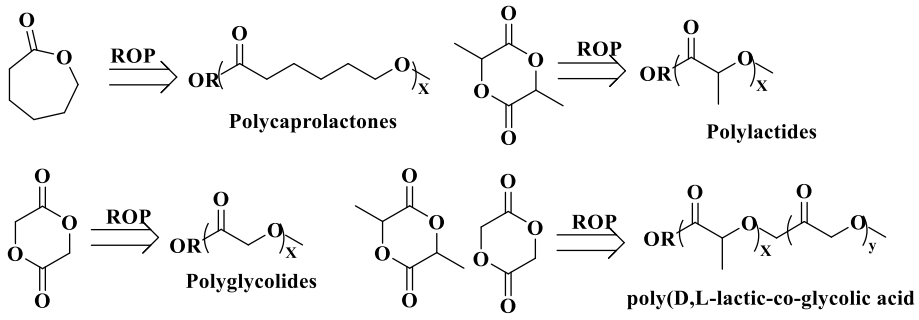

Scheme 2.1 *Synthesis of the polyester from Ring Opening polymerization strategy.*

Last one-decade, significant efforts has been taken to enhance the hydrolytic and environmental stability of the PLLA,[18] and also to overcome the slow enzymatic-biodegradation of PCL chains by various side chain functionalization[19] for drug delivery in cancer[20,21,22] and antimicrobial agents[23,24]. On the contrary, polycondensation approach for aliphatic polyesters has been noticed with limited success in commercial exploration due to poor mechanical properties, low molecular weights, limited enzymatic- or microbial assisted biodegradation, etc[25]. 1,4-Cyclohexane dicarboxylic acid (from DuPont)[26], sebasic acid[27], adipic acid[28] and

succinic acid[29] based aliphatic polyesters are some of the important examples for polycondensation approach.

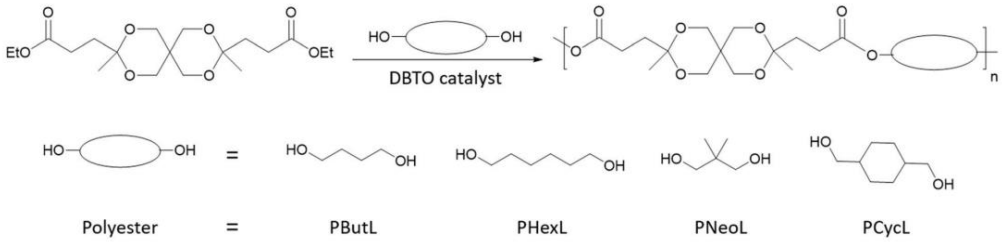

Scheme 2.2 *Synthesis of the polyester from Polycondensation Strategy from levulinic acid-based monomer with different diols. (Adapted from Green Chem., 2021, 23, 5706–5723).*

Recently, bio-based carboxylic acids such as vanillic acid[30],levulinic acid[31], azelaic acid[32], sulfur-containing dicarboxylic acids[33,34] and bio-based diols such as D-mannitol[35,36], (R)-1,3-butanediol[29], isosorbide[37,38], camphor-derived diol[39], and plant oils[40] were explored to make fully aliphatic or aliphatic-aromatic hybrid polyesters. In general, majority of the efforts in the bio-derived aliphatic polyesters are focused to primarily study their thermal and mechanical properties to establish structure-property relationships; and very rarely their biomedical application has been explored. This is partially associated with the lacking of solubility or dispersibility of the bio-derived polyesters in water or aqueous medium which is essential requirement for their application in biosystems. Therefore, new efforts are required to trace bio-derived monomers for aliphatic polyesters and preferably employ solvent-free polycondensation strategy for their long-term impact in biomedical industry.

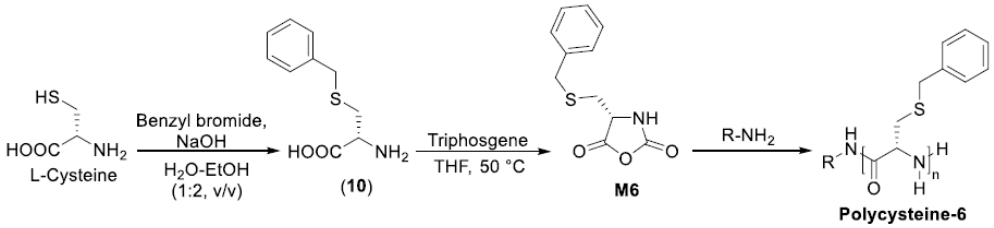

Scheme 2.3 *Synthesis of poly L-Cysteine (Adapted from Biomacromolecules 2022, 23, 6, 2667–2684).*

L-Amino acids are natural bio-derived monomers associated with significant structural-diversity to cater the design and development of biodegradable polymers.[5,41,42] ROP of N-carboxylic anhydride monomers is one of the most studied synthetic strategy to build α-helical[43,44,45] and β-sheet polypeptides[46,47] and their block copolymers.

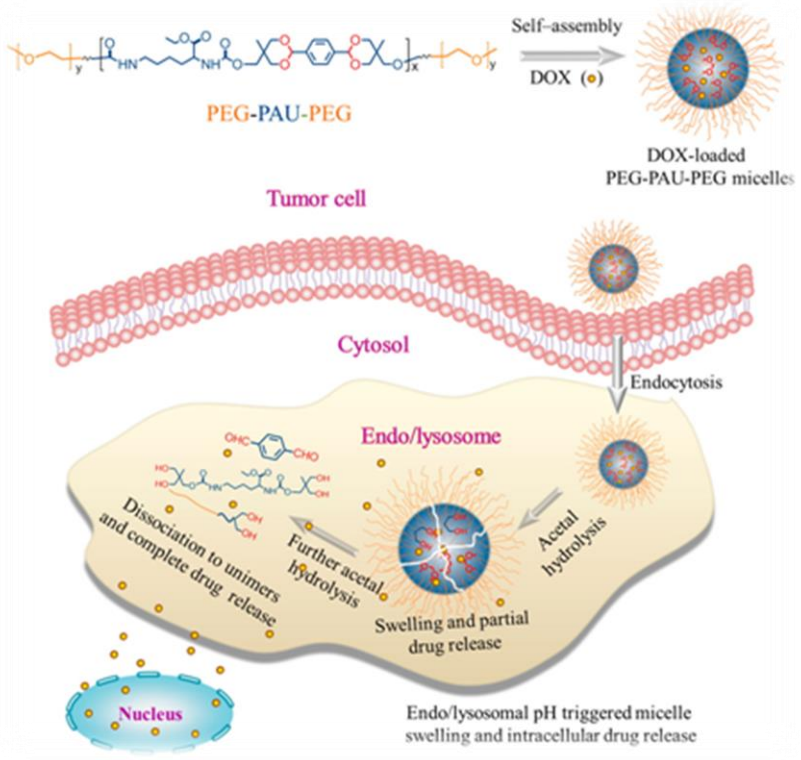

Figure 2.1 *Acid-degradable PEG-PAU-PEG Triblock Copolymer Micelles for pH-Triggered Intracellular DOX Delivery (Adopted Biomacromolecules,* ***2015****, 16, 2228-2236).*

L-Amino acids were converted into α-hydroxy acids and their cyclic monomers were subjected to ROP to produce poly(α-hydroxy acid)s[48,49]. Polycondensation strategy has been reported to build non-peptide polymer analogues from L-amino acid resources such as poly(ester-amide)s[50,51,52,53], poly(acetal-urethane)s[54], poly(disulfide-urethane)s[55], poly(disulfide amide)s[56], polycarbonates[57,58,59,60], and poly(ester-urea-urethanes)[61], etc. Enzyme-catalyzed strategy was also reported for the polyesters[62,63] and very recently the process was improved to make high molecular weight helical chiral polyesters[64]. We have introduced solvent free melt polycondensation strategy for L-amino acid-based monomers to make new classes of non-peptide polymers such as poly(ester-urethane)s[65,66,67] and polyurethanes[68], etc. These polymers were also suitably

modified into pH and enzyme[69], thermo-responsive[70], redox-responsive[71] nano-assembles. L-amino acid-based polymers were also chemically conjugated with fluorophores to build intracellular-responsive FRET bioprobes in cancer research.[72,73]

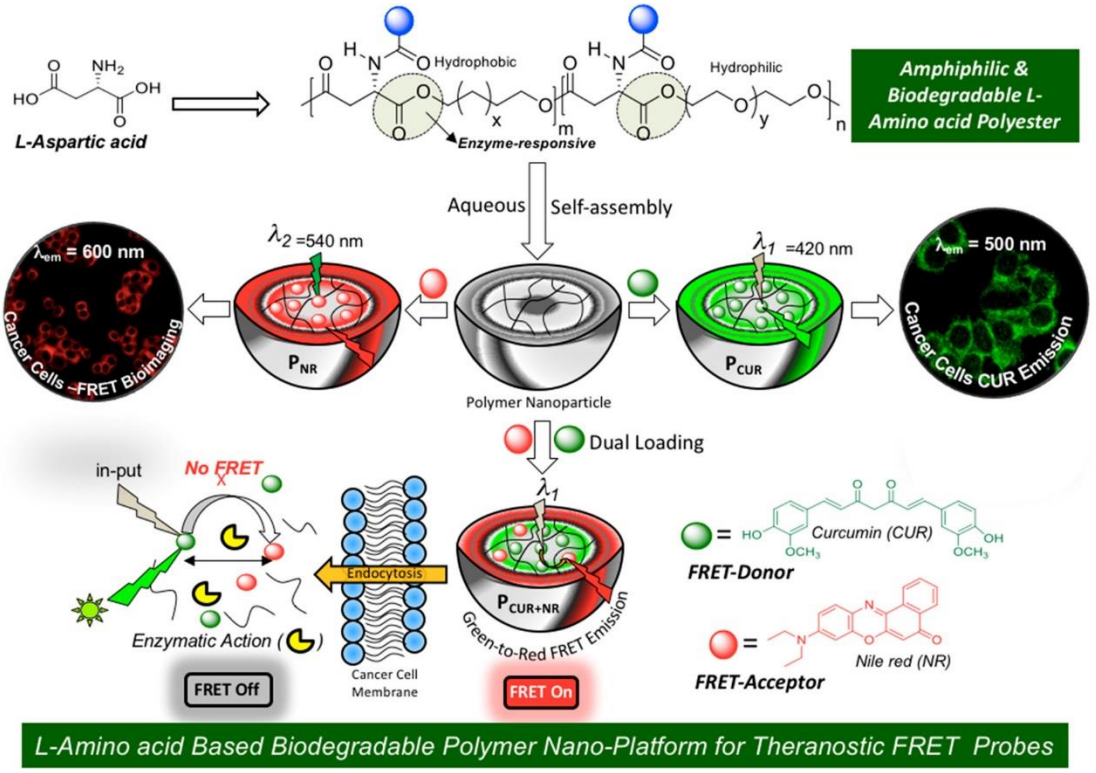

Figure 2.2 *Polyester based FRET probe for drug delivery and bioimaging (Adopted ACS Appl. Bio Mater. 2019, 2, 12, 5245–5262).*

L-Aspartic, L-glutamic acid and L-serine were tailor-made into Boc-protected or acetal-protected diester monomers and they were subjected to thermo-selective melt transesterification to make linear and hyperbranched polymers[74,67,75]. The linear polymers were subjected to post-polymerization de-protection to yield amine-functionalized[74] or hydroxyl functionalized polyesters. [75] It is understandable from the above discussions that bio-derived functional monomers and polymers are highly relevant to replace the existing petroleum-based polymer products in domestic and biomedical applications. Further, more than 50 % of the current prodrug market is based on enzymatically-biodegradable aliphatic ester chemical linkages[76]; and therefore, new synthetic efforts for the development of L-amino acid based aliphatic polyesters is highly relevant and urgently required. Our efforts emphasized that solvent-free melt polymerization strategy to L-amino acid-based monomers have huge potential and the strategy is not just limited to few monomer designs. Here, we report design and development of new classes of amide-functionalized aliphatic polyesters and expand

the scope of synthesis to accomplish one of the first examples of thermo- and enzyme dual-responsive amphiphilic polyesters for drug delivery in cancer research. Large number of monomers based on L-aspartic acid were tailor-made and new aliphatic polyesters were made for tunable thermal properties. Amphiphilic polymer nano-scaffold was successfully encapsulated with anticancer drugs or biomarkers, and potential of these new classes of biodegradable polyesters in drug delivery in breast cancer cell lines as shown in Figure 2.3

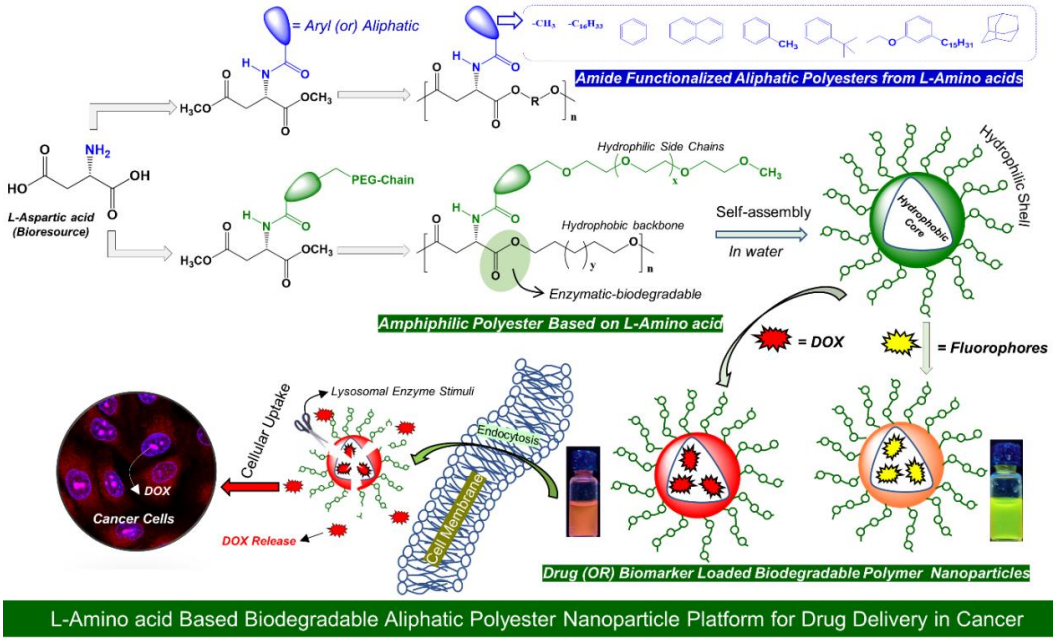

Figure 2.3 *Development of amide-functionalized aliphatic polyesters from L-aspartic acid by solvent-free melt polycondensation strategy and its enzyme-responsive drug delivery in cancer cells.*

The present study deals with the designing and developing of amide-substituted aliphatic polyesters from L-aspartic acid and explore their enzyme-responsive drug delivery aspects in cancer research. For this purpose, the carboxylic acid groups of L-aspartic acid were converted to dimethyl-ester and the amine was masked as amide by using aryl or aliphatic carboxylic acids. The monomers were polymerised with diol to produce high molecular weight polyesters and their molecular weight and thermal properties were studied in detail. Polyethylene glycol 350 monomethyl ether was anchored in the L-aspartic acid to make PEGlated monomer which yielded side chain amphiphilic polyester for producing self-assembled nano-particles. The polymer nanoparticles were found to be thermo-responsive. The water insoluble drug and dyes such as doxorubicin, curcumin, Rose Bengal, 8-hydroxypyrene-1,3,6-trisulfonic acid trisodium salt were loaded in hydrophobic core of micellar nanoparticles. The aliphatic

polyester backbone underwent lysosomal enzymatic-biodegradation to release the drugs or dye under physiological conditions. Cytotoxicity profiles revealed high biocompatibility the polymers and non-toxic towards both cancerous (MCF 7) as well as non- cancerous cell lines (WT MEF) while their drug loaded polymer NPs were found to be effective in inhibiting the growth of cancer cells. Temperature and time-dependent confocal microscopic studies were done to study their cellular uptake in cancer cell lines.

2.2 Experimental Section

2.2.1 Materials and Methods

L-Aspartic acid, acetic anhydride, benzoic acid, 4-hydroxybenzoic acid, 2-naphthoic acid, toluic acid, tertbutyl benzoic acid, adamantane acetic acid, polyethylene glycol (PEG-350) monomethyl ether, 3-pentadecyl phenol, stearic acid, 1,12 dodecandiol, Polyethylene glycol (PEG-400), pyrene, titanium (IV) butoxide ($Ti(OBu)_4$), tin(II) octoate ($Sn(Oct)_2$), dibutyltin dilaurate (DBTDL) , cadmium (II) acetate ($Cd(OAc)_2$) , zinc(II) acetate ($Zn(OAc_2)$), lanthanum(III) chloride, Horse liver esterase enzyme, tetrazolium salt, 3-(4, 5 dimethylthiazolyl)-2,5 diphenyltetrazolium bromide (MTT), dimethyl sulphoxide (DMSO), 4′,6-diamidino-2-phenylindole (DAPI), doxorubicin hydrochloride (DOX. HCl), 4 % paraformaldehyde, rose bengal (RB), and curcumin (CUR) were purchased from Sigma-Aldrich. Many other reagents, solvent and salts were purchased from local market and used without further purification. The human breast cancer cell (MCF 7) and Wild type mouse embryonic fibroblast (WT MEF) were maintained on complete media in an incubator supplied with CO_2 and O_2 about 5% and 1% respectively.

2.2.2 General Procedures

The structures of monomers and polymers were characterised by using 400 MHz JEOL and 400 MHz Brucker NMR spectrophotometers. Chemical shifts are reported in terms of δ units, which is expressed in ppm, the deuterated chloroform was used as internal standard the residual proton peak appears at 7.26 ppm. The molecular weight of monomers and compounds of intermediate step were analysed using HRMS-ESI-Q-time of flight LCMS and Applied Biosystems 4800 PLUS MALDI TOF. The monomers, intermediates and the polymers were characterised by Fourier transform infrared spectroscopy (ATR-FTIR) using Bruker alphaT Fourier transform infrared

spectrophotometer. The molecular weights and polydispersity index (PDI) of polyester was analysed using size exclusion chromatography (SEC) analysis. The concentration of polymer sample was kept as 5mg/mL in HPLC Grade THF. 100 µl of sample was injected. GPC was performed using THF as eluent and The SEC column were calibrated using narrow disperse polystyrene from molecular weight range 1k to 100k. SEC analysis was performed with system equipped with an isocratic pump (Viscotek VE 1122 pump) and a differential refractometer (DRI) detector (Viscotek VE 3580 RI). For SEC with THF as the eluent, separations were performed using serially connected size exclusion columns (two T6000M, General Mixed Organic 8 × 300 mm, from Viscotek) at 25 °C using 1.0 mL/min flow rate, and molecular weights were determined from the calibration curve generated from narrow polystyrene standards. TA Q20 Differential Scanning Calorimeter and PerkinElmer thermal analyser were used for the analysis of thermal decomposition and thermal phase transitions (T_g, T_m and T_c) at 10 ºC/min under nitrogen atmosphere as reported earlier[65]. The size of polymeric nano particle was determined using dynamic light scattering technique (DLS). Nano ZS-90 apparatus from Malvern Instruments was used. The concentration of polymeric Nanoparticle sample was maintained as 0.1mg/mL. The instrument works on the principle of light scattering of laser of 633nm. The polymeric nanoparticles in Brownian motion scatter light. The detector is placed in 90º angle to record fluctuations in scattered light collected and the instrument generates autocorrelation function [g^2 (t)] using which Diffusion coefficient was obtained using cumulant method. Instrument utilizes stock Einstein method to calculate the diameter of nanoparticle. Absorbance and Fluorescence Studies was carried out for Drug/Dye loaded nanoparticle. A PerkinElmer Lambda 45 UV−vis spectrophotometer was utilised for the absorption studies. Emission and Excitation spectra was recorded on a SPEX Fluorolog HORIBA JOBIN VYON fluorescence spectrophotometer. This instrument utilises 450 W Xe lamp as the source of excitation at room temperature. The morphology of polymeric nanoparticle was analysed by microscopic techniques. FESEM samples were prepared taking 0.1mg/mL concentration of nanoparticle which was drop casted on silicon wafer. Samples were subjected to gold coating. The gold coated layer protects sample from high voltage and make it conducting. FESEM analysis was done using Zeiss Ultra Plus scanning electron microscope. The morphology of polymeric nanoparticle was further confirmed TEM. The samples were drop casted on Formvar-coated copper grid. Samples were stained using uranyl acetate. The TEM Images were acquired using a

Technai-300 instrument. The Concentration of formazan was determined by taking absorbance readings at 570 nm at a Varioskan FLASH instrument. The polymeric nanoparticle samples were lyophilize using A Christ Alpha 1-2 LD plus. The cellular uptake studies were carried out using live cells and fixed cell experiments. The cells were imaged using LSM710 confocal microscope which utilizes 405, 488, and 561 nm lasers. 63X Oil immersion lens was used.

2.2.3 Synthesis of Dimethyl benzoyl-L-aspartate (M1)

L-Aspartic acid (10.0 g, 0.07 mol) was immersed in methanol (100.0 mL) and kept at 0 ºC. Thionyl chloride (21.0 mL, 34.5 g, 0.29 mol) was added dropwise at 0 ºC. under the atmosphere of nitrogen and then the reaction mixture was brought to 25 ºC and stirred for 30 min. The reaction mixture was subjected to reflux at 70 ºC for 6 h under nitrogen atmosphere. Excess of thionyl chloride and methanol were removed by distillation and the residue was washed with diethyl ether to get white solid product. Yield =14.5 g (98%). The resultant dimethyl ester-L-aspartic acid aminium salt (**compound-1**) was directly used without further purification. Compound -1 (10.0 g, 0.05 mol) was dissolved in dry dichloromethane (100.0 mL) with triethylamine (14.0 mL, 10.2g, 0.10 mol). Benzoyl chloride (5.3mL, 6.3 g, 0.04 mol) was added dropwise under nitrogen condition at 0 ºC. The reaction mixture was allowed to warm to 25 ºC and stirred for 6 h. The dichloromethane was removed by rotary evaporator and the product was extracted in ethyl acetate. The organic layer was dried over anhy. Na_2SO_4 and the solvent was removed by rotary evaporator to obtain solid product. It was further purified silica-gel column using ethyl acetate and pet ether 1:10 (v/v). Yield = 9.7 g (80 %) ^{1}H NMR (400 MHz, $CDCl_3$) δ ppm 7.82 (2 H, m) 7.53 (1 H, d, *J*=7.34 Hz) 7.46 (2 H, m) 7.24 (2 H, d, *J*=7.34 Hz) 5.08 (1 H, m) 3.81 (3 H, s) 3.72 (3 H, s) 3.16 (1 H, dd, *J*=17.24, 4.28 Hz) 3.00 (1 H, dd, *J*=17.24, 4.52 Hz). ^{13}C NMR (101 MHz, $CDCl_3$) δ ppm 171.77, 171.26, 166.92, 133.55, 131.92, 128.62, 127.14, 52.93, 52.09, 48.84, 36.04. FTIR (cm^{-1}) 3330, 3004, 2954, 1737, 1646, 1603, 1578, 1531, 1487, 1438, 1345, 1278, 1217, 1173, 1103, 1076, 1049, 1000, 895, 845, 802, 716. MALDI-TOF: calculated. For C13H15NO5 [M + Na] $^{+}$: 288.0848; found: 288.7138 (M+ Na^{+}). HRMS(ESI): calculated [M + Na] $^{+}$: 288.0848 found: 288.0851.

2.2.4 Synthesis of Dimethyl (4-methylbenzoyl)-L-aspartate (M2)

4-Methyl benzoic acid (5.0 g, 0.03 mol) refluxed with thionyl chloride (10 mL, 0.14 mol) at 80 ºC for 6 h under nitrogen atmosphere. Excess thionyl chloride was removed by distillation, and the resultant 4-methyl benzoyl chloride (5.0 g, 0.03mol) in dry dichloromethane (100.0 mL) was added dropwise into compound-1 (6.5 g, 0.03mol) and triethylamine (7.0mL, 5.0g 0.05mol) in dry dichloromethane (50.0 mL). The rest of the procedure is same as described for monomer **M1**. Yield = 7.9 g (87 %) ^{1}H NMR (400 MHz, $CDCl_3$) δ ppm 7.71 (2 H, d, *J*=8.24 Hz) 7.25 (3 H, m) 7.19 (1 H, d, *J*=7.78 Hz) 5.07 (1 H, m) 3.80 (3 H, s) 3.71 (3 H, s) 3.15 (1 H, dd, *J*=17.40, 4.12 Hz) 2.98 (1 H, dd, *J*=17.40, 4.58 Hz) 2.40 (3 H, s). ^{13}C NMR (101 MHz, $CDCl_3$) δ ppm 171.46, 171.01, 166.60, 142.10, 130.33, 128.92, 126.82, 52.55, 51.72, 48.49, 35.74, 21.13. FTIR (cm^{-1}) 3339, 3030, 2954, 1736, 1646, 1613, 1534, 1500, 1438, 1344, 1283, 1216, 1179, 1105, 1046, 998, 896, 839, 754, 687. MALDI-TOF: calculated. For C14H17NO5 m/z $[M + Na]^+$: 302.1004; found: $[M + Na]^+$: 302.7708

2.2.5 Synthesis of Dimethyl (4-(tert-butyl) benzoyl)-L-aspartate (M3)

4-Ter. butyl benzoic acid (5.0 g, 0.03 mol) refluxed with thionyl chloride (10 mL, 0.14 mol) at 80 ºC for 6 h under nitrogen atmosphere. Excess thionyl chloride was removed by distillation, and the resultant 4-methyl benzoyl chloride (5.0 g, 0.02mol) in dry dichloromethane (100.0 mL) was added dropwise into compound-1 (6.5 g, 0.03mol) and triethylamine (7.7mL, 5.6g 0.07mol) in dry dichloromethane (60.0 mL). The rest of the procedure is same as described for monomer **M1**. Yield= 6.5g (79%) ^{1}H NMR (400 MHz, $CDCl_3$) δ ppm 7.76 (2 H, m, *J*=8.24 Hz) 7.47 (2 H, m, *J*=8.24 Hz) 7.23 (1 H, s) 5.08 (1 H, s) 3.80 (3 H, s) 3.71 (3 H, s) 3.13 (1 H, s) 3.01 (1 H, s) 1.34 (10 H, s). ^{13}C NMR (101 MHz, $CDCl_3$) δ ppm 171.79, 171.34, 166.85, 155.50, 130.64, 126.99, 125.56, 52.90, 52.07, 48.79, 36.09, 34.95, 31.12. FTIR (cm^{-1}) 3340, 2958, 2871, 1737, 1643, 1613, 1534, 1499, 1438, 1409, 1364, 1344, 1268, 1207, 1175, 1096, 1048, 1015, 897, 851, 773, 710. MALDI-TOF: calculated For C17H23NO5 $[M + Na]^+$: 344.1474; found: $[M + Na]^+$: 344.9114.

2.2.6 Synthesis of Dimethyl (2-naphthoyl)-L-aspartate (M4)

2-Naphthoic acid (5.0 g, 0.03 mol) refluxed with thionyl chloride (20 mL, 0.27 mol) at 80 ºC for 6 h under nitrogen atmosphere. Excess thionyl chloride was removed by

distillation, and the resultant 2-napthoyl chloride (5.0g, 0.02mol) in dry dichloromethane (100.0 mL) was added dropwise into compound-1 (7.8 g, 0.039mol) and triethylamine (12.0 mL, 8.7 g 0.08 mol) in dry dichloromethane (120.0 mL). The rest of the procedure is same as described for monomer **M1**. Yield =5.0g (60 %) ^{1}H NMR (400 MHz, $CDCl_3$) δ ppm 8.35 (1 H, s) 7.93 (4 H, m) 7.57 (2 H, s) 7.42 (1 H, br. s.) 5.13 (1 H, s) 3.83 (3 H, s) 3.73 (3 H, s) 3.17 (1 H, s) 3.06 (1 H, m). ^{13}C NMR (101 MHz, $CDCl_3$) δ ppm 171.83, 171.34, 166.97, 134.92, 132.54, 130.73, 129.02, 128.52, 127.85, 127.79, 127.74, 126.82, 123.56, 52.96, 52.11, 48.97, 36.11, -0.02. FTIR (cm^{-1}) 3339, 3058, 2953, 2362, 1740, 1647, 1531, 1438, 1343, 1304, 1219, 1174, 1093, 1049, 998, 907, 865, 827, 776, 665. MALDI-TOF: calculated. For C17H17NO5 m/z [M + Na] $^{+}$: 338.1004; found: [M +Na] $^{+}$: 338.8675 HRMS (ESI): m/z [M + H] $^{+}$: 316.11; found: [M +H] $^{+}$: 316.1190

2.2.7 Synthesis of Dimethyl acetyl-L-aspartate (M5)

The dimethyl ester-L-aspartic acid aminium salt (**compound-1**) (15 g, 0.076 mol) was dissolved in a mixture of triethylamine (15.9mL, 11.5g, 0.011 mol) and dry dichloromethane (100 mL). when the aspartate dimethyl ester was dispersed in mixture of dry dichloromethane and triethyl amine. acetic anhydride (5.7 mL, 6.2 gm, 0.06) was added in a dropwise to the reaction mixture under ice cold condition. After addition, the reaction mixture was allowed to warm to room temperature and then reaction performed for 12 h under nitrogen atmosphere. The dichloromethane was removed by rotary evaporator. Product was extracted in ethyl acetate by work up with water and the obtained viscous liquid was further purified by column chromatography using ethyl acetate and pet ether as eluent 1:10 (V/V). Yield = 7.8g (63%) ^{1}H NMR (400 MHz, $CDCl_3$) δ ppm 6.67 (1 H, d, *J*=7.34 Hz) 4.85 (1 H, dq, *J*=8.28, 4.25 Hz) 3.75 (3 H, s) 3.68 (3 H, s) 3.02 (1 H, m) 2.85 (1 H, m) 2.03 (3 H, s). ^{13}C NMR (101 MHz, $CDCl_3$) δ ppm 171.62, 171.53, 171.11, 170.35, 52.75, 51.97, 51.89, 48.42, 35.94, 35.87, 22.87, 22.83, FTIR (cm^{-1}) 3340, 2958, 2871, 1737, 1643, 1613, 1534, 1499, 1438, 1409, 1364, 1344, 1268, 1207, 1175, 1096, 1048, 1015, 897, 851, 773, 710. MALDI-TOF: calculated. For C8H13NO5 [M + H] $^{+}$: 204.08; found: [M + H] $^{+}$: 204.397.

2.2.7 Synthesis of Dimethyl (2-(3-pentadecylphenoxy) acetyl)-L-aspartate (M6)

Pentadecyl-phenoxy acetic acid (10 gm, 0.03mol) refluxed with thionyl chloride (40mL, 0.34mol)) at 80 ºC for 6 h under nitrogen atmosphere. Excess thionyl chloride was removed by distillation, and the resultant 2-(3-pentadecylphenoxy) acetyl chloride. The 2-(3-pentadecylphenoxy) acetyl chloride (10.5 gm, 0.03mol) in dry dichloromethane (100.0 mL) was added dropwise into compound-1 (Compound I), (8.2gm,0.04mol) and triethylamine (11.4 mL, 8.0 g 0.08 mol) in dry dichloromethane (120.0 mL). The rest of the procedure is same as described for monomer **M1**. Yield= 12 g (88%) ^{1}H NMR (400 MHz, $CDCl_3$) δ ppm 7.58 (1 H, br. s.) 7.22 (1 H, s) 6.86 (1 H, s) 6.78 (2 H, s) 4.97 (1 H, s) 4.53 (2 H, s) 3.77 (3 H, s) 3.67 (3 H, s) 3.06 (1 H, s) 2.89 (1 H, s) 2.59 (2 H, s) 1.58 (5 H, s) 1.26 (25 H, s) 0.89 (3 H, s). ^{13}C NMR (101 MHz, $CDCl_3$) δ ppm 171.45, 170.99, 168.74, 157.44, 145.35, 129.68, 122.61, 115.33, 111.97, 67.44, 53.18, 52.34, 48.30, 36.29, 36.25, 32.19, 31.68, 29.96, 29.88, 29.80, 29.63, 22.97, 14.40. FTIR (cm^{-1}) 3420, 2922, 2852, 1739, 1681, 1587, 1522, 1488, 1438, 1368, 1256, 1212, 1162, 1058, 997, 852, 777, 720, 694. HRMS (ESI): m/z calcd. For $C_{29}H_{47}NO_6$ $[M + H]^+$: 528.3301; found: $[M + Na]^+$: 526.8652.

2.2.8 Synthesis of Dimethyl stearoyl-L-aspartate (M7)

Stearic acid (4.5g, 0.016mol) refluxed with thionyl chloride (20mL, 0.27mol) at 80 ºC for 6 h under nitrogen atmosphere. Excess thionyl chloride was removed by distillation, and the resultant stearoyl chloride (5.0g, 0.016mol in dry dichloromethane (40.0 mL) was added dropwise into compound-1 (3.27g, 0.016mol) and triethylamine (5mL, 3.6g, 0.03mol) in dry dichloromethane (40.0 mL). The rest of the procedure is same as described for monomer **M1**. Yield= 7.3g (65%). ^{1}H NMR (400 MHz, $CDCl_3$) δ ppm 6.46 (1 H, br. s.) 4.87 (1 H, s) 3.77 (3 H, s) 3.70 (3 H, s) 3.02 (1 H, s) 2.88 (1 H, s) 2.23 (2 H, s) 1.62 (5 H, br. s.) 1.26 (30 H, s) 0.89 (3 H, s). ^{13}C NMR (101 MHz, $CDCl_3$) δ ppm 172.94, 171.66, 171.29, 52.77, 51.99, 48.26, 36.49, 36.09, 31.90, 29.67, 29.63, 29.58, 29.47, 29.34, 29.31, 29.14, 25.50, 22.66, 14.10. FTIR (cm^{-1}) 3340, 2958, 2871, 1737, 1643, 1613, 1534, 1499, 1438, 1409, 1364, 1344, 1268, 1207, 1175, 1096, 1048, 1015, 897, 851, 773, 710. MALDI-TOF: calculated. For $C_{24}H_{45}NO_5$ $[M + H]^+$: 428.33; found: $[M + H]^+$: 428.756.

2.2.9 Synthesis of Dimethyl(adamantane-1-carbonyl)-L-aspartate (M8)

1- Adamantane acetic acid (3g, 0.015mol) refluxed with thionyl chloride (10mL, 0.13mol) at 80 ºC for 6 h under nitrogen atmosphere. Excess thionyl chloride was removed by distillation, and the resultant adamantane-1-acetyl chloride (3g, 0.014mol) in dry dichloromethane (100.0 mL) was added dropwise into compound-1 (2.7g, 0.028mol) and triethyl amine (6mL, 4.3g, 0.04mol) in dry dichloromethane (120.0 mL). The rest of the procedure is same as described for monomer **M1**. Yield= 3.25g (72%). ^{1}H NMR (400 MHz, $CDCl_3$) δ ppm 6.38 (1 H, d, *J*=7.83 Hz) 4.86 (1 H, m) 3.77 (3 H, s) 3.69 (3 H, s) 3.04 (1 H, dd, *J*=17.12, 4.40 Hz) 2.88 (1 H, dd, *J*=17.24, 4.52 Hz) 1.98 (5 H, m) 1.65 (13 H, m) ^{13}C NMR (101 MHz, $CDCl_3$) δ ppm 171.68, 171.26, 170.68, 77.32, 76.69, 52.72, 51.98, 51.38, 48.31, 42.43, 42.25, 36.67, 36.09, 32.82, 28.58. FTIR (cm−1) 3882, 3744, 3294, 2901, 2847, 1735, 1649, 1530, 1437, 1341, 1272, 1201, 1169, 1124, 1097, 1051, 999, 852, 734, 700, 646, 629. HRMS (ESI): m/z calcd. For C24H45NO5 $[M + H]^+$: 338.19; found: $[M + H]^+$: 428.756.

2.2.10 Synthesis of Polyethylene glycol monomethyl ether methane sulphonate (Compound 2)

PEG 350 monomethyl ether (10g, 0.028mol) along with dry dichloromethane (50ml) was taken in clean round bottomed flask. At 0 ºC methane sulphonic acid (4.8g, 0.042mol) was added to reaction mixture using dropping funnel. Then the reaction was shifted to room temperature. The reaction was performed under nitrogen atmosphere for 12 h. the product was extracted in dichloromethane by doing work up with acidic water. Followed by washing organic layer with brine. The organic layer was the concentrated over rotary evaporator to get yellow coloured product. Yield=11.2g (94%). ^{1}H NMR (400 MHz, $CDCl_3$) δ ppm 4.38 (2 H, m) 3.77 (2 H, dd, *J*=5.26, 3.79 Hz) 3.66 (24 H, m) 3.55 (2 H, m) 3.38 (3 H, s) 3.09 (3 H, s). ^{13}C NMR (101 MHz, $CDCl_3$) δ ppm 84.09, 83.77, 83.45, 78.36, 77.05, 76.94, 76.93, 75.88, 75.45, 65.43, 44.14.

2.2.11 Synthesis of methyl 4-hydroxybenzoate (Compound 3)

4-Hydroxyl benzoic acid (10g, 0.072mol) was taken in clean round bottomed flask to that methanol (100ml) was added and concentrated sulphuric acid (5ml) was added. The reaction was refluxed for 12 h. at 70 ºC. After completion of the reaction methanol

was removed by rotary evaporator followed by crude product was purified by workup in ethyl acetate and acidic water. Ethyl acetate layer was dried over Na_2SO_4 layer and concentrated to get white solid product. Yield=9.92g (90%). ^{1}H NMR (400 MHz, $CDCl_3$) δ ppm 7.96 (2 H, m, *J*=8.80 Hz) 6.88 (2 H, m, *J*=8.80 Hz) 3.90 (4 H, s). ^{13}C NMR (101 MHz, $CDCl_3$) δ ppm 176.62, 167.63, 160.56, 131.92, 121.94, 115.29, 77.32, 76.69, 52.09, 20.65.

2.2.12 Synthesis of Methyl benzoate of polyethylene glycol monomethyl ether (Compound 4)

Methyl 4-hydroxybenzoate (5.4g, 0.035mol) was taken in clean round to bottomed flask. Anhydrous K_2CO_3 (8.3g, 0.06mol) and dry acetonitrile (100ml) was added. Reaction mixture was kept for reflux at 80 ºC. after 0.4 h mesylated Polyethylene glycol monomethyl ether (10g, 0.02mol) was added. The reaction was performed at 70 ºC under nitrogen atmosphere for 12h. after completion of the reaction acetonitrile was removed. The crude product was purified by workup on ethyl acetate and water. The product was further purified by column chromatography. Yield= 10g (100%) ^{1}H NMR (400 MHz, $CDCl_3$) δ ppm 7.97 (2 H, m, *J*=8.80 Hz) 6.93 (2 H, m, *J*=8.80 Hz) 4.18 (2 H, m) 3.87 (5 H, m) 3.68 (23 H, m) 3.54 (2 H, d, *J*=4.89 Hz) 3.37 (3 H, s). ^{13}C NMR (101 MHz, $CDCl_3$) δ ppm 170.13, 170.10, 162.79, 131.97, 122.17, 114.10, 77.3, 76.68, 71.71, 70.66, 70.41, 70.34, 70.27, 69.36, 67.41, 58.82.

2.2.13 Synthesis of 4- polyethylene glycol monomethyl ether benzoic acid (Compound 5)

Methyl benzoate of polyethylene glycol monomethyl ether (10g, 0.02mol) was taken in clean round bottomed flask to that methanol (50 ml) was added. Followed by that sodium hydroxide (4g, 0.1mol) was added. The reaction mixture was kept for reflux for 48 h. After completion of the reaction methanol was removed by rotary evaporator. The reaction mixture was dissolved in ethyl acetate and extracted against acidic water. The ethyl acetate layer was dried anhydrous sodium sulphate and concentrated over rotary evaporator to get product. Yield: 9.2g (94%) ^{1}H NMR (400 MHz, $CDCl_3$) δ ppm 7.98 (2 H, m, *J*=8.80 Hz) 6.91 (2 H, m, *J*=8.80 Hz) 4.16 (2 H, d, *J*=9.54 Hz) 3.86 (2 H, br. s.) 3.71 (2 H, br. s.) 3.62 (20 H, br. s.) 3.52 (2 H, br. s.) 3.35 (3 H, s) ^{13}C NMR (101 MHz, $CDCl_3$) δ ppm 170.13, 170.10, 162.79, 131.97, 122.17, 114.10, 77.3 , 76.68, 71.71, 70.66, 70.41, 70.34, 70.27, 69.36, 67.41, 58.82.

2.2.14 Synthesis of Dimethyl (4-(polyethylene glycol monomethyl ether 350) benzoyl)-L-aspartate monomer: (M-PEG)

4- Polyethylene glycol monomethyl ether benzoic acid (10g, 0.02mol) refluxed with thionyl chloride (40ml, 0.83mol) at 80 ºC for 6 h under nitrogen atmosphere. Excess thionyl chloride was removed by distillation, and the resultant). PEG 350 acid chloride in dry dichloromethane (100.0 mL) was added dropwise into compound-1 (7.9g ,0.04mol) and triethylamine (11.1 mL, 8g 0.08mol) in dry dichloromethane (120.0 mL). The rest of the procedure is same as described for monomer **M1**. Yield= 8.72 (65%). ^{1}H NMR (400 MHz, $CDCl_3$) δ ppm 7.76 (2 H, m, *J*=8.80 Hz) 7.14 (1 H, d, *J*=7.83 Hz) 6.94 (2 H, m, *J*=8.80 Hz) 5.04 (1 H, m) 4.16 (2 H, m) 3.86 (2 H, m) 3.78 (3 H, s) 3.68 (24 H, m) 3.53 (2 H, m) 3.36 (3 H, s) 3.12 (1 H, dd, *J*=17.12, 4.16 Hz) 2.96 (1 H, dd, *J*=17.24, 4.52 Hz). ^{13}C NMR (101 MHz, $CDCl_3$) δ ppm 172.94, 171.66, 171.29, 52.77, 51.99, 48.26, 36.49, 36.09, 31.90, 29.67, 29.63, 29.58, 29.47, 29.34, 29.31, 29.14, 25.50, 22.66, 14.10. FTIR (cm−1) 3340, 2874, 1737, 1651, 1606, 1575, 1538, 1500, 1440, 1348, 1297, 1250, 1177, 1095, 946, 847,768, 697, 653. MALDI-TOF: m/z calculated For C30H49NO14 $[M + H]^+$: 669.8; found: $[M + Na]^+$: 670.8.

2.2.15 Synthesis of Benzoyl-L-aspartate polyester (P1)

General procedure for melt polycondensation is described for the polymerization of monomer M1 with 1,12 dodecanediol. In a cleaned and dried polymerization tube, dimethyl benzoyl-L-aspartate M1 (0.6 g, 0.0022 mol) and 1,12 dodecanediol (0.45g, 0.0022 mol) were melted together at 80 ºC and purged with nitrogen to remove moisture and oxygen. $Ti(OBu)_4$ (1 mol%) was added as catalyst and the polymerization was proceeded for 4 h at 140 ºC with constant stirring under nitrogen purge. During this step, the more than 90 % of the methanol condensate was removed. Subsequently, the polymerization was carried out under reduced pressure of 10^{-2} mbar to get viscous polymer product. Polymer was dissolved in dichloromethane and purified by precipitating in hexane. Yield = 0.89g (98 %). ^{1}H NMR (400 MHz, $CDCl_3$) δ ppm 7.80 (2 H, s) 7.52 (1 H, s) 7.44 (2 H, s) 7.26 (1 H, br. s.) 5.03 (1 H, br. s.) 4.18 (2 H, s) 4.08 (2 H, s) 3.10 (1 H, m.) 2.99 (1 H, m) 1.62 (4 H, br. s.) 1.23 (16 H, br. s.). ^{13}C NMR (101 MHz, $CDCl_3$) δ ppm 171.30, 170.84, 166.91, 133.68, 131.82, 128.57, 127.09, 66.07, 65.26, 49.00, 36.25, 29.51, 29.46, 29.21, 29.17, 28.49, 28.42, 25.85, 25.76. FTIR (cm^{-1})

3344, 2924, 2853, 2361, 1732, 1650, 1603, 1579, 1526, 1485, 1465, 1393, 1342, 1273, 1180, 1100, 1045, 993, 898, 801, 771, 713.

2.2.16 Synthesis of 4-Methylbenzoyl)-L-aspartate polyester (P2)

Dimethyl (4-methylbenzoyl)-L-aspartate M2 (0.6g, 0.0022mol) and 1,12 dodecanediol (0.44g, 0.0022mol) were polymerized using $Ti(OBu)_4$ catalyst as described for the polymer P1. Yield=0.89g (97%). ^{1}H NMR (400 MHz, $CDCl_3$) δ ppm 7.69 (2 H, s) 7.24 (3 H, s) 5.02 (1 H, br. s.) 4.17 (2 H, s) 4.07 (2 H, s) 3.08 (1 H, br. m.) 2.99 (1 H, br. m.) 2.39 (3 H, s) 1.60 (4 H, s.) 1.23 (17 H, br. s.) ^{13}C NMR (101 MHz, $CDCl_3$) δ ppm 171.45, 171.06, 167.00, 142.42, 130.95, 129.34, 127.23, 66.16, 65.36, 49.07, 36.42, 29.65, 29.60, 29.50, 29.34, 29.29, 28.62, 28.54, 25.97, 25.88, 21.58, 0.08,. FTIR (cm^{-1}) 3344, 2924, 2853, 2361, 1732, 1646, 1613, 1532, 1498, 1464, 1393, 1342, 1267, 1184, 1100, 1043, 898, 836, 803, 751, 723, 664.

2.2.17 Synthesis of (4-(Tert-butyl) benzoyl)-L-aspartate Polyester (P3)

Dimethyl (4-(tert-butyl) benzoyl)-L-aspartate monomer (0.6g, 0.0018mol) and 1,12 dodecanediol (0.37g, 0.0018mol) were polymerized using $Ti(OBu)_4$ catalyst as described for the polymer P1. Yield=0.84g (98%). ^{1}H NMR (400 MHz, $CDCl_3$) δ ppm 7.75 (2 H, m, *J*=8.31 Hz) 7.46 (2 H, m, *J*=8.31 Hz) 7.21 (1 H, d, *J*=7.83 Hz) 5.03 (1 H, m) 4.18 (2 H, t, *J*=6.60 Hz) 4.07 (2 H, t, *J*=6.72 Hz) 3.12 (1 H, dd, *J*=17.12, 4.16 Hz) 2.97 (1 H, dd, *J*=17.12, 4.40 Hz) 1.61 (6 H, m) 1.33 (27 H, m). ^{13}C NMR (101 MHz, $CDCl_3$) δ ppm 171.61, 171.23, 167.12, 155.67, 131.15, 127.27, 125.82, 66.34, 65.54, 49.28, 36.64, 35.24, 31.44, 29.85, 29.80, 29.54, 29.50, 28.83, 28.75, 26.17, 26.09. FTIR (cm^{-1}) 3344, 2924, 2853, 2361, 1732, 1650, 1603, 1579, 1526, 1485, 1465, 1393, 1342, 1273, 1180, 1100, 1045, 993, 898, 801, 771, 713.

2.2.18 Synthesis of (2-Naphthoyl)-L-aspartate polyester (P4)

Dimethyl (2-naphthoyl)-L-aspartate monomer (0.6g, 0.0019mol) and 1,12 dodecanediol (0.38g, 0.0019mol) were polymerized using $Ti(OBu)_4$ catalyst as described for the polymer P1. Yield=0.84g (96%). ^{1}H NMR (400 MHz, $CDCl_3$) δ ppm 8.33 (1 H, s) 7.88 (4 H, br. s.) 7.55 (2 H, s) 7.40 (1 H, s) 5.11 (1 H, br. s.) 4.20 (2 H, s) 4.09 (2 H, br. s.) 3.14 (1 H, br. s.) 3.06 (1 H, br. s.) 1.65 (4H, br. s.) 1.20 (6 H, br. s.). ^{13}C NMR (101 MHz, $CDCl_3$) δ ppm 171.37, 170.93, 166.98, 134.88, 132.54, 130.86,

128.99, 128.49, 127.80, 127.72, 126.78, 123.55, 66.12, 65.30, 49.14, 36.32, 29.48, 29.21, 28.51, 28.44, 25.86, 25.78. FTIR (cm^{-1}) 3344, 3357 2924, 2853, 2361, 1732, 1650, 1600, 1526, 1503, 1464, 1435, 1392, 1338, 1299, 1200, 1090, 1044, 989, 910, 865, 825, 775, 760, 664.

2.2.19 Synthesis of Acetyl-L-aspartate polyester (P5)

Dimethyl acetyl-L-aspartate (0.5g, 0.0024mol) and 1,12 dodecanediol (0.49g, 0.0024mol) were polymerized using $Ti(OBu)_4$ catalyst as described for the polymer P1. Yield = 0.78g (95%). ^1H NMR (400 MHz, $CDCl_3$) δ ppm 7.80 (s, 2 H) 7.44 (s, 3 H) 7.23 (s, 1 H) 5.03 (br. s., 1 H) 4.18 (s, 2 H) 4.08 (s, 2 H) 3.11 (br. s., 1 H) 2.99 (br. s., 1 H) 1.64 (br. s., 5 H) 1.15 - 1.45 (m, 18 H). ^{13}C NMR (101 MHz, $CDCl_3$) δ ppm 171.18, 170.80, 169.85, 65.97, 65.19, 62.94, 48.57, 36.27, 32.75, 29.50, 29.47, 29.37, 29.21, 29.15, 28.48, 28.40, 25.83, 25.74, 23.08. FTIR (cm^{-1}) 3344, 2924, 2853, 2361, 1732, 1650, 1603, 1579, 1526, 1485, 1465, 1393, 1342, 1273, 1180, 1100, 1045, 993, 898, 801, 771, 713.

2.2.20 Synthesis of (2-(3-Pentadecylphenoxy) acetyl)-L-aspartate polyester (P6)

Dimethyl (2-(3-pentadecylphenoxy) acetyl)-L-aspartate monomer (0.85g, 0.0016mol) and 1,12 dodecanediol (0.34g, 0.0016mol were polymerized using $Ti(OBu)_4$ catalyst as described for the polymer P1. Yield=0.75g (98%). ^1H NMR (400 MHz, $CDCl_3$) δ ppm 7.59 (1 H, s) 7.20 (1 H, s) 6.83 (1 H, s) 6.77 (2 H, s) 4.91 (1 H, br. s.) 4.51 (2 H, s) 4.15 (2 H, s) 4.03 (2 H, s) 3.03 (1 H, br. s.) 2.87 (1 H, m) 2.58 (2 H, s) 1.60 (7 H, br. s.) 1.26 (43 H, s) 0.88 (3 H, s). ^{13}C NMR (101 MHz, $CDCl_3$) δ ppm 170.68, 170.27, 168.27, 157.19, 145.01, 129.35, 122.26, 115.01, 111.67, 67.18, 66.08, 65.28, 48.15, 36.26, 35.96, 31.90, 31.39, 29.68, 29.58, 29.52, 29.35, 29.28, 29.21, 28.48, 28.40, 25.86, 25.75, 22.67, 14.11. FTIR (cm^{-1}) 3425, 2922, 2852, 2361, 1738, 1687, 1588, 1519, 1488, 1462, 1394, 1353, 1258, 1198, 1061, 990, 873, 773, 721, 694.

2.2.21 Synthesis of Stearoyl-L-aspartate polyester (P7)

Dimethyl stearoyl-L-aspartate monomer (0.6g, 0.0014mol) and 1,12 dodecanediol (0.28g, 0.0014mol) were polymerized using $Ti(OBu)_4$ catalyst as described for the polymer P1. Yield=0.77g (97%). ^1H NMR (400 MHz, $CDCl_3$) δ ppm 6.48 (1 H, br. s.) 4.84 (1 H, br. s.) 4.14 (2 H, s) 4.07 (2 H, s) 3.00 (1 H, br. s.) 2.86 (1 H, br. s.) 2.22 (2 H, s) 1.63 (7 H, br. s.) 1.26 (45 H, br. s.) 0.89 (3 H, s). ^{13}C NMR (101 MHz, $CDCl_3$) δ

ppm 173.24, 171.53, 171.16, 66.23, 65.46, 48.70, 36.80, 36.57, 34.67, 32.19, 29.97, 29.93, 29.85, 29.80, 29.62, 29.54, 29.48, 28.92, 28.79, 28.72, 26.15, 26.06, 25.85, 25.28, 22.96, 14.39. FTIR (cm^{-1}) 3318, 2918, 2850, 2362, 1732, 1647, 1534, 1465, 1394, 1358, 1287, 1175, 1053, 993, 755, 721, 665.

2.2.22 Synthesis of (Adamantane-1-carbonyl)-L-aspartate polyester(P8)

Dimethyl (adamantane-1-carbonyl)-L-aspartate: Monomer (0.32g, 0.001mol) and 1,12 dodecanediol (0.36g, 0.001mol were polymerized using $Ti(OBu)_4$ catalyst as described for the polymer P1. Yield=0.82g (91%). ^{1}H NMR (400 MHz, $CDCl_3$) δ ppm 6.39 (1 H, d, *J*=7.58 Hz) 4.84 (1 H, m) 4.15 (2 H, t, *J*=5.99 Hz) 4.07 (2 H, t, *J*=6.72 Hz) 3.65 (1 H, s) 3.03 (1 H, dd, *J*=17.12, 4.16 Hz) 2.86 (1 H, dd, *J*=17.24, 4.52 Hz) 1.98 (5 H, br. s.) 1.70 (4 H, m) 1.59 (16 H, m) 1.28 (20 H, m) ^{13}C NMR (101 MHz, $CDCl_3$) δ ppm 171.5, 171.20, 66.29, 65.53, 51.76, 48.74, 42.79, 37.00, 36.68, 33.16, 29.85, 29.80, 29.56, 29.51, 28.9, 28.81, 28.75, 26.17, 26.08, 26.02 , 1.30, 0.28 . FTIR (cm^{-1}) 2903, 2850, 1732, 1650, 1515, 1452, 1355, 1261, 1198, 1178, 1042, 803, 734.

2.2.23 Synthesis of (4-(Polyethylene glycol monomethyl ether 350) benzoyl)-L-aspartate polyester (P-PEG)

Dimethyl (4-(polyethylene glycol monomethyl ether 350) benzoyl)-L-aspartate Monomer (0.7g, 0.0018mol) and 1,12 dodecanediol (0.21g, 0.0018mol) were polymerized using $Ti(OBu)_4$ catalyst as described for the polymer P1.Yield=0.87g (97%). ^{1}H NMR (400 MHz, $CDCl_3$) δ ppm 7.75 (2 H, m, *J*=8.56 Hz) 7.13 (1 H, d, *J*=7.58 Hz) 6.93 (2 H, m, *J*=8.56 Hz) 5.00 (1 H, m) 4.16 (4 H, t, *J*=4.77 Hz) 4.06 (2 H, t, *J*=6.85 Hz) 3.86 (2 H, t, *J*=4.65 Hz) 3.68 (21 H, m) 3.53 (2 H, m) 3.36 (3 H, s) 3.07 (1 H, d, *J*=4.16 Hz) 2.97 (1 H, d, *J*=4.40 Hz) 1.61 (4 H, dt, *J*=13.82, 6.79 Hz) 1.26 (16 H, m). ^{13}C NMR (101 MHz, $CDCl_3$) δ ppm 171.29, 170.93, 161.62, 128.91, 114.31, 77.31, 76.68, 71.78, 70.73, 70.41, 70.34, 69.44, 67.45, 65.97, 65.19, 58.89, 48.95, 36.27, 29.42, 29.11, 28.42, 28.35, 25.77, 25.68, 0.91, -0.09, FTIR (cm^{-1}) 3780, 3699, 3660, 3343, 2924, 2857, 2361, 1736, 1657, 1606, 1577, 1533, 1499, 1460, 1349, 1295, 1252, 1219, 1179, 1102, 949, 848, 805, 771, 652.

2.2.24 Self-assembly P-PEG

The self-assembly of polymer was studied in water using dialysis method. Polymer (5.0 mg) was taken in clean vial and it was dissolved in 2.0 mL HPLC grade dimethyl sulphoxide. To that 3.0 mL Milli Q water was added drop wise. The solution was stirred for 4 h followed and it was transferred to dialysis tube of MWCO of 1kD. Dialysis was performed against water was replenished after regular interval of time till 24 hours to remove DMSO completely. All the polymers studied for their self-assembly using similar protocol.

2.2.25 DOX loading in polymeric Nanoparticles

5mg of polymer was take in cleaned 25ml vial 2mL of HPLC grade dimethyl sulphoxide was added. 0.5 mg of doxorubicin hydrochloride was added. The doxorubicin hydrochloride was pre-neutralised with the help of triethyl amine. The above mixture was added with 3mL Milli Q water drop wise. This mixture solution was transferred to 1 kD molecular weight cut-off dialysis bag. Then dialysis was performed against Milli Q water for 24 hours. Water was replenished after regular interval of time. The drug loaded polymeric solution was further purified by passing through 0.22µ filter.The drug loading efficiency (DLE) and drug loading content (DLC) were determined by Absorbance spectroscopy using the following equations[6]:

$$\text{Drug or Dye Loading Content (\%)} = \frac{\text{weight of drug or dye in nanoparticle}}{\text{weight of polymer taken}} * 100$$

$$\text{Drug or Dye Loading Efficiency(\%)} = \frac{\text{weight of drug or dye in nanoparticle}}{\text{weight of drug in feed}} * 100$$

2.2.26 CMC determination

The polymer was studied for their self-assembly using pyrene encapsulation method. Critical micellar concentration was determined using fluorescence spectroscopy utilizing pyrene as probe. In this experiment, the pyrene acts as environmental sensitive probe. The concentration of pyrene was maintained as 0.6 µM and the concentration of polymer was varied ranging from 0.5 mg/mL to 10^{-9} mg/mL. Polymeric solution was sonicated for 3 h followed by equilibrating 12 h of time. The samples were purged with nitrogen and fluorescence spectra was recorded. The pyrene was excited at 337 nm and

spectra was collected from 347-500 nm. The ratio of vibronic transition I_1 / I_3 vs logarithm of concentration is plotted to determine the critical micellar concentration (CMC) the break point in the graph corresponds to CMC.

2.2.27 In vitro drug release kinetics

As the nanoparticle synthesized is made up of polyester backbone, it is known to enzymatic cleavage in presence of enzyme under physiological condition[75]. The DOX loaded nanoparticle was subjected to release kinetics in presence of enzyme esterase. The *in vitro* experiment was set up at 37 ºC and pH of buffer was maintained as 7.4. The polymeric nanoparticle was taken in 1X PBS enzyme was 10 U was added. This solution transferred to 1kD dialysis bag and was dialysed against 2 mL 1X PBS. As a control, dialysed solution of DOX loaded nanoparticle was subjected to similar conditions except presence of enzyme. The solution from outside dialysis bag was taken and quantified for their concentration of DOX using absorbance spectroscopy. The concentration of released DOX was quantified over regular interval of time.

2.2.28 Cell Viability Assay (MTT Assay)

The cell viability and biocompatibility of the polymer alone and drug or dye loaded nano particle were studied using MTT assay. The human breast cancer cell (MCF 7) and Wild type mouse embryonic fibroblast (WT MEF) cells were used for these experiments. The experimental procedure is as follows 1000 cells per well were grown in 96 well plate in 100 µL complete media for 16 hours. Then media was aspirated to from 96 well plate and polymeric sample with or without drug or dye was dissolved in complete media and about 300 µL of the samples were added in each well. The complete media was prepared by DMEM media with 1% of penicillin streptomycin solution and 10 % of fetal bovin serum. The cells in 96 well plates were grown for 72 hours in incubator supplied with CO_2 and O_2 about 5% and 1% respectively. After completion of 72 hours the media was aspirated and solution of MTT (0.5mg/mL) in complete media was added and the plates were again incubated for 4 hours. The live cells are having mitochondrial reductase enzyme which convert MTT to formazan crystal. After 4h media was aspirated from the 96 well plates and the HPLC grade Dimethyl sulphoxide was added 100 µL per well. The formazan crystal get dissolved and provide purple colour solution and The plate was the inserted in varioscan microplate reader to record absorbance at 570 nm from each well. From the

concentration of formazan percentage cell viability was calculated by comparing the control value.

2.2.29 Cellular Uptake Studies for Drug or Dye loaded Polymeric Nanoparticles

The cellular uptake of drug or dye loaded polymeric nanoparticle was carried out by fixed cell imaging. To carry out the experiments. The cancerous cell that is MCF 7 was utilized. 10^5 cells were grown on coverslips in 6 well plate. For that purpose, clean and sterilized coverslips was kept in 6 well plate to that 10^5 cells were added along with 2mL complete media. Cells were incubated at 37 °C for 16 h under 5 % CO_2 and 1 % O_2. The polymeric sample prepared by mixing lyophilised solution of polymer along with complete media. This Polymeric solution was added to 6 well plate containing 10^5 cells. The plate was incubated for 4 hours at above-mentioned conditions. These cells were fixed on microscopic slide by following the procedure as follows. media was aspirated from 6 well plate the cells were washed twice with 1 X PBS. In next step cells were added with 4 % solution of paraformaldehyde in water and it was kept for 20 min undisturbed at 4°C. After that cells were washed with 1x PBS twice and finally solution of DAPI was added to it was allowed it treat for 1 min. Excess of DAPI was washed with 1X PBS. On microscopic slides 40 % glyceraldehyde solution was added cover slip was fixed to it using nail paint. The position of cover slip was placed in such a way that the stained cells get exposed to glyceraldehyde solution. The fixed slide was dried for 12-18 hours and it was imaged using Leica SP8 confocal microscopy and processed using ImageJ software.

2.2.30 Hemolysis Assay Compatibility of polymer sample toward RBCs were determined using hemolysis assay. Polymer sample was prepared by dissolving 100µg/mL of polymer solution in 1 X PBS. For hemolysis assay, blood was freshly withdrawn from C57BL/6 mice and RBCs were extracted using centrifugation at 8000 rpm followed by preparation of 5% v/v solution in PBS. 100 µL of polymer solution (in PBS) was added to 100 µL of RBC solution and samples were incubated for 37 ºC for an hour. The experiment was performed in triplicates. 1% solution of Triton-X-100 was used as positive control while PBS was taken as negative control. The samples were centrifuged at 8000 rpm for 5 min and observance of RBC pellet at the bottom of eppendorf was an indication of polymeric biocompatibility. Percentage hemolysis was determined according to reported procedure[24].

2.3 Results and Discussion

2.3.1 Synthesis of monomers

L-Aspartic acid is a natural L-amino acid resource having trifunctional groups consisting of two carboxylic acid and one amine units. The acid groups were converted into dimethoxy ester by esterification using thionyl chloride in methanol to produce aminium salt of L-aspartic dimethyl ester (compound 1). This amine group was masked using various commercial carboxylic acids such as adamantane acetic acid, benzoic acid, toluic acid, 4-t-butyl benzoic acid, stearic acid, and naphthoic acid, and acetic anhydride and their chemical structure of the monomers are shown in Scheme 1. Natural resource-based 3-pentadecyl phenol was attached with acid[77] handle which used to make amide-substituted monomer (see Scheme 2.4).

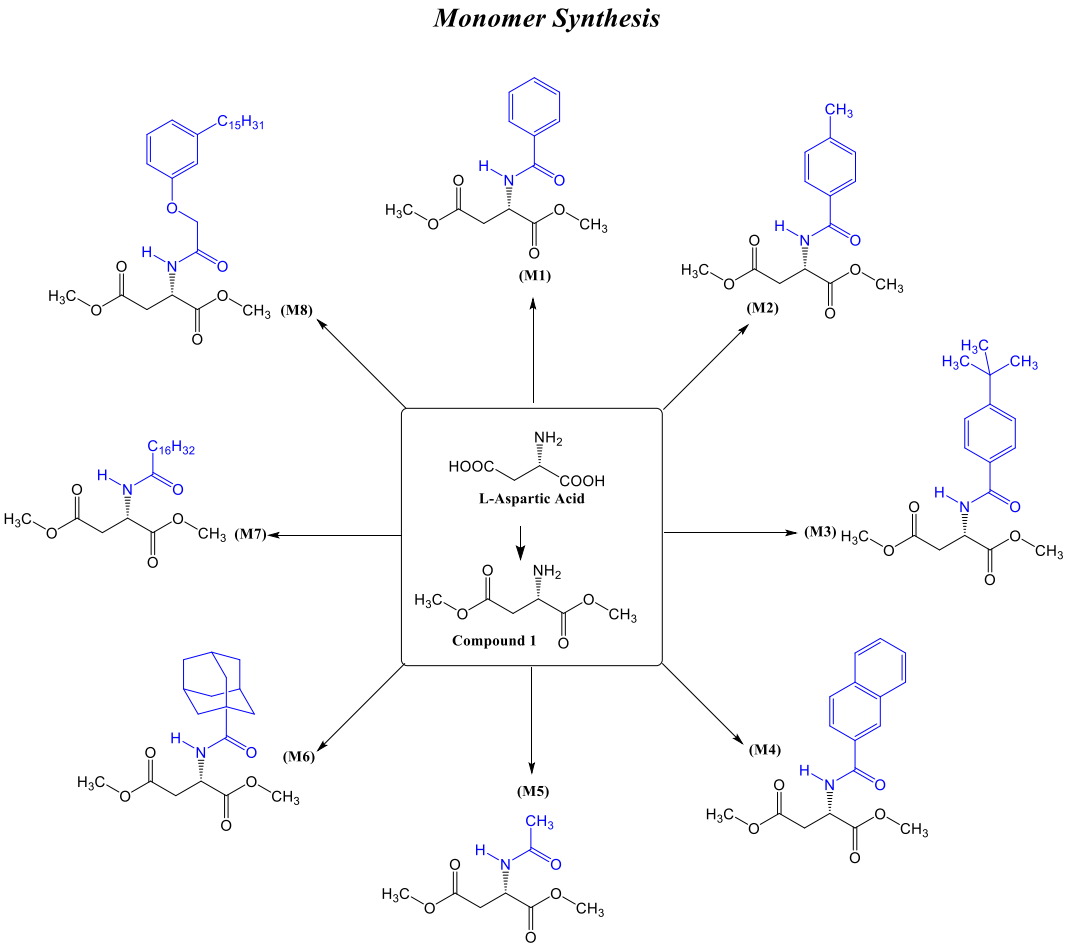

Scheme 2.4 *Synthesis of amide-functionalized L- aspartic acid diester monomers.*

Thermogravimetric analysis of these L-aspartate monomers (Appendix Figure S1) was confirmed their thermal stability up to 180 ºC and established their suitability for solvent free melt polymerisation reactions.

Polymer Synthesis

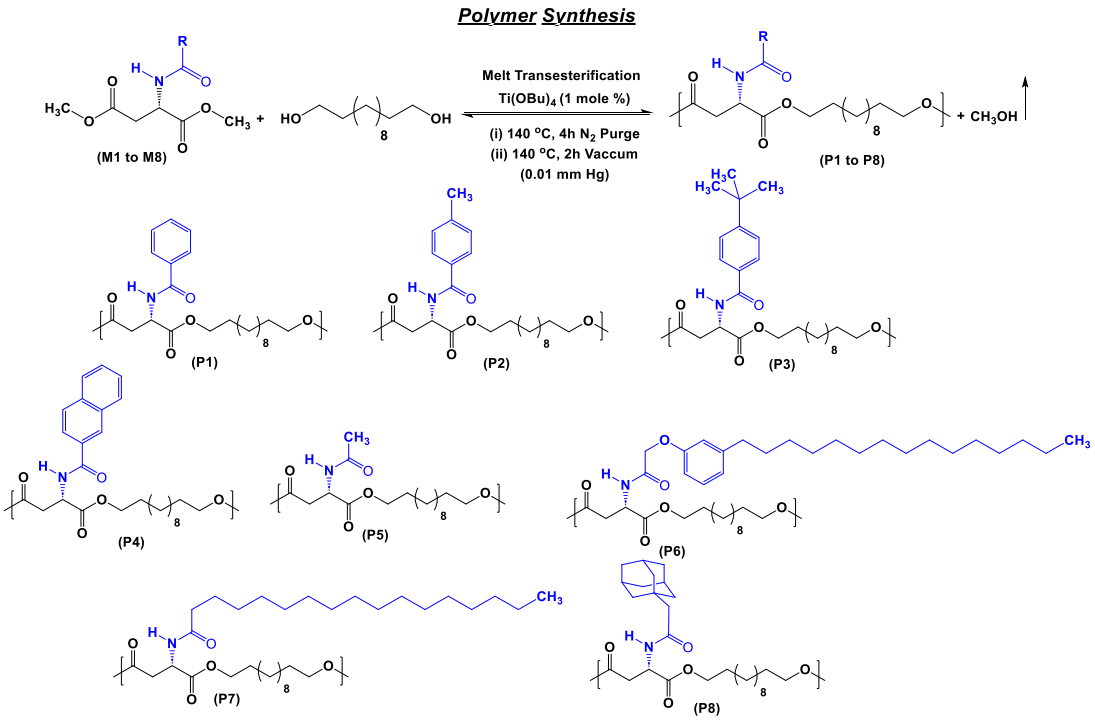

Scheme 2.5 *Melt transesterification process to produce new L-aspartate polyesters.*

The procedure for the polymer synthesis is explained as follows. The L-aspartic monomers were reacted with 1, 12 dodecanediol in test tube shaped reactor and the polymerization was carried out at 140 ºC using 1 mol % of $Ti(OBu)_4$ as a catalyst. The polycondensation process takes place in two stages: (i) initially under nitrogen purging, the nucleophilic attack of the hydroxyl group of diol on carbonyl ester of monomer result in the removal of methanol to produce oligomers of 4-8 repeating units, and (ii) in the second stage, these oligomers further undergo polycondensation under high vacuum (0.01mbar) and the melt viscosity of polymer increased with the formation of high molecular weight of polymers. The polymers were purified by dissolving in THF and re-precipitate into methanol. The polymers were labelled as P1 to P8 and their chemical structures are shown in Scheme 2.5

The polymer was characterized by ^{1}H-NMR and ^{13}C- NMR as shown in Figure 2.4. L-aspartic dimethyl ester is unsymmetrical monomer and the methyl ester peaks were observed at 3.81 and 3.72 ppm (proton-a and a', Figure 2.4a). Upon polycondensation, new ester peaks appeared at 4.08 and 4.18 ppm (proton f an f', Figure 2.4b) and the amide side chain substitution was remained inert during polymerisation

and their peaks are intact. In the ^{13}C-NMR spectra, the monomer methyl ester carbon in the monomer at 52.15 and 53.03 ppm (Figure 2.4c) were completely vanished in the polymer spectrum and new ester peaks appeared at 65.45 and 66.34 ppm (Figure 2.4d).

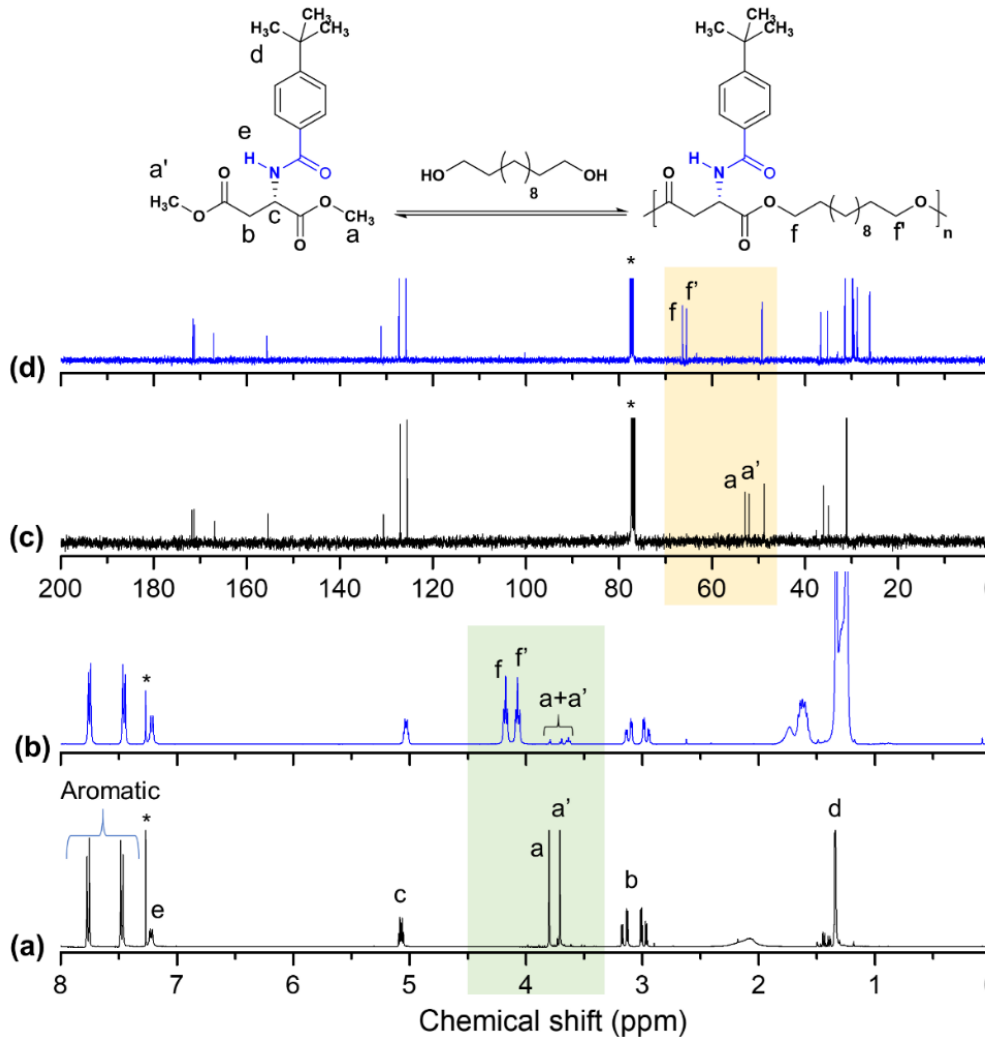

Figure 2.4 *(a) ^{1}H-NMR spectra of dimethyl (4-(tert-butyl) benzoyl)-L-aspartate monomer (M3) and (b) polymer P3 in $CDCl_3$ as solvent. (c) ^{13}C- NMR spectra of dimethyl (4-(tert-butyl) benzoyl)-L-aspartate monomer (M3) and (d) (4-(tert-butyl) benzoyl)-L-aspartate polyester (P3) in $CDCl_3$. The peaks were assigned alphabetical order. Asterisk refers to the solvent peak.*

Similar NMR analysis was carried out for other polymers to confirm their structures in Appendix Figure S2 to S8. The number of repeating units in the polymer chain was determined from ^{1}H-NMR spectroscopy by comparing the integration of new polyester-CH_2 (protons f+f', in Figure 2b) versus methyl ester -OCH_3 which appeared at the chain ends (proton – a and a', in Figure 2b). By this analysis, the number repeating unit in P3 (from Figure 2b) was estimated to be 33-35 repeating unit which corresponding to more

than 97 % conversion [X_n = 1/(1-p)] of monomers to polymers. The number average molecular weight of polymer from NMR were calculated using equation $M_n = X_n \times M_o$; where M_o-repeating unit mass. **Table 2.1** summarizes the % conversion (p), degree of polymerization (X_n or n), and the ^{1}H-NMR based number average molecular weights for polymers P1 to P8. The polymers were produced in 97-98 % conversion with molecular weights of 20,000 g/mol. This result suggests that 97 to 98 % conversion in melt polycondensation is excellent results for new polymer synthesis in the laboratory scale to produce nearly 50 repeating units (more than 99 % conversion is possible only in industrial scale reactions). In solution polycondensation, the organic solvent removal is addition step required to be handled; thus, solution polymerization is not considered to be eco-friendly. Further, the solubility parameters of the monomers and polymers are required to be optimized in order to carryout homogeneous polymerization in solution. Thus, the solution polymerization process is typically chosen if the solvent free melt or bulk polymerization is not possible. In case of melt polycondensation, both monomers are melted (no solvent) and stirred at high temperature to yield the polymer products. In this route as log as we could maintain the temperature of the polymerization above the melting point of the polymers, the reaction proceeds homogeneously. This process typically followed industrial-scale and we make few tons of PET every year by melt polycondensation process. Therefore, the synthesis of polyesters by melt polycondensation process, in principle, could be taken up to industrial scale in long-term. Further for biomedical applications, solvent free process makes more cleaner polymers which is an added advantage.

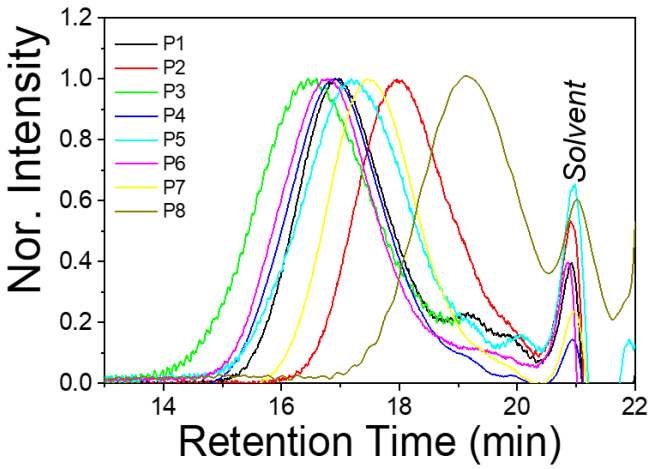

Figure 2.5 *SEC chromatograms of polymers in THF as eluent the column was calibrated with polystyrene standard.*

Table 2.1. *Degree of polymerization and molecular weight of polymers were determined by NMR and SEC.*

Polymer	Monomer	% Conv (p)[a]	X_n[b]	M_n[c] (g/mol)	M_n[d] (g/mol)	M_w[d] (g/mol)	M_w/M_n
P1	*M1*	*98*	*50*	*22900*	*10000*	*19000*	*1.9*
P2	*M2*	*97*	*33*	*13800*	*10300*	*21000*	*2.1*
P3	*M3*	*97*	*33*	*17400*	*19800*	*38800*	*1.9*
P4	*M4*	*98*	*50*	*16000*	*10900*	*23800*	*2.1*
P5	*M5*	*97*	*33*	*11200*	*10200*	*24000*	*2.3*
P6	*M6*	*97*	*33*	*21200*	*13000*	*26800*	*2.1*
P7	*M7*	*96*	*25*	*16700*	*14400*	*24400*	*1.7*
P8	*M8*	*94*	*16*	*7400*	*6000*	*10900*	*1.8*

[a)] Percentage conversion (p) was estimated from ^{1}H NMR. [b)] The degree of polymerization was calculated from ^{1}H NMR using Carothers equation (X_n=1/1-p). [c)]The number average molecular weight (M_n) was calculated using the formula $M_n=M_o \times X_n$ Where M_o is mass of repeating unit. [d)]Molecular weights were determined by SEC using THF as eluent at 25 °C.

The polymers were subjected to molecular weight determination using size exclusion chromatography (SEC) in tetrahydrofuran (THF) solvent. The chromatograms of the polymers in Figure 2.5 revealed that polymers were produced in mono-model distribution confirming the formation of uniform chain length. The number and weight average molecular weights M_n and M_w of polymers were determined in the range of M_n = 6.0 to 19.8 x10^3 g/mol and M_w = 10.9 to 38.8 x10^3 g/mol, respectively. The polydispersity of the polymers was produced closer to 2 which is typically expected for higher conversion (X_w/X_n = 1+p; "p" in mole fraction). The molecular weights obtained from SEC was slightly lower compared to ^{1}H- NMR which is attributed to the usage of polystyrene standards for SEC calibration.

2.3.3 Kinetics of polymerisation

Among all the monomers, M3 was found to produce higher molecular weights along with 1,12 dodecanediol. Lower diol analogues were not tried in the present study since 1, 12 dodecanediol found to be one of the best candidates to yield high molecular weight polymer based on our previous reports[65]. t-Butyl benzoic monomer **M3** was employed to study the kinetics of polymerisation along with 1,12 dodecanediol using 1 mol % of Ti-catalyst as shown in Figure 2.6a. Aliquots were collected at intervals and they were analysed by ^{1}H-NMR as shown in Figure 2.6b, the ^{1}H-NMR spectra of the aliquots are stalked plotted from 30 min to 360 min time interval. From ^{1}H-NMR spectra of the kinetics of the polymerisation it can be observed that at the initial stage of the polymerisation the peaks at 3.7-3.8 ppm can be clearly see which represent

methyl ester of the monomer M3 which shows reduction in intensity of the peak as the polymerisation continues. While the new peak at in the range of 4.1-4.2 ppm confirms the formation of polyester backbone, as it can be seen in Figure 5b the methyl ester peak of monomer gets reduced during polymerisation and new peak backbone peak get increase as the polycondensation progresses. ^{1}H NMR analysis showed that all the polymers were produced 94-98% conversion irrespective of their side chains in the Table 2.1(Page no 89). This implies that the process is very robust and employable to wide ranges of monomers. To understand the kinetics of polymerization, we have chosen M3 monomer (in Figure 2.6) and the ^{1}H NMR was employed to estimate the % conversation vs molecular weight. In principle, the kinetics of the polymerization of other monomers would also expect to follow the similar trend since the melt transesterification process is same in all the cases.

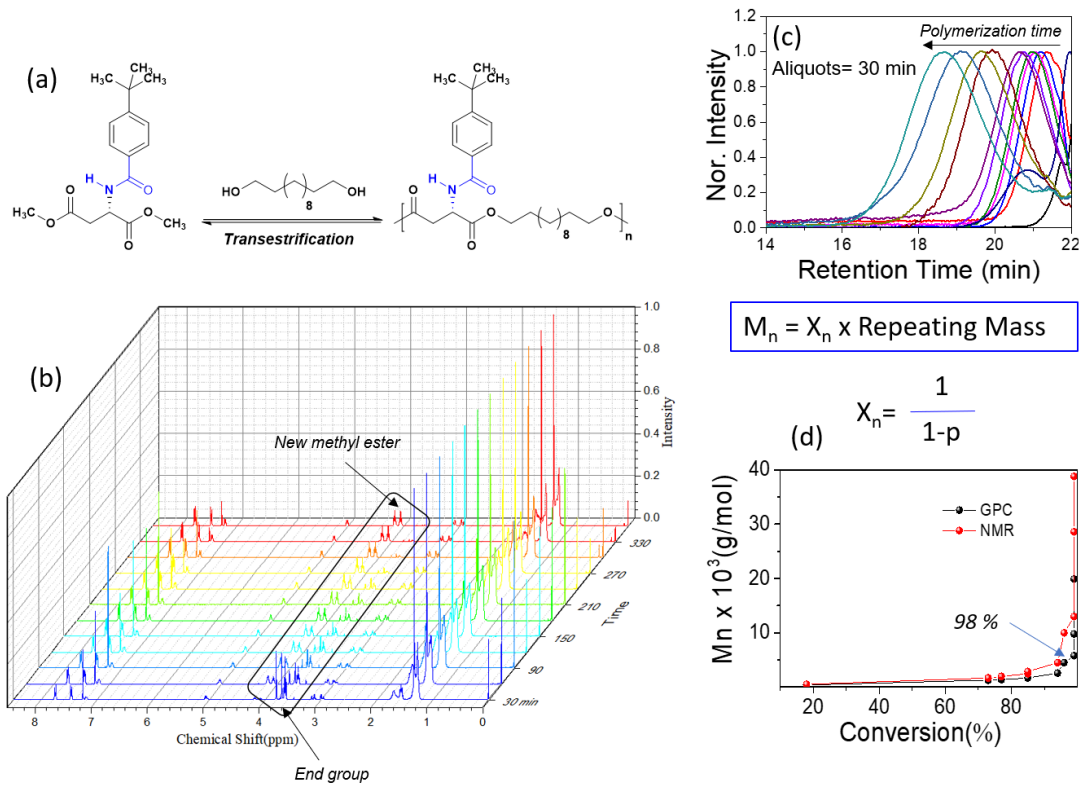

Figure 2.6 *(a)Scheme for the kinetics of the polymerization. (a) ^{1}H NMR spectra of kinetic of polymerisation of P-3. Aaliqoutes were collected each after 30 min for NMR analysis in $CDCl_3$ (b) SEC chromatograms of polymer aliquots taken at various time interval in the polymerization kinetics of P3. (c) Plot on M_n versus the % conversion for the polymerization kinetics of P3.*

The collected aliquots were further characterised with SEC in the THF column. As shown in Figure 2.6c, the SEC chromatogram showed bimodal distribution at the initial stage of polymerisation, and with the progress of the reaction the polymer showed monomodal distribution and appeared at low retention time with respect to the formation of higher molecular weight chains. The molecular weight of the polymer was calculated from the ^{1}H-NMR spectra which is discussed as Figure 2.6a, First the number of repeating units (X_n) of the polymer is calculated by comparing the integration of new appearing peak of the polymer backbone 4.1-4.2 ppm with the end group peak at 3.7-3.8 ppm. From the number of repeating units (X_n), number average molecular weights (M_n) were calculating the formula shown in Figure 2.6. The plots of M_n versus reaction in Figure 2.6d revealed that formation of higher molecular weight polymers with the progress of the reaction time and M_n was obtained to 40,000 g/mol (based on NMR). The nature of the plot further confirms the polymerisation is procced by the polycondensation method. TGA profile of the polymer aliquots as shown in Appendix Figure S9 which shows that with increase in polymerisation time stability of the polymer chain increases.

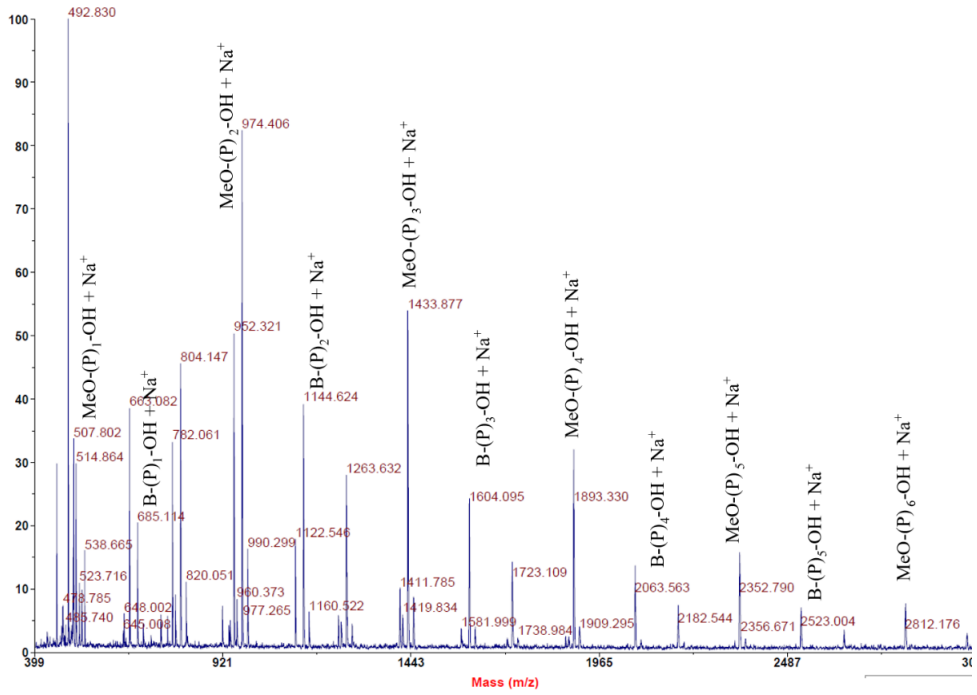

Figure 2.7 *MALDI TOF of polymer aliquots P3 at 150 minutes fraction. Repeating Unit Mass=455g/mol.*

MALDI-TOF analysis of polymer aliquots was carried out in DHB matrix. The polymer chain was analyzed various mass fragments. From the analysis of the MALDI-TOF of the polymer aliquots different fragments of the polymer chains were observed

with different end groups with sodiated or potassiated peaks as shown in Figure 2.7. The MALDI-TOF spectra further confirms the stability of the L-aspartic monomer for melt polymerization reaction to yield high molecular weight polymer products, in addition to that there was no peak of macrocycle was observed.

2.3.4 Catalyst Screening

The catalyst screening experiment was performed to trace the best catalyst for the transesterification polycondensation. Based on our lab literature report various catalyst was chosen. Transesterification catalyst such as $Zn(OAc)_2$, $Cd(OAc)_2$, $LaCl_3$, $Ti(OBu)_4$, dibutyl tin dilaurate, $Sn(Oct)_2$ were chosen based on our earlier experience[66]. The polymerization was carried out with similar setup as explained for P3, Except the catalyst was changed.

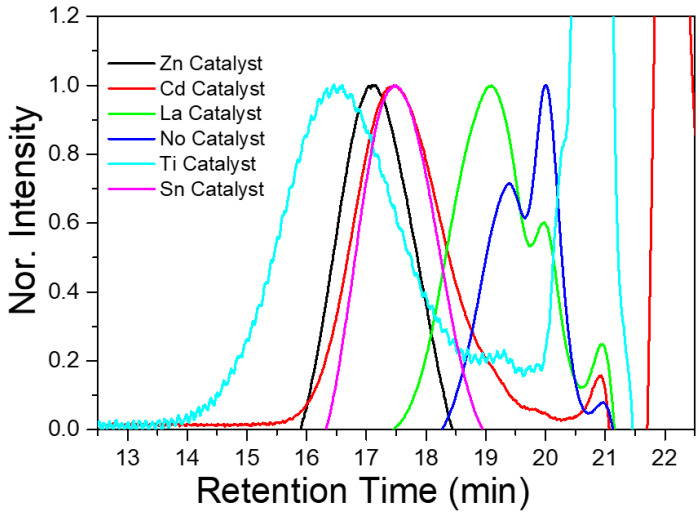

Figure 2.8 *SEC Profile of the polymer P3 synthesized using various catalyst.*

Table 2.2 *Table containing the SEC molecular weights of the polymers in THF at 25 ºC.*

.

Catalyst	M_n^a	M_w^a	M_w/M_n
$Ti(OBu)_4$	*19800*	*38800*	*1.9*
$Sn(Oct)_2$	*5600*	*9900*	*1.7*
DBTO	*5400*	*11200*	*2.0*
$Cd(OAc)_2$	*5400*	*10400*	*1.9*
$Zn(OAc)_2$	*5400*	*10400*	*1.9*
$LaCl_3$	*1300*	*1900*	*1.3*
No Catalyst	*1100*	*1300*	*1.1*

[a)] Molecular weights were determined by SEC using THF as eluent at 25 °C.

Among the various transition metal catalyst, $Ti(OBu)_4$ produced highest molecular weights i.e 19800 g/mol for the L-aspartic acid monomer while other catalyst produce low molecular weight polymer in the range of 5000 to 6000g/mol. While in absence of the catalyst the only oligomer was produced. In the Figure 2.8 SEC chromatogram of the polymers produced from different catalysts are plotted. Polymer synthesized from Ti catalyst showed lowest retention time in SEC as compare to other polymers. The molecular weight t M_n, M_w and PDI of the polymers are summarized in Table 2.2.

2.3.5 Thermal Characterization

The polymers were analysed for their thermal properties using thermogravimetric analysis (TGA) and differential scanning calorimetry (DSC). Thermogravimetric analysis data is show in Figure 2.9. The thermogram revealed that polymers are highly stability all the polymer are stable in the range of 280-300 °C irrespective of their different side chain. All the polymer showed decomposition hump at 380-450 °C this is due to polyester backbone.

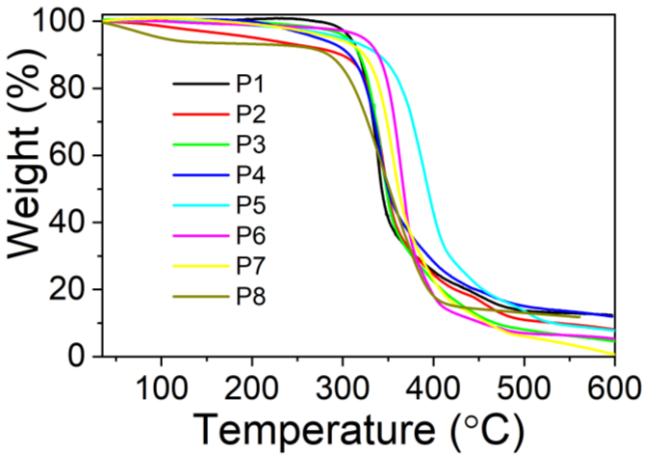

Figure 2.9 *TGA Thermogram of the polymers under nitrogen atmosphere*

The nature of the polymer was determined by Differential scanning calorimetry (DSC). The DSC of the polymers was carried out under the nitrogen atmosphere from the temperature range -50 ºC to 150 ºC. DSC thermogram of the polymers shown as Figure 2.10 revealed that the polymer with different aryl side chain such as benzoyl, Toluyl, 4 Tert butyl benzoyl and Napthoyl in polymer P1, P2, P3 and P4 respectively were found to be amorphous in nature. (See Figure 2.10).

If we compare these polymers side chain containing polymers comparing the first three polymers in the series all these found to be amorphous the first polymer (P1) containing benzoyl group at a side chain found to be having glass transition (T_g) value -7 ºC which expected to have π-π interaction in the solid state. This kind of interaction is hindered in the polymers P2 and P3. In P2 methyl group at the para position of benzoyl which hinders π-π interaction which led to increase in the glass transition (T_g) value -6 ºC. Further bulker group i.e., Ter. Butyl group at para of benzoyl group in the PE-3 increased T_g -1ºC. While like P1 π-π interaction possible in the P4 polymer resulting in to low T_g value as -1ºC. These polymers exhibited glass transition temperature T_g < 10 ºC.

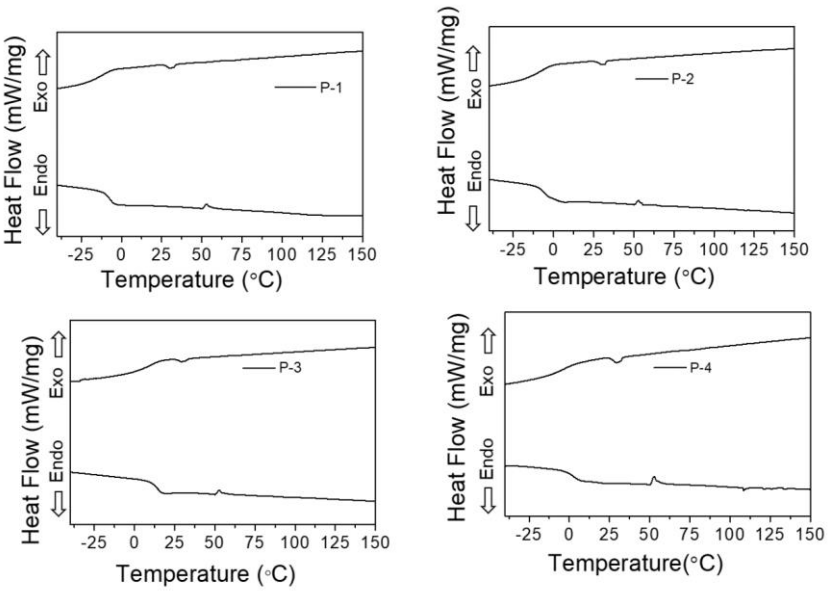

Figure 2.10 *DSC profile of polymer P1 to P4. (DSC was performed at 10 ºC/min under N_2 atmosphere).*

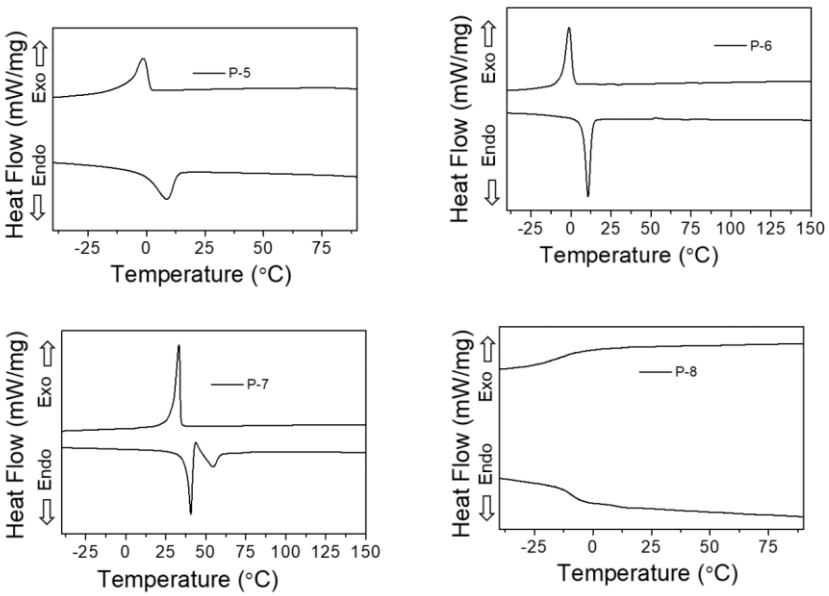

Figure 2.11 *DSC profile of polymer P5 to P8. (DSC was performed at 10 ºC/min under N_2 atmosphere).*

Whereas long aliphatic side chain polymers were found to semi-crystalline (Figure 2.11). Among the series of the polymers P5, P6 and P7 was found to be semicrystalline. In case of P6 pentadecyl unit as side chain while P7 contains stearic as side chain. In both of these cases side chain long aliphatic linkage is responsible for crystalline nature of the polymers. These long chains undergo packing due to inter or intramolecular van der Waals interaction between aliphatic in the microdomain of polymer matrix to give crystallinity to the polymers as shown in Figure S14. Thermal properties of the polymer are summarized in Table 2.3. The polymers exhibited glass transition temperature T_g < 10 ºC. the polymer P6 showed melting transition at 10 ºC with enthalpy of transition 36 J/g while P7 has shown slightly higher melting point at 42 ºC and enthalpy of melting 49 J/g. The P5 showed melting point 8 ºC with enthalpy of melting 30 J/g. The polymer with bulky rigid side chain such as adamantane group as side found to show amorphous in nature with Tg value close to 10 ºC. Thermal characterisation data including TGA and DSC are summarized in the Table 2.3

Table 2.3 *Thermal properties of L-Aspartic acid-based polyester*

Polymer	T_d (°C) [a]	T_g(°C)[b]	T_m(°C)[c]	ΔHm(J/g)[d]	T_c(°C)[e]	ΔHc(J/g)[f]
P1	*280*	*-7.0*	-	-	-	-
P2	*250*	*-6.0*	-	-	-	-
P3	*270*	*-1.0*	-	-	-	-
P4	*280*	*-3.0*	-	-	-	-
P5	*250*	-	*8*	*30*	*-1*	*25*
P6	*260*	-	*40.0*	*36.96*	*33.1*	*36.34*
P7	*240*	-	*10.0*	*69.3*	*-1.0*	*62.8*
P8	*280*	*-10.0*	-	-	-	-

[a)] Temperature of decomposition (T_d) determined from TGA. [b)] The glass transition temperature (T_g) was determined from second heating cycle of DSC thermogram. [c)]Melting point (T_m) of the polyester determined heating cycle of DSC thermogram. [d)] Enthalpy of Melting determined from area under the curve of heating cycle of the of DSC thermogram. [e)] Temperature of Crystallization (T_c) of the polyester determined cooling cycle of DSC thermogram. [f)] Enthalpy of crystallization determined from area under the curve of cooling cycle of the of DSC thermogram.

The above analysis suggested that depending upon the side chain substitution one could readily fine-tuned the semi-crystalline nature of the L-aspartic acid-based polyesters. These aliphatic polyesters were found to be exhibiting good thermal properties; thus, these natural resource derived L-amino acid-based polyesters may have long-term impact in thermoplastic applications. Due to rigid structure and high hydrophobicity, these polymers were found to be not soluble in aqueous medium, and therefore, further structure engineering was introduced to bring appropriate amphiphilicity for aqueous self-assembly to demonstrate their drug delivery capabilities.

2.3.6 Synthesis of PEGlated Monomer

To incorporate appropriate amphiphilicity, a new L-aspartic monomer anchored with polyethylene glycol side chain was designed as shown in Scheme 2.6. PEG-350 monomethyl ether was mesylated using methane sulphonyl chloride to produce compound **2** and then this was coupled with 4-hydroxyl benzoic ester (**3**) to get PEGlated benzoic ester derivative (**4**).

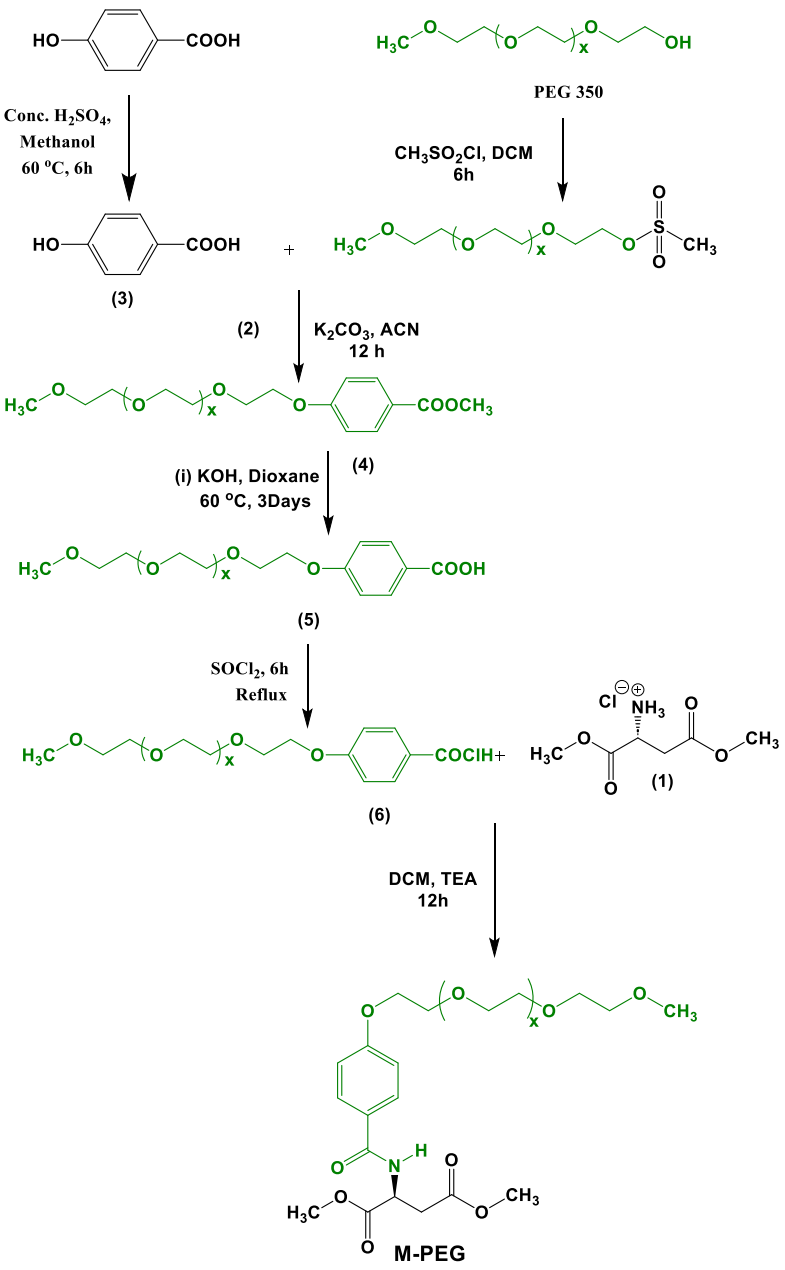

Scheme 2.6 *Synthetic of L- Aspartic acid containing PEG 350 side chain monomer M-PEG.*

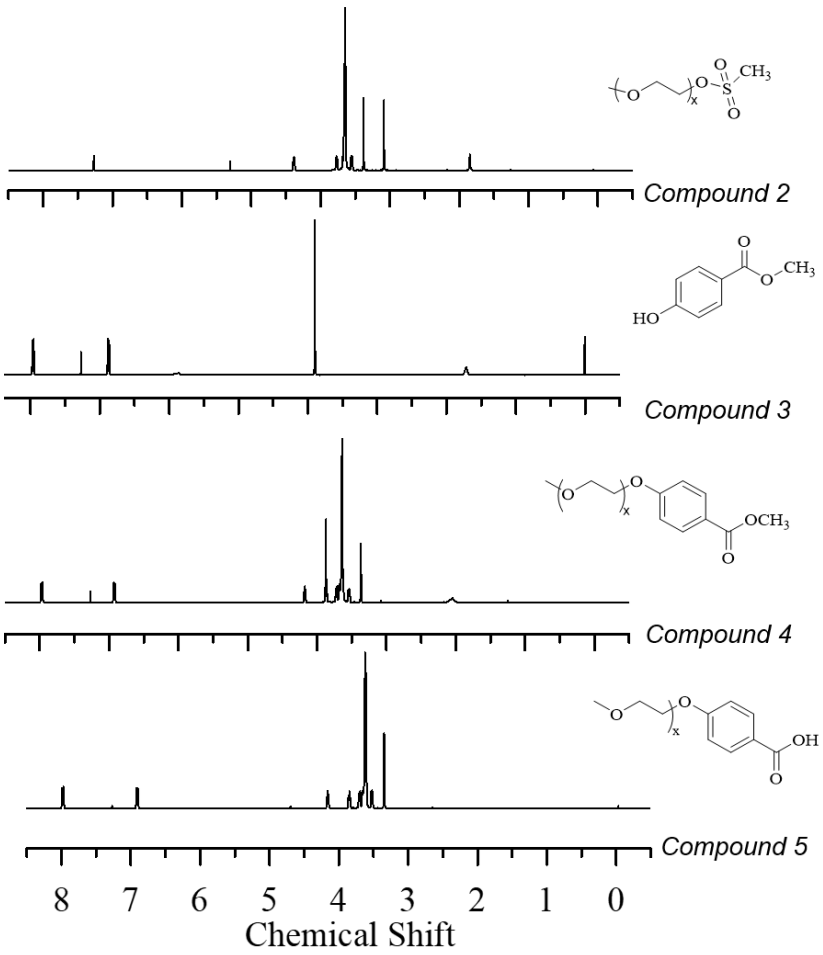

Figure 2.12 *^{1}H NMR spectra of the compounds in $CDCl_3$.*

The resultant methyl ester (**4**) was hydrolysed to corresponding carboxylic acid (**5**) and its acid chloride (**6**) coupled with to L-aspartic ester compound **1** to produce PEGlated monomer **M-PEG.** ^{1}H NMR spectra of compound 2 to 5 is provided as Figure 2.12.

2.3.7 Synthesis of PEGlated Amphiphilic polyester

The monomer M-PEG was polymerized with 1,12 dodecanediol using $Ti(OBu)_4$ to yield amphiphilic polyester **P-PEG** and structure of the polymer was characterized by ^{1}H NMR and ^{13}C-NMR (See Figure 2.13).

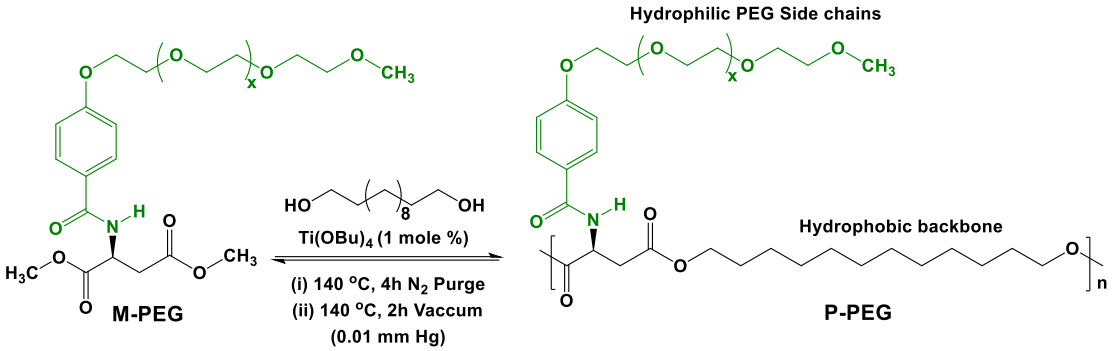

Scheme 2.7 *Synthetic of L- Aspartic acid containing PEG 350 side chain polymer P-PEG.*

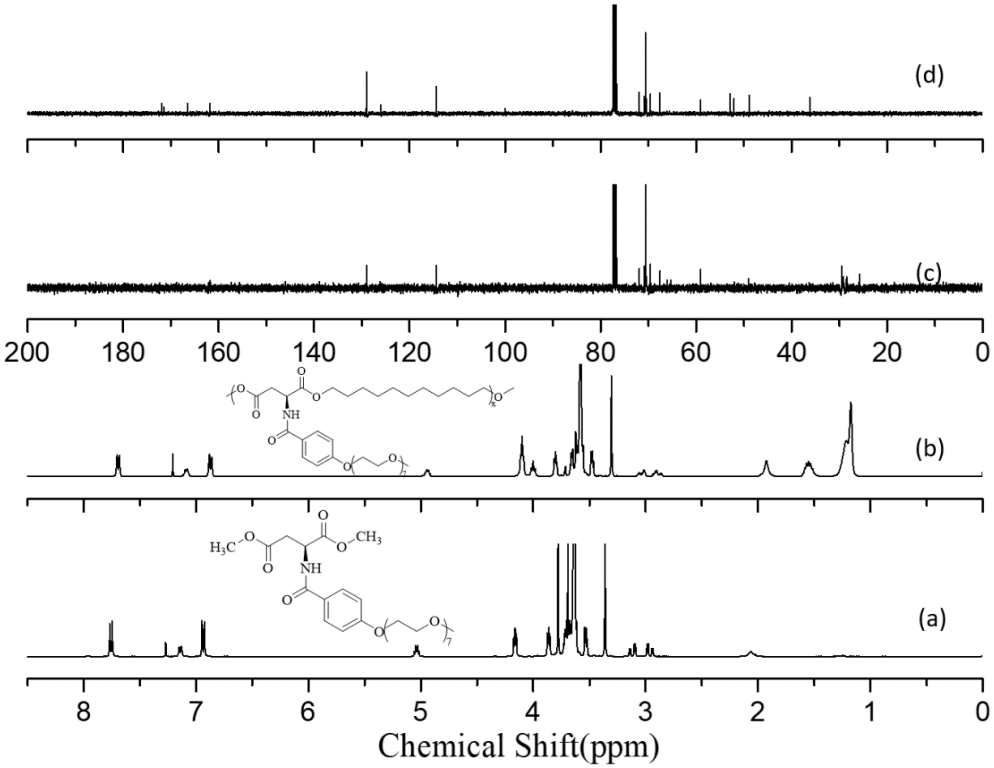

Figure 2.13 *^{1}H NMR spectra of monomer M-PEG (a) and its polymer P-PEG (b). ^{13}C NMR spectra of monomer M-PEG (c) and its polymer P-PEG (d). The spectra were recorded in $CDCl_3$*

Unlike the polymers P1 to P8, the exact determination of X_n by ^{1}H-NMR analysis for P-PEG was not feasible due to the overlap of peaks of the -CH_2CH_2O- of the PEG units along with the $COOCH_3$ end groups. ^{13}C-NMR spectrum of the P-PEG indeed confirmed the disappearance of the carbon atoms in the $COOCH_3$ end groups confirming the formation of high molecular weight polymers.

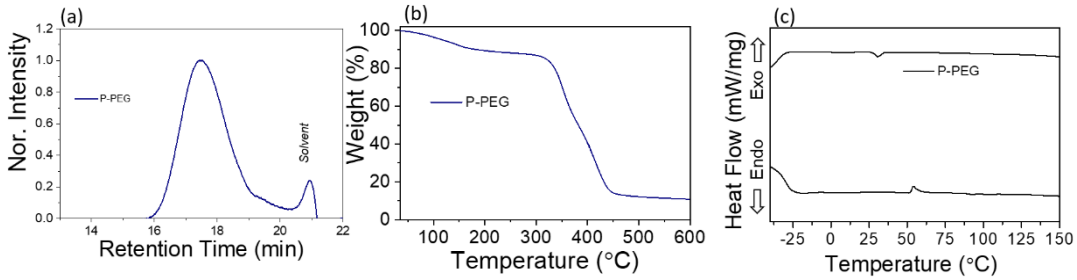

Figure 2.14 *(a) SEC chromatograms of P-PEG in THF as eluent the column was calibrated with polystyrene standard. (b) TGA Thermogram of P-PEG (c) DSC profile of P-PEG.*

SEC of the P-PEG polymer was found to be mono-model distribution with respect to the formation of homogeneous chain lengths (Figure 2.14a); The P-PEG polymer found to produce M_n = 5.6 x10^3 g/mol and M_w = 9.8 x10^3 g/mol with polydispersity index 1.7. The reason for the estimation of low molecular weight for the PEGylated polymer is attributed to the mismatch of the hydrodynamic volume of the polystyrene standard used the SEC calibration (a similar trend was observed in our earlier reports)[67,70]. Similarly the thermal characterisation was carried out using TGA and DSC, P-PEG polymer was found to thermally stable to higher temperature of 350 ºC (See Figure 2.14b). The P-PEG showed amorphous nature with glass transition temperature -30 ºC as shown in Figure 2.14c.

2.3.8 Self-assembly of amphiphilic polyester

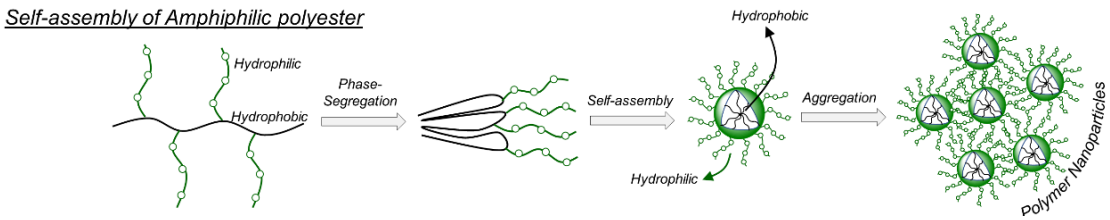

Figure 2.15 *Schematic representation of P-PEG polymer nanoparticle self-assembly in water.*

The P-PEG was comprised of aliphatic polyester hydrophobic backbone and flexible PEGlated hydrophilic side chains and this brought amphiphilic balance which is essential for the self-assembly of polymers in aqueous medium. The polymer was self-assembled by dissolving the polymer (5.0 mg) in DMSO+water mixture (2/3 v/v) and dialyzed using semi-permeable membrane having molecular weight cut-off (MWCO) of 1.0 kDa for 48 h. During this process, the hydrophobic back bone is anticipated to undergo phase segregation into a amphiphiles which self-assembled in to

spherical micelles having hydrophobic core and hydrophilic shell. Subsequent aggregation of the micelles produced aggregated micelles and the entire process is schematically shown in Figure 2.15

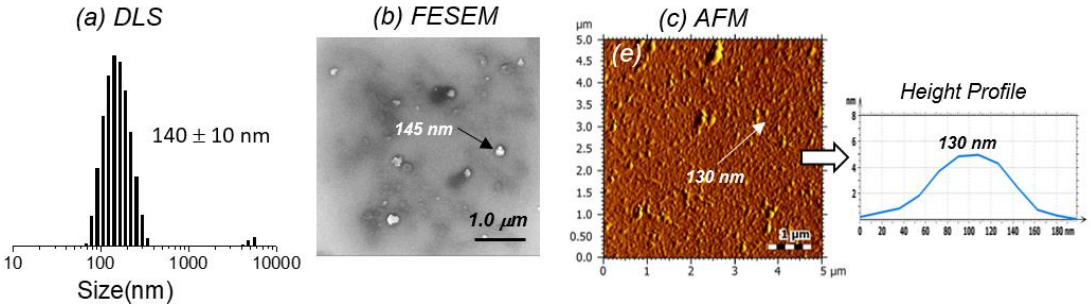

Figure 2.16 *(a) DLS histogram of dialyzed P-PEG solution at 0.1 mg/mL in water (b) FE-SEM image and (c) AFM image along with height profile of P-PEG nanoparticle at 0.1 mg/mL in water.*

The dialysed polymer solution was subjected to dynamic light scattering (DLS) and size of the nanoparticle was found to be in the range of 140 nm±10 in Figure 2.16b. The DLS histogram distribution exhibited polydispersity index of 0.5 suggesting that polymeric nanoparticle is formed in uniform size. The morphology of the polymeric nanoparticle was determined by FESEM and AFM and the images are shown in Figure 2.16b and Figure 2.16c, respectively. FE-SEM image showed the existence of spherical nanoparticle with size of 140 ± 10 nm. AFM image showed the size of the nanoparticle as 130 ± 10nm its spherical shape was further confirmed from the AFM height profile. The size of the aqueous self-assembly of P-PEG by DLS was matching very well that of the FESEM and AFM images confirming the formation of spherical nanoparticles.

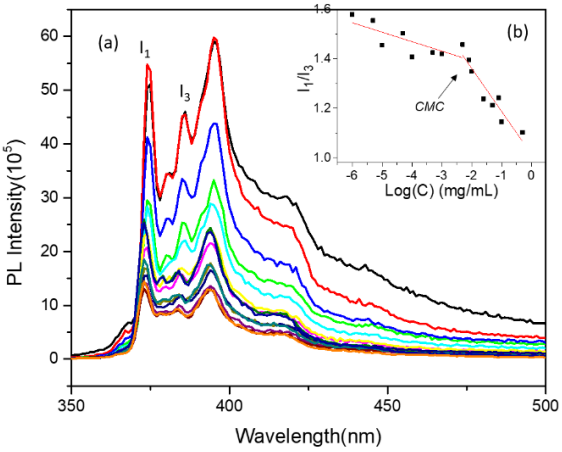

Figure 2.17 *(a)Pyrene emission spectra of CMC Experiment. Pyrene chromophore was excited at (λ_{Ex}= 337 nm and emission collected from 350-500 nm. (b) Plot of I_1/I_3 vs concentration of the P-PEG.*

The critical micelle concentration (CMC) of P-PEG polyester was determined using pyrene as probe following earlier report[6]. The concentration of the pyrene was maintained as 0.6 µM and the polymer concentration was varied from $1.0x10^{-3}$ g/mL to $1.0x10^{-9}$ g/mL. The pyrene was excited at 337 nm and emission spectra was recorded from 350-500nm as shown in Figure 2.17a and the ratio of I_1/I_3 peak was plotted against the P-PEG concentration as shown in Figure 2.17b. The break point with respect to CMC was found to be 4.8µg/mL which agrees with previously reported literature value for PEGlated polymers[67,70]. CMC values for small molecules are reported in the mM, while in case of the polymer it can be reported wither by mM or mg/mL which is acceptable in the literature. Since the structure of the polymers significant vary with respect to the side chains, it is better to follow the mg/mL so that the comparison could be made. Further, the DLC and DLE value and MTT assay data (all biological studies) are also typically reported in mg/mL. Therefore, CMC is mentioned in mg/mL for better clarity.

2.3.10 Thermo-responsive amphiphilic polyester

The polymer P-PEG was found to be thermo-responsive as shown in Figure 2.18a. At ambient temperature (25 °C), the polymer was completely soluble in water whereas the solution became turbid and the polymer chains phase separate up on heating above its lower critical solution temperature (LCST). The polymer chains are soluble in water due to hydration of polyethylene glycol chain (below LCST); however, above LCST the hydrogen bonding between the PEG-oxygen to the surrounded water molecule became feeble as a result the polymers precipitate which in turn increases the turbidity of the aqueous medium.

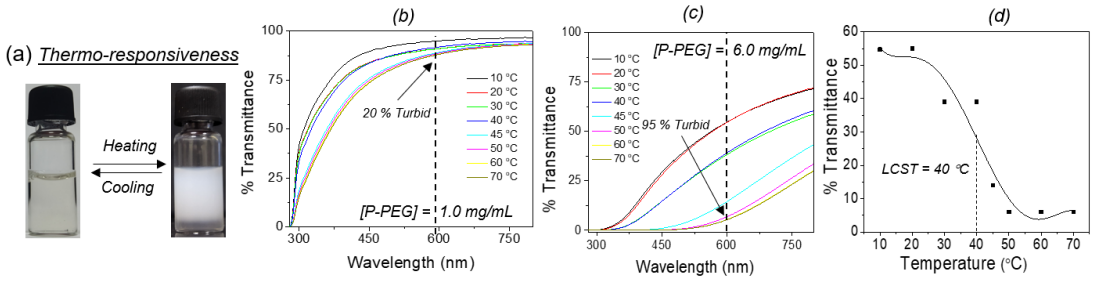

Figure 2.18 *(a) Photograph of vials showing thermo-responsive behavior in the heating and cooling cycles. Variable temperature transmittance at 600 nm of the P-PEG in water for 1.0 mg/mL (b) and 6.0 mg/mL (c) concentrations in the heating cycle. (d) Plot of % transmittance versus the heating temperature of P-PEG at 6.0 mg/mL.*

To study the thermo-responsive nature of the P-PEG sample, it was subjected to temperature dependent transmittance measurement using UV-Vis spectrophotometer. Variable temperature spectra are shown in Figure 2.18b and Figure 2.18c for two different concentrations of P-PEG at 1.0 mg/mL and 6.0 mg/mL, respectively. The plot of % transmittance at O.D. = 600 nm (much away from the absorbance range of polymer) versus the temperature exhibited clear break point at much higher polymer concentrations (Figure 2.18d). The thermo-responsiveness at 1.0 mg/mL was found to be weak whereas the turbidity increased significantly nearly up to 95 % at 6.0 mg/mL. PEGlated polymers of L-lysine polyurethanes and L-tyrosine poly(ester-urethane) s in our previous attempts[67,70] exhibited strong LCST trend at low polymer concentration (1.0 mg/mL), and therefore, they were explored for the thermo-responsive drug delivery concept in cancer cell lines. However, the present L-aspartate based PEGlated polyester exhibited relatively LCST at higher polymer concentration which restrict their exploration as stimuli for drug release. This may be attributed to the fact that both L-tyrosine and L-lysine polymers possessed hydrogen bonding interaction in the polymer backbone via urethane (or carbamate) linkages which is completely lacking in the polyester system. Despite the polyesters were indeed structurally engineered with side-chain hydrogen bonding unit, they lack strong thermo-responsive characteristics. This implies that further structural engineering may be required to optimise the thermo-responsive in L-aspartate polyesters and separate efforts required to address this aspect. Nevertheless, it is important to note that the L-aspartate polyester has two aliphatic ester linkages per repeating unit; thus, the polymer chains are highly suitable for lysosomal enzymatic-biodegradation at intracellular compartments for drug delivery which is an added advantage compared to earlier system.

2.3.11 Drug or Biomarker Encapsulation in polymer Nanoparticles

To study the encapsulation capability of the P-PEG nanoparticles drug molecules such as doxorubicin (DOX), camptothecin (CPT), curcumin (CUR); and biomarkers like Rose Bengal (RB), Nile Red (NR), Rhodamine-B (RhB) and 8-hydroxy-pyrene-1,3,6-trisulfonic acid sodium salt (HPTS) were attempted by dialysis method. Typically, 5.0 mg of the polymer and 0.5 mg of the cargo were taken in DMSO+ water (2.0+3.0 mL) solvent mixtures and dialyzed against Milli Q water for 48 h. Among all the cargoes

attempt for loading only DOX, CUR, RB and HPTS showed very stable encapsulation in the P-PEG.

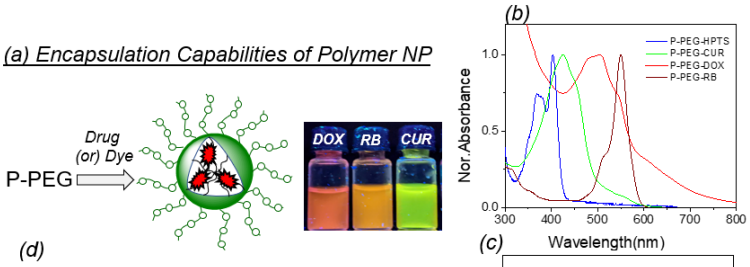

(d)

Sample	Drug/Dye	DLC (%)	DLE (%)
P-PEG-RB	RB	1.8	18.2
P-PEG-DOX	DOX	4.5	45.0
P-PEG-CUR	CUR	3.8	38.0
P-PEG-HPTS	HPTS	3.4	34.2

Figure 2.19 *(a) Schematic diagram of drug (or dye) loaded P-PEG self-assembly in water. The photograph of vials showing P-PEG-DOX, P-PEG-RB and P-PEG-CUR nanoparticle under photoexcitation using UV lamp. (b) Absorption spectra of drug (or dye) loaded P-PEG nanoparticles. (c) Emission spectra of drug (or dye) loaded nanoparticles (λ_{exc} at absorbance maxima). (d)Table containing the drug (or dye) loading content (DLC) and drug (or dye) loading Efficiency (DLE).*

The photographs of the vials and the table in Figure 2.19a summarizes these drug or dye loaded samples. The drug (or dye) loading content (DLC) and drug (or dye) loading efficiency (DLE) were determined by absorbance spectroscopy. Among the various cargoes DOX was loaded 4.5% while other cargoes such as CUR, HPTS and RB was loaded in lower amount i.e., 3.8%, 3.4% and 1.8%, respectively (See Figure 2.19d). These samples are referred as P-PEG-DOX, P-PEG-CUR, P-PEG-RB, and P-PEG-HPTS. In Figure 2.20a, the DLS of the DOX loaded samples exhibited the existence of 75 ± 10 nm sized nanoparticles. Morphology of P-PEG-DOX was found to be spherical in shape with average diameter of 100 nm which is confirmed by FESEM in Figure 2.20b and AFM in Figure 2.20c. DLS histograms of P-PEG-CUR, P-PEG-RB, and P-PEG-HPTS also confirmed the existence of <200 nm nanoparticles (Figure 2.21).

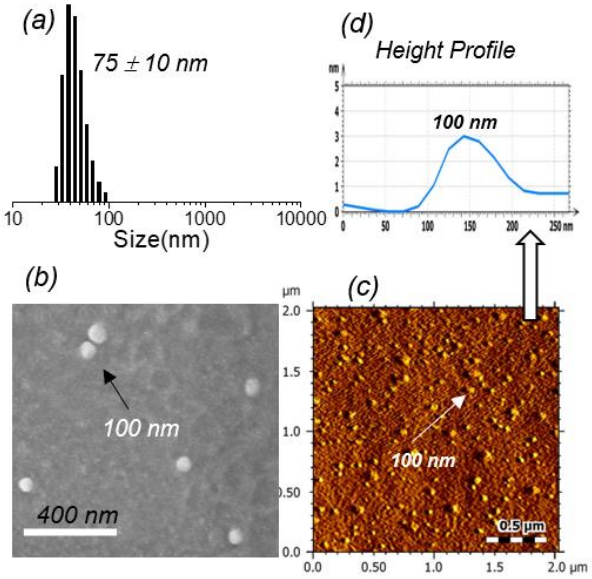

Figure 2.20 *(a) DLS histogram for of P-PEG-DOX nanoparticle at 0.1 mg/ml. (b)FE-SEM image and (c) AFM-image (d) of P-PEG-DOX nanoparticles.*

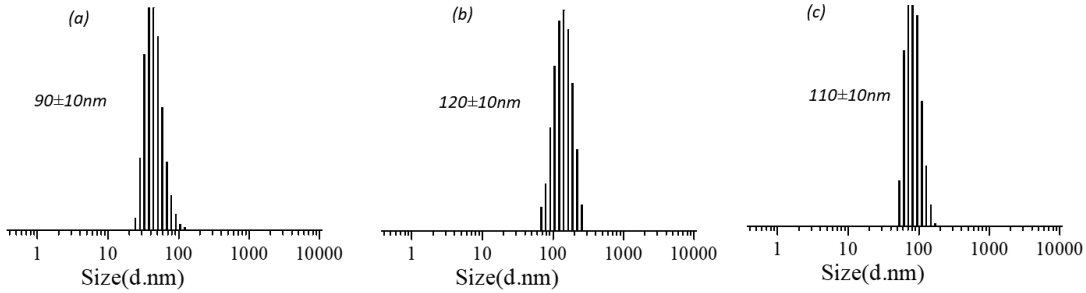

Figure 2.21 *DLS profile for (a) P-PEG-CUR, (b) P-PEG-RB, and (c) P-PEG-HPTS. Concentration = 0.1 mg/ml.*

The drug or dye loaded nanoparticle was subjected to study photophysical using absorbance and emission spectra. Absorbance and emission spectra of drug or dye loaded nanoparticle is shown in Figure 2.19b and Figure 2.19c, respectively. The λ_{max} of absorbance and emission maxima of the drug and dye loaded P-PEG samples are similar to that of their free drugs and dyes [75]. This implies that the newly designed PEGlated L-aspartate polymer nanoparticle was efficient in loading wide ranges of cargoes in the nanocavity and the photophysical properties of the drug or dye chromophores were also retained in aqueous medium for bioimaging applications.

2.3.12 Enzyme-Responsive Release

Lysosomal-enzymes at the intracellular compartments are very well known to biodegrade aliphatic polyester polymeric nanoparticle to release the drug molecules as

shown in Figure 2.22a[73].To study the drug releasing capabilities of P-PEG polymer NP, *in vitro* experiment was designed in such a manner that polymer was incubated with the esterase enzyme under physiological condition. P-PEG-DOX sample was incubated with 10 U horse liver esterase enzyme at physiological temperature 37 ºC and pH of the PBS was maintained at 7.4

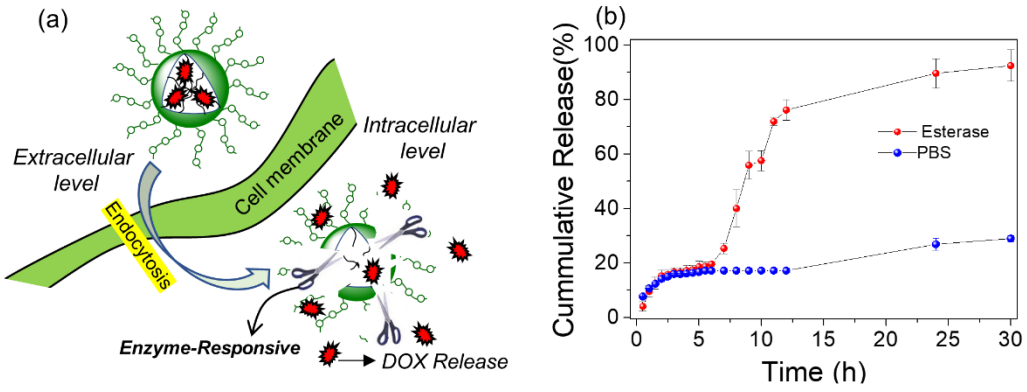

Figure 2.22. *(a) Schematic representation of cellular uptake by endocytosis and doxorubicin release from PE-PEG-DOX nanoparticle by the action of lysosomal enzymes at the intracellular level. (b) Doxorubicin release profile from PE-PEG-DOX nanoparticle with and without of esterase enzyme at 37 ℃ in pH= 7.4.*

. The polymeric solution with enzyme was added to dialysis tube of 1 kD. The PBS 7.4 pH was taken in outer reservoir so that the released doxorubicin can be monitored. The concentration of doxorubicin released was monitored using absorbance spectroscopy and the cumulative DOX release was estimated and plotted in Figure 2.22b. As a control experiment doxorubicin release kinetics in absence to enzyme also studied in PBS alone at pH 7.4. The plot in Figure 6b proved that nearly 92 % drug was released in presence of enzyme. The 20 % leaching out of DOX from the NP in the absence of enzyme is attributed the effect of PBS salt in the partial destabilization of the NP at 37 ºC. The drug release kinetics follows two-step release patterns during initial 6 h both the sample with esterase and without esterase enzyme shows equal amount of DOX release this is due to disassembly of the polymeric nanoparticle after this stage esterase enzyme acts on the polymer backbone causing the enzyme triggered release of the DOX. This experiment mimics the action of various enzyme at intracellular compartment of the cell and validated the enzymatic-biodegradation of the tailor-made P-PEG NPs. The process of endocytosis is an energy dependent process

which is assisted at normal physiological temperature while the free DOX is taken up by the cells using simple diffusion [75].

2.3.13 Temperature dependent endocytosis

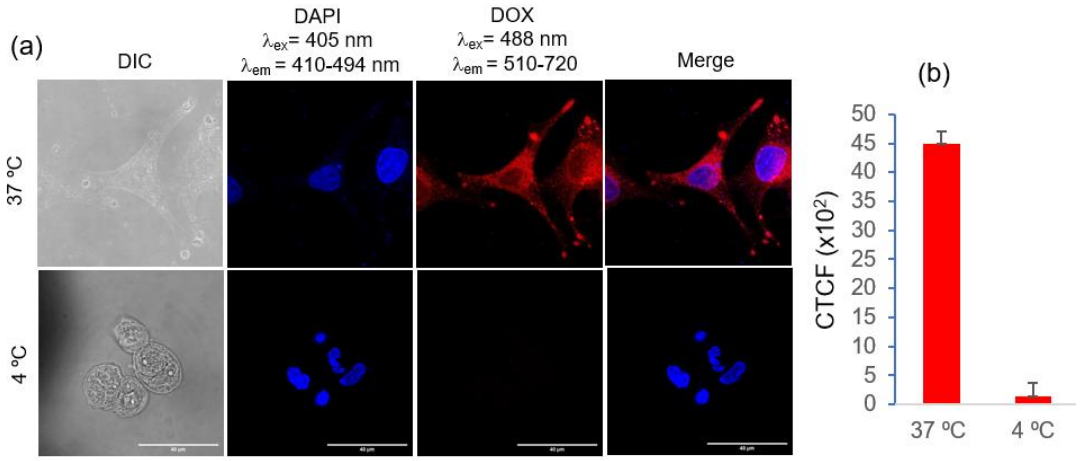

Figure 2.23: *(a) Confocal microscopy images of temperature dependent cellular uptake of P-PEG-DOX at 37 ºC and 4 ºC. (b) Plot of CTCF values against the incubation temperature.*

To prove the nanoparticle is taken by endocytosis temperature dependent experiment was carried out. About 10^5 cells were grown in two separate 6 well plate for 24 h. P-PEG-DOX with DOX concentration was maintained as 5µg/mL and the plots were separately incubated at 37 ºC and at 4 ºC for 4h. After 4h, the cells were fixed with 4 % paraformaldehyde and stained with DAPI and subjected for confocal microscopic imaging. DOX was excited with 488 nm laser and signals were acquired from 510-720 nm whereas the DAPI was excited using 405 nm laser and signals acquired from 410-494 nm. The images in Figure 2.23a clearly evident that the DOX has been substantially taken up by the cells at 37 °C while negligible amount was seen at 4 °C. The amount of DOX taken up by the cells was further quantified by CTCF calculation and plotted in Figure 2.23b. Corrected total cell fluorescence (CTCF) = Integrated density– (area of selected cell × mean fluorescence of background readings[75]. It was observed that at the physiological temperature P-PEG-DOX was taken up by the cells is 10 time higher as compare to P-PEG-DOX at 4 ºC. Hence, the cellular uptake studies revealed that newly designed L-aspartate amphiphilic polyester

P-PEG has excellent ability to endocytosis under physiological temperature and also susceptible to enzymatic-biodegradation to deliver the cargoes at the intracellular level.

2.3.14 Haemolysis Study of polymer nanoparticles

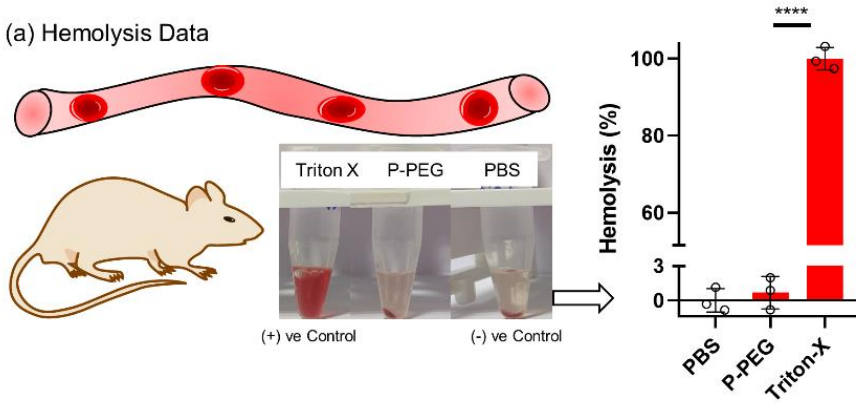

Figure 2.24. *Haemolysis study of P-PEG (0.1 mg/mL) with Triton-X as positive control and PBS as negative control. Corresponding data shown in photograph of centrifuge tube). (****p<0.0001). Each point represents mean ± SEM (n = 3)*

For any polymeric biomaterial, it is vital to understand its biocompatibility with different cell types at physiological condition. In blood, RBCs are the most abundant cell type and for polymeric intravenous delivery, it should be hemocompatible[23,24]. To determine its compatibility, 0.1 mg/mL P-PEG polymer solution (in PBS) was incubated with RBC solution for one hour at 37 ºC in static incubator. The solution was taken in eppendorf and centrifuged at 8000 rpm for 5 min. In case of positive control (0.1 % Trx), the whole solution appeared red in colour (as shown in Figure 2.24) due to complete lysis of RBCs while for negative control (in PBS), an undisturbed RBC pellet was observed at the bottom of the eppendorf which accounts for no lysis. In case of polymer sample (P-PEG), RBCs were found to be completely intact at the bottom of the eppendorf (see Figure 7a photograph). The % hemolysis for P-PEG polymer sample along with positive (0.1% Trx) and negative control (PBS) is plotted in Figure 2.24. For P-PEG polymeric sample, % hemolysis value was found to be 2 % which was significantly lower as compared to positive control which confirms that polymer is extremely compatible to RBCs and can be employed for intravenous delivery.

2.3.15 Cytotoxicity studies of the polymer and loaded cargo

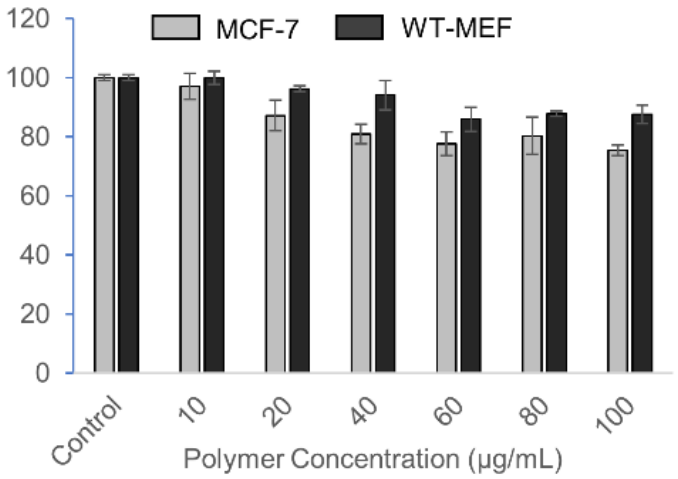

Figure 2.25. *Cytotoxicity of P-PEG in MCF 7 and WT MEF cell lines for 72 h incubation. [10^3 cells are used for seeding in the cytotoxicity studies].*

MTT assay was employed to study cytotoxicity of polymer nanoparticle in nascent form and loaded with DOX anticancer drug or RB and HPTS biomarkers. To study cytotoxicity two different cell lines were chosen non-cancerous WT MEF (Wild type Mouse embryonic fibroblast, non-cancerous cell line) and other breast cancerous cell lines MCF 7. The concentration of polymer alone was studied from 1.0 µg/mL to 100 µg/mL as shown in Figure 2.25.

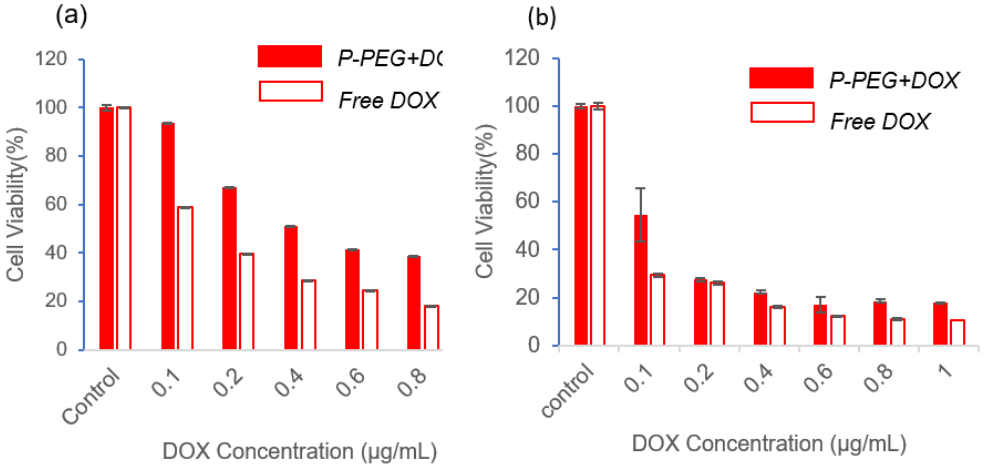

Figure 2.26. *Cytotoxicity of free doxorubicin and PE-PEG-DOX nanoparticle in (a)MCF cell line (b) WT MEF. [10^3 cells are used for seeding in the cytotoxicity studies].*

The polymer P-PEG was found to be non-toxic towards both normal and cancerous cell lines. The P-PEG-DOX and free DOX were studied for their cytotoxicity and the concentration of DOX was maintained in the range of 0.1 µg/mL to 1.0 µg/mL.

The IC_{50} value was found to be 0.4 µg/mL and 1.0 µg/mL for free DOX and P-PEG-DOX in Figure 2.26. The IC_{50} value for the DOX delivery from the P-PEG NP platform is comparable to that of other polymeric scaffolds reported earlier[77,70].

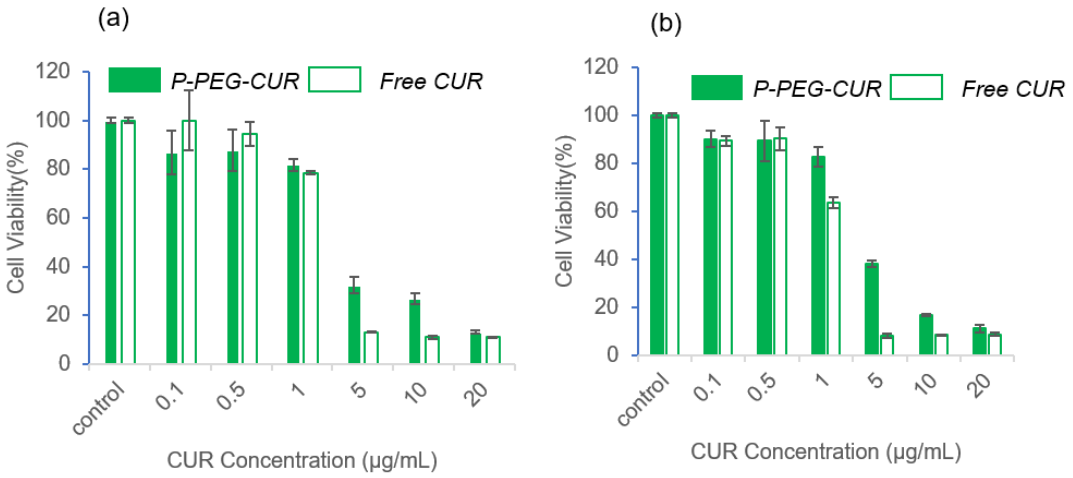

Figure 2.27 *Cytotoxicity of free curcumine and PE-PEG-CUR nanoparticle in (a)MCF cell line (b) WT MEF. [10^3 cells are used for seeding in the cytotoxicity studies].*

Anti-inflammatory drug curcumin was also tested for toxicity in MCF 7 and WT MEF; The concentration of CUR was maintained from 0.1µg/mL to 20µg/ml. It was found that Free CUR and P-PEG-CUR are equally effective in inhibiting the cancer cell growth. Both the sample were able to inhibit the growth of cancer cells up to 70 % at the concentration of 5µg/mL (see Figure 2.27). The bio-probes loaded samples P-PEG-HPTS and P-PEG-RB and these bio-probe in free form were found to be non-toxic toward both WT MEF and MCF 7 in Figure 2.28.

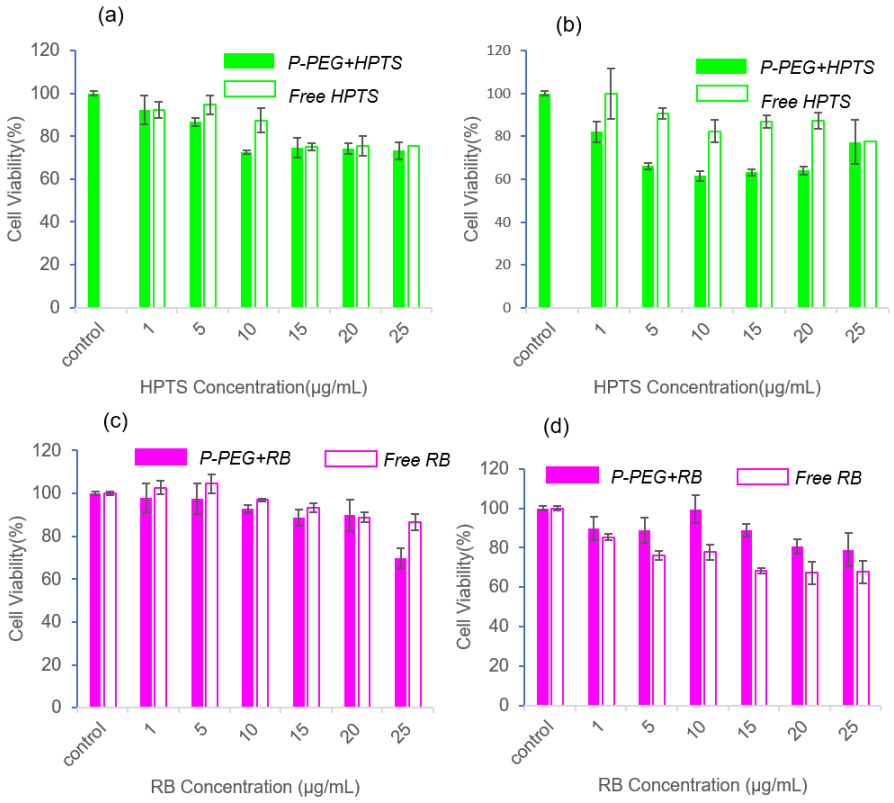

Figure 2.28 *Cytotoxicity of free HPTS and PE-PEG-HPTS nanoparticle in (a) MCF cell line (b) WT MEF. Cytotoxicity of free RB and PE-PEG-RB nanoparticle in (c)MCF cell line (d) WT MEF. [10^3 cells are used for seeding in the cytotoxicity studies].*

2.3.16 Cellular Uptake Studies

The ability of P-PEG polymer to transport the loaded cargoes (DOX, CUR, RB and HPTS) across the cell membrane for their cellular uptake was studied in MCF 7 cell line. The experiment was setup to study the uptake of drug and dye in free and loaded form. 10^5 Cells were seeded on glass cover slip and grown for 24 h. Concentration of fluorophore was kept same for free dye and loaded dye as 5 µg. The cells along with fluorophore was incubated for 6 h and fixed. The mechanism of uptake of polymeric nanoparticle was studied at the cellular level using confocal laser scanning microscopy (CLSM).

When the cellular uptake of the Free HPTS and P-PEG-HPTS was carried outby incubating the MCF 7 cells with concentration of HPTS about 5 µg. The uptake was studied for the period of 6h and the nuclei of the cells were stained with Acridine Orange (AO). The nuclear staining agent DAPI cannot be in this as it could interfere with HPTS signal. HPTS were excited using 405 nm laser and collection was done in

range of 410 nm-494 nm and AO was excited using 488 nm laser and collection of the AO was done in a range 510 nm-570 nm. From confocal images it was observed that HPTS was taken up by the cells in both free and P-PEG-HPTS form as shown in Figure 2.29a.

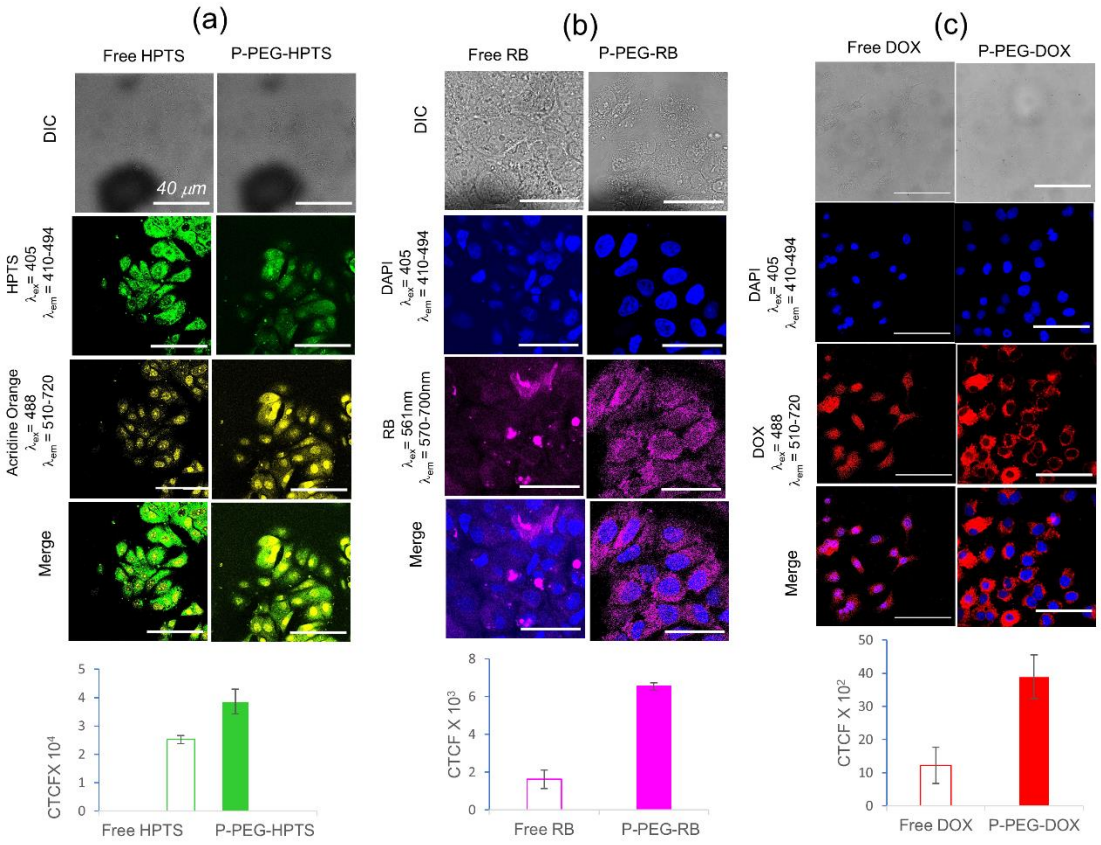

Figure 2.29 *Confocal images of cellular uptake and corresponding their CTCF values of (a) free HPTS and P-PEG-HPTS, (b) free RB and P-PEG-RB, and (c) free DOX and P-PEG-DOX in MCF 7 cell line. The images were recoded for fixed cells after 6 h incubation [10^5 cells were seeded]. Concentration of the RB, DOX and HPTS were maintained as 5.0 μg/mL.*

The green signal from the cells refers to the presence of HPTS while yellow colour is given to AO. Merge images shows that Free HPTS after 6h of incubation, found to be localised in cytoplasm while P-PEG-HPTS taken up by the cells shows signal were also observed in nucleus along with the cytoplasm. In case of P-PEG-HPTS uptake merge image shows presence of intense yellow signal at nucleus. The uptake of the HPTS was further confirmed by the CTCF calculation. It was found that P-PEG-HPTS was taken up more compare to free HPTS.

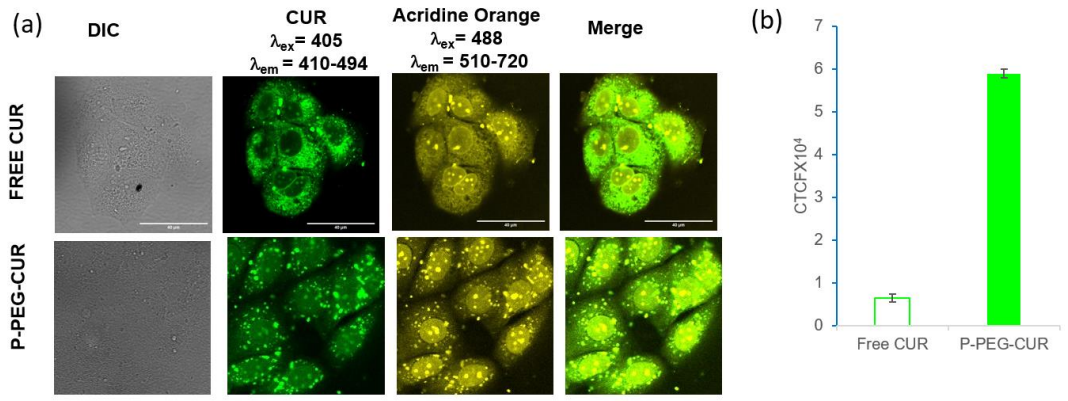

Figure 2.30 *(a)Confocal images of cellular uptake and (b)corresponding their CTCF values of free CUR and P-PEG-CUR in MCF cell line. The images were recoded for fixed cells after 6 h incubation [10^5 cells were seeded]. Concentration of the CUR HPTS were maintained as 5.0 µg/mL. Scale bar = 40µm.*

Uptake studies of anti-inflammatory drug curcumin (CUR) was also performed for 6h in MCF 7 cells. Free CUR and P-PEG-CUR concentration was maintained as 5 µg. Nuclei was stained with AO. Confocal Images of the cells were carried out by using similar settings as used for HPTS samples. λ_{max} of CUR is at 420nm therefore 405nm laser was used to excite CUR and emission signals were collected at 410 nm-494 nm and AO was excited using 488 nm laser and collection of the AO was done in a range 510 nm-570 nm, signal from curcumin is shown in green colour while AO signal marked with yellow colour. Figure 2.30 shows that free CUR predominantly found in the cytoplasm while P-PEG-CUR sample was taken up by cells signals were found nuclei along with cytoplasm which is indicated by intense yellow colour in merge image. CTCF plot shows that P-PEG-CUR was taken up 5-fold more as compare to free CUR.

RB and P-PEGRB uptake was also quantified by CLSM images, DAPI was used to stain the nuclei in this case. After the 6h of incubation of fluorophore. It was observed that RB in free form was up taken in very less quantity as compare to P-PEG-RB. Figure 2.29b show confocal images pink colour from cells is due to presence of RB inside the cells, blue colour shows nuclei due to DAPI staining. CTCF plot further confirm that P-PEG-RB was taken up in more quantity as compare to free RB.

2.3.17 Time dependent Cellular uptake studies of Free DOX vs P-PEG-DOX

The cellular uptake for both free DOX and polymer loaded with DOX i.e., P-PEG-DOX was studied using MCF 7 cell line to demonstrate ability of drug loaded nanoparticle to deliver the drug. The DOX is very well-known anticancer drug with kills the cells by intercalation between the base pairs for DNA double stranded helix and disrupts the mechanism of topoisomerase II enzyme of DNA repair which lead to death of the cell. The experiment was setup to study cellular uptake 10^5 Cells were grown on the coverslips for 24 h. Then the cells were exposed to DOX about 5µg of DOX added to the cells and allowed to uptake for 4 h. After uptake the cells were fixed and stained with DAPI as it is known to exclusively stain nucleus. DOX was excited with 488 nm laser and signals were acquired from 510-720 nm whereas the DAPI was excited using 405 nm laser and signals acquired from 410-494 nm as mentioned earlier.

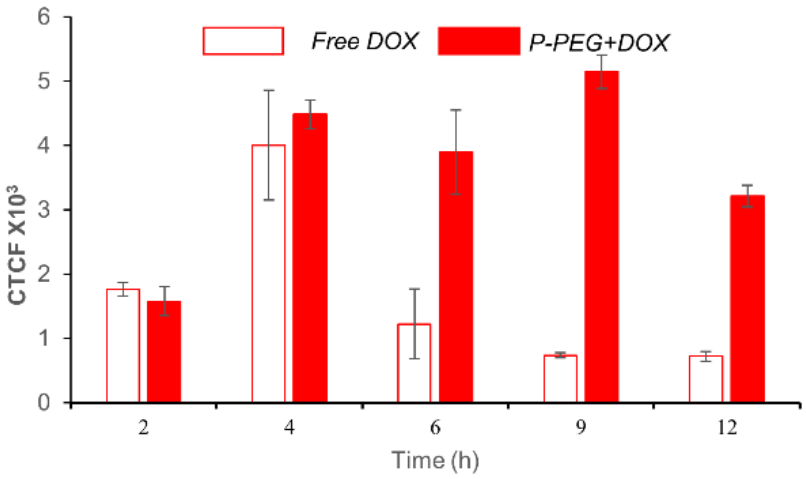

Figure 2.31 *Plot of CTCF values against the incubation time*

In Figure 2.31, it was found that DOX loaded nanoparticles were shown emission was coming from cytoplasm while free DOX directly reaches to nucleus. Overlay merge of two images taken at DOX channel and DAPI channel produce magenta colour. it was further confirmed that free DOX was predominantly found inside the nucleus while DOX loaded inside the polymer NPs showed emission form both nucleus and the cytoplasm. Free DOX is small molecule and it would readily excrete from the cytosol by the p-glycoprotein pump (have pore diameter of 5 nm) which is very well acceptable and reported phenomena in biological studies. On the other hand, the larger size polymer NPs (~ 100 nm) retained in the cytosol and not

possible to excrete by p-glycoprotein pump that enabled their prolonged internalization in the cells. This results in the enhanced intensity of the polymer+DOX compared to that of DOX alone. The mechanism of cellular uptake was further studied to study in a time dependent manner. The free DOX and P-PEG-DOX nanoparticles were exposed to cell lines such as at different time point such as 2h, 4h, 6h, 9h and 12h. The CLSM images are shown in Figure 2.32.

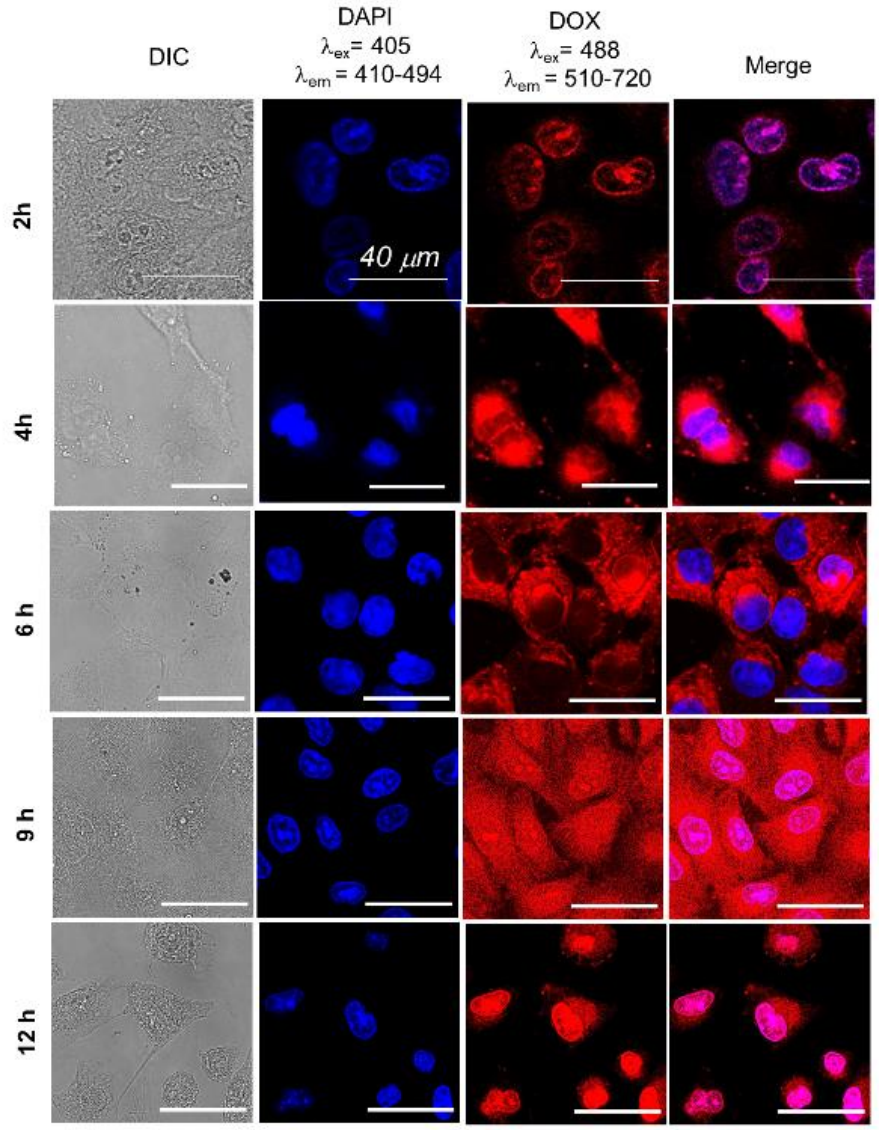

Figure 2.32 *Time-dependent cellular uptake P-PEG-DOX at various time interval as 2h, 4h, 6h, 9h, and 12h in MCF 7 cell line. The concentration of DOX was maintained as 5.0 μg/mL.*

The amount of the DOX inside the cells were calculated by CTCF calculation. It was found that free DOX was taken up by the cell very fast as compare to DOX loaded inside the polymer NPs. The free DOX enters the cell by passive diffusion process while the polymer NPs enters the cell by process of endocytosis. Free DOX as it is taken up faster by the cell it is also cleared up quickly by efflux pump of Multi Drug Resistance (MDR) Cells. To overcome this resistance polymer NPs helps as they are larger in size. Free DOX was taken up by the cells in 6h and also cleared up in before 9h as shown in Figure 2.33.

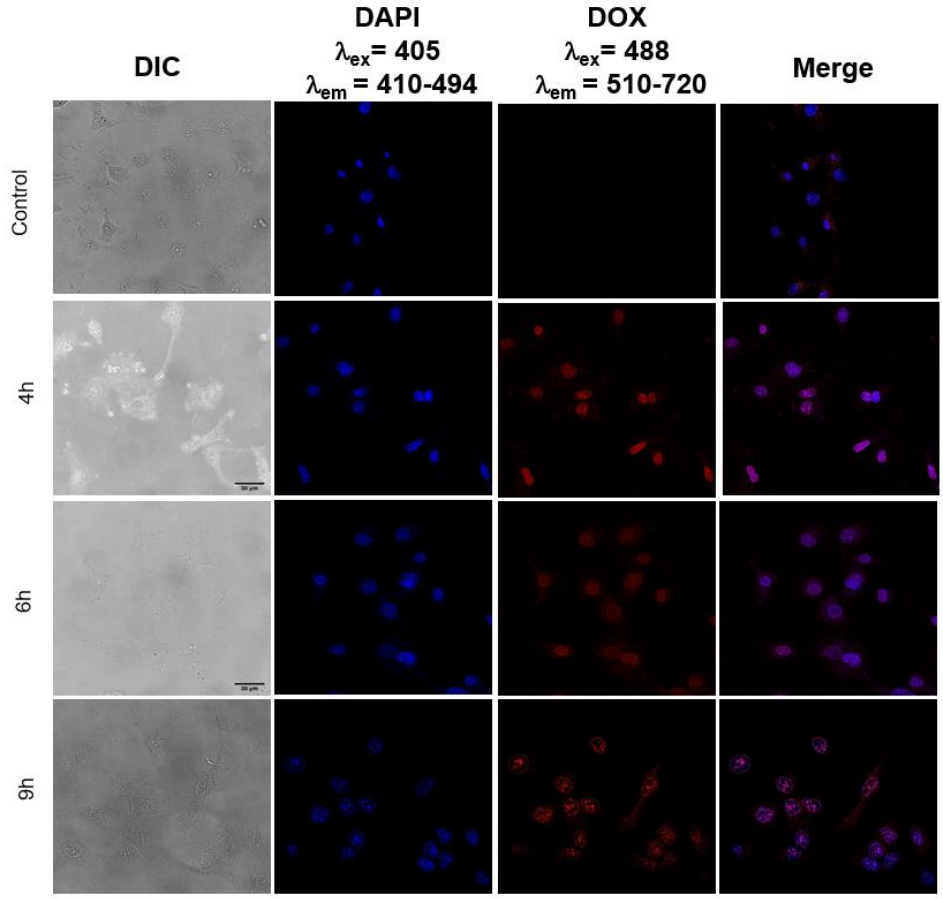

Figure 2.32 *Time-dependent cellular uptake fixed cell imaging of Free DOX at various time interval as 4h, 6h, 9h, and 12h. The concentration of DOX was maintained as 5.0 µg/mL. Scale bar = 30µm.*

While polymer NPs enters inside the cell by the process of endocytosis, which is energy dependent process. The nanoparticle is taken by the cell slowly to lysosome were polymer gets degraded by the action of enzymes and release the loaded cargo in side cytoplasm and the DOX reaches inside nucleus. The present investigation reports the development of amide-substituted L-aspartic acid; however, the approach is not restricted to few selected examples, and in principle, the approach could be expanded

to wide ranges of aliphatic polyesters with different functionality for instance the amide-handle could also be expanded to anchoring fluorophores, drug molecules or targeting agents, etc. Currently efforts are taken in these lines to expanded the scope of the melt polycondensation strategy to L-amino acid-based polyesters development.

2.4 Conclusion

L-Aspartic acid based different side chain containing amide functionalised polymer was synthesized using melt polycondensation strategy. Various aromatic and aliphatic acid were conjugated to dimethyl ester monomer and polymerised with 1,12 dodecane diol to produce high molecular weight polyester. These polymers were characterised with the help of NMR and SEC and was found to produce high molecular weight polymers. Titanium tetrabutaoxide ($Ti(OBu)_4$) found to produce highest molecular weight polymer as compare to other catalyst. Kinetic of polymerisation was studied using ^1H NMR and SEC, the plot Mn vs percentage conversion(p) obtained shows the similar trends as anticipated for polycondensation process. TGA data shows that the polymers are stable in the range of 280-300 ºC. Thermal behaviour of the polymers shows that all the polymers amorphous (with T_g below 10 ºC) in nature except the polymer containing long pendent chain such as stearate and penta decyl phenol as side chain. Then to make the polymer water soluble the P-PEG functionalised polymer was designed which was capable of undergoing self-assembly in aqueous medium to produce spherical nanoparticle. These polymer NPs were found to be capable of loading drugs and biomarker such as doxorubicine (DOX), curcumin (CUR), rose bengal (RB) and 8-hydroxypyrene-1,3,6-trisulfonic acid trisodium salt (HPTS). Biodegradable nature of the polyester backbone was indirectly proved by *in vitro* drug release kinetics. The polymer alone nanoparticle was found to be biocompatible with both normal (WT MEF) and cancerous cell lines (MCF 7). While the drug loaded polymer NPs i.e P-PEG-DOX and P-PEG-CUR showed inhibition in the growth of WT MEF and MCF 7 cells. The uptake of drug loaded polymer micelle was confirmed by confocal microscopy. CTCF calculations shows that the P-PEG-DOX was taken up by the cell in higher amount as compare to free DOX. Time and temperature dependent cellular uptake study showed that polymer NPs taken up by the process of endocytosis while free drug was taken up by the cells by diffusion process. The present investigation emphasized on development of amide functionalised polyester from L-aspartic acid and its application as efficient drug delivery nanocarrier.

2.5 References:

(1) Hasani-sadrabadi, M. M.; Sarrion, P.; Nakatsuka, N.; Young, T. D.; Taghdiri, N.; Ansari, S.; Aghaloo, T.; Li, S.; Khademhosseini, A.; Weiss, P. S.; Moshaverinia, A. Hierarchically Patterned Polydopamine- Containing Membranes for Periodontal Tissue Engineering. *ACS Nano* **2019**, *13*, 3830–3838. https://doi.org/10.1021/acsnano.8b09623.

(2) Liang, Y.; He, J.; Guo, B. Functional Hydrogels as Wound Dressing to Enhance Wound Healing. *ACS Nano* **2021**, *15*, 12687–12722. https://doi.org/10.1021/acsnano.1c04206.

(3) Xu, H.; Yao, Q.; Cai, C.; Gou, J.; Zhang, Y.; Zhong, H.; Tang, X. Amphiphilic Poly(Amino Acid) Based Micelles Applied to Drug Delivery: The in Vitro and in Vivo Challenges and the Corresponding Potential Strategies. *J. Control. Release* **2015**, *199*, 84–97. https://doi.org/10.1016/j.jconrel.2014.12.012.

(4) Yin, L.; Song, Z.; Kim, K. H.; Zheng, N.; Tang, H.; Lu, H.; Gabrielson, N.; Cheng, J. Reconfiguring the Architectures of Cationic Helical Polypeptides to Control Non-Viral Gene Delivery. *Biomaterials* **2013**, *34*, 2340–2349. https://doi.org/10.1016/j.biomaterials.2012.11.064.

(5) Sun, H.; Meng, F.; Dias, A. A.; Hendriks, M.; Feijen, J.; Zhong, Z. α-Amino Acid Containing Degradable Polymers as Functional Biomaterials: Rational Design, Synthetic Pathway, and Biomedical Applications. *Biomacromolecules* **2011**, *12*, 1937–1955. https://doi.org/10.1021/bm200043u.

(6) Malhotra, M.; Surnar, B.; Jayakannan, M. Polymer Topology Driven Enzymatic Biodegradation in Polycaprolactone Block and Random Copolymer Architectures for Drug Delivery to Cancer Cells. *Macromolecules* **2016**, *49*, 8098–8112. https://doi.org/10.1021/acs.macromol.6b01793.

(7) Chen, R.; Funnell, J. L.; Quinones, G. B.; Bentley, M.; Capadona, J. R.; Gilbert, R. J.; Palermo, E. F. Poly(pro-Curcumin) Materials Exhibit Dual Release Rates and Prolonged Antioxidant Activity as Thin Films and Self-Assembled Particles. *Biomacromolecules* **2023**, 24, 204-307. https://doi.org/10.1021/acs.biomac.2c01135.

(8) Yang, P. B.; Davidson, M. G.; Edler, K. J.; Brown, S. Synthesis, Properties, and Applications of Bio-Based Cyclic Aliphatic Polyesters. *Biomacromolecules* **2021**, *22*, 3649–3667. https://doi.org/10.1021/acs.biomac.1c00638.

(9) Jérôme, C.; Lecomte, P. Recent Advances in the Synthesis of Aliphatic Polyesters by Ring-Opening Polymerization. **2008**, *60*, 1056–1076. https://doi.org/10.1016/j.addr.2008.02.008.

(10) Surnar, B.; Jayakannan, M. Delivery under the Gastrointestinal Tract. *Biomacromolecules* **2013**, *14*, 4377–4387.

(11) Buzin, P.; Lahcini, M.; Schwarz, G.; Kricheldorf, H. R. Aliphatic Polyesters by Bismuth Triflate-Catalyzed Polycondensations of Dicarboxylic Acids and Aliphatic Diols. *Macromolecules* **2008**, *41*, 8491–8495.

(12) Cai, Q.; Bai, T.; Zhang, H.; Yao, X.; Ling, J.; Zhu, W. Catalyst-Free Synthesis of Polyesters via Conventional Melt Polycondensation. *Mater. Today* **2021**, *51*,

155–164. https://doi.org/10.1016/j.mattod.2021.07.024.

(13) Labet, M.; Thielemans, W. Synthesis of Polycaprolactone : A Review W. *Chem. Soc. Rev.* **2009**, *38*, 3484–3504. https://doi.org/10.1039/b820162p.

(14) Woodruff, M. A.; Hutmacher, D. W. Progress in Polymer Science The Return of a Forgotten Polymer — Polycaprolactone in the 21st Century. *Progress in Polymer Science* **2010**, *35*, 1217–1256. https://doi.org/10.1016/j.progpolymsci.2010.04.002.

(15) Kamaly, N.; Yameen, B.; Wu, J.; Farokhzad, O. C. Degradable Controlled-Release Polymers and Polymeric Nanoparticles : Mechanisms of Controlling Drug Release. *Chem. Rev* **2016,** *116*, 2602-2663. https://doi.org/10.1021/acs.chemrev.5b00346.

(16) Middleton, J. C.; Tipton, A. J. Synthetic Biodegradable Polymers as Orthopedic Devices. *Biomaterials* **2000**, *21*, 2335-2346. https://doi.org/10.1016/S0142-9612(00)00101-0.

(17) Aliphatic, H.; Design, P.; Trollsås, M.; Lee, V. Y.; Mecerreyes, D.; Lo, P.; Mo, M.; Miller, R. D.; Hedrick, J. L. Hydrophilic Aliphatic Polyesters: Design, Synthesis, and Ring-Opening Polymerization of Functional Cyclic Esters. *Macromolecules* **2000**, 4619–4627. https://doi.org/10.1021/ma992161x.

(18) Samadi, N.; Van Nostrum, C. F.; Vermonden, T.; Amidi, M.; Hennink, W. E. Mechanistic Studies on the Degradation and Protein Release Characteristics of Poly(Lactic-Co-Glycolic-Co-Hydroxymethylglycolic Acid) Nanospheres. *Biomacromolecules* **2013**, *14*, 1044–1053. https://doi.org/10.1021/bm301900t.

(19) Rainbolt, E. A.; Washington, K. E.; Biewer, M. C.; Stefan, M. C. Recent Developments in Micellar Drug Carriers Featuring Substituted Poly(ε-Caprolactone)S. *Polym. Chem.* **2015**, *6*, 2369–2381. https://doi.org/10.1039/C4PY01628A.

(20) Surnar, B.; Sharma, K.; Jayakannan, M. Core-Shell Polymer Nanoparticles for Prevention of GSH Drug Detoxification and Cisplatin Delivery to Breast Cancer Cells. *Nanoscale* **2015**, *7*, 17964–17979. https://doi.org/10.1039/c5nr04963f.

(21) Surnar, B.; Jayakannan, M. Triple Block Nanocarrier Platform for Synergistic Cancer Therapy of Antagonistic Drugs. *Biomacromolecules* **2016**, *17*, 4075–4085. https://doi.org/10.1021/acs.biomac.6b01608.

(22) Kulkarni, B.; Surnar, B.; Jayakannan, M. Dual Functional Nanocarrier for Cellular Imaging and Drug Delivery in Cancer Cells Based on π-Conjugated Core and Biodegradable Polymer Arms. *Biomacromolecules* **2016**, *17*, 1004–1016. https://doi.org/10.1021/acs.biomac.5b01654.

(23) Ghosh, R.; Malhotra, M.; Ravindra, R.; Sathe, M.; Jayakannan, M. Biodegradable Polymer Theranostic Fluorescent Nanoprobe for Direct Visualization and Quantitative Determination of Antimicrobial Activity. *Biomacromolecules* **2020,** *21*, 2896-2912. https://doi.org/10.1021/acs.biomac.0c00653.

(24) Ghosh, R.; Jayakannan, M. Theranostic FRET Gate to Visualize and Quantify Bacterial Membrane Breaching. *Biomacromolecules* **2022** *ASAP* . https://doi.org/10.1021/acs.biomac.2c01202.

(25) Vert, M. Aliphatic Polyesters: Great Degradable Polymers That Cannot Do Everything. *Biomacromolecules* **2005**, *6*, 538–546. https://doi.org/10.1021/bm0494702.
(26) Martin, E. V; Kibler, C. J. (12) United States Patent. **2002**, *1* (12).
(27) Guo, B.; Chen, Y.; Lei, Y.; Zhang, L.; Zhou, W. Y.; Rabie, A. B. M.; Zhao, J. Biobased Poly(Propylene Sebacate) as Shape Memory Polymer with Tunable Switching Temperature for Potential Biomedical Applications. *Biomacromolecules* **2011**, *12*, 1312–1321. https://doi.org/10.1021/bm2000378.
(28) Moyori, T.; Tang, T.; Takasu, A. Dehydration Polycondensation of Dicarboxylic Acids and Diols Using Sublimating Strong Brønsted Acids. *Biomacromolecules* **2012**, *13*, 1240–1243. https://doi.org/10.1021/bm300231d.
(29) Derosa, C. A.; Kua, X. Q.; Bates, F. S.; Hillmyer, M. A. Step-Growth Polyesters with Biobased (R)-1,3-Butanediol. *Ind. Eng. Chem. Res.* **2020**, *59*, 15598–15613. https://doi.org/10.1021/acs.iecr.0c03009.
(30) Pang, C.; Zhang, J.; Wu, G.; Wang, Y.; Gao, H.; Ma, J. Renewable Polyesters Derived from 10-Undecenoic Acid and Vanillic Acid with Versatile Properties. *Polym. Chem.* **2014**, *5*, 2843–2853. https://doi.org/10.1039/c3py01546g.
(31) Valsange, N. G.; Garcia Gonzalez, M. N.; Warlin, N.; Mankar, S. V.; Rehnberg, N.; Lundmark, S.; Zhang, B.; Jannasch, P. Biobased Aliphatic Polyesters from a Spirocyclic Dicarboxylate Monomer Derived from Levulinic Acid. *Green Chem.* **2021**, *23*, 5706–5723. https://doi.org/10.1039/d1gc00724f.
(32) Mincheva, R.; Delangre, A.; Raquez, J. M.; Narayan, R.; Dubois, P. Biobased Polyesters with Composition-Dependent Thermomechanical Properties: Synthesis and Characterization of Poly(Butylene Succinate-Co-Butylene Azelate). *Biomacromolecules* **2013**, *14*, 890–899. https://doi.org/10.1021/bm301965h.
(33) Duarte, M. E.; Huber, B.; Theato, P.; Mutlu, H. The Unrevealed Potential of Elemental Sulfur for the Synthesis of High Sulfur Content Bio-Based Aliphatic Polyesters. *Polym. Chem.* **2020**, *11*, 241–248. https://doi.org/10.1039/c9py01152h.
(34) Ahmed, A. M.; Kainulainen, T. P.; Sirviö, J. A.; Heiskanen, J. P. Renewable Furfural-Based Polyesters Bearing Sulfur-Bridged Difuran Moieties with High Oxygen Barrier Properties. *Biomacromolecules* **2022**, *23*, 1803–1811. https://doi.org/10.1021/acs.biomac.2c00097.
(35) Lavilla, C.; Alla, A.; Martínez De Ilarduya, A.; Muñoz-Guerra, S. High Tg Bio-Based Aliphatic Polyesters from Bicyclic d-Mannitol. *Biomacromolecules* **2013**, *14*, 781–793. https://doi.org/10.1021/bm301854c.
(36) Lavilla, C.; De Ilarduya, A. M.; Alla, A.; García-Martín, M. G.; Galbis, J. A.; Muñoz-Guerra, S. Bio-Based Aromatic Polyesters from a Novel Bicyclic Diol Derived from d-Mannitol. *Macromolecules* **2012**, *45*, 8257–8266. https://doi.org/10.1021/ma3013288.
(37) Zakharova, E.; Martínez, A.; Ilarduya, D.; León, S. Sugar-Based Bicyclic Monomers for Aliphatic Polyesters : A Comparative Appraisal of Acetalized Alditols and Isosorbide. *Des. Monomers Polym.* **2017**, *20*, 1–10.

https://doi.org/10.1080/15685551.2016.1231038.

(38) Xu, Y.; Hua, G.; Hakkarainen, M.; Odelius, K. Isosorbide as Core Component for Tailoring Biobased Unsaturated Polyester Thermosets for a Wide Structure-Property Window. *Biomacromolecules* **2018**, *19*, 3077–3085. https://doi.org/10.1021/acs.biomac.8b00661.

(39) Pang, C.; Jiang, X.; Yu, Y.; Chen, L.; Ma, J.; Gao, H. Copolymerization of Natural Camphor-Derived Rigid Diol with Various Dicarboxylic Acids: Access to Biobased Polyesters with Various Properties. *ACS Macro Lett.* **2019**, *8*, 1442–1448. https://doi.org/10.1021/acsmacrolett.9b00570.

(40) Nomura, K.; Binti Awang, N. W. Synthesis of Bio-Based Aliphatic Polyesters from Plant Oils by Efficient Molecular Catalysis: A Selected Survey from Recent Reports. *ACS Sustain. Chem. Eng.* **2021**, *9*, 5486–5505. https://doi.org/10.1021/acssuschemeng.1c00493.

(41) Nayak, K.; Ghosh, P.; Khan, H. Side-Chain Amino-Acid-Based Polymers : Self-Assembly and Bioapplications. *Polym Int* **2022**, *71*, 411-425. https://doi.org/10.1002/pi.6278.

(42) Jain, S.; John, A.; George, C. E.; Johnson, R. P. Tyrosine-Derived Polymers as Potential Biomaterials : Synthesis Strategies , Properties , and Applications. *Biomacromolecules* **2023,** *ASAP*. https://doi.org/10.1021/acs.biomac.2c01232.

(43) Deming, T. J. Methodologies for Preparation of Synthetic Block Copolypeptides: Materials with Future Promise in Drug Delivery. *Adv. Drug Deliv. Rev.* **2002**, *54* , 1145–1155. https://doi.org/10.1016/S0169-409X(02)00062-5.

(44) Deming, T. J. Synthesis of Side-Chain Modified Polypeptides. *Chem. Rev* 2016**,** *116*, 786-808. https://doi.org/10.1021/acs.chemrev.5b00292.

(45) Carlsen, A.; Lecommandoux, S. Current Opinion in Colloid & Interface Science Self-Assembly of Polypeptide-Based Block Copolymer Amphiphiles. *Curr. Opin. Colloid Interface Sci.* **2009**, *14*, 329–339. https://doi.org/10.1016/j.cocis.2009.04.007.

(46) Nisal, R.; Jayakannan, M. Tertiary-Butylbenzene Functionalization as a Strategy for β-Sheet Polypeptides. *Biomacromolecules* **2022**, *23*, 2667–2684. https://doi.org/10.1021/acs.biomac.2c00416.

(47) Kricheldorf, H. R. Polypeptides and 100 Years of Chemistry of a -Amino Acid N -Carboxyanhydrides Angew. Chem. Int. Ed. **2006**, *45*, 5752–5784. https://doi.org/10.1002/anie.200600693.

(48) Yin, Q.; Yin, L.; Wang, H.; Cheng, J. Synthesis and Biomedical Applications of Functional Poly(α-Hydroxy Acids) via Ring-Opening Polymerization of O-Carboxyanhydrides. *Acc. Chem. Res.* **2015**, *48*, 1777–1787. https://doi.org/10.1021/ar500455z.

(49) Basu, A.; Kunduru, K. R.; Katzhendler, J.; Domb, A. J. Poly(α-Hydroxy Acid)s and Poly(α-Hydroxy Acid-Co-α-Amino Acid)s Derived from Amino Acid. *Adv. Drug Deliv. Rev.* **2016**, *107*, 82–96. https://doi.org/10.1016/j.addr.2016.08.003.

(50) Sun, H.; Cheng, R.; Deng, C.; Meng, F.; Dias, A. A.; Hendriks, M.; Feijen, J.; Zhong, Z. Enzymatically and Reductively Degradable α-Amino Acid-Based

Poly(Ester Amide)s: Synthesis, Cell Compatibility, and Intracellular Anticancer Drug Delivery. *Biomacromolecules* **2015**, *16*, 597–605. https://doi.org/10.1021/bm501652d.

(51) Deng, M.; Wu, J.; Reinhart-King, C. A.; Chu, C. C. Synthesis and Characterization of Biodegradable Poly(Ester Amide)s with Pendant Amine Functional Groups and in Vitro Cellular Response. *Biomacromolecules* **2009**, *10*, 3037–3047. https://doi.org/10.1021/bm9006437.

(52) Wu, J.; Wu, D.; Mutschler, M. A.; Chu, C. C. Cationic Hybrid Hydrogels from Amino-Acid-Based Poly(Ester Amide): Fabrication, Characterization, and Biological Properties. *Adv. Funct. Mater.* **2012**, *22*, 3815–3823. https://doi.org/10.1002/adfm.201103147.

(53) Fonseca, A. C.; Gil, M. H.; Simões, P. N. Biodegradable Poly(Ester Amide)s - A Remarkable Opportunity for the Biomedical Area: Review on the Synthesis, Characterization and Applications. *Prog. Polym. Sci.* **2014**, *39*, 1291–1311. https://doi.org/10.1016/j.progpolymsci.2013.11.007.

(54) Huang, F.; Cheng, R.; Meng, F.; Deng, C.; Zhong, Z. Micelles Based on Acid Degradable Poly(Acetal Urethane): Preparation, Ph-Sensitivity, and Triggered Intracellular Drug Release. *Biomacromolecules* **2015**, *16*, 2228–2236. https://doi.org/10.1021/acs.biomac.5b00625.

(55) Lu, W.; Wang, X.; Cheng, R.; Deng, C.; Meng, F.; Zhong, Z. Biocompatible and Bioreducible Micelles Fabricated from Novel α-Amino Acid-Based Poly(Disulfide Urethane)s: Design, Synthesis and Triggered Doxorubicin Release. *Polym. Chem.* **2015**, *6*, 6001–6010. https://doi.org/10.1039/c5py00828j.

(56) Wu, J.; Zhao, L.; Xu, X.; Bertrand, N.; Choi, W. I.; Yameen, B.; Shi, J.; Shah, V.; Mulvale, M.; Maclean, J. L.; FaroKhzad, O. C. Hydrophobic Cysteine Poly(Disulfide)-Based Redox-Hypersensitive Nanoparticle Platform for Cancer Theranostics. *Angew. Chemie - Int. Ed.* **2015**, *54*, 9218–9223. https://doi.org/10.1002/anie.201503863.

(57) Aamer, K. A.; Genson, K. L.; Kohn, J.; Becker, M. L. Impact of Polymer-Bound Iodine on Fibronectin Adsorption and Osteoblast Cell Morphology in Radiopaque Medical Polymers: Tyrosine-Derived Polycarbonate Blends as a Model System. *Biomacromolecules* **2009**, *10*, 2418–2426. https://doi.org/10.1021/bm900327b.

(58) Chun, Y.; Kohn, J. Tyrosine-PEG-Derived Poly(Ether Carbonate)s as New Biomaterials. Part I: Synthesis and Evaluation. *Biomaterials* **1999**, *20*, 253–264. https://doi.org/10.1016/S0142-9612(98)00169-0.

(59) Bourke, S. L.; Kohn, J. Polymers Derived from the Amino Acid L-Tyrosine: Polycarbonates, Polyarylates and Copolymers with Poly(Ethylene Glycol). *Adv. Drug Deliv. Rev.* **2003**, *55*, 447–466. https://doi.org/10.1016/S0169-409X(03)00038-3.

(60) Sheihet, L.; Piotrowska, K.; Dubin, R. A.; Kohn, J.; Devore, D. Effect of Tyrosine-Derived Triblock Copolymer Compositions on Nanosphere Self-Assembly and Drug Delivery. *Biomacromolecules* **2007**, *8*, 998–1003.

https://doi.org/10.1021/bm060860t.

(61) He, M.; Ro, L.; Liu, J.; Chu, C.-C. Folate-Decorated Arginine-Based Poly(Ester Urea Urethane) Nanoparticles as Carriers for Gambogic Acid and Effect on Cancer Cells. *J. Biomed. Mater. Res. Part A* **2017**, *105*, 475–490. https://doi.org/https://doi.org/10.1002/jbm.a.35924.

(62) Naolou, T.; Busse, K.; Kressler, J. Synthesis of Well-Defined Graft Copolymers by Combination of Enzymatic Polycondensation and "Click" Chemistry. *Biomacromolecules* **2010**, *11*, 3660–3667. https://doi.org/10.1021/bm1011085.

(63) Yang, B.; Wang, G.; Xia, B.; Zhong, M.; Fan, P.; Chen, F.; Fei, Z. Enzymatic Synthesis of Chiral Polyamide via Condensation of Natural Source Amino Acid Diesters and Diamine. *Macromol. Chem. Phys.* **2021**, *222*, 1–6. https://doi.org/10.1002/macp.202100162.

(64) Zhang, Y.; Xia, B.; Li, Y.; Lin, X.; Wu, Q. Substrate Engineering in Lipase-Catalyzed Selective Polymerization of d -/ l -Aspartates and Diols to Prepare Helical Chiral Polyester. *Biomacromolecules* **2021**, *22*, 918–926. https://doi.org/10.1021/acs.biomac.0c01605.

(65) Anantharaj, S.; Jayakannan, M. Polymers from Amino Acids: Development of Dual Ester-Urethane Melt Condensation Approach and Mechanistic Aspects. *Biomacromolecules* **2012**, *13*, 2446–2455. https://doi.org/10.1021/bm300697h.

(66) Anantharaj, S.; Jayakannan, M. Catalysts and Temperature Driven Melt Polycondensation Reaction for Helical Poly(Ester-Urethane)s Based on Natural L-Amino Acids. *J. Polym. Sci. Part A Polym. Chem.* **2016**, *54*, 1065–1077. https://doi.org/10.1002/pola.27970.

(67) Aluri, R.; Jayakannan, M. One-Pot Two Polymers: ABB′ Melt Polycondensation for Linear Polyesters and Hyperbranched Poly(Ester-Urethane)s Based on Natural l-Amino Acids. *Polym. Chem.* **2015**, *6*, 4641–4649. https://doi.org/10.1039/c5py00602c.

(68) Joshi, D. C.; Saxena, S.; Jayakannan, M. Development of l -Lysine Based Biodegradable Polyurethanes and Their Dual-Responsive Amphiphilic Nanocarriers for Drug Delivery to Cancer Cells. *ACS Appl. Polym. Mater.* **2019**, *1*, 1866–1880. https://doi.org/10.1021/acsapm.9b00413.

(69) Saxena, S.; Jayakannan, M. Enzyme and PH Dual Responsive L-Amino Acid Based Biodegradable Polymer Nanocarrier for Multidrug Delivery to Cancer Cells. *J. Polym. Sci. Part A Polym. Chem.* **2016**, *54*, 3279–3293. https://doi.org/10.1002/pola.28216.

(70) Aluri, R.; Saxena, S.; Joshi, D. C.; Jayakannan, M. Multistimuli-Responsive Amphiphilic Poly(Ester-Urethane) Nanoassemblies Based on l -Tyrosine for Intracellular Drug Delivery to Cancer Cells. *Biomacromolecules* **2018**, *19*, 2166–2181. https://doi.org/10.1021/acs.biomac.8b00334.

(71) Anantharaj, S.; Jayakannan, M. Melt Polycondensation Approach for Reduction Degradable Helical Polyester Based on L-Cystine. *J. Polym. Sci. Part A Polym. Chem.* **2016**, *54*, 2864–2875. https://doi.org/10.1002/pola.28172.

(72) Saxena, S.; Jayakannan, M. π-Conjugate Fluorophore-Tagged and Enzyme-Responsive l -Amino Acid Polymer Nanocarrier and Their Color-Tunable

Intracellular FRET Probe in Cancer Cells. *Biomacromolecules* **2017**, *18*, 2594–2609. https://doi.org/10.1021/acs.biomac.7b00710.

(73) Saxena, S.; Pradeep, A.; Jayakannan, M. Enzyme-Responsive Theranostic FRET Probe Based on l -Aspartic Amphiphilic Polyester Nanoassemblies for Intracellular Bioimaging in Cancer Cells. *ACS Appl. Bio Mater.* **2019**, *2*, 5245–5262. https://doi.org/10.1021/acsabm.9b00450.

(74) Anantharaj, S.; Jayakannan, M. Amyloid-Like Hierarchical Helical Fibrils and Conformational Reversibility in Functional Polyesters Based on l-Amino Acids. *Biomacromolecules* **2015**, *16*, 1009–1020. https://doi.org/10.1021/bm501903t.

(75) Saxena, S.; Jayakannan, M. Development of L-Amino-Acid-Based Hydroxyl Functionalized Biodegradable Amphiphilic Polyesters and Their Drug Delivery Capabilities to Cancer Cells. *Biomacromolecules* **2020**, *21*, 171–187. https://doi.org/10.1021/acs.biomac.9b01124.

(76) Rautio, J.; Kumpulainen, H.; Heimbach, T.; Oliyai, R. Prodrugs : Design and Clinical Applications. *Nature Reviews Drug Discovery* **2008**, *7*, 255–270. https://doi.org/10.1038/nrd2468.

(77) Pramod, P. S.; Takamura, K.; Chaphekar, S.; Balasubramanian, N.; Jayakannan, M. Dextran Vesicular Carriers for Dual Encapsulation of Hydrophilic and Hydrophobic Molecules and Delivery into Cells. *Biomacromolecules* **2012,** *3627*−3640. https://doi.org/10.1021/bm301583s.

(78) Chandra Joshi, D.; Ashokan, A.; Jayakannan, M. L -Amino Acid Based Phenol- and Catechol-Functionalized Poly(Ester-Urethane)s for Aromatic π-Interaction Driven Drug Stabilization and Their Enzyme-Responsive Delivery in Cancer Cells . *ACS Appl. Bio Mater.* **2022,** *5*, 5432-5444. https://doi.org/10.1021/acsabm.2c00775.

Chapter 3

Fluorophore-Tagged Theranostic Polyester Nano-assemblies for Drug Delivery in-Vitro and In-vivo

Abstract

Present study deals with design and development of tetra phenyl ethylene (TPE) fluorescent Tagged biodegradable polyester from L-aspartic acid for design of polymer self-assembly with theranostic application in cancer cells. The synthetic strategy involves synthesis of the acetal functionalised TPE Tagged polymer which can subsequently converted into desired hydroxyl functionalised TPE Tagged polymer. The new monomer designed with acetal and TPE as side chain pendant monomer which was polymerized by polycondensation with 1, 12 dodecane diol to produces acetal functionalised TPE Tagged polymer with different composition of two monomers. On selective deprotection of the acetal group from the polymer yielded hydroxyl functionalised TPE Tagged polymer. The polymer having TPE chromophore shows the aggregation induced emission (AIE) properties based on the solvent composition of the environment. Polymer showed interesting thermal properties, Thermostability of the polymer was found up to 250 ºC with semicrystalline nature of the polymer. The semicrystalline nature in the polymer introduced due to the due to π-π interaction between the pendant TPE unit of the polymer chain in solid state, this nature was further enhanced by the combined effect of the hydrogen bond and π-π interaction in the polymer chains. At level of the solution, the polymer form nano assemblies in water with size less than 250nm with biomarker such as Rhodamine B (RhB) and rose Bengal (RB) or drug doxorubicin (DOX) encapsulation capabilities. The photophysical properties of the NPs using absorbance, emission spectroscopy and lifetime measurement established the energy transfer through Forster resonance energy transfer (FRET) process. The phenomena of the FRET further utilised to demonstrate the interaction between the polymer and loaded cargo at the cellular level by bioimaging using CSLM. NPs found biocompatible with cancer and normal cell lines and also does not show any cytotoxic effect toward human red blood cells (RBCs). *In vivo* biodistribution of the NPs loaded with IR780 was carried out by IVIS imaging setup which suggest better life time of the NPs with IR780 as compare to free IR780.

3.1 Introduction

Theranostic self-assemblies represent a promising class of nanosystems for the targeted delivery of therapeutic drugs or genes in cancer therapy.[1-4] These nanocarriers, constructed using fluorescent chromophores, harness their unique properties of absorbance and emission in the visible to infrared spectrum. They can be administered in the body at lower concentrations, offering improved treatment efficiency[5,6]. Within the realm of fluorescent polymers, various strategies have been reported, involving the conjugation of fluorescent molecules to polymers. These constructs undergo self-assembly in aqueous environments and can respond to external stimuli, such as changes in pH, enzyme activity, or redox reactions, enabling precise cellular-level analysis. [7-10] The array of polymeric self-assembly options includes unimolecular micelles[11], aggregated micelles[12], polymersomes[13,14], liposomes[15,16], supramolecular assemblies[17], inorganic nanoparticles[18], and more.

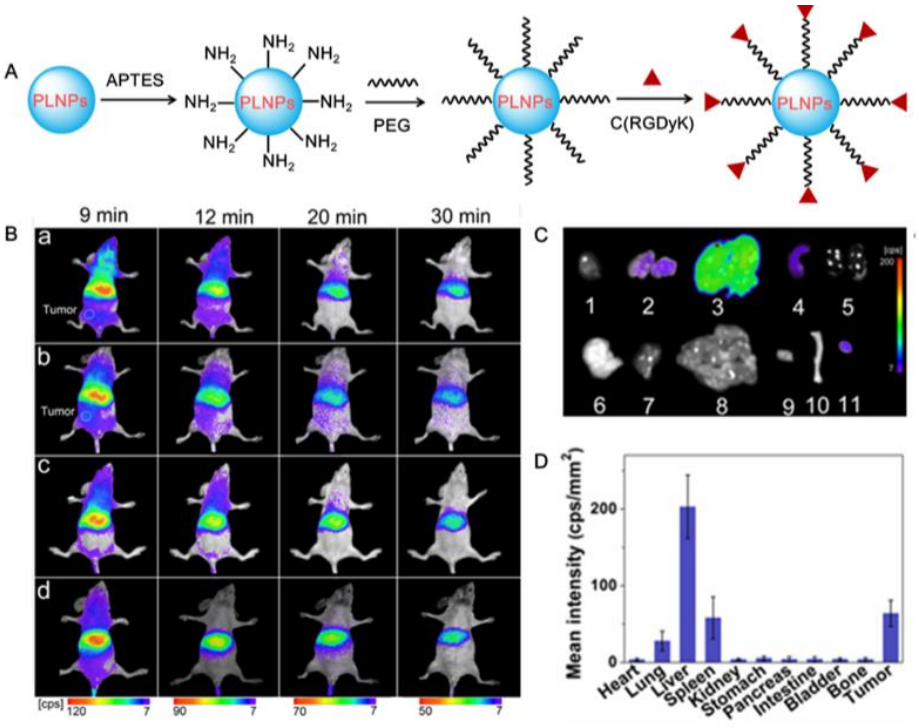

Figure 3.1 *Development of fluroscent Inorganic nanoparticles for tumour targeted imaging.(Adapted from Acc. Chem. Res.* **2018**, *51*, 5, 1131-1143.*)*

Within the realm of fluorescent polymer systems found in existing literature, one noteworthy category involves polyaromatic molecules. Under aqueous conditions, these polyaromatic systems engage in π-π interactions among their chromophores, resulting in a phenomenon known as aggregation-induced quenching (ACQ). The strong aggregation within polyaromatic systems leads to a reduction in the emission intensity of the polymers, particularly in the context of intracellular bioimaging applications[19,20]. When these polyaromatic systems come into proximity or converge within nanocavities during the formation of polymeric nanoparticles, they not only quench the emission of the fluorescent polymer but also diminish the emitted signals originating from the loaded cargo.

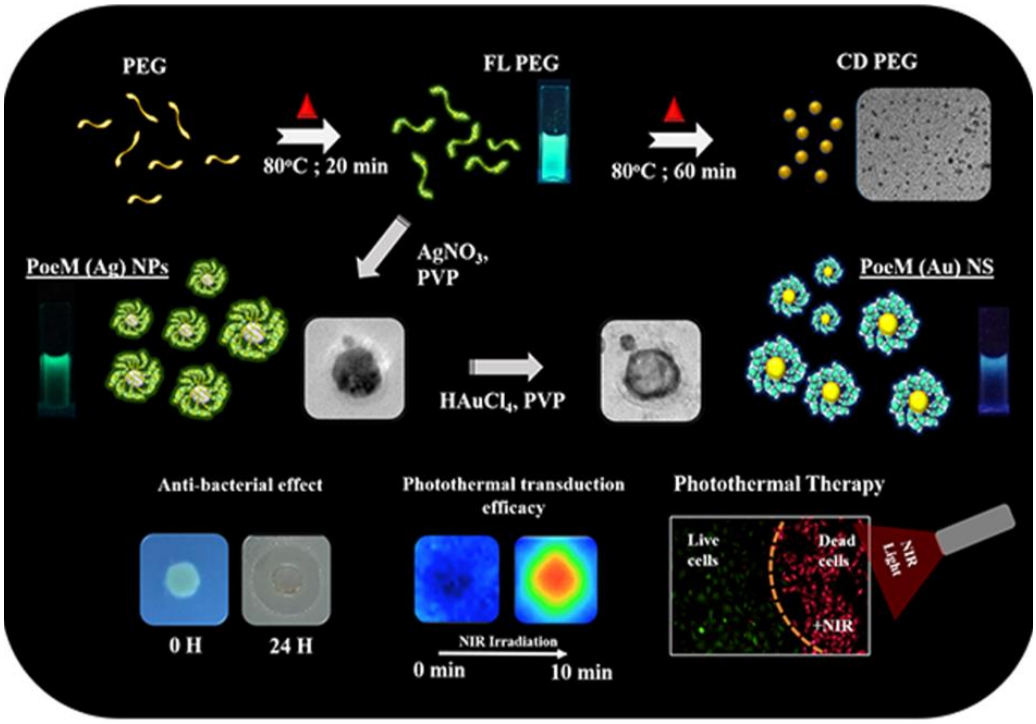

Figure 3.2 *fluroscent polymers for drug delivery in cancer cells and antibacterial applications. (Adapted from ACS Appl.Polym. Mater.2020,2,1388−1397.)*

Over the past decade, the concept of aggregation-induced emission (AIE), as introduced by Ben Zong Tong et al., has gained prominence. This innovative approach involved the synthesis of a range of molecules that exhibit enhanced emission intensity upon aggregation, marking a departure from the previously discussed aggregation-caused quenching (ACQ). Notably, they explored diverse fluorescent structures, such as Hexaphenylsilole, which produces emissions when intramolecular rotation is

restricted. The underlying principles of AIE hold significant potential for the advancement of fluorescent-tagged nanoparticles, opening new avenues for their development and applications[21-25].

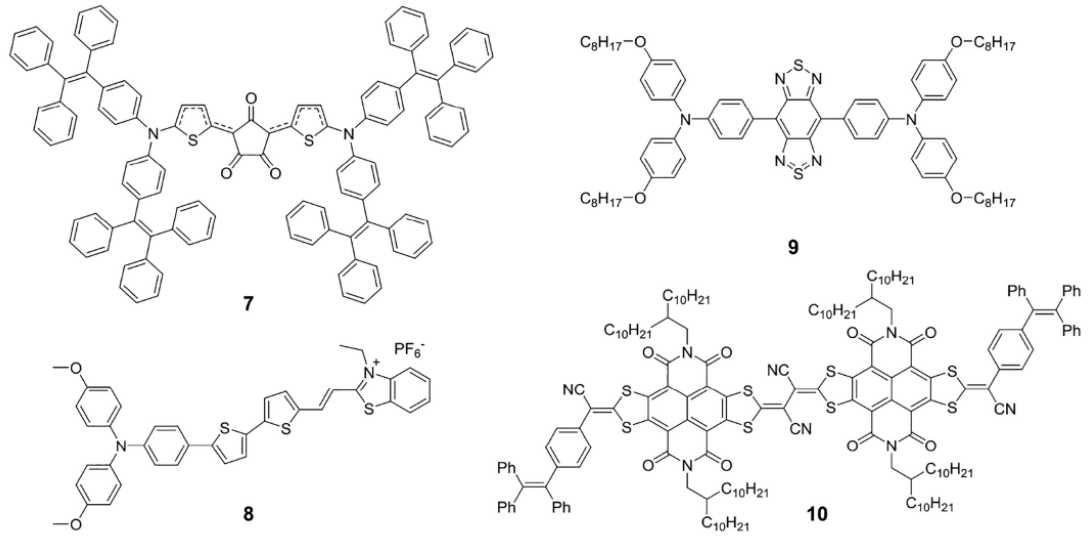

Figure 3.3 *Chemical Structure of the aggregation induced emission chromophore(Adapted from ACS Appl. Polym. Mater. 2021, 3, 2290−23091397.)*

Förster or fluorescence resonance energy transfer (FRET) stands as a potent non-invasive fluorescence probing technique[26]. It operates on the principle of selective photoexcitation energy transfer occurring between donor and acceptor chromophores, all within nano-confinements of ≤ 50 Å[27]. The versatility of FRET has led to its application in a multitude of areas, including real-time tumor imaging[28-29], monitoring drug release kinetics[30-31], investigating the self-assembly of amphiphilic block copolymers[32], exploring protein folding under physiological conditions[33-34], studying quadruplex-to-duplex[35] transitions in DNA[36], probing molecular interactions at mammalian cell surfaces[37-38], enabling two-photon imaging in cancers[39-40], and even sensing bilirubin in human serum[41], among other uses.

In recent decades, substantial progress in the field of conducting polymers for optoelectronic devices has unveiled new opportunities for water-soluble cationic π-conjugated polymers as luminescent bio-probes[42]. Notably, cationic and water-soluble polyfluorenes have emerged as pivotal π-conjugated polymers in FRET applications[43,49]. Additionally, polyacrylates-based random and block copolymers, with optical chromophores incorporated into their side chains, have been explored for FRET applications. Nevertheless, the persisting challenge of non-biodegradability associated

with the rigid C-C backbone in π-conjugated polymers and acrylates continues to be a significant hurdle to their widespread adoption in biomedical research.[50-51]

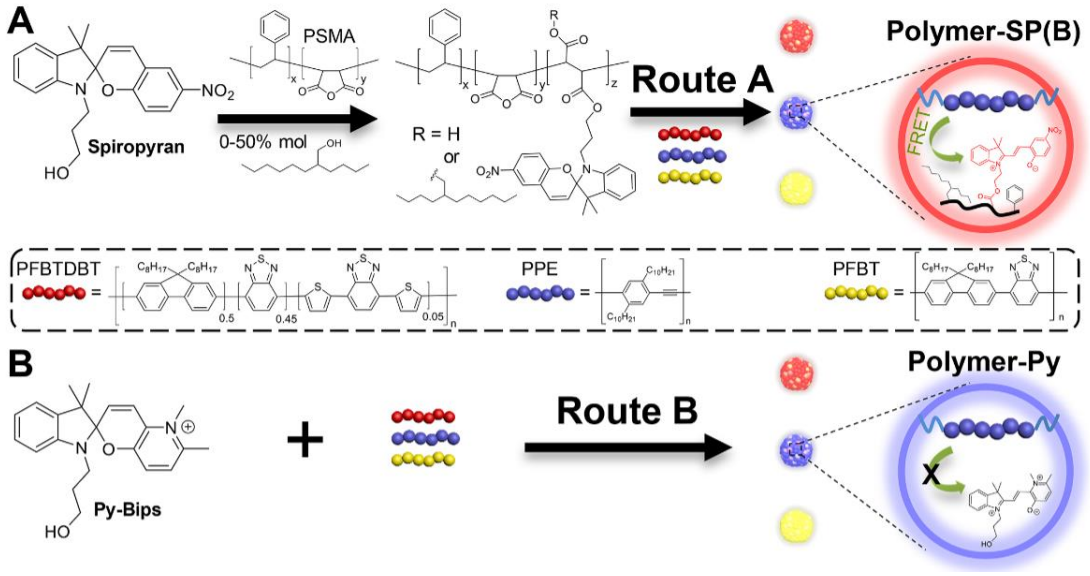

Figure 3.4 *Fluroscent polymer based on AIE flurophore composed of the carbon-carbon backbone (Adapted from ACS Appl. Mater. Interfaces2017, 9, 30918−30924).*

There is a need to develop the fluorescent nanocarrier based drug delivery system which should be biodegradable and biocompatible. In our lab we developed the biodegradable polymer from L-amino acid resource using melt polycondensation strategy, were the new classes of the polymer such as Poly(ester urethane)s[52-55], Polyurethanes[56] and Polyesters[57-63] from L-amino acid, this methodology was further expanded for the development of stimuli responsive polymers such as pH, redox, enzyme etc. The present approach here, we come up with development of biodegradable polyester for L-aspartic acid resource, not just for the bioimaging in the cancer cells but also intermolecular interaction between the polymer and the loaded cargo Using FRET as a tool.

In this chapter we have constructed biodegradable hydroxyl functionalised tetraphenyl ethylene (TPE) Tagged polymer capable to form FRET probe with biomarkers such as rose bengal(RB) and rhodamine B (RhB) and anticancer drug doxorubicin (DOX). The synthesis involves use natural amino acid i.e., L-aspartic acid,

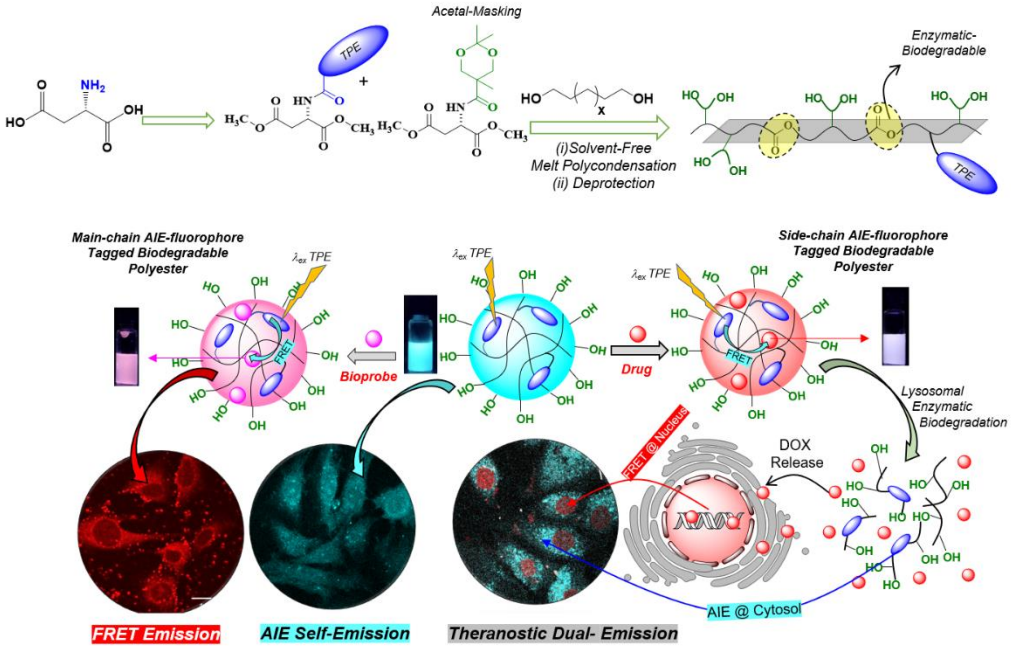

Figure 3.5 *Development of enzyme responsive TPE tagged hydroxyl functionalised polyester nanoparticles for theranostic fluorescent probe for drug delivery in cancer cells.*

The L-aspartic acid was converted to two different melt polymerizable units, acetal masked monomer and TPE Tagged monomer these monomers were developed the chemistry as first the aspartic acid was converted in to the dimethyl ester and amine of it was modified as amide with acetal masked acid and TPE Tagged acid. On polymerisation by melt polycondensation these of these two monomers along 1, 12 dodecane diol produced acetal functionalised TPE Tagged polyester which well characterised for its structural and thermal properties. The polymer was subsequently deprotected with trifluoracetic acid to produce hydroxyl functionalised TPE Tagged polyester. The hydrophilic and hydrophobic balance in the polymer was control by the varying the acetal and TPE monomer ratio in the at the stage of polycondensation. The deprotected polymer was showed change in thermal properties. The polyester found to be semi-crystalline nature due to presence of π-π interaction between the TPE group and hydrogen bonding in polymer matrix because of hydroxyl group contribute toward glass transition temperature (T_g) and semi-crystalline nature of the polymer. The hydroxyl functionalised TPE Tagged polymer produced nanoparticle in water by dialysis method and encapsulated drug doxorubicin or biomarker rose bengal and rhodamine B inside the hydrophobic nanocavity. The intermolecular energy transfer between TPE from the polymer chain and loaded drug or biomarker inside the micelle

was studied using FRET as tool in polymer NPs. From the photophysical characterisation it was clear that TPE and RB/RhB/DOX act as FRET pair, and TPE acts as donor while RB/RhB/DOX acts as acceptor. FRET was further established through photophysical characterisation such as absorbance, emission and lifetime measurement. The FRET tool has also helped to calculate Forster distance, FRET efficiency, lifetime of the donor in presence and absence acceptor. Horse liver esterase enzyme action successfully demonstrate the biodegradable nature of the polymer which leads to enzyme responsive release of the loaded cargo. The nascent polymer and polymer NPs loaded biomarker do not cause any toxic effect to the both normal and cancer cell lines, while NPs with doxorubicin were able to deliver the doxorubicin and able to kill the cancerous cells. Cellular uptake of the NPs and intermolecular interaction between TPE and RB/RhB/DOX studied by bioimaging in the cancer cells. The polymer NPs were able to delivered the loaded cargo in the body of a live mice, biodistribution studies further suggested that polymer NPs can better deliver the biomarker as compare to free form of biomarker which was proved by time dependent live imaging of the mice by IVIS imaging.

3.2 Experimental Section

3.2.1 Materials & Methods

4-Hydroxy benzophenone, 4,4 Dihydroxy benzophenone, Benzophenone, Titanium tetra chloride ($TiCl_4$), Tetrahydrofuran (THF), Zinc (Zn) powder, Hydrochloric acid (HCl), Ethyl acetate, Pet ether, Potassium carbonate (K_2CO_3), Dimethyl formamide (DMF), Acetonitrile (ACN), Ethyl chloroacetate, Potassium hydroxide (KOH), Dioxane, Aspartic acid, Thionyl chloride ($SOCl_2$), Methanol, 1, 12 Dodecanediol, Chloro-ethoxyethanol, 2,2 Dimethoxy propane, 2,2-Bishydroxymethyl propionic acid, Para toluene sulfonic acid (p-TSA), Dry acetone, Triethylamine (TEA), Anhydrous Sodium Sulphate (Na_2SO_4), Diisopropylethylamine (DIPEA), N′-ethylcarboiimide hydrochloride (EDC-HCl), Hydroxy benzotriazole (HOBt), Titanium tetra-butaoxide ($Ti(OBu)_4$), Trifluroacetic acid(TFA). Doxorubicin hydrochloride (DOX.HCl), Rose Bengal (RB), Rhodamine B (RhB), 4',6-diamidino-2-phenylindole (DAPI), 3-(4,5-dimethylthiazol-2-yl)-2,5-diphenyl tetrazolium bromide (MTT), Dimethyl sulphoxide (DMSO), Milli Q water, 1 % (v/v) penicillin–streptomycin (Pen-Strep), Fatal bovine serum (FBS), Dulbecco's Modified Eagle's Medium (DMEM), 0.5

% Trypsin, 6 well plate, 96 well plate, 4% paraformaldehyde (PFA). Other chemicals were purchase locally and used without purification. Mammalian cells such as Wild type mouse embryonic fibroblast (WT MEF), MCF 7 and SKOV3 Cells were cultured and maintained at 37 ºC, 5% CO_2 atmosphere in complete media which is made up of DMEM, FBS and Pen-Strep solution.

3.2.2 General Procedure

The structures of monomers and polymers were characterised by ^{1}H and ^{13}C Nuclear magnetic resonance (NMR) spectroscopy using 400 MHz JEOL NMR & 400 MHz Brucker spectrophotometer. Chemical shifts are reported in terms of δ units, which is expressed in ppm, The Deuterated Chloroform was used as internal standard the residual proton peak appears at 7.26 ppm. The molecular weight of monomers and compounds of intermediate step were analysed using HRMS-ESI-Q-time of flight LCMS. The monomers, intermediates compound and the polymers were characterised for their Attenuated total reflectance-Fourier transform infrared spectroscopy (ATR-FTIR) using Bruker alpha Fourier transform infrared spectrophotometer. The frequency was mentioned in cm^{-1}. The relative molecular weight and polydispersity index of polyester was analysed using Size exclusion chromatography (SEC) analysis. The concentration of polymer sample was kept as 5mg/ml in HPLC Grade THF, 100µL of sample was injected. SEC was performed using THF as eluent and The SEC column were calibrated using narrow disperse polystyrene from molecular weight range 1000 to 100k g/mol. SEC analysis was performed with system equipped with an isocratic pump (Viscotek VE 1122 pump) and a differential refractometer (DRI) detector (Viscotek VE 3580 RI). For SEC with THF as the eluent, separations were performed using serially connected size exclusion columns (two T6000M, General Mixed Organic 8 × 300 mm, from Viscotek) at 25 °C and at a flow rate of 1.0 mL/min, and molecular weights were determined from the calibration curve generated from narrow polystyrene standards. Thermal stability of the polymers was determined using PerkinElmer thermal analyser at a heating rate of 10ºC/min in nitrogen atmosphere. Thermal analysis of all polymers was performed using TA Q20 Differential Scanning Calorimeter. All the polymers were heated to melt before recording in order to remove previous thermal history. Polymers were heated and cooled at a rate of 10º C/min in nitrogen atmosphere. The size of polymeric nanoparticle was determined using dynamic light scattering technique (DLS). Nano ZS-90 apparatus from Malvern Instruments was used. The

concentration of polymeric nanoparticle sample was maintained as 0.1mg/mL. The instrument works on the principle of light scattering of laser of 633nm. The polymeric nanoparticles in Brownian motion scatter light. The detector is placed in 90 angle to record fluctuations in scattered light collected and the instrument generates autocorrelation function [g^2 (t)] using which Diffusion coefficient was obtained using cumulant method. Instrument utilizes stock Einstein method to calculate the diameter of nanoparticle. The photophysical studies of the polymer was carried out by absorbance and fluorescence. A PerkinElmer Lambda 45 UV−vis spectrophotometer was utilised for the absorption studies. Emission and excitation spectra were recorded on a SPEX Fluor log HORIBA JOBIN VYON fluorescence spectrophotometer. This instrument utilises 450 W Xe lamp as the source of excitation at room temperature. The morphology of polymeric nanoparticle was analysed by microscopic techniques such as Field emission scanning electron microscopy (FESEM), for that samples were prepared taking 0.1mg/ml concentration of nanoparticle which was drop casted on silicon wafer which were subjected to gold coating. The gold coated layer protects sample from high voltage and make it conducting. FESEM analysis was done using Zeiss Ultra Plus scanning electron microscope. Cell viability of the polymer determined by MTT assay; the concentration of formazan was determined by taking absorbance readings at 570 nm at a Vairoscan FLASH instrument. The polymeric nanoparticle samples were lyophilize using A Christ Alpha 1-2 LD plus. The cellular uptake was studied by confocal microscopy, the fixed cell acquired using 405, 488, and 561 nm lasers of a CLSM710 confocal microscope.

3.2.3 Esterification of aspartic acid (Compound 1)

L-Aspartic acid (10.0 g, 0.07 mol) was added with dry methanol (100 mL) in a two-neck RB flask (250mL). Thionyl chloride (21.0 mL, 34.5 g, 0.29 mol) under ice cold condition added dropwise under nitrogen atmosphere. Then reaction allowed to attain room temperature and it was refluxed for 6 hrs by under nitrogen atmosphere. The excess of methanol and thionyl chloride were removed by vacuum distillation. The residue white solid was washed with diethyl ether to get white solid product obtained yield =14.8 g (98%).

3.2.4 Synthesis of 2,2,5-Trimethyl-1,3-dioxane-5-carboxylic Acid (Compound 2)

2,2-Bishydroxymethyl propionic acid (20.0 g, 0.015 mol) and para toluene sulfonic acid (p-TSA) (1.40 g, 0.008 mol) was taken in a two-neck round-bottom flask in dry acetone (100.0 mL). Dimethoxy propane (37 mL, 0.22 mol) was added dropwise to the above solution, and the reaction mixture was stirred for 4 h at 25 °C. Triethylamine was added to neutralize the excess pTSA, and the acetone was removed by rota-evaporation. The product was extracted in ethyl acetate. It was dried over anhydrous Na_2SO_4, and the solvent was removed to get crystalline powder as product. Yield = 23.4 g (90%). ^{1}H NMR (400 MHz, CHLOROFORM-*d*) d ppm 4.19 (2 H, d, *J*=11.98 Hz) 3.67 (2 H, d, *J*=11.98 Hz) 1.41 (3 H, s) 1.44 (3 H, s) 1.21 (3 H, s). ^{13}C NMR (101 MHz, CHLOROFORM-*d*) δ ppm 18.10, 21.73, 24.72, 41.38, 65.48, 76.37, 76.69, 97.97, 179.80. FTIR (cm−1) 2989, 1714, 1458, 1381, 1248, 1200, 1160, 1072, 987, 932, 824, 756, 715. HR-MS (ESI+): m/z [M + H+] Calculated for C8H14O2 [M+] = 175.0926; found = 175.0971.

3.2.5 Synthesis of 4-(1,2,2-triphenylvinyl) phenol (Compound 3)

Benzophenone (15.00 g, 0.08mol), 4-hydroxy benzophenone (16.31 g, 0.08mol) and Zinc powder (13g, 0.2mol) was taken in clean two neck round bottomed flask under inert condition dry THF (100ml) was transferred to the reaction mixture. The reaction was then placed under ice cold condition for 30 min and titanium tetra-chloride (10.5ml, 18.2g, 0.09mol) was added dropwise. After complete addition of titanium tetra-chloride reaction mixture was shifted to room temperature and kept for 30 min. The reaction was performed at 80°C under nitrogen atmosphere for 12 h. The reaction mixture was brought to room temperature. The product was extracted by doing workup with DCM and 0.1M HCl solution. The organic layer was taken in separate flask and dried over anhydrous sodium sulphate and the product was further purified by column chromatography ethyl acetate: pet ether. 1:10 V/V Yield =5.6 g (32 %). ^{1}H NMR (400 MHz, CHLOROFORM-*d*) d ppm 7.07 (16 H, m) 6.91 (2 H, m, *J*=8.70 Hz) 6.57 (2 H, m, *J*=8.70 Hz) 4.68 (1 H, s). ^{13}C NMR (101 MHz, CHLOROFORM-*d*) d ppm 153.95, 143.96, 143.85, 140.39, 140.16, 136.35, 132.70, 131.34, 131.31, 128.10, 127.68, 127.58, 126.35, 126.24, 114.56, 77.31, 76.68, FTIR (cm−1) 3530, 3024, 1605, 1508, 1441, 1327, 1261, 1168, 1101, 1073, 1028, 910, 809, 747, 699. HR-MS (ESI+): m/z [M + H+] Calculated for C26H20O [M+] = 348.1514; Found =348.1521.

3.2.6 Synthesis of Ethyl 2-(4-(1,2,2-triphenylvinyl) phenoxy) acetate (Compound 4)

4-(1,2,2-triphenylvinyl) phenol (Compound 1) (10 g, 0.028mol) and K_2CO_3 (11. 6g, 0.084mol) was taken in clean 250ml round bottomed flask to that 100 mL of dry DMF was added. The reaction mixture was stirred at 80 ºC for 30min and then ethyl chloroacetate (5.2ml,0.043mol) was added. The reaction was performed for 18h. DMF was removed by doing work up with ice cold water and ethyl acetate. The ethyl acetate layer was extracted and dried over anhydrous sodium sulphate to get the crude product which was further purified by gel column using ethyl acetate: pet ether solvent. 1:10 V/V Yield= 4.0 g (65 %).^{1}H NMR (400 MHz, CHLOROFORM-*d*) d ppm 7.07 (16 H, m) 6.95 (2 H, m) 6.65 (2 H, m) 4.55 (2 H, s) 4.26 (2 H, q, *J*=7.33 Hz) 1.29 (3 H, t, *J*=7.10 Hz). ^{13}C NMR (101 MHz, CHLOROFORM-*d*) d ppm 168.88, 156.29, 143.84, 143.81, 143.75, 140.40, 140.23, 137.14, 132.54, 131.34, 131.29, 127.69, 127.58, 126.37, 126.27, 113.77, 77.31, 76.68, 65.35, 61.30, 14.14 (1 C, s). FTIR (cm−1) 3053, 1759, 1601, 1504, 1441, 1289, 1176, 1077, 1028, 911, 825, 745, 698. HR-MS (ESI+): m/z [M + H+] Calculated for C30H26O3 [M+] = 435.1960; found =435.1949.

3.2.7 Synthesis of 2-(4-(1,2,2-triphenylvinyl) phenoxy) acetic acid (Compound 5)

In a round bottomed flask ethyl 2-(4-(1,2,2-triphenylvinyl) phenoxy) acetate (10g, 0.02 mmol), KOH (3.8 g, 0.07mol) was taken in a clean round bottomed flask. The reaction mixture was dissolved in 100mL of dioxane and refluxed at 70 ºC for 12 h. The solvent dioxane was removed from reaction mixture by using rotary evaporator. The crude product was purified by solvent extraction with ethyl acetate and acidic water. The organic layer was concentrated over rotary evaporator to get product and it was further purified by column chromatography in ethyl acetate: pet ether solvent system. 1:10 V/V Yield = 3.6 g (98 %). ^{1}H NMR (400 MHz, CHLOROFORM-*d*) d ppm 7.06 (18 H, m) 6.67 (2 H, d, *J*=8.56 Hz) 4.61 (2 H, s). ^{13}C NMR (101 MHz, CHLOROFORM-*d*) d ppm 174.11, 156.12, 144.07, 144.04, 143.98, 140.90, 140.39, 137.90, 132.98, 131.63, 131.59, 128.04, 127.94, 127.91, 126.73, 126.67, 126.63, 114.08, 77.63, 77.31, 65.04 (1 C, s). FTIR (cm−1) 1053, 1724, 1601, 1504, 1439, 1216, 1176, 1076, 908, 824, 731, 697. HR-MS (ESI+): m/z [M + H+] Calculated for C28H22O3 [M+] = 406.1569; found = 406.1563.

3.2.8 Synthesis of Dimethyl (2,2,5-Trimethyl-1,3-dioxane-5-carbonyl) Aspartate (M-Ac)

Aspartic dimethyl ester amine salt (20.0 g, 0.1 mol) (Compound **1**) was taken in the clean two neck round bottomed flask, in this flask dimethylaminopyridine (DMAP) (13.6 mL, 0.11 mol) was added as base while dry dichloromethane (DCM) (150.0 mL) was added as solvent and stirred at 25 °C until it dissolves completely. N′-ethylcarboiimide hydrochloride (21.3 g, 0.11 mol) and 2,2,5-Trimethyl-1,3-dioxane-5-carboxylic Acid (compound 5) (14.0 g, 0.080 mol) were added to the above solution, and the reaction was carried out by stirring at 25 °C for 30 h. The DCM was removed from reaction mixture using rotary-evaporator, and the crude product was extracted in ethyl acetate. The resultant product was purified using silica column in 30% ethyl acetate in pet ether. The solvent was evaporated to get pale yellow liquid as a product. Yield = 17.8 g (70%). ^{1}H NMR (400 MHz, CHLOROFORM-*d*) d ppm 8.00 (1 H, d, *J*=7.63 Hz) 4.85 (1 H, m) 3.89 (1 H, m) 3.80 (1 H, m) 3.71 (5 H, m) 3.61 (3 H, s) 2.96 (1 H, dd, *J*=16.78, 4.58 Hz) 2.83 (1 H, dd, *J*=16.78, 4.58 Hz) 1.40 (6 H, d, *J*=3.05 Hz) 0.93 (3 H, s) ^{13}C NMR (101 MHz, CHLOROFORM-*d*) d ppm 174.20, 170.69, 98.02, 76.68, 76.36, 66.42, 66.35, 52.12, 51.42, 48.10, 39.63, 35.76, 27.84, 17.82, 17.10 (1 C, s). FTIR (cm−1) 3366, 2945, 1737, 1660, 1519, 1440, 1371, 1199, 1079, 1041, 917, 827, 688. HR-MS (ESI+): m/z [M + H+] Calculated for C28H22O3 [M+] = 340.1372; found = 340.1368.

3.2.9 Synthesis of dimethyl (2-(4-(1,2,2-triphenylvinyl) phenoxy) acetyl)-L-Aspartate (M-TPE)

2-(4-(1,2,2-triphenylvinyl) phenoxy) acetic acid (4g, 0.089mol) was taken in two neck round bottomed flask to that thionyl chloride (30ml, 0.25 mol) was added at 25^{o}C. The reaction mixture was refluxed at 80 ^{o}C for 6 hrs under nitrogen atmosphere. After the reaction excess of thionyl chloride was removed by vacuum distillation, the product produced 2-(4-(1,2,2-triphenylvinyl) phenoxy) acetyl chloride (4.17g, 0.089mol) in reaction was dissolved in dry dichloromethane (100ml). In another two necks round bottom flask aspartate diester (Compound 1) (2.9g, 0.014mol) was dissolved in a mixture of dry dichloromethane (120mL) with triethylamine (4ml, 2.9g 0.03mol). In this reaction mixture 2-(4-(1,2,2-triphenylvinyl) phenoxy) acetyl chloride was added dropwise under ice cold condition in an inert atmosphere. The reaction mixture was stirred at room temperature for 6h. The solvent was removed from the reaction mixture

and crude product was further purified by column chromatography with pet ether/ ethyl acetate 1:10 (v/v). Yield = 17.8 g (87%) ^{1}H NMR (400 MHz, CHLOROFORM-*d*) d ppm 7.55 (1 H, d, *J*=8.31 Hz) 7.05 (17 H, m) 6.69 (2 H, d, *J*=8.80 Hz) 4.94 (1 H, m) 4.46 (2 H, s) 3.77 (3 H, s) 3.68 (3 H, s) 3.07 (1 H, dd, *J*=17.24, 4.52 Hz) 2.86 (1 H, dd, *J*=17.12, 4.65 Hz). ^{13}C NMR (101 MHz, CHLOROFORM-*d*) d ppm 171.23, 170.72, 168.14, 155.57, 143.81, 143.74, 140.69, 140.09, 137.76, 132.75, 132.64, 131.32, 127.92, 127.79, 127.69, 127.66, 126.49, 126.45, 126.39, 114.03, 77.39, 77.06, 76.74, 67.11, 52.94, 52.15, 48.00, 36.03 (1 C, s). FTIR (cm−1) 3419, 3023, 2953, 1739, 1683, 1601, 1504, 14440, 1366, 1215, 1175, 1058, 847, 755, 701. HR-MS (ESI+): m/z [M + H+] Calculated for C28H22O3 [M+] = 550.2185; found = 550.2230.

3.2.10 Synthesis of acetal functionalised polymer (P-Ac)

The melt polycondensation for the synthesis of the acetal homopolymer is explained as followed. The M-Ac (0.6g, 0.0018mol) and 1,12 dodecane diol (0.38g, 0.0018mol) were taken in test shape polymer tube. The polymer tube was subjected to higher temperature of 140 ºC after complete melting of the monomers, $Ti(OBu)_4$ 1 mol %. The polymerisation setup was then subjected continuous flow of the nitrogen gas for 4h followed by the constant vacuum of 0.1 mBar. The resulted polymer was purified in methanol. Yield = 1.20g (95%). ^{1}H NMR (400 MHz, CHLOROFORM-*d*) d ppm 8.04 (1 H, d, *J*=7.58 Hz) 4.89 (1 H, br. s.) 4.14 (2 H, s) 4.06 (2 H, s) 3.94 (1 H, s) 3.87 (1 H, s) 3.77 (2 H, d, *J*=15.41 Hz) 3.00 (1 H, s) 2.90 (1 H, s) 1.61 (4 H, br. s.) 1.47 (6 H, s) 1.25 (17 H, br. s.) 1.01 (3 H, s). ^{13}C NMR (101 MHz, CHLOROFORM-*d*) δ ppm 17.38, 18.16, 25.45, 25.51, 27.99, 28.12, 28.17, 28.89, 28.94, 29.18, 29.24, 36.15, 39.83, 48.39, 64.80, 65.49, 66.57, 76.36, 76.69, 98.19, 170.51, 174.30.

3.2.11 Synthesis of hydroxyl functionalised polymer (P-OH)

The P-Ac (0.9g, 2mmol) was taken in clean round bottomed flask; dichloromethane was added to the reaction flask. The reaction mixture was shifted to 0ºC, under this condition trifluoro acetic acid was added. 2ml of the water was added to the reaction mixture and reaction was carried out for 2h. After completion of the reaction, the dichloromethane was removed on the rotary evaporator. The resultant polymer was purified by dialysis in water by using 3Kd dialysis. The polymer was lyophilised to get sticky powder. Yield = 0.80 g (95%). ^{1}H NMR (400 MHz, CHLOROFORM-*d*) d ppm 8.04 (1 H, d, *J*=7.58 Hz) 4.89 (1 H, br. s.) 4.14 (2 H, s) 4.06 (2 H, s) 3.94 (1 H, s) 3.87 (1 H, s) 3.77 (2 H, d, *J*=15.41 Hz) 3.00 (1 H, s) 2.90 (1 H, s) 1.61 (4 H, br. s.) 1.47 (6

H, s) 1.25 (17 H, br. s.) 1.01 (3 H, s). 13C NMR (100 MHz, CDCl3) δ ppm: 174.1, 171.7, 97.8, 66.9, 65.8, 64.6, 48.3, 39.9, 36.4, 29.4, 28.4, 24.8, 18.1, and 17.7.

Synthesis of acetal functionalised TPE Tagged polymers

3.2.12 Synthesis of $PTPE_4$

The general procedure for the synthesis of described in detail for the $PTPE_4$ polymer. In this polymer synthesis the molar ratio of the two monomers M-Ac (0.6g,0.0018mol) and M-TPE (0.054g, 0.0001mol) was kept as 96:04 respectively with the ratio of 100 % of 1,12 dodecanediol (0.4g, 0.0019mol). M-Ac and M-TPE was taken in clean polymerization tube along with 1,12 dodecanediol, the polymerisation mixture was melted at 140 ºC and 1 mol % of the $Ti(OBu)_4$ catalyst was taken. The polymerisation performed in two steps, in the first step the polymerisation performed with 4h continuous nitrogen purge. And in the second step 0.01mbar vacuum was applied for 2h. Yield= 1.0g (98%). ^{1}H NMR (400 MHz, CHLOROFORM-*d*) δ ppm 1.00 (s, 3 H) 1.17 - 1.37 (m, 17 H) 1.40 - 1.49 (m, 6 H) 1.51 - 1.69 (m, 4 H) 2.86 (dd, *J*=16.76, 4.63 Hz, 1 H) 3.01 (dd, *J*=16.76, 4.25 Hz, 1 H) 3.75 (dd, *J*=11.94, 3.06 Hz, 2 H) 3.80 - 3.99 (m, 2 H) 4.04 (t, *J*=6.69 Hz, 2 H) 4.13 (t, *J*=6.63 Hz, 2 H) 4.81 - 4.96 (m, 1 H) 8.02 (d, *J*=7.75 Hz, 1 H). ^{13}C NMR (101 MHz, CHLOROFORM-*d*) δ ppm 0.24, 17.97, 18.77, 26.03, 26.10, 28.57, 28.70, 28.76, 29.46, 29.51, 29.66, 29.75, 29.81, 33.03, 36.75, 40.43, 49.00, 63.18, 65.38, 65.56, 66.07, 67.16, 77.32, 77.64, 98.77, 114.22, 126.69, 127.85, 127.99, 131.51, 132.95, 171.07, 174.89.

3.2.13 Synthesis of $PTPE_{10}$

M-Ac (0.59g, 0.0017mol), M-TPE (0.10g, 0.0001mol) and 1,12 dodecane diol(0.4g, 0.0019mol) was polymerised by reported procedure explained for $PTPE_4$ Similar procedure was followed as for $PTPE_4$, only the molar ratio of the monomers was changed. Yield= 1.2g (97%). ^{1}H NMR (400 MHz, CHLOROFORM-*d*) δ ppm 0.98 (s, 3 H) 1.23 (br. s., 17 H) 1.44 (br. s., 6 H) 1.51 - 1.69 (m, 4 H) 2.86 (br. s., 1 H) 2.98 (br. s., 1 H) 3.74 (d, *J*=11.51 Hz, 2 H) 3.84 (br. s., 1 H) 3.92 (br. s., 1 H) 4.03 (br. s., 2 H) 4.12 (br. s., 2 H) 4.87 (br. s., 1 H) 6.98 (br. s., 1 H) 7.05 (br. s., 1 H) 8.01 (d, *J*=7.38 Hz, 1 H). ^{13}C NMR (101 MHz, CHLOROFORM-*d*) δ ppm 17.60, 18.41, 25.66, 25.72, 28.20, 28.33, 28.39, 29.09, 29.13, 29.38, 29.43, 32.66, 36.13, 36.22, 36.38, 40.06, 48.03, 48.62, 62.74, 65.00, 65.18, 65.69, 65.95, 66.79, 66.97, 76.68, 77.32, 98.40, 113.86, 126.22, 126.27, 127.48, 127.52, 127.62, 131.14, 132.58, 137.53, 139.93, 140.51, 143.58, 143.64, 155.47, 167.87, 170.11, 170.56, 170.69, 174.52.

3.2.14 Synthesis of $PTPE_{20}$

M-Ac (0.5g, 0.0016mol), M-TPE (0.2g,0.004mol) and 1,12 dodecane diol (0.4g, 0.002mol) was polymerised by reported procedure explained for $PTPE_4$ Similar procedure was followed as for $PTPE_4$, only the molar ratio of the monomers was changed. Yield= 1.0g (98%). ^{1}H NMR (400 MHz, CHLOROFORM-*d*) δ ppm 1.02 (s, 2 H) 1.18 - 1.40 (m, 17 H) 1.41 - 1.52 (m, 5 H) 1.52 - 1.68 (m, 4 H) 2.88 (dd, *J*=16.78, 4.58 Hz, 1 H) 3.03 (dd, *J*=16.78, 4.58 Hz, 1 H) 3.73 - 3.83 (m, 2 H) 3.85 - 4.01 (m, 2 H) 4.06 (t, *J*=6.87 Hz, 2 H) 4.15 (t, *J*=6.48 Hz, 2 H) 4.83 - 4.96 (m, 1 H) 6.91 - 7.16 (m, 3 H) 8.04 (d, *J*=7.63 Hz, 1 H). ^{13}C NMR (101 MHz, CHLOROFORM-*d*) δ ppm -0.03, 0.99, 17.71, 18.51, 25.77, 25.84, 28.31, 28.45, 28.50, 29.21, 29.26, 29.51, 29.56, 32.78, 36.49, 40.17, 48.12, 48.72, 65.12, 65.30, 65.82, 66.08, 66.89, 67.06, 76.69, 77.32, 98.51, 113.96, 126.38, 127.59, 127.63, 127.72, 131.25, 132.69, 143.68, 155.56, 167.97, 170.23, 170.83, 174.62

3.2.15 Synthesis of $PTPE_{30}$ Similar procedure was followed as for $PTPE_4$, only the molar ratio of the monomers was changed. M-Ac (0.43g, 0.0013mol), M-TPE (0.32g, 0.0006mol) and 1,12 dodecane diol (0.4g, 0.0019mol) was polymerised by reported procedure explained for PTPE4. Yield= 1.1g (99%). ^{1}H NMR (400 MHz, CHLOROFORM-*d*) δ ppm 1.01 (s, 2 H) 1.17 - 1.40 (m, 17 H) 1.40 - 1.53 (m, 5 H) 1.53 - 1.72 (m, 4 H) 2.88 (dd, *J*=16.40, 4.96 Hz, 1 H) 3.03 (dd, *J*=16.78, 4.58 Hz, 1 H) 3.77 (dd, *J*=11.83, 3.43 Hz, 2 H) 3.84 - 4.00 (m, 2 H) 4.06 (t, *J*=6.87 Hz, 2 H) 4.15 (t, *J*=6.48 Hz, 2 H) 4.44 (s, 1 H) 4.83 - 4.96 (m, 1 H) 6.67 (d, *J*=9.16 Hz, 1 H) 6.87 - 7.06 (m, 2 H) 7.09 (d, *J*=6.10 Hz, 2 H) 8.04 (d, *J*=8.39 Hz, 1 H)^{13}C NMR (101 MHz, CHLOROFORM-*d*) δ ppm 17.69, 18.49, 25.75, 25.82, 28.29, 28.42, 28.48, 29.19, 29.23, 29.48, 29.54, 32.75, 36.21, 36.47, 40.15, 48.10, 48.71, 62.95, 65.09, 65.28, 65.79, 66.05, 66.87, 67.05, 76.69, 77.31, 98.49, 113.94, 126.36, 126.41, 127.57, 127.61, 127.70, 131.23, 132.66, 137.62, 140.01, 140.60, 143.65, 143.72, 155.54, 167.96, 170.21, 170.67, 170.80, 174.61.

Synthesis of hydroxyl functionalised TPE tagged copolyester:

3.2.15 Synthesis of $PTPE_4$-OH

The procedure is described in detail for the deprotection of the acetal group from the polymer. The polymer $PTPE_4$ (0.5g, 0.001mol) was taken in the clean round and dissolved in 2ml of dichloromethane. At the 0 ºC TFA (1mL, 0.013mol) was added to the reaction mixture dropwise. After 15 min of time interval 1ml water was added to

the reaction. The reaction carried out for 2h, the dichloromethane and water were removed from the reaction mixture by rotary evaporator. The resultant polymer was purified by dialysis in water for 12h. Yield:0.42g (86%).^{1}H NMR (400 MHz, CHLOROFORM-*d*) δ ppm 1.09 (s, 1 H) 1.28 (br. s., 14 H) 1.55 (br. s., 2 H) 1.63 (br. s., 2 H) 2.32 (br. s., 4 H) 2.63 (s, 1 H) 2.86 (d, *J*=11.91 Hz, 1 H) 3.00 (br. s., 1 H) 3.64 (s, 2 H) 3.79 (br. s., 2 H) 4.08 (s, 1 H) 4.14 (s, 1 H) ^{13}C NMR (101 MHz, CHLOROFORM-*d*) δ ppm -0.34, 17.03, 25.38, 28.14, 28.82, 29.06, 29.12, 29.18, 29.22, 32.44, 35.72, 40.48, 48.38, 62.75, 65.14, 65.93, 67.96, 76.36, 76.69, 130.95, 163.22, 170.72,.

3.2.16 Synthesis of PTPE$_{10}$-OH

PTPE$_{10}$-OH (0.5g, 0.001mol) and TFA (1mL, 0.013mol) was taken Similar procedure was followed as for PTPE$_4$-OH, only the molar ratio of the monomers was changed. Yield: 0.45 g (90%). ^{1}H NMR (400 MHz, CHLOROFORM-*d*) δ ppm 1.09 (s, 1 H) 1.28 (br. s., 15 H) 1.57 (br. s., 4 H) 2.63 (s, 3 H) 2.87 (br. s., 1 H) 3.00 (br. s., 1 H) 3.64 (s, 2 H) 3.78 (br. s., 2 H) 4.07 (br. s., 1 H) 4.16 (br. s., 1 H) 4.88 (br. s., 1 H) 7.02 (br. s., 1 H) 7.11 (br. s., 1 H). ^{13}C NMR (101 MHz, CHLOROFORM-*d*) δ ppm -0.03, 17.37, 25.69, 28.45, 29.14, 29.37, 29.43, 29.50, 29.54, 32.74, 36.05, 48.69, 63.06, 65.46, 66.27, 76.69, 77.31, 113.98, 126.39, 127.60, 131.27, 132.70, 171.04.

3.2.17 Synthesis of PTPE$_{20}$-OH

PTPE$_{10}$-OH (0.5g, 0.001mol) and TFA (1mL, 0.013mol) was taken Similar procedure was followed as for PTPE$_4$-OH, only the molar ratio of the monomers was changed. Yield: 0.42 g (87%). ^{1}H NMR (400 MHz, CHLOROFORM-*d*) δ ppm 1.09 (s, 1 H) 1.28 (br. s., 16 H) 1.57 (br. s., 4 H) 2.64 (s, 4 H) 2.88 (br. s., 1 H) 3.00 (br. s., 1 H) 3.65 (s, 2 H) 3.76 (br. s., 2 H) 4.07 (br. s., 1 H) 4.16 (br. s., 1 H) 4.89 (br. s., 1 H) 7.02 (br. s., 1 H) 7.11 (br. s., 2 H). ^{13}C NMR (101 MHz, CHLOROFORM-*d*) δ ppm -0.03, 17.37, 25.69, 28.38, 29.14, 29.37, 29.51, 29.54, 32.75, 40.81, 63.07, 65.45, 76.68, 77.31, 113.98, 126.40, 127.64, 127.74, 131.26, 132.70, 171.03,

3.2.18 Synthesis of PTPE$_{30}$-OH

PTPE$_{10}$-OH (0.5g, 0.001mol) and TFA (1mL, 0.013mol) was taken Similar procedure was followed as for PTPE$_4$-OH, only the molar ratio of the monomers was changed. Yield: 0.41 g (85%). ^{1}H NMR (400 MHz, CHLOROFORM-*d*) δ ppm 1.09 (s, 1 H) 1.27 (br. s., 17 H) 1.58 (br. s., 4 H) 2.63 (s, 1 H) 2.76 - 2.94 (m, 1 H) 2.99 (br. s., 3 H) 3.66 (br. s., 2 H) 3.77 (br. s., 2 H) 4.06 (br. s., 1 H) 4.15 (br. s., 1 H) 6.68 (s, 1 H) 6.95 (s, 1

H) 7.01 (br. s., 2 H) 7.10 (br. s., 2 H) .^{13}C NMR (101 MHz, CHLOROFORM-*d*) δ ppm -0.03, 17.37, 25.69, 28.38, 29.14, 29.37, 29.51, 29.54, 32.75, 40.81, 63.07, 65.45, 76.68, 77.31, 113.98, 126.40, 127.64, 127.74, 131.26, 132.70, 171.03.

3.2.19 Determination of critical aggregation concentration (CAC) experiment

2.3 mg of the $PTPE_{18}$-OH polymer was dissolved in 1.15mL of the DMSO, the final concentration of the stock was made as 2mg/mL. using this stock, the concentration of the polymer was varied from the 20 mg/mL to 400 mg/mL in 10 % DMSO and 90 % water combination. The fluorescence spectra of the above samples were recorded by exciting λ_{exc} = 330 nm and emission spectra was collected at 340nm to 700nm.

3.2.20 Solvent dependent aggregation (SDA) Experiment

3.16 mg of the $PTPE_{18}$-OH polymer was dissolved in 1.08mL of the DMSO, the final stock of the polymer become 2mg/mL. From this stock 100 mg of the polymer was taken in each vail and the it was dissolved in varying composition of the DMSO and water combination. The ratio of DMSO to water was varied from 100 % DMSO to 10 % DMSO and 90 % water. The sample was the subjected absorbance and fluorescence studies. The fluorescence spectra were recorded at 340nm to 700nm by exciting samples at 330nm.

3.2.21 Self-Assembly of hydroxyl functionalised TPE conjugated polymers

The polymeric nanoparticle synthesized by the dialysis method. Hydroxyl functionalised TPE conjugated polymer was self-assembled by dialysis method. The polymer was taken 5.0mg and dissolved in the 2ml of dimethyl suphoxide water was added to it drop wise with continuous stirring. This solution then transferred to 1kd dialysis bag and dialysed against Milli Q water for 24h, the water in the reservoir was changed over regular interval of time

3.2.22 Encapsulation of Drug/Dye

Similar protocol was adapted as mentioned in the previous section. 5.0mg of polymer was taken in 2ml of dimethyl sulphoxide about 0.5mg dye or drug was taken and dissolved in it. The milli Q water about 3.0 ml was added to it drop by drop over 30 min with continues stirring. The resultant solution was dialysed in 1Kd dialysis bag against water for 24h. The unencapsulated drug or dye leaches out in the solution while the if the solution retains the drug or dye it shows fluorescent dye solution inside the nanoparticle which can be further studied by photophysical studies.

3.2.23 Cytotoxicity experiments of the polymer nanoparticle

For the use of anticancer application polymer should be biocompatible with the both cancer cells and normal cells. The cell viability studies for the polymer were carried out for polymer alone as well as the polymer nanoparticle loaded with drug or dye. PTPE polymer, PTPE-RhB, PTPE-RB and PTPE-DOX was studied for toxicity by MTT assay. The cytotoxicity was studied for WT MEF and MCF 7 cancer cell lines. Similar protocol was followed as explained earlier chapter.

3.2.24 Haemolysis

Cytotoxicity of the polymer was studied for red blood cells of Bulb C mice. The blood collected from the retro-orbital sinus of the mice. The mice blood was then diluted with 1X PBS. The polymer sample was prepared by dissolving the polymer in 1 X PBS, was incubated with mice blood at 37 ºC for 1h. Followed by it was subjected to the rotation of 800rpm for 5 min. If the RBCs pallets settles then it as polymer is compatible with the RBC. The plasma collected about 100µl from the supernatant and absorbance was recorded at 480nm in varioscan.

3.2.25 Biodistribution in vivo Imagining

Female balb/c mice of 8–12-week-old (~ 25 g in weight) were used for the biodistribution studies using IVIS. Total 8 mice were randomly divided into 3 groups. The first group (n=3) were injected with free IR-780 dye, the second group (n=3) were injected with IR-780 loaded polymer nanoparticles and the last group (n=2) were injected with PBS. All the injections of free IR-780 or IR-780 loaded nanoparticles in PBS (100 µL) were done intraperitonially while maintaining the IR-780 dosage at 0.5 mg/kg. The blood was collected from anesthetized mice via retro-orbital plexus puncture at the various time points (4 h, 24 h, 48 h post injection) from alternate sides. In case of bleeding the absorbable hemostatic gelatin sponge (AbGel) was used. The biodistribution of the free IR-780 dye and the dye loaded polymer nanoparticles were monitored in real time by employing IVIS spectrum (Perkin Elmer). Wherein, the mice were anesthetized and imaged at time points 4 h, 24 h, 48 h and 72h to capture both the dorsal and ventral view using the excitation and emission filter of λexc = 745 nm and λem = 820 nm respectively. At the end of 48 h, the Mice were euthanized by overdose of anaesthesia (isoflurane) and perfused with PBS prior to organ harvesting. The harvested organs were used for *whole-organ* imaging analysis employing the same

excitation and emission filters. From the collected blood, plasma samples were isolated by centrifugation and inoculated (10 µL) in each well of 96-well plate and subsequently diluted 10 times with PBS. These samples were then subjected to the IVIS imaging using similar filters (as mentioned above). The average radiance was calculated from the instrument software and used to quantify the amount of the dye IR-780.

3.3 Result and Discussion

The fluorescent Tagged hydroxyl functionalised polyester was designed using naturally source of L- aspartic acid. For this purpose, tetraphenyl ethylene (TPE) conjugated monomer was synthesized which is referred as M-TPE. Tetraphenyl ethylene (TPE) is very well-known fluorophore which is known to show aggregation induced emission (AIE) property. Another monomer was designed with acetal masked pendant group which is referred as M-Ac, these both monomers with serve as comonomer for melt polycondensation polymerisation.

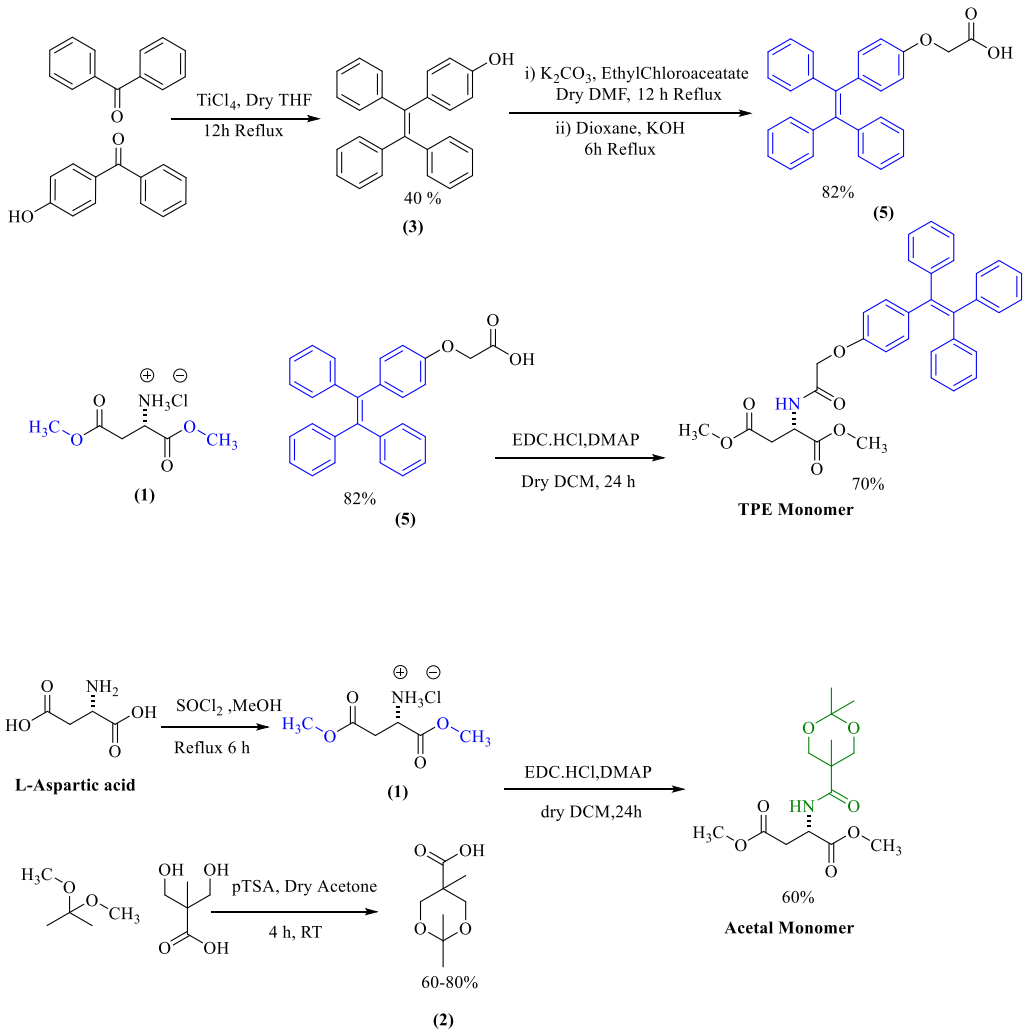

Scheme 3.1 *Synthesis of aspartic diester monomer i.e M-Ac and M-TPE*

3.3.1 Synthesis of monomers

The detail strategy for the synthesis of monomers is as follows; L-aspartic acid was esterified with thionyl chloride in methanol to produce dimethoxy aspartate ammiunium hydrochloride salt (compound 1). The amine salt of compound 1 was neutralised using a base and coupled 2,2,5-Trimethyl-1,3-dioxane-5-carboxylic acid (compound 2) to produce Dimethyl (2,2,5-Trimethyl-1,3-dioxane-5-carbonyl) aspartate (M-Ac). The compound 2,2,5-Trimethyl-1,3-dioxane-5-carboxylic acid (compound 2) was synthesized, using bis (hydroxyl methyl) propionic acid with 2,2 methoxy propanol under acidic condition of p-toluyl sulphonic acid in dry acetone. The ^{1}H and ^{13}C NMR spectra of the compound 2 and M-Ac monomer is shown in Figure 3.6

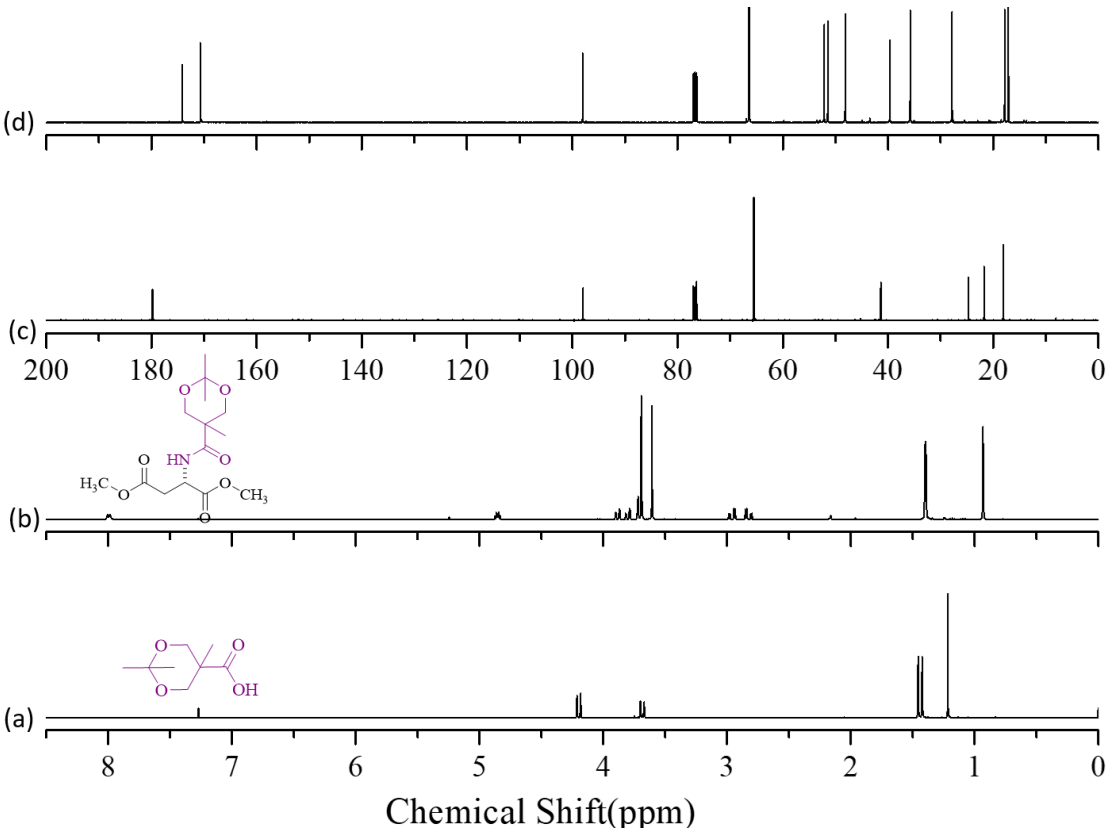

Figure 3.6 *Chemical structure of compond 2 and M-Ac and 1H and 13C Spectra of the Compound 2 and M-Ac. Spectra of (a) and (c) belongs to compound 2 while spectra (b) and (d) belongs to M-Ac.*

A new TPE conjugated fluorescent monomer (M-TPE) was prepared by multiple step organic reaction. In this reaction benzophenone and 4-hydroxy

benzophenone were coupled to form 4-hydroxyl tetraphenyl ethylene (compound 3) using $TiCl_4$ and Zn by Mc Murry coupling. The hydroxyl group was alkylated using ethyl chloroacetate under basic condition to produce Ethyl 2-(4-(1,2,2-triphenylvinyl) phenoxy) acetate (compound 4), ethyl ester of compound 4 was hydrolysed produce 2-(4-(1,2,2-triphenylvinyl) phenoxy) acetic acid (compound 5) under basic conditions. Compound 5 was coupled treated with thionyl chloride to produce respective acid chloride which subsequently reacted with compound 1 to produce dimethyl (2-(4-(1,2,2-triphenylvinyl) phenoxy) acetyl)-L-aspartate (M-TPE), the reaction scheme

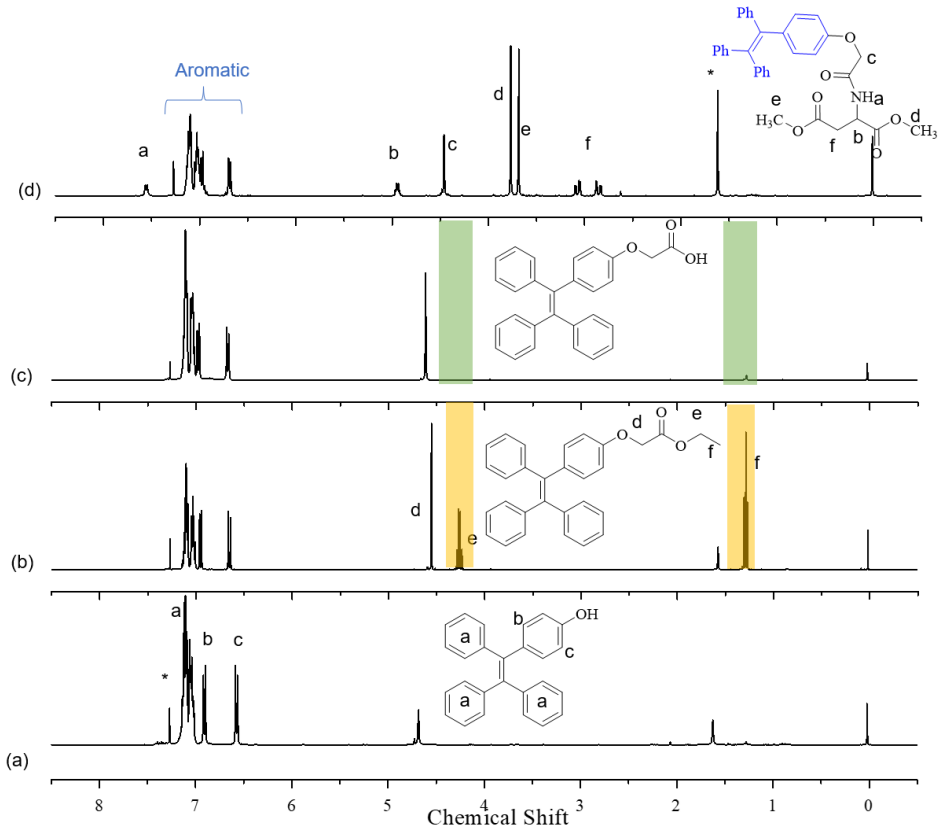

shown as Scheme-1.

Figure 3.7 *Chemical structure of compond 3 to compound 5 and M-TPE and ^1H NMR spectra.*

The structure of M-TPE and intermediate compounds 2 to compound 5 was confirmed by using ^1H and ^{13}C spectroscopy, the ^1H NMR spectra of the intermediate compounds and M-TPE is shown as Figure 3.7. (^{13}C NMR spectra of the intermediate compounds and M-TPE is provided as Appendix Figure S10). These synthesized monomers were studies for their thermal stability using thermogravimetric analysis

(TGA), both the M-TPE and M-Ac were found to be stable at the melt polycondensation temperature as shown in Appendix Figure S11.

3.3.2 Synthesis of Copolymers

The copolymers were prepared taking different molar ratio of M-TPE and M-Ac with respect to 1,12 dodecane diol as shown in Scheme 3.2. The polymerisation was carried out via solvent free melt polycondensation process. The synthetic procedure for 10 % TPE Tagged acetal functionalised polyester is discussed in details.

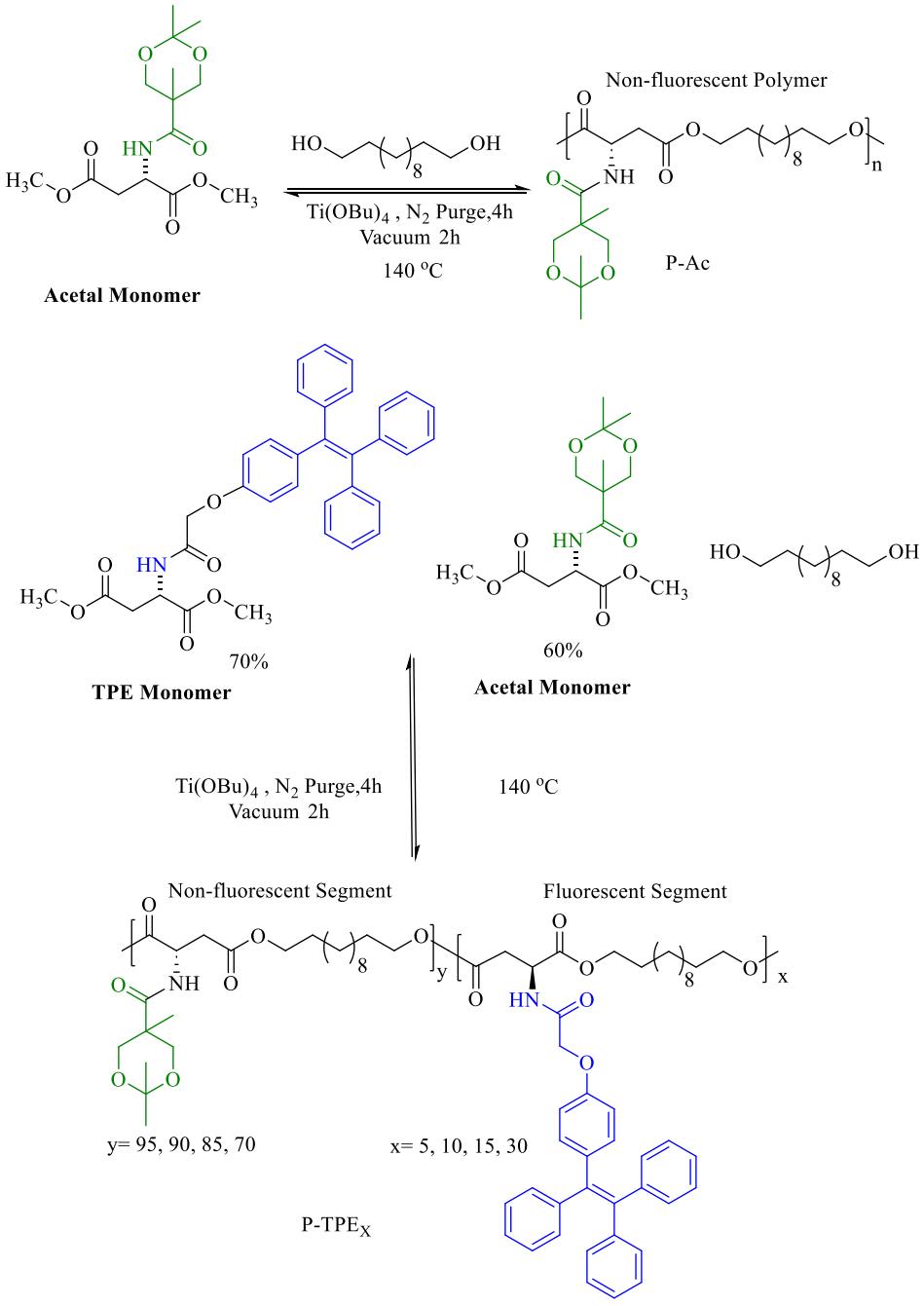

Scheme 3.2 *Synthesis of L aspartic acid based homopolymer P-Ac and Copolymer from M-TPE and M-Ac using melt polycondensation strategy.*

The molar ratio of the monomers was taken as 10 % of M-TPE and 90 % of M-Ac with respect to these two monomers 1,12 dodecane diol (DD) was taken as 100%. Both monomers were taken into test tube shaped polymerisation tube along with 1,12 dodecane diol (DD). This polymerisation mixture was then subjected to high temperature as at 140 °C which is well above its melting point and nitrogen purging was carried out for 15 minutes followed by that 1 mole % of $Ti(OBu)_4$ was added as catalyst. Then the polymerisation continued for 4h continuous nitrogen purge followed by vacuum for 2h of magnitude of 0.01mBar. During the melt condensation process at high temperature hydroxyl group of alcohol acts as nucleophile which attack on ester carbonyl centre. The carbonyl centre was polarised by catalyst making it more prone to nucleophilic attack leaving methanol as by product. Melt polycondensation was performed by two steps, first step involves the condensation under nitrogen purge which involve the condensation reaction between monomers and diol continuous nitrogen purge to remove excess of by-product methanol for 4h. In the next step vacuum about 10^{-2} mbar was applied for 2h. During the polycondensation process side chain, the amide pendant acetal and TPE remain inert and does not interfere in polycondensation. Following the same protocol series of copolymers were prepared using different molar ratio of M-TPE and M-Ac. For making polyester, ratio of these two monomers were maintained as 05:95, 10:90, 20:80 and 30:70. The structure of synthesized polyester was confirmed by ^{1}H and ^{13}C nuclear magnetic resonance spectroscopy. The ^{1}H spectra of M-Ac, M-TPE and their copolymer is shown in Figure 3.8

The NMR spectra of the monomers and polymer is shown as Figure 3.8. In the ^{1}H NMR monomer as shown in Figure 3.8a the methyl peak of dimethyl ester monomer of L-aspartate in M-Ac appears at 3.60 ppm and 3.68 ppm similarly methyl ester peak in M-TPE appears at 3.68 ppm and 3.77 ppm as singlets (See Figure 3.8b) in both of these cases the methyl esters peaks are Tagged by orange colour. After the formation of polyester new ester peaks appear as triplet at 4.05 and 4.15 ppm which belonging to ester backbone of the polyester as shown in Figure 3.8c. Formation of polyester linkage was further confirmed by ^{13}C spectroscopy methyl ester peak for the monomers appeared in the range of 51-53 ppm which disappears and new ester peak appeared in range of 64-67 ppm.

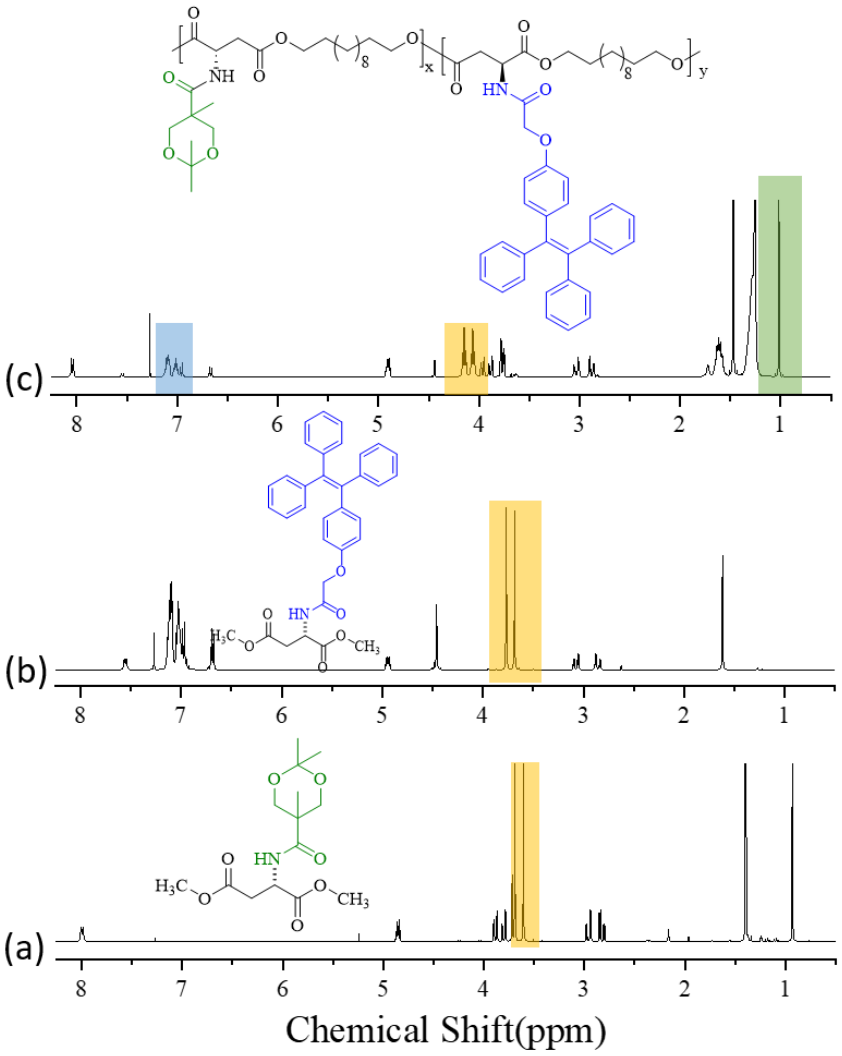

Figure 3.8 *^{1}H NMR spectra of the M-Ac (a) and M-Ac (b) and their copolymer PTPE$_x$ (c).*

The % TPE incorporated inside the copolymer was determined by ^{1}H NMR spectra, comparing the ratio of integration of two different peaks from acetal and TPE monomer as shown in Figure 3.8c. The acetal and TPEs ^{1}H NMR peak used for the calculation of the TPE content Tagged by green and blue colour respectively. For example, the copolymer was aimed to incorporate the 10 % of the M-TPE and 90 % of M-Ac but according to NMR it showed 9 % of M-TPE and 91 % of M-Ac incorporated. The notation P-Ac refers to the polyester with acetal side chain while co-polyester referred as PTPE$_4$ corresponding polymer with 4 % M-TPE unit and 96 % M-Ac units. The polymers are named as PTPE$_X$ where 'X' represents that the polymer with X % of the TPE monomer incorporated likewise other polymers are denoted as PTPE$_4$, PTPE$_9$,

$PTPE_{18}$ and $PTPE_{27}$. Which are having 4, 9, 18 and 27 % of TPE monomer incorporated. The copolymers prepared was characterised with the ^{1}H and ^{13}C nuclear magnetic resonance spectroscopy (Appendix Figure S12 to S15).

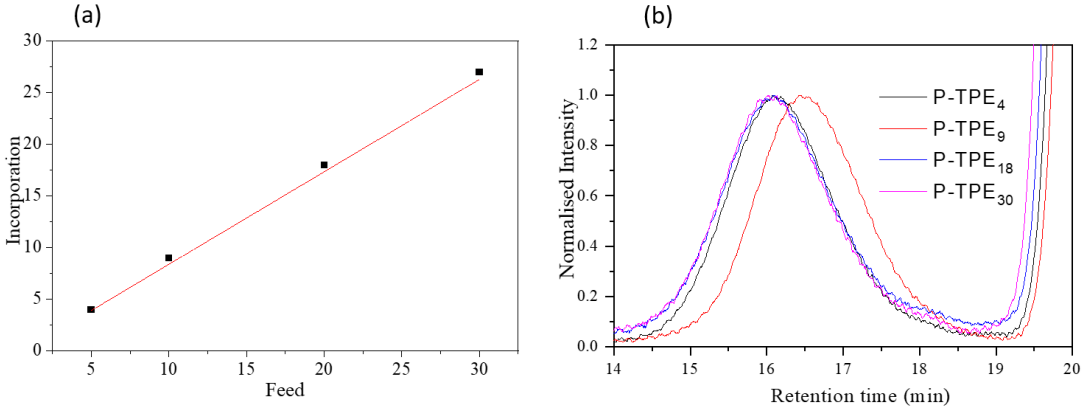

Figure3.9*(a) Plot of feed vs incorporation of the TPE monomer in polycondensation (b)SEC chromatograms of polymers in THF as eluent.*

The plot feed vs incorporation provided as Figure 3.9(a) from the plot, it can be clear stated that using this method one can make polyester of choice with exact control over incorporation of TPE monomer. These synthetic copolymers were characterised by size exclusion chromatography (SEC) in tetrahydrofuran (THF) solvent as eluent as at 35ºC. The SEC chromatogram for the synthesized polymers is shown in Figure 3.9b, polymers shows that polymers mono-model distribution. The number average molecular weight (M_n) was found to be in the range of 5.8 X 10^3 to 8.5 X 10^3 g/mol and weight average molecular weight (M_w) was found to be in the range of 10.3 X 10^3 to 15.8 X 10^3 g/mol with the polydispersity index in the range of 1.5 to 2.1. The data is summarised in the form of Table 3.1.

Figure 3.1*. Table containing feed and incorporation of the monomer in the polymer, molecular weights of polymers determined from SEC and polydispersity index.*

Table contains the incorporation of TPE units and molecular weights of polymers

Polymer	TPE Monomer (in Feed)	TPE in Polymer (^{1}H-NMR)[a]	M_n (g/mol)[b]	M_w (g/mol)[b]	PDI
P-Ac	0	0	12000	20000	1.7
$PTPE_4$	5	4	8500	15800	1.8
$PTPE_9$	10	9	6800	10300	1.5
$PTPE_{18}$	20	18	6700	12000	1.8
$PTPE_{27}$	30	27	5800	12500	2.1

[a] Amount of TPE unit incorporation in the polymer was estimated by 1H-NMR analysis. [b] Size exclusion chromatography molecular determination was done in THF solvent at 35 °C using polystyrene standard for calibration

3.3.3 Synthesis of Hydroxyl functionalised TPE tagged polymer

The above synthesized copolymers were subjected to pendant acetal group deprotection in with strong acid such as trifluoroacetic acid to produce hydroxyl functionalised TPE tagged polymer as shown in Scheme 3.3

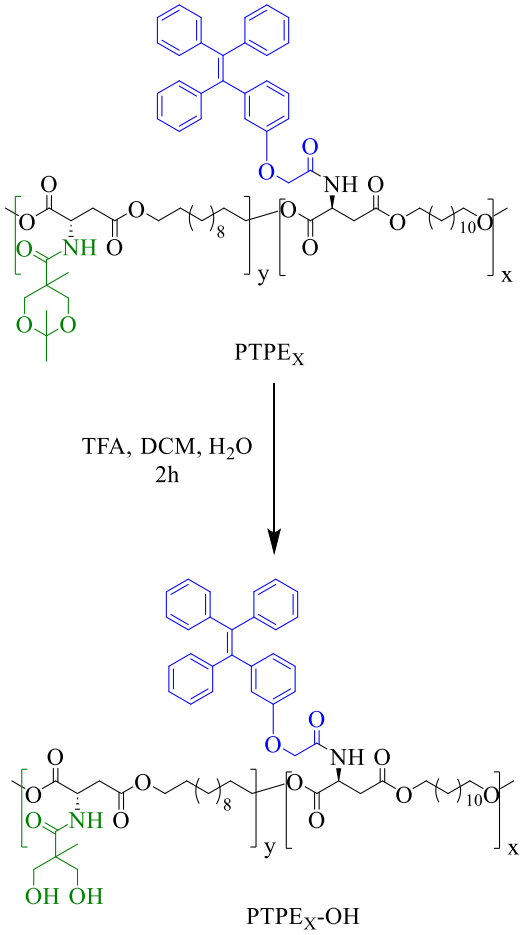

Scheme 3.3 *Synthesis of Hydroxyl functionalised TPE tagged Polyester from L-Aspartic acid.*

The deprotected polymers were characterised using ^{1}H and ^{13}C NMR spectroscopy. As shown in the Figure 3.10(a) ^{1}H NMR spectra of copolymer the presence of acetal peak at 1.47 ppm which is Tagged with orange coloured, after conversion of acetal group to the hydroxyl group from the copolymer was confirmed by disappearance peak of the acetal group as Tagged green region in the ^{1}H NMR spectra Figure 3.10(b). The polymers were designated by name with respect to their acetal counterpart for example PTPE$_4$-OH was obtained by deprotection of acetal group from PTPE$_4$ polyester. All other copolymers were successfully deprotected by optimised procedure and characterised with the help of NMR spectroscopy. Stack plot ^{1}H NMR spectra of copolymer is shown in Appendix Figure S16.

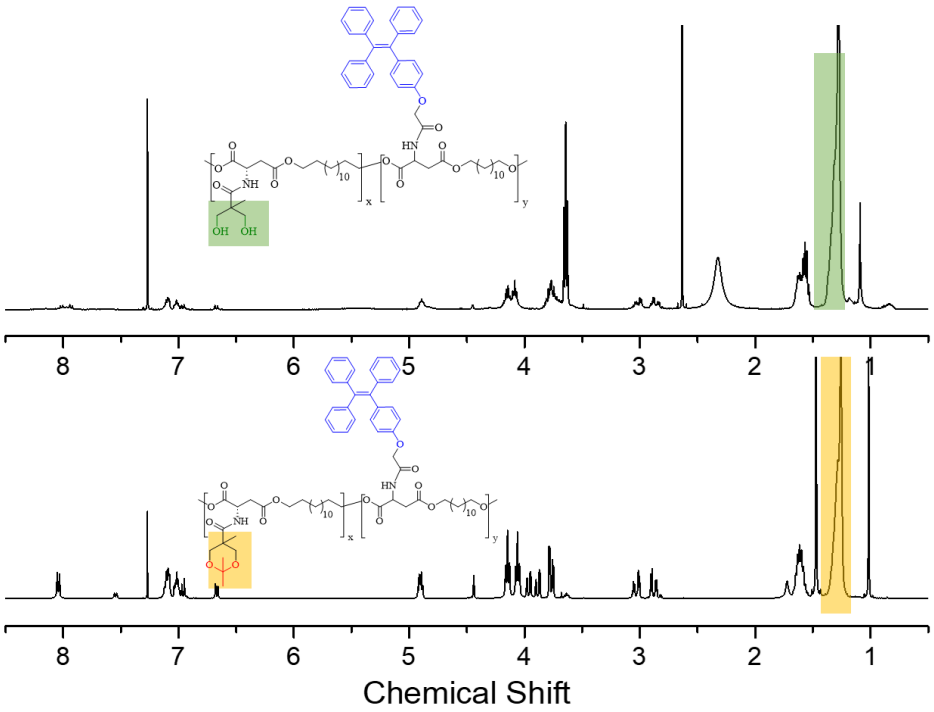

Figure 3.10. *^{1}H NMR spectra of the copolymer before (a) and after deprotection(b).*

The hydroxyl functionalised TPE Tagged polymer was then characterised with SEC with tetrahydrofuran as eluent, SEC chromatogram provided in Figure 3.11. After deprotection the molecular weight of hydroxyl functionalised TPE tagged polymers drastically reduced to 1500 to 2000 the obtained polymer molecular weight was underestimated due presence of hydroxyl group which may lead to reduction in hydrodynamic volume of the polymer as compare in a to Polystyrene standard using which the instrument which was calibrated, the molecular weight is summarised in the form of Table 3.2.

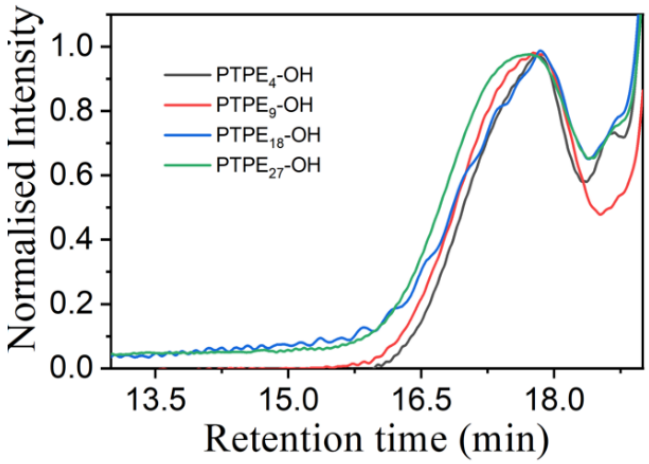

Figure 3.11 *SEC chromatograms of polymers in THF as eluent*

***Figure 3.2**. Table containing, molecular weights of polymers determined from SEC and polydispersity index.*

Polymer	M_n (g/mol) [a]	M_w (g/mol) [a]	PDI
$PTPE_4$-OH	1500	2000	1.3
$PTPE_9$-OH	1500	1800	1.2
$PTPE_{18}$-OH	1500	2000	1.3
$PTPE_{27}$-OH	1500	1900	1.2

(a) Molecular weights determined from size exclusion chromatography in using THF as eluent at 25 ºC.

3.3.4 Thermal Characterisation Acetal vs Hydroxyl copolymers

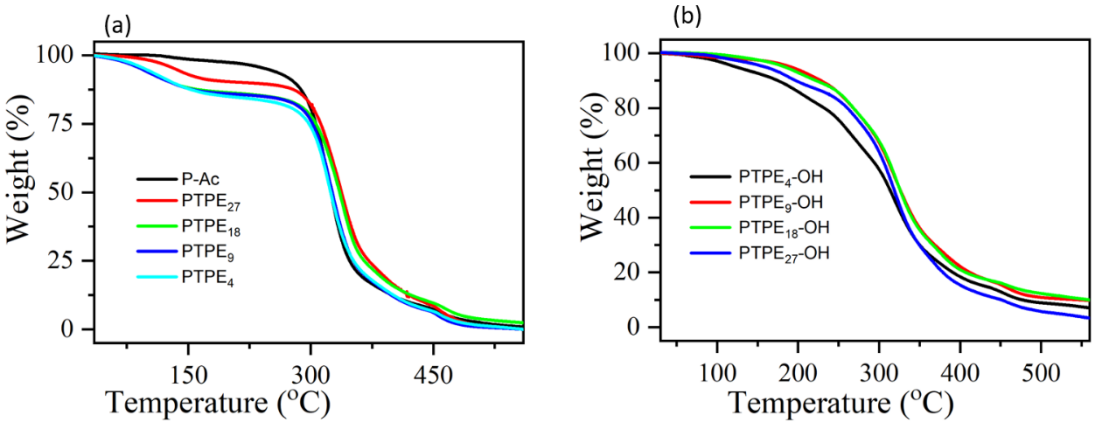

. ***Figure 3.12** TGA thermogram of the copolymer (a) for $PTPE_x$ (b) for $PTPE_x$-OH.*

The copolymers were then subjected to thermal characterisation using Thermogravimetric analysis (TGA) and Differential scanning calorimetry (DSC). TGA profile of the random copolymer suggest that the polymers are stable up to 350 °C with bimodal decomposition pattern as shown in Figure 3.12a for acetal copolymer after the deprotection of acetal to the hydroxyl group thermal stability varied and polymers found to be thermal stability up to 300 °C which is relatively less as compare to acetal counterpart (See Figure 3.12b). The homo-polymer of acetal P-Ac was found to be amorphous in nature on conversion to hydroxyl functionalised polyester (See Figure 3.13a) it remained amorphous and was found to increase the glass transition "T_g" value due to presence hydrogen bonding interaction between the polymer chains.

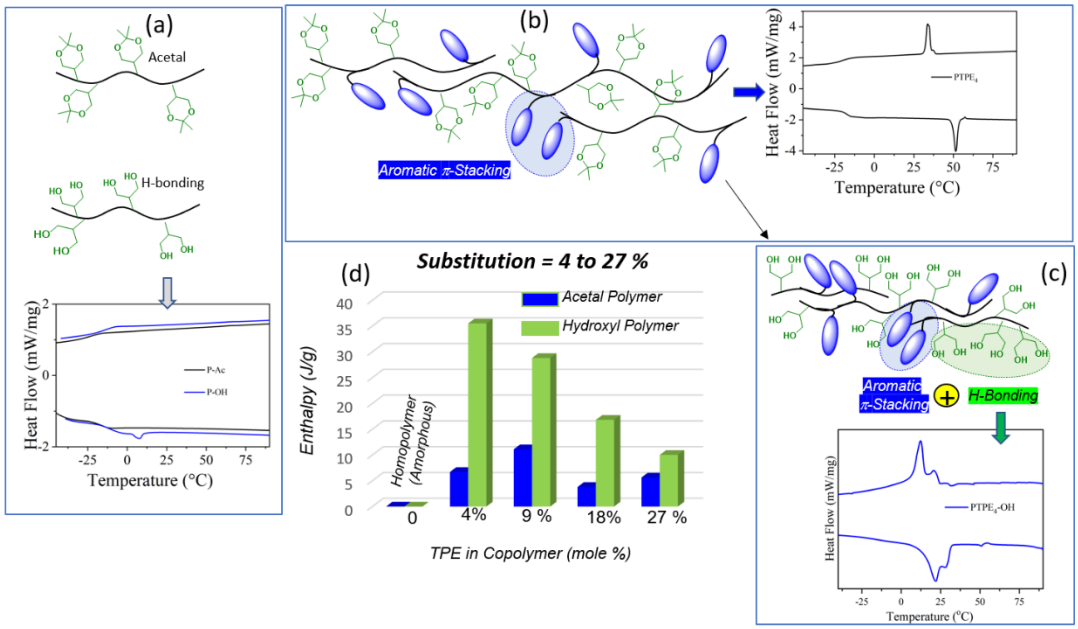

Figure 3.13 *Schematic representation and DSC data of P-Ac and P-OH (a) $PTPE_4$ (b)and $PTPE_4$-OH(c) DSC data shown summarized as histogram(d).*

The polymer system showed interesting thermal properties in the solid state, while on interesting result in thermal properties were observed, in case of $PTPE_x$ as the copolymer composed of acetal and TPE monomer, the polymer becomes semicrystalline, this semicrystalline nature of the polymer attributed to presence of TPE unit, the π-π interaction between the TPE pendant of the polymer segment causes the development of nucleating site inside the polymer matrix. All the polymer shows semicrystalline nature with melting point close to 50°C irrespective to their composition. DSC thermogram for acetal functionalised TPE tagged polymer is shown as the polymer showed Figure 3.13b. After the deprotection copolymer remains semi-crystalline nature of the polymer but with there is increase in the crystalline nature of the polymer as reflected from the increase in the enthalpy of the melting (ΔH_m). Increased crystalline nature due to two factors that is π-π interaction between TPE units and hydrogen bonding between hydroxyl functional group in the polymer chains. The glass transition temperature (T_g) of the polymer increased while the melt transition (T_m)

and crystallization transition shifts to lower temperature close to 25°C. DSC thermogram for hydroxyl functionalised TPE tagged polymer is shown as Figure 3.13c.

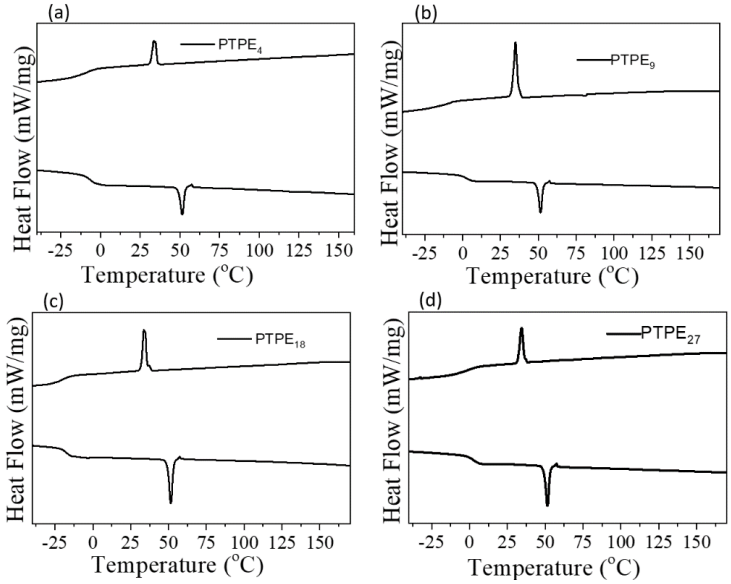

Figure 3.14 *DSC data for (a)PTPE4 (b) PTPE9 (c) PTPE18 and (d) PTPE27*

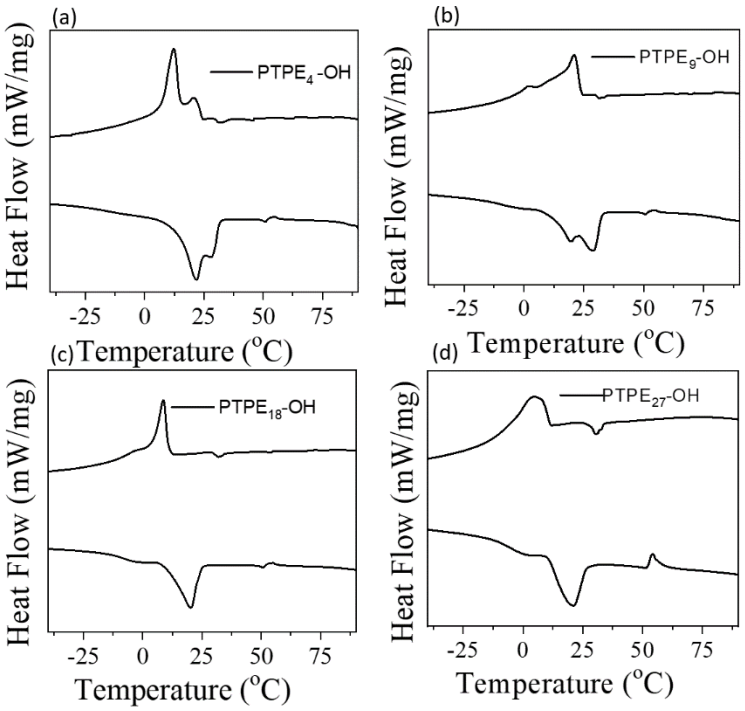

Figure 3.15 *DSC data for (a)PTPE4 (b) PTPE9 (c) PTPE18 and (d) PTPE27*

DSC thermogram of all the polymers are shown as Figure 3.14. and Figure 3.15. Thermal characterisation data is summarised in the form of plot as shown in the Figure 3.13d. The plot containing TPE content vs enthalpy of the melting (ΔH_m), As shown

the polymer P-Ac (without TPE unit) was found to be amorphous with no enthalpy of melting, When TPE was introduce in polymer melting enthalpy was observed. When we compare acetal vs hydroxyl counterpart of the polymer it showed enhancement in there in crystalline nature. The polymer $PTPE_4$-OH showed maximum crystalline nature, further increase in the TPE content resulted in decreases in semicrystalline nature. Thermal characterisation data of the polyester is summarised in the form of Table 3.3.

Figure 3.3 *Table containing thermal characterization data of the polymers*

Table contains the thermal characterisation data of the polymers

Polymer	T_d (°C) [a]	T_g(°C)[b]	T_m(°C)[c]	ΔHm(J/g)[d]	T_c(°C)[e]	ΔHc(J/g)[f]
P-Ac	350	-15	-	-	-	-
$PTPE_4$	350	-17	52	6.7	34	7.7
$PTPE_9$	350	-7	52	11.1	35	10.5
$PTPE_{18}$	350	-6.6	52	3.8	33	3.9
$PTPE_{27}$	350	-7	52	5.6	34	5.3

[a] Temperature of decomposition (T_d) determined from TGA. [b] The glass transition temperature (T_g) was determined from second heating cycle of DSC thermogram. [c]Melting point (T_m) of the polyester determined heating cycle of DSC thermogram. [d] Enthalpy of Melting determined from area under the curve of heating cycle of the of DSC thermogram. [e] Temperature of Crystallization (T_c) of the polyester determined cooling cycle of DSC thermogram. [f] Enthalpy of crystallization determined from area under the curve of cooling cycle of the of DSC thermogram.

3.3.5 Aqueous Self-Assembly

After studying the solid-state properties of the $PTPE_x$ copolymers, the hydroxyl functionalised TPE Tagged polymer with different content of the TPE was studied for their self-assembly in water by dialysis method. All the polymers were self-assembled using same protocol. 5.0 mg of the polymer was dissolved in the 2 mL of HPLC Grade dimethyl sulphoxide with constant stirring 3mL of milli Q water was added to the solution dropwise. The resultant 5mL of solution was transferred to 3kD dialysis bag and dialysed against water for 48h. Among the various copolymer all the polymers were soluble in water except the $PTPE_{27}$-OH was not found to be forming stable nanoparticle and precipitate out in water. The images of dialysed solution under normal light and UV light are provided as Appendix Figure S17. After dialysis solution appears to be cloudy under normal light while the presence of TPE chromophore is indicated by bright blue fluorescence from the solution under UV light. The photophysical properties of the polymer solution was carried out by absorbance and emission. The

polymer solution showed the absorbance maxima at 330nm while emission maxima was observed at 470nm. It was observed that even after maintaining equal concentration of TPE in the solution as the TPE content is increasing emission also increases this is due to the property of AIE as shown in Appendix Figure18. Among the different copolymer synthesized as mentioned earlier the $PTPE_{27}$-OH was not found to be forming stable nanoparticle, $PTPE_{18}$-OH was taken for further studies with aim polymer with highest content of TPE unit which is able to form stable nanoparticles.

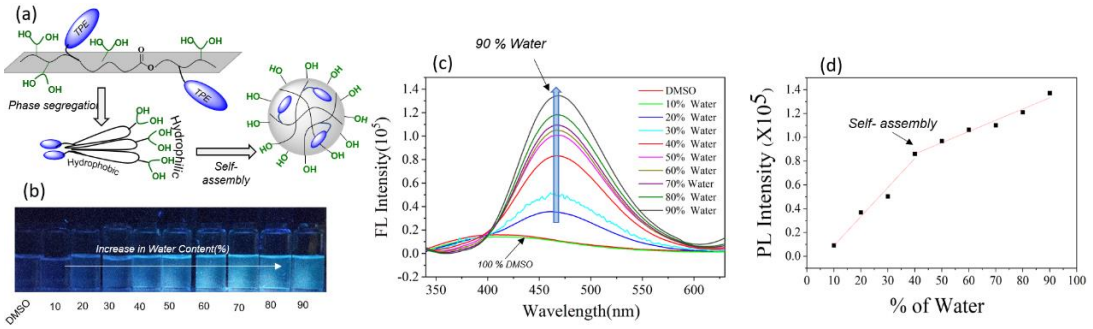

Figure 3.16 *(a) Schematic representation of self-assembly of $PTPE_{18}$-OH (b) photograph of vial containing $PTPE_{18}$-OH at different solvent combination upon photoexcitation under UV light (c) Emission spectra of the polymer in different water-DMSO combination, concentration of the $PTPE_{18}$-OH was maintained as 100µg/mL. (d) Plot PL emission intensity vs solvent combination showing break point at 40% water in DMSO-water combination*

The hydroxyl functionalised TPE Tagged polymer, $PTPE_{18}$-OH composed of two segments TPE pendant side chain and backbone contributes as hydrophobic portion of the polymer while hydroxyl group acts as hydrophilic segment. When the $PTPE_{18}$-OH self-assemble in aqueous system polymer undergo self-assembly in such a fashion that first polymer undergoes phase segregation then form micelle as shown in Figure 3.16(a). As the polymer composed of TPE unit which is known show the phenomena of aggregation induced emission upon in the solution aggregation. To study AIE phenomena on self-assembly, solvent dependent aggregation of the polymer was studied by maintaining the constant concentration of the polymer in water-dimethyl sulphoxide combination. Dimethyl sulphoxide being the good solvent for the polymer, it is expected that polymer will be in expanded chain confirmation while as content of water will increase the polymer undergoes aggregation to form self-assembled structure. The photograph of vial shows increases in intensity of fluorescent polymer upon increase in the water content of the polymer solution. The corresponding emission spectra of the solution is shown as Figure 3.16b. The emission intensity of the polymer

aggregate in DMSO shows no emission as polymer is in extended chain confirmation. With increase in water content polymer chains start to undergo aggregation. TPE polymer shows aggregation induced emission peak at 470nm. (See Figure 3.16c). As the polymer content increases emission of TPE aggregation which resulted in the increases in the emission intensity from the solution, this due to phenomena on aggregation induced emission. To rule out the possibility of increase in molar extension coefficient with increase in water content, the solutions was studied for their absorbance. It was found that absorbance of the solution remains constant. As shown in Appendix Figure S19. The emission maxima were plotted w. r. t. water content and it was found that emission intensity at 470nm increases with increase in water content linearly up to 40 %. The break points above 40 % there is slow increase in emission intensity. The break point corresponds to formation TPE nanoparticles.

3.3.6 Determination of critical aggregation concentration

To determine the concentration at which polymer chains comes close to each other to form polymer nanoparticles is referred as critical aggregation concentration (CAC). For the determination of CAC, the property of the TPE to undergo AIE was exploited. In aqueous environment, below certain concentration, polymer chains are freely soluble in water and TPE pendant (fluorophore) are also shows less emission. When the polymer concentration increases polymer chains starts coming close to each other and shows enhancement in the emission of the TPE, this is due to the fact that when TPE molecule come close to each other and undergo aggregation.

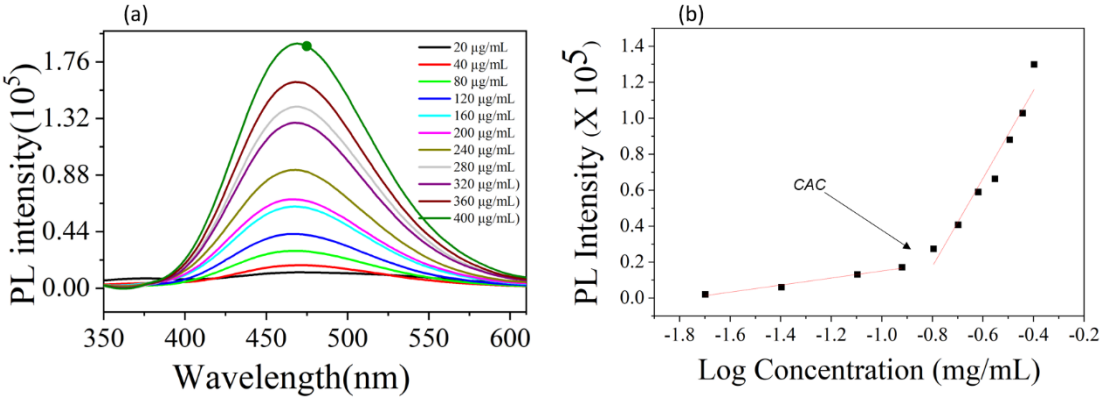

Figure 3.17 *(a) Emission spectra for the PTPE$_{18}$-OH at various polymer concentration ranging from 20µg/mL to 400µg/mL. (b) Plot PL emission intensity vs concentration of the PTPE$_{16}$-OH in 90% water in DMSO-water combination.*

When TPE molecules are in free form in good solvent upon excitation at its absorbance maxima, the TPE molecules mainly release its energy rotation of the double bond and monomeric emission peak at 350nm but when the TPE molecules undergo aggregation there is formation of new peak due to aggregation induced emission at 470nm. In the polymer system chain comes close to each other the TPE molecules undergo aggregation due to that there is restriction in the intramolecular rotation of phenyl group of the TPE molecule which results in enhancement in photo luminance (PL) intensity which can be directly corelated with formation of polymeric nanoparticle due to aggregation. This can be a direct method to detect the aggregation of polymer chains to determine CAC of the polymer in water. To determine the CAC of the $PTPE_{18}$-OH polymer, stock of $PTPE_{18}$-OH polymer was taken at the various concentration of increasing from the range of 20 µg/mL to 400 µg/mL. The polymer was dissolved in 10 % DMSO and 90 % water concentration. This polymer solution was the subjected to photophysical characterisation such as absorbance and fluorescence (see Figure 3.17a) absorbance spectra of the polymer solutions is shown as Appendix Figure S20. The absorbance does not show much increase as compare to fluorescence as shown Figure 3.17a. The corresponding plot concentration of polymer vs fluorescence at 470 nm is as shown in Figure 3.17b. The break point at 180 µg/mL corresponds to critical aggregation concentration.

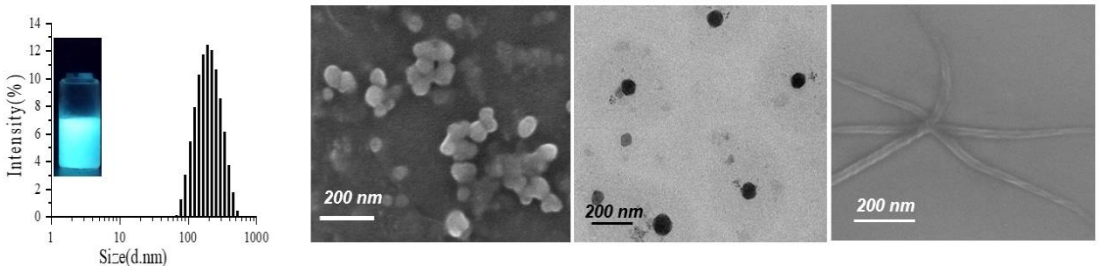

Figure 3.18 *(a) DLS of data for $PTPE_{18}$-OH nanoparticles at concentration 0.1mg/mL. (b) FESEM data for $PTPE_{18}$-OH nanoparticles (c) HR-TEM data for $PTPE_{18}$-OH nanoparticles. (d) $PTPE_{18}$-OH nanofiber drop-casted in THF.*

The synthesized polymeric nanoparticle was studied for size using dynamic light scattering (DLS) and morphology by FESEM and HR-TEM and. DLS data is shown as Figure 3.18(a) which suggest that polymer nanoparticle of size 250±10 nm, the photograph dialysed solution of polymer sample under UV light shows fluorescent blue emission under UV light. The polymer morphology was confirmed using HR TEM and

FESEM. It showed that polymer forms nanoparticle with spherical morphology with size of nanoparticle was 100±10 nm. (See Figure 3.18b and Figure 3.18c). The polymer showed the formation of helical nanofiber when dissolved and drop casted in THF as shown in Figure 3.18d.

3.3.7 Drug or Biomarker Encapsulation

The TPE Tagged hydroxyl functionalised polymer PTPE$_{18}$-OH was utilised for loading drug doxorubicin (DOX), Rose bengal (RB), Rhodamine B and (RhB) biomarker. The doxorubicin was chosen as drug and biomarker such as Rhodamine B (RhB) rose and Bengal (RB) was chosen to encapsulate inside the nanoparticle. The drug (or biomarker) encapsulation was carried out by using dialysis method.

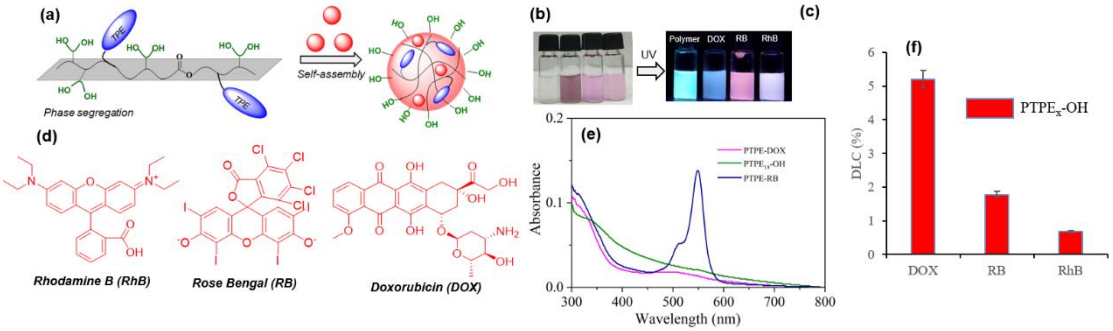

Figure 3.19 *(a) Schematic representation of loading of cargo in PTPE$_{18}$-OH nanoparticles. photograph of vial containing drug/ dye loaded nanoparticles under normal light (b) and photoexcitation by UV light (c). Chemical structure of the loaded cargo(d) Absorbance spectra of PTPE$_{18}$-OH nanoparticles(e). Plot containing drug/ dye loading content (DLC) of various cargo (f).*

The typical procedure for encapsulation drug (or dye) involves following steps, for example 5.0 mg of the and PTPE$_{18}$-OH polymer along with 0.5 mg of the drug doxorubicin, the drug is in the form of hydrochloride salt it was neutralised with triethyl amine solution. was dissolved in 3.0 ml dimethyl sulphoxide and water was added to this mixture dropwise to start self-assembly, this solution was then transferred to 1kD dialysis membrane dialysed against Milli Q water for 48 h to form doxorubicin loaded nanoparticle the mechanism of the drug (or dye) loading is depicted in Figure 3.19a. The polymer loaded cargo show fluorescent illumination under normal light and UV light as shown in Figure 3.19b and 3.19c. The nascent polymer nanoparticle sample produces strong blue fluorescence upon photoexcitation by UV light while loaded nanoparticles showed different coloured depending upon loaded dye. The chemical structure of the loaded cargos is shown in figure 3.19d. The drug/dye loaded

nanoparticle was then subjected to absorbance studies. The absorbance spectra showed the presence of two absorbance maxima the first absorbance maxima belong to TPE chromophore at 330 nm and other loaded cargo shown peak at their respective wavelength. Such as presence of doxorubicin was observed by peak at 490 nm. While in case of RB and RhB loaded polymer nanoparticle λ_{max} was observed at 550nm (See Figure 3.19e). These drugs (or dye) loaded nanoparticle was measured for drug (or dye) loading content (DLC) and drug (or dye) loading efficiency (DLE) using absorbance spectroscopy using Lambert-Beers law. The molar extension co-efficient for DOX, RB and RhB was 11500, 90400 and 10600 L mol^{-1} cm^{-1} respectively for calculating DLC and DLE. The DLE and DLC was summarised in the form of plot Figure 3.19f. The polymer showed DLC for rose bengal 3.1 % while doxorubicin and RhB was loaded 5.1 % and 1 % respectively. The drug (or dye) loading efficiency (DLE) was found to be 31 % , 51 % and 10 % for Rose Bengal, doxorubicin and Rhodamine B respectively. The doxorubicin loaded nanoparticle was referred as PTPE-DOX while RB and RhB loaded nanoparticle was referred as PTPE-RB and PTPE-RhB respectively. The polymer without TPE was is referred POH which was also attempted to load as drug doxorubicin and biomarkers such as RB and RhB, POH showed loading of doxorubicin and RB but was unable to load RhB. The nanoparticle without TPE were referred as POH-DOX and POH-RB.

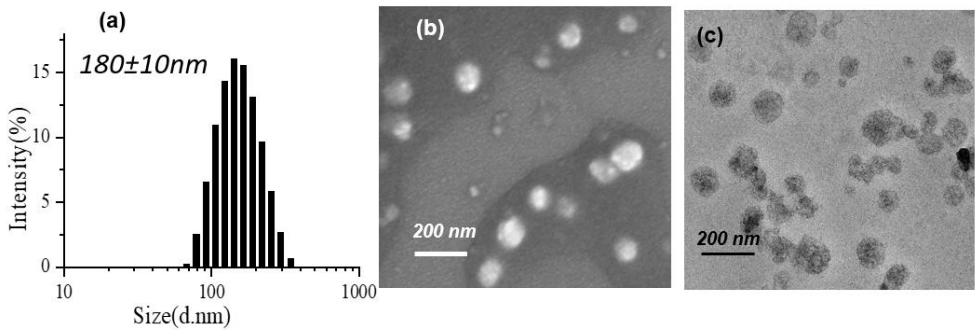

Figure 3.20 (a) *(a) DLS of data for PTPE-DOX nanoparticles at concentration 0.1mg/mL. (b) FESEM data for $PTPE_{18}$-OH-DOX nanoparticles (c) HR-TEM data for PTPE-DOX nanoparticles.*

The size of the nanoparticle was determined by dynamic light scattering (DLS), the PTPE-DOX is shown in Figure 3.20a after loading drug (or dye) the nanoparticle found to be produce below 200nm. FESEM data of the polymer shows the PTPE-DOX form nanoparticle of spherical morphology with diameter of 150±10 nm which corroborated

with DLS data (See Figure 3.20b). The PTPE-DOX nanoparticles were further characterised for its structure using HR-TEM, which suggest the similar result as by FESEM, HR-TEM image shown in the Figure 3.20c.

3.3.8 Photophysical Properties and FRET probes

In the nanoparticle PTPE-DOX, inside the nanocavity there are two chromophore that is TPE and doxorubicin is in close vicinity enough that there is probability of transfer of energy between two different chromophores. Figure 3.21a shows the schematic representation for energy level diagram for energy transfer between two chromophores via FRET process. During the FRET process the when one molecule of higher energy level when excited it releases energy so that, the chromophore in the closed vicinity can absorb released energy utilised by nearby chromophore to excite give emission spectra of later. The chromophore which absorbs higher energy referred as **donor** and molecules gets energy from donor is referred as **acceptor.** In this case TPE acts as donor and loaded chromophore DOX acts as acceptor in this case.

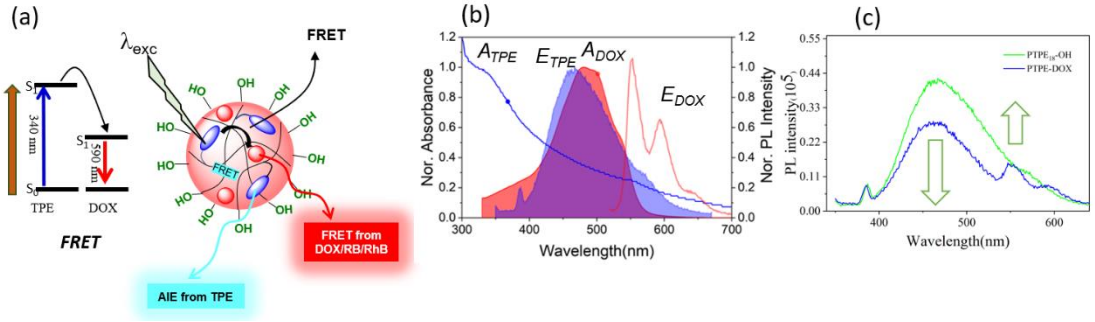

Figure 3.21 *(a) Schematic representation for energy level diagram for energy transfer by FRET process and energy transfer between two chromophores by FRET process in in nanoparticle* PTPE-OH-DOX. *(b) Spectra of Absorbance and emission spectra of PTPE and DOX to study spectral overlap. (c) Emission of spectra of PTPE along with PTPE-DOX.*

The molecular structure of donor and acceptor is provided as Figure 3.21b polymer micelle having hydrophobic core occupied by TPE molecule for example PTPE-DOX polymer NPs, in the hydrophobic core of the micelle TPE and doxorubicin are in close vicinity (See Figure 3.21b). The intermolecular interaction between TPE and DOX was studied by fluorescence measurement. Nanoparticle solution of PTPE-DOX, PTPE-RB and PTPE-RhB was subjected to emission of the chromophore. All samples were prepared by maintaining optical density of 0.1 OD for the TPE. As a

control polymer was without TPE was prepared which completely hydroxyl functionalised polymer. For the phenomena of FRET, the two molecules should show some characteristic properties which includes the pair of the molecules should acts as donor and acceptor. These pair of acceptors should show the overlap integral. This property was studied by comparison between overlap between emission spectra of TPE and absorption spectra of doxorubicin and it was found that there is an overlap between them. (See Figure 3.21c). there is 94 % overlap of absorbance spectra of the doxorubicin with emission spectra of TPE in PTPE-DOX system. When the PTPE-18-OH NPs in water molecule excited at 330nm, the polymers show TPE self-emission with λ_{em}= 470nm. When the PTPE-DOX system with concentration of TPE 0.1 OD was excited at 330nm it showed the reduction in the TPE self-emission at 470nm and showed emission peak from DOX. This is due to the transfer of energy form donor molecule TPE to the acceptor DOX. There was reduction in energy of the TPE sample and transfer of energy from TPE to doxorubicin due to FRET. Similar kind of study was also performed from PTPE-RB and PTPE-RhB systems as shown in Appendix Figure S21 and S22. There is 38% overlap between absorbance spectra of the RB with emission spectra of TPE in PTPE-RB system. FRET phenomena were also observed in PTPE-RB after exciting nanoparticle PTPE-RB at 330nm there was emission signal observed from TPE and RB.

(a)

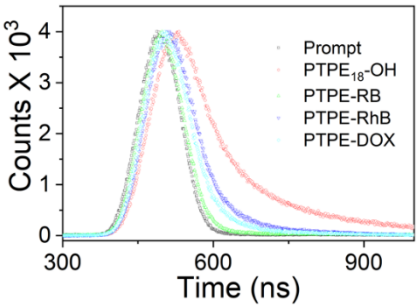

(b)

Sample	Overlap integral	Time (ns)	E_{FRET}	R(A)
PTPE-DOX	5.46 X10^{14}	0.27	74	25.3
PTPE-RB	1.45X10^{15}	0.4	86	29.8
PTPE-RhB	1.70X10^{15}	1.2	65	30.6
PTPE$_{18}$-OH	-	3.5	-	-

Figure 3.22 *(a) TCSPC plot for PTPE polymer and PTPE loaded cargo and (b) corresponding table containing fluorescence lifetime decay constant, efficiency of energy transfer, Forster distance etc.*

There were no such FRET phenomena was observed in case of polymer nanoparticle without TPE. The sample without TPE such as POH-DOX and POH-RB samples were also studied for photophysical characterisation using absorbance and emission spectroscopy. As expected, absorbance spectra did not show any at 330nm

but only absorbance observed from the loaded chromophore, Further emission spectra of POH-DOX and POH-RB only showed signal from DOX and RB respectively when excited at their respective absorbance maxima. The PTPE-RhB sample showed FRET between TPE and RhB with overlap integral of 38%. FRET phenomena were further studied using time correlated single photon counting (TCSPC) spectroscopy. The lifetime of donor in the nanoparticle studied as PTPE-DOX and PTPE-OH i.e., with and without acceptor respectively. The lifetime of donor is referred as T_D and lifetime of donor in presence of acceptor is defined as T_{DA}. TCSPC measurement was carried out by exciting TPE using 340nm nano-LED lamp up to 10000 counts, the decay profiles showed in Figure 3.22a. For the sample PTPE-DOX, TPE molecules relax very fast in presence of doxorubicin which shows life time 0.27 ns while in absence of doxorubicin polymer NPs on exciting at 340nm life time 3.5 ns which is more as compare PTPE-DOX. The other system showed similar observation such as in case of PTPE-RB and PTPE-RhB system the lifetime of TPE was observed as 0.4ns and 1.2ns respectively (See Figure 3.22b). The FRET efficiency between donor and acceptor was calculated using equation $E_{FRET} = 1-T_{DA}/T_{D.}$ where T_{DA} is lifetime of donor in presence of acceptor and T_D is life time of donor in absence of acceptor. As the FRET is distance depend process, it is essential that the donor and acceptor must be in close vicinity, the distance between the donor and acceptor should be less than 50 A^o. In this system of PTPE-DOX, PTPE-RB and PTPE-RhB distance between TPE and other loaded chromophore were found to be in the 25-30 A^o (See Figure 3.22b) which is very less as compare to Forster distance 50 A^o and in all the cases FRET efficiency was found to be above 50%. The details information about FRET calculation is provided in appendix and related information such as Forster distance FRET efficiency, overlap integral, life times of TPE is summarised in the form of table in Figure 3.22b.

3.3.9 Enzyme responsive release of DOX

The L aspartic acid-based hydroxyl functionalised polymer earlier in lab was having hydroxyl group as a pendant. The current case the polymer was modified in such a manner it is having both hydroxyl group and TPE as side chain pendant. The polymer PTPE-OH backbone is comprised of fully aliphatic linkage which known to undergo cleavage by the action esterase enzyme under physiological condition as shown in Figure 3.23a.

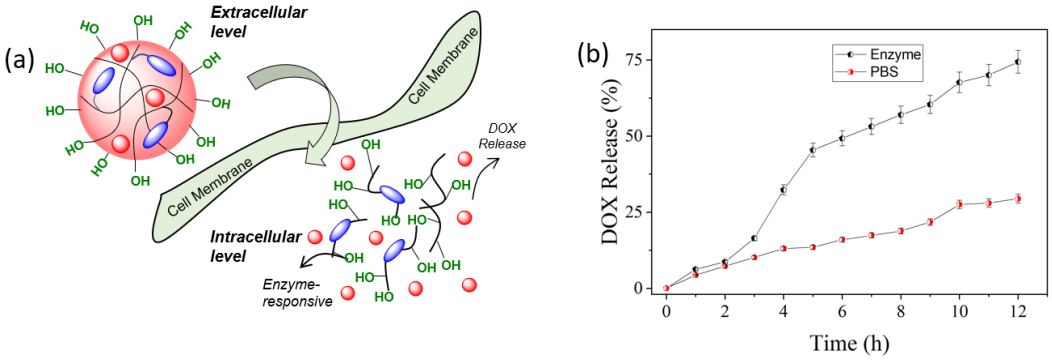

Figure 3.23 *(a) Schematic representation of process of endocytosis of PTPE-DOX by MCF 7 cell lines degradation of the polymer nanoparticles due to enzymes in lysosomal compartment inside the cells. (b) Cumulative doxorubicin release profile from PTPE-DOX nanoparticle with and without of esterase enzyme at 37 ℃ in pH= 7.4.*

The release of doxorubicin from PTPE-DOX by the action esterase enzyme was studied using dialysis method as reported earlier (ref). PTPE-DOX sample was incubated with 10 U horse liver esterase enzyme under physiological condition such 37 ºC and 7.4 pH. This mixture was then added to dialysis bag (1Kd) and dialysed against 20 % PBS solution and studied using absorbance spectroscopy cumulative doxorubicin release was plotted against time as shown in Figure 3.23b in presence of enzyme 80% of doxorubicin was released. As compare to our earlier system[58] which fully hydroxyl functionalised polyester was composed aliphatic polyester linkages in a backbone and hydroxyl group as pendant, which was capable to encapsulate various drugs and dye but it has poor enzymatic degradability such resulted in release of drug up to only 30%. The present polymer is composed of TPE side chain in addition to hydroxyl group which changes hydrophilic hydrophobic balance of the polyester. As a control experiment was performed without enzyme which shows leaching of drug up to 30% (See Figure 3.23b).

3.3.10 Cell viability and biocompatibility

The biocompatibility of polymer nanoparticle was studied by (3-[4,5-dimethylthiazol-2-yl]-2,5 diphenyl tetrazolium bromide) (MTT) assay (ref) in three different cell lines which includes normal cell lines WT MEF and cancer cell lines Breast cancer cells (MCF 7) and ovarian cancer cells (SKOV 3) cells. Similar procedure was followed as performed earlier. 10^3 Cells were seeded per well in 96 well plate and grown for 18h along with complete media. After the completion of incubation, the

media was removed from the 96 well plate and it was replaced with fresh media with polymer samples. The concentration of the sample was maintained in the range 10 µg/mL to 100 µg/mL and as a control the cells were grown with complete media alone. Then the plate was incubated for 72h, and then it was added with MTT solution. The concentration of the farmazan crystal produce was studied by varioscan and cell viability was calculated by comparing with control. As shown in Figure 3.24a, the

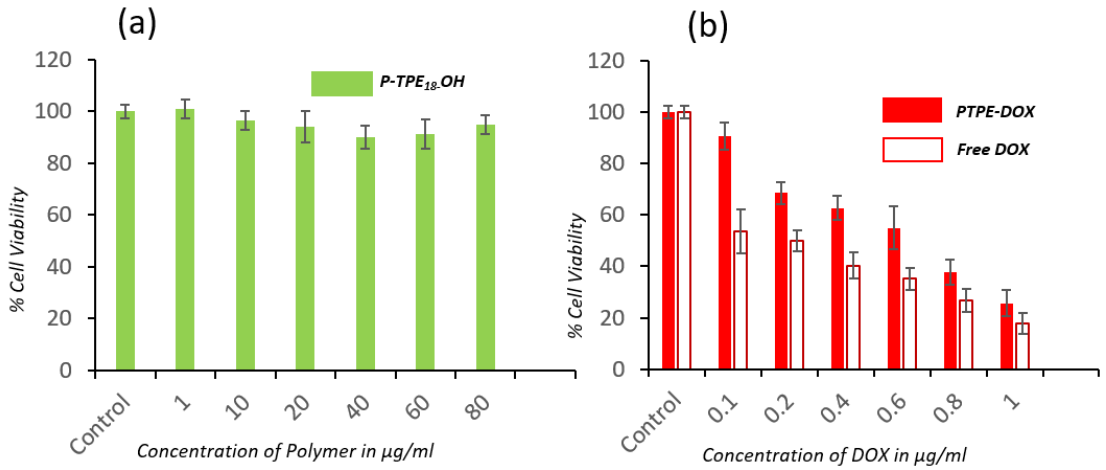

polymer alone was found to be biocompatible in all the three cells lines up to 100 µg/mL

Figure 3.24 *(a) Cell viability of thePTPE$_{18}$-OH polymer (b) Cell viability of the PTPE-DOX and Free DOX in MCF 7 cell line. [10^3 cells are used for seeding in the cytotoxicity studies].*

Cytotoxicity of Free doxorubicin vs PTPE-DOX towards the MCF 7 cell lines is shown in Figure 3.24b, PTPE-DOX cytotoxicity study was performed in the range of 0.1 µg/mL to 1 µg/mL. The PTPE-DOX was able to deliver doxorubicin the kill cancer cells. In both the cases that is free doxorubicin and PTPE-DOX there is inhibition of the cell growth was observed but free DOX showed more killing as compare to PTPE-OH-DOX. This can be attributes to slow release of doxorubicin from PTPE-DOX as compare to free DOX.

3.3.11 Cellular Uptake

The ability of the nanoparticle to deliver the drug was studied at the cellular level by confocal microscopy. As the polymer sample was found to be biocompatible in the normal and cancer cell lines it was taken to study the uptake of PTPE NPs. For this purpose, 100000 cells of SKOV3 cells lines were seeded on the 6 well plate on the glass coverslip and grown for 16h along with the complete media. After incubation old media

was aspirated and fresh media PTPE-OH, PTPE-RB, PTPE-RhB and PTPE-DOX was then incubated for 6h with the cells. The cells were fixed on slide imaged under confocal microscopy. As shown Figure 3.25a First panel shows that PTPE-OH polymer alone taken up by the cells, TPE was excited with 405 nm laser and collection was done in the range of 410nm-494nm and along with it the cells were excited at different laser to check any other emission from the cells. The first panel shows that on excitation using different laser only emission from TPE was observed with is indicated by cyan colour in the image. No emission in the DOX channel due to absence of the DOX inside the polymer apart from DOX there were no emission observed in other channels when excited with 488nm and 561 lasers

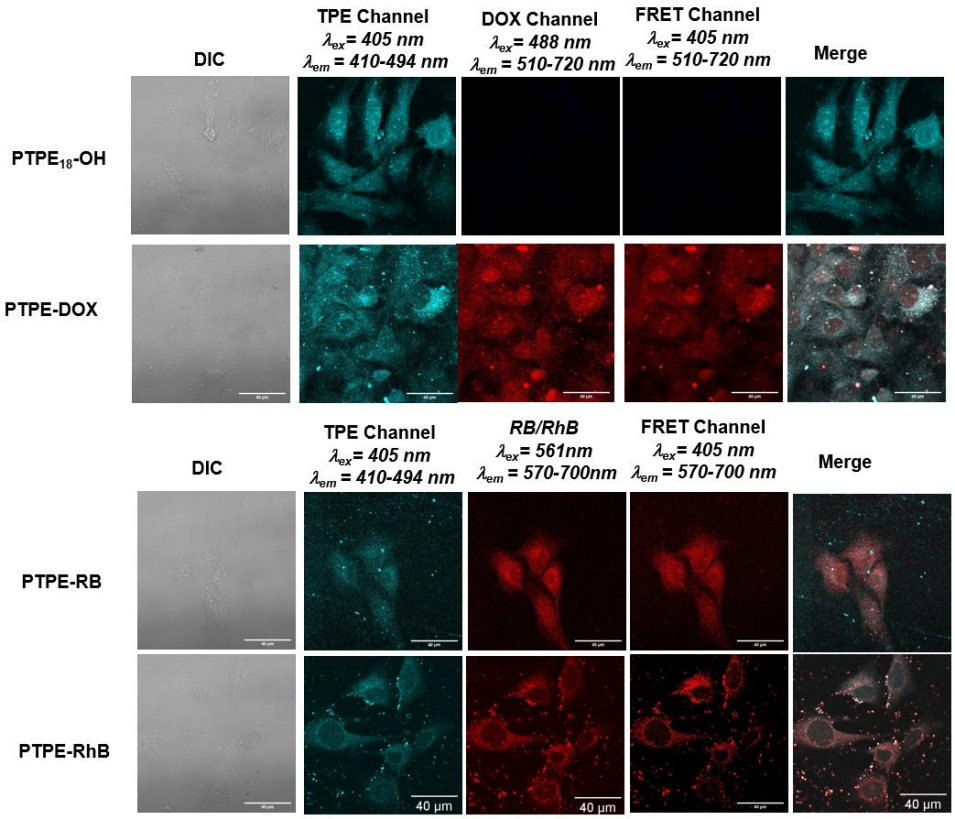

Figure 3.25: *Cellular uptake studies for (a) PTPE-OH polymer alone (b) PTPE-DOX(c) PTPE-RB and (d)PTPE-RhB in the SKOV 3 cells lines. Scale bar= 40µm*

Uptake studied for sample taken up PTPE-DOX further confirms the uptake of the nanoparticle, TPE was excited at 405 nm laser while DOX was excited using 488nm laser emission of DOX shown by the red colour. As the both TPE and DOX are in close vicinity inside the cells. FRET channel was also added where cells were excited using 405nm laser and collection was done at the DOX channel. The FRET phenomena were

also observed at the cellular level due to transfer of energy from TPE to DOX. (See Figure 3.25b). Similarly, the cellular uptake studies were performed for PTPE-RB and PTPE-RhB nanoparticles was carried out, In the confocal microscopy rose Bengal and Rhodamine B was excited using 561nm laser and collection was done from 570-620nm self-emission of the RB and RhB observed. Location of the TPE inside the cells is determined from exciting cell with 405 laser and collection at 410-494nm, in both PTPE-RB and PTPE-RhB uptake studies TPE signal was observed in the cytoplasm of the cells. The loaded cargo RhB and RB was also observed found inside the cytoplasm of the cells. The merge images show the location of the TPE and RB are the same. The study FRET process inside the cells, the cells were excited by using 405 nm laser and collection was done from 570-620nm. (See Figure 3.25c and Figure 3.25d) which show first TPE molecule gets and then transfer the energy to RB or RhB.

3.3.12 Haemolysis

For *in vivo* study in the polymer should be nontoxic toward the Red Blood Cells (RBCs) of the mice. To check the biocompatibility of the $PTPE_{18}$-OH with RBCs, haemolysis experiments was performed by the reported procedure in earlier chapter. The blood was freshly withdrawn for retro-orbital sinus of the Bulb C mice and incubated with solution of the $PTPE_{18}$-OH at the concentration of 1mg/ml in PBS for 1h at 37 ºC.

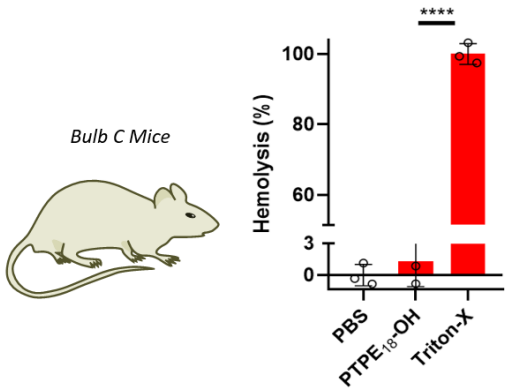

Figure 3.26 *Haemolysis study of $PTPE_{18}$-OH (0.1 mg/mL) with Triton-X as positive control and PBS as negative control. (****p<0.0001). Each point represents mean ± SEM (n = 3)*

After the incubation blood samples were centrifuged at 8000rpm for 10 min. The haemolytic nature of the sample is compared with Triton X as the positive control while PBS was taken as negative control. After the centrifugation if the sample is non

haemolytic then RBCs for palette at centrifuge tube. The clear plasma of the blood was the collected as supernatant and absorbance was measured at 480 nm. The absorbance data further confirms the non-haemolytic nature of the $PTPE_{18}$-OH as shown in the plot Figure 3.3.26. The found to be biocompatible with RBCs as shown in plot polymer shows <2% haemolysis.

3.3.13 In Vivo biodistribution Studies

Considering the non-haemolytic nature of $PTPE_{18}$-OH, The $PTPE_{18}$-OH was taken for *in vivo* biodistribution studies. The $PTPE_{18}$-OH was attempted to encapsulate with IR 780 which is NIR active biomarker. The polymer found to encapsulated the IR780 in the form of polymer nanoparticle drug loading content (DLC) 1%. (See Figure 3.27)

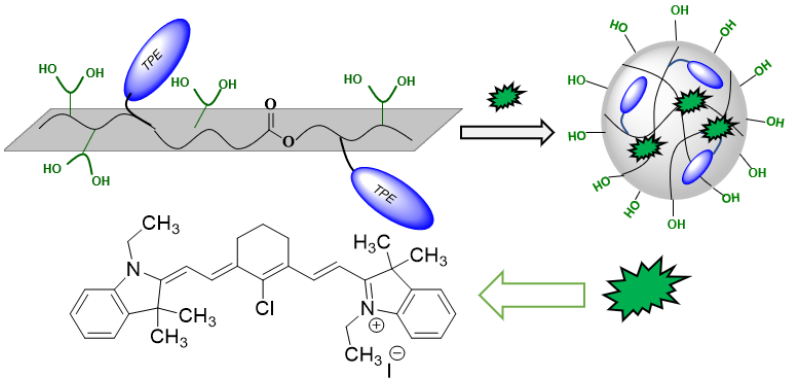

Figure 3.27 *Schematic representation of loading of IR 780 biomarker in the nanoparticle.*

The biodistribution of the biomarker was studied in the mice by using IVIS imaging setup. The IVIS imaging setup helps to study live monitoring of IR780 biomarker inside body of a live mice without causing side effects. The experiment was carried out on Bulb C mice of age 2–3-month-old through intra-peritoneal injection. The biodistribution experiments were performed in three different sets (i) set of mice which was injected with only PBS as a negative control (ii) set of mice injected with free IR780 dissolved in PBS (ii) set of mice injected with sample PTPE-IR780. All the three set of mice were compared during course of experiment. The concentration of IR780 was maintained as 0.5 mg/Kg of the body of the mice in PBS as medium, After the injection the body imaging of mice was done in a time dependent manner, the interval of IVIS imaging includes 4h, 24h, 48h and 72h.

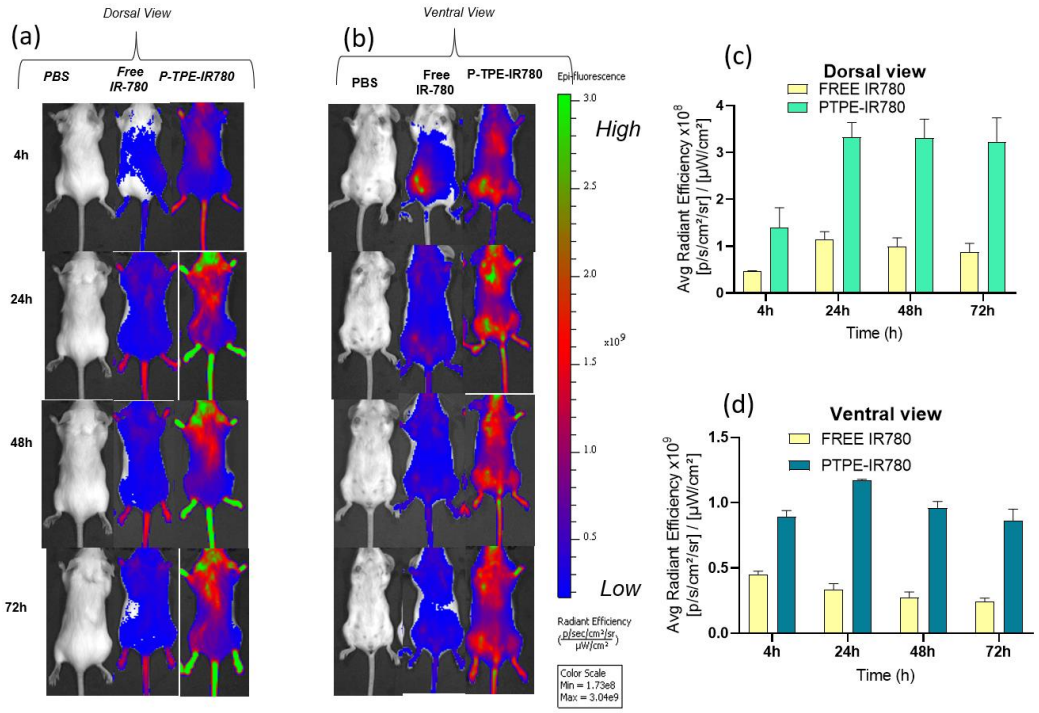

Figure 3.28 *Images of the mice for kinetics of the biodistribution (a) dorsal view (b) ventral view. plot corresponding to the intensity of the signal (c) dorsal view (d) ventral view*

The imaging was conducted from dorsal and ventral view as shown in the Figure 3.28a and Figure 3.28b. The first set of the mice in the panel does not show any signal from IR780 from dorsal and ventral view when subjected to excitation to signal 745nm wavelength and collection was done IR region as the PBS was considered as negative control for the experiment. The second set of the mice was subjected to the free IR780 imaging was done in the time dependent manner post injection. As you can see in case of the dorsal view the intensity of the IR780 is quite low in the body with over increase in the time spread across the body, while in case of the dorsal view 4h post injection most of the IR780 remains inside the intraperitoneal cavity and with time it slowly diffuses out. The IR780 loaded in the form of the polymer nanoparticle when injected in the mice showed interesting result the both the dorsal and the ventral view showed presence of the IR780 the maximum intensity is compare to the free IR780 this could be due the increase in the life time of the IR780 as compare to free IR780. The quantification of the bio distribution was carried out using average radiant efficiency which is plotted over time. The data is shown as Figure 3.28c and Figure 3.28d. The biodistribution studies showed better life time of nanoparticle as compare to the free IR780, which could be due to the renal clearance by kidney. The presence of the IR780

was further confirmed in the blood plasma, the blood was collected from the mice retro-orbital in plasma was extracted by centrifugation, IVIS imaging data shows the similar result as done for live mice. The mice with IR 780 polymer NPs showed higher signal as compare to free IR 780 (See Figure 3.29a). Similar trend was observed for both 24h and 48h time point as reflected in the corresponding plot.

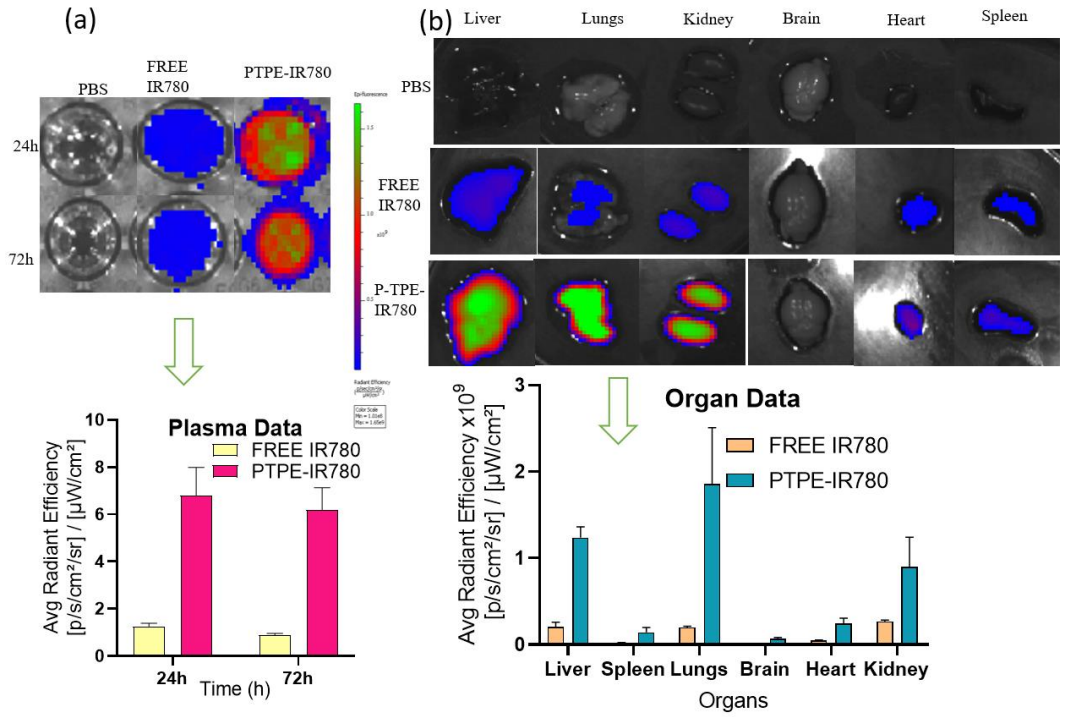

Figure 3.29 *Representative photograph of different time point the plasma by IVIS Imaging setup (b) Plot corresponding to the different time point the plasma by IVIS Imaging (c) Photograph of the mice organ for sacrifice ex vivo imaging(d). Plot corresponding to the mice organ for sacrifice ex vivo imaging.*

To comprehensively assess organ-level biodistribution, the mice were sacrificed after 72 hours of imaging. Major organs such as the brain, heart, liver, spleen, and kidneys were meticulously collected for analysis using the IVIS imaging setup. As shown in Figure 3.29b, the first panel pertained to mice injected with PBS alone, revealing no emission signal. In contrast, the second and third panels corresponded to mice administered with free IR780 and PTPE-IR780 nanoparticles, respectively. Among these vital organs, no detectable signal was observed from the brain. Subsequently, only faint signals were noted in the heart and spleen, suggesting minimal cardiotoxicity in both free and P-TPE-IR780 formulations. In stark contrast, more robust signals emanated from the kidneys, liver, and lungs, indicating effective clearance mechanisms through renal or hepatic pathways. These findings were

substantiated by the radiance intensity plot, underscoring the superior delivery capabilities of polymer nanoparticles compared to free IR780. In conclusion, this extensive study not only sheds light on the biodistribution patterns of IR780 but also highlights the potential advantages of utilizing polymer nanoparticles as an efficient delivery vehicle for IR780 in biomedical applications.

3.4 Conclusion

L-aspartic acid based new monomers was designed and polymerised using melt polycondensation strategy to produce fluorescent tagged polyester. The copolymer was well characterised for structural properties which ^{1}H NMR studies further confirms reliability of the method to produce copolymer with exact composition. SEC chromatography further confirms the moderate molecular weight built up. The acetal group of the polymer subsequently deprotected to get hydroxyl functionalised TPE tagged polymer, which was found stable up to 300 ºC. DSC profile of the polymer provides interesting result. The semi crystallinity in the polymer induces by the π-π interaction in the polymer chains which creates the nucleating site after deprotection the semi crystalline nature further induced due to π-π interaction and hydrogen bonding interaction synergistic effect. Polymer showed AIE properties in the solution state studies, the CAC value of the polymer determined using the AIE property of the polymer. The polymers were capable to form nano-assemblies in aqueous state able to encapsulate hydrophilic and hydrophobic dyes. The polymer nanoparticles were characterised for their size and shape using FEEM and HR-TEM which showed nanoparticle with spherical morphology with sub nano-meter size. As the polymer nanoparticle photophysical properties emission spectra and lifetime measurements which confirms the FRET phenomena in the nanocavity of the nanoparticles. The polymer found to be biocompatible with normal and cancer cells and showed successful carrier for the drug delivery in the cells. The interaction between polymer chain and loaded cargo also employed to study FRET at the cellular level. *In vivo* biodistribution was carried out in the Bulb C mice using IVIS imaging setup, which further confirms the utilisation of polymer based nanocarrier for delivery of cargo.

3.4 References

(1) Kelkar, S. S.; Reineke, T. M. Theranostics: Combining Imaging and Therapy. *Bioconjug Chem* **2011**, *22* (10), 1879–1903. https://doi.org/10.1021/bc200151q.

(2) Ho, D.; Sun, X.; Sun, S. Monodisperse Magnetic Nanoparticles for Theranostic Applications. *Accounts of Chemical Research*. October 18, 2011, pp 875–882. https://doi.org/10.1021/ar200090c.

(3) Li, C.; Liu, S. Polymeric Assemblies and Nanoparticles with Stimuli-Responsive Fluorescence Emission Characteristics. *Chemical Communications* **2012**, *48* (27), 3262–3278. https://doi.org/10.1039/c2cc17695e.

(4) Li, K.; Liu, B. Water-Soluble Conjugated Polymers as the Platform for Protein Sensors. *Polymer Chemistry*. May 2010, pp 252–259. https://doi.org/10.1039/b9py00283a.

(5) Melancon, M. P.; Zhou, M.; Li, C. Cancer Theranostics with Near-Infrared Light-Activatable Multimodal Nanoparticles. *Accounts of Chemical Research*. October 18, 2011, pp 947–956. https://doi.org/10.1021/ar200022e.

(6) Lee, J. E.; Lee, N.; Kim, T.; Kim, J.; Hyeon, T. Multifunctional Mesoporous Silica Nanocomposite Nanoparticles for Theranostic Applications. *Acc Chem Res* **2011**, *44* (10), 893–902. https://doi.org/10.1021/ar2000259.

(7) Liu, G.; Wang, X.; Hu, J.; Zhang, G.; Liu, S. Self-Immolative Polymersomes for High-Efficiency Triggered Release and Programmed Enzymatic Reactions. *J Am Chem Soc* **2014**, *136* (20), 7492–7497. https://doi.org/10.1021/ja5030832.

(8) Liu, H. W.; Li, K.; Hu, X. X.; Zhu, L.; Rong, Q.; Liu, Y.; Zhang, X. B.; Hasserodt, J.; Qu, F. L.; Tan, W. In Situ Localization of Enzyme Activity in Live Cells by a Molecular Probe Releasing a Precipitating Fluorochrome. *Angewandte Chemie - International Edition* **2017**, *56* (39), 11788–11792. https://doi.org/10.1002/anie.201705747.

(9) Zhu, A.; Miao, K.; Deng, Y.; Ke, H.; He, H.; Yang, T.; Guo, M.; Li, Y.; Guo, Z.; Wang, Y.; Yang, X.; Zhao, Y.; Chen, H. *Dually PH/Reduction-Responsive Vesicles for Ultrahigh-Contrast Fluorescence Imaging and Thermo-Chemotherapy-Synergized Tumor Ablation*.

(10) Jiwpanich, S.; Ryu, J. H.; Bickerton, S.; Thayumanavan, S. Noncovalent Encapsulation Stabilities in Supramolecular Nanoassemblies. *J Am Chem Soc* **2010**, *132* (31), 10683–10685. https://doi.org/10.1021/ja105059g.

(11) Jiwpanich, S.; Ryu, J. H.; Bickerton, S.; Thayumanavan, S. Noncovalent Encapsulation Stabilities in Supramolecular Nanoassemblies. *J Am Chem Soc* **2010**, *132* (31), 10683–10685. https://doi.org/10.1021/ja105059g.

(12) Surnar, B.; Jayakannan, M. Stimuli-Responsive Poly(Caprolactone) Vesicles for Dual Drug Delivery under the Gastrointestinal Tract. *Biomacromolecules* **2013**, *14* (12), 4377–4387. https://doi.org/10.1021/bm401323x.

(13) Meng, F.; Zhong, Z.; Feijen, J. Stimuli-Responsive Polymersomes for Programmed Drug Delivery. *Biomacromolecules* **2009**, *10* (2), 197–209. https://doi.org/10.1021/bm801127d.

(14) Hu, X.; Zhang, Y.; Xie, Z.; Jing, X.; Bellotti, A.; Gu, Z. Stimuli-Responsive Polymersomes for Biomedical Applications. *Biomacromolecules*. American Chemical Society March 13, 2017, pp 649–673. https://doi.org/10.1021/acs.biomac.6b01704.

(15) Petersen, A. L.; Hansen, A. E.; Gabizon, A.; Andresen, T. L. Liposome Imaging Agents in Personalized Medicine. *Advanced Drug Delivery Reviews*. October 2012, pp 1417–1435. https://doi.org/10.1016/j.addr.2012.09.003.

(16) Lee, S. M.; Nguyen, S. T. Smart Nanoscale Drug Delivery Platforms from Stimuli-Responsive Polymers and Liposomes. *Macromolecules*. December 10, 2013, pp 9169–9180. https://doi.org/10.1021/ma401529w.

(17) Sun, S. K.; Wang, H. F.; Yan, X. P. Engineering Persistent Luminescence Nanoparticles for Biological Applications: From Biosensing/Bioimaging to Theranostics. *Acc Chem Res* **2018**, *51* (5), 1131–1143. https://doi.org/10.1021/acs.accounts.7b00619.

(18) Li, P.; Zhang, D.; Zhang, Y.; Lu, W.; Zhang, J.; Wang, W.; He, Q.; Théato, P.; Chen, T. Aggregation-Caused Quenching-Type Naphthalimide Fluorophores Grafted and Ionized in a 3d Polymeric Hydrogel Network for Highly Fluorescent and Locally Tunable Emission. *ACS Macro Lett* **2019**, *8* (8), 937–942. https://doi.org/10.1021/acsmacrolett.9b00337.

(19) Zuo, Y.; Wang, X.; Wu, D. Uniting Aggregation-Induced Emission and Stimuli-Responsive Aggregation-Caused Quenching, Single Molecule Achieved Multicolour Luminescence. *J Mater Chem C Mater* **2019**, *7* (46), 14555–14562. https://doi.org/10.1039/c9tc05258e.

(20) Ma, Z.; Chen, Y.; Zuo, W.; Zhu, M. Synthesis and Fabrication of a Betulin-Containing Polyolefin Electrospun Fibrous Mat for Antibacterial Applications. *ACS Biomater Sci Eng* **2022**, *8* (12), 5110–5118. https://doi.org/10.1021/acsbiomaterials.2c01092.

(21) Yuan, Y.; Kwok, R. T. K.; Zhang, R.; Tang, B. Z.; Liu, B. Targeted Theranostic Prodrugs Based on an Aggregation-Induced Emission (AIE) Luminogen for Real-Time Dual-Drug Tracking. *Chemical Communications* **2014**, *50* (78), 11465–11468. https://doi.org/10.1039/C4CC05255B.

(22) Lu, N.; Gao, X.; Pan, M.; Zhao, B.; Deng, J. Aggregation-Induced Emission-Active Chiral Helical Polymers Show Strong Circularly Polarized Luminescence in Thin

Films. *Macromolecules* **2020**, *53* (18), 8041–8049. https://doi.org/10.1021/acs.macromol.0c00638.

(23) Zhang, N.; Chen, H.; Fan, Y.; Zhou, L.; Trépout, S.; Guo, J.; Li, M. H. Fluorescent Polymersomes with Aggregation-Induced Emission. *ACS Nano* **2018**, *12* (4), 4025–4035. https://doi.org/10.1021/acsnano.8b01755.

(24) Rouillon, J.; Ali, L. M. A.; Hadj-Kaddour, K.; Marie-Luce, R.; Simon, G.; Onofre, M.; Denis-Quanquin, S.; Jean, M.; Albalat, M.; Vanthuyne, N.; Micouin, G.; Banyasz, A.; Gary-Bobo, M.; Monnereau, C.; Andraud, C. Assembly of Aggregation-Induced Emission Active Bola-Amphiphilic Macromolecules into Luminescent Nanoparticles Optimized for Two-Photon Microscopy In Vivo. *Biomacromolecules* **2022**, *23* (6), 2485–2495. https://doi.org/10.1021/acs.biomac.2c00232.

(25) Fruhwirth, G. O.; Fernandes, L. P.; Weitsman, G.; Patel, G.; Kelleher, M.; Lawler, K.; Brock, A.; Poland, S. P.; Matthews, D. R.; Keri, G.; Barber, P. R.; Vojnovic, B.; Ameer-Beg, S. M.; Coolen, A. C. C.; Fraternali, F.; Ng, T. How Förster Resonance Energy Transfer Imaging Improves the Understanding of Protein Interaction Networks in Cancer Biology. *ChemPhysChem*. Wiley-VCH Verlag February 25, 2011, pp 442–461. https://doi.org/10.1002/cphc.201000866.

(26) Li, X.; Mu, J.; Liu, F.; Tan, E. W. P.; Khezri, B.; Webster, R. D.; Yeow, E. K. L.; Xing, B. Human Transport Protein Carrier for Controlled Photoactivation of Antitumor Prodrug and Real-Time Intracellular Tumor Imaging. *Bioconjug Chem* **2015**, *26* (5), 955–961. https://doi.org/10.1021/acs.bioconjchem.5b00170.

(27) Chen, J.; Zhong, W.; Tang, Y.; Wu, Z.; Li, Y.; Yi, P.; Jiang, J. Amphiphilic BODIPY-Based Photoswitchable Fluorescent Polymeric Nanoparticles for Rewritable Patterning and Dual-Color Cell Imaging. *Macromolecules* **2015**, *48* (11), 3500–3508. https://doi.org/10.1021/acs.macromol.5b00667.

(28) Han, X.; Liu, D. E.; Wang, T.; Lu, H.; Ma, J.; Chen, Q.; Gao, H. Aggregation-Induced-Emissive Molecule Incorporated into Polymeric Nanoparticulate as FRET Donor for Observing Doxorubicin Delivery. *ACS Appl Mater Interfaces* **2015**, *7* (42), 23760–23766. https://doi.org/10.1021/acsami.5b08202.

(29) Chen, H.; Kim, S.; Li, L.; Wang, S.; Park, K.; Cheng, J.-X. *Release of Hydrophobic Molecules from Polymer Micelles into Cell Membranes Revealed by Fö Rster Resonance Energy Transfer Imaging*; 2008; Vol. 6.

(30) Rajdev, P.; Basak, D.; Ghosh, S. Insights into Noncovalently Core Cross-Linked Block Copolymer Micelles by Fluorescence Resonance Energy Transfer (FRET) Studies. *Macromolecules* **2015**, *48* (10), 3360–3367. https://doi.org/10.1021/acs.macromol.5b00559.

(31) Miyake-Stoner, S. J.; Miller, A. M.; Hammill, J. T.; Peeler, J. C.; Hess, K. R.; Mehl, R. A.; Brewer, S. H. Probing Protein Folding Using Site-Specifically Encoded Unnatural

Amino Acids as FRET Donors with Tryptophan. *Biochemistry* **2009**, *48* (25), 5953–5962. https://doi.org/10.1021/bi900426d.

(32) Maity, H.; Reddy, G. Folding of Protein L with Implications for Collapse in the Denatured State Ensemble. *J Am Chem Soc* **2016**, *138* (8), 2609–2616. https://doi.org/10.1021/jacs.5b11300.

(33) He, F.; Tang, Y.; Yu, M.; Feng, F.; An, L.; Sun, H.; Wang, S.; Li, Y.; Zhu, D.; Bazan, G. C. Quadruplex-to-Duplex Transition of G-Rich Oligonucleotides Probed by Cationic Water-Soluble Conjugated Polyelectrolytes. *J Am Chem Soc* **2006**, *128* (21), 6764–6765. https://doi.org/10.1021/ja058075w.

(34) Lin, W.; Du, Y.; Zhu, Y.; Chen, X. A Cis-Membrane FRET-Based Method for Protein-Specific Imaging of Cell-Surface Glycans. *J Am Chem Soc* **2014**, *136* (2), 679–687. https://doi.org/10.1021/ja410086d.

(35) Rana, S.; Elci, S. G.; Mout, R.; Singla, A. K.; Yazdani, M.; Bender, M.; Bajaj, A.; Saha, K.; Bunz, U. H. F.; Jirik, F. R.; Rotello, V. M. Ratiometric Array of Conjugated Polymers-Fluorescent Protein Provides a Robust Mammalian Cell Sensor. *J Am Chem Soc* **2016**, *138* (13), 4522–4529. https://doi.org/10.1021/jacs.6b00067.

(36) Wang, Y.; Li, S.; Feng, L.; Nie, C.; Liu, L.; Lv, F.; Wang, S. Fluorescence Ratiometric Assay Strategy for Chemical Transmitter of Living Cells Using H2O2-Sensitive Conjugated Polymers. *ACS Appl Mater Interfaces* **2015**, *7* (43), 24110–24118. https://doi.org/10.1021/acsami.5b07172.

(37) Huang, Y.; Qiu, F.; Shen, L.; Chen, D.; Su, Y.; Yang, C.; Li, B.; Yan, D.; Zhu, X. Combining Two-Photon-Activated Fluorescence Resonance Energy Transfer and Near-Infrared Photothermal Effect of Unimolecular Micelles for Enhanced Photodynamic Therapy. *ACS Nano* **2016**, *10* (11), 10489–10499. https://doi.org/10.1021/acsnano.6b06450.

(38) Qiu, F.; Huang, Y.; Zhu, X. Fluorescent Unimolecular Conjugated Polymeric Micelles for Biological Applications. *Macromol Chem Phys* **2016**, *217* (2), 266–283. https://doi.org/10.1002/macp.201500283.

(39) Lee2, J.-K.; Schrock, R. R.; Baigent, D. R.; Friend, R. H. *A New Type of Blue-Light-Emitting Electroluminescent Polymer*; 1996; Vol. 28.

(40) Senthilkumar, T.; Asha, S. K. Selective and Sensitive Sensing of Free Bilirubin in Human Serum Using Water-Soluble Polyfluorene as Fluorescent Probe. *Macromolecules* **2015**, *48* (11), 3449–3461. https://doi.org/10.1021/acs.macromol.5b00043.

(41) Qi, J.; Chen, C.; Ding, D.; Tang, B. Z. Aggregation-Induced Emission Luminogens: Union Is Strength, Gathering Illuminates Healthcare. *Advanced Healthcare Materials*. Wiley-VCH Verlag October 24, 2018. https://doi.org/10.1002/adhm.201800477.

(42) Malik, A. H.; Hussain, S.; Iyer, P. K. Aggregation-Induced FRET via Polymer-Surfactant Complexation: A New Strategy for the Detection of Spermine. *Anal Chem* **2016**, *88* (14), 7358–7364. https://doi.org/10.1021/acs.analchem.6b01788.

(43) Zhu, C.; Yang, Q.; Liu, L.; Wang, S. Visual Optical Discrimination and Detection of Microbial Pathogens Based on Diverse Interactions of Conjugated Polyelectrolytes with Cells. *J Mater Chem* **2011**, *21* (22), 7905–7912. https://doi.org/10.1039/c0jm04424e.

(44) Martínez-Tome, M. J.; Esquembre, R.; Mallavia, R.; Mateo, C. R. Formation of Complexes between the Conjugated Polyelectrolyte Poly{[9,9-Bis(6'-n,n,Ntrimethylammonium) Hexyl]Fluorene-Phenylene} Bromide (HTMA-PFP) and Human Serum Albumin. *Biomacromolecules* **2010**, *11* (6), 1494–1501. https://doi.org/10.1021/bm100123t.

(45) Huang, Y.; Qiu, F.; Chen, D.; Shen, L.; Xu, S.; Guo, D.; Su, Y.; Yan, D.; Zhu, X. Color-Convertible, Unimolecular, Micelle-Based, Activatable Fluorescent Probe for Tumor-Specific Detection and Imaging In Vitro and In Vivo. *Small* **2017**, *13* (20). https://doi.org/10.1002/smll.201604062.

(46) Allazetta, S.; Hausherr, T. C.; Lutolf, M. P. Microfluidic Synthesis of Cell-Type-Specific Artificial Extracellular Matrix Hydrogels. *Biomacromolecules* **2013**, *14* (4), 1122–1131. https://doi.org/10.1021/bm4000162.

(47) Chandra Joshi, D.; Ashokan, A.; Jayakannan, M. L -Amino Acid Based Phenol- and Catechol-Functionalized Poly(Ester-Urethane)s for Aromatic π-Interaction Driven Drug Stabilization and Their Enzyme-Responsive Delivery in Cancer Cells. *ACS Appl Bio Mater* **2022**, *5* (11), 5432–5444. https://doi.org/10.1021/acsabm.2c00775.

(48) Anantharaj, S.; Jayakannan, M. Polymers from Amino Acids: Development of Dual Ester-Urethane Melt Condensation Approach and Mechanistic Aspects. *Biomacromolecules* **2012**, *13* (8), 2446–2455. https://doi.org/10.1021/bm300697h.

(49) Anantharaj, S.; Jayakannan, M. Catalysts and Temperature Driven Melt Polycondensation Reaction for Helical Poly(Ester-Urethane)s Based on Natural L-Amino Acids. *J Polym Sci A Polym Chem* **2016**, *54* (8), 1065–1077. https://doi.org/10.1002/pola.27970.

(50) Aluri, R.; Jayakannan, M. One-Pot Two Polymers: ABB′ Melt Polycondensation for Linear Polyesters and Hyperbranched Poly(Ester-Urethane)s Based on Natural l-Amino Acids. *Polym Chem* **2015**, *6* (25), 4641–4649. https://doi.org/10.1039/c5py00602c.

(51) Joshi, D. C.; Saxena, S.; Jayakannan, M. Development of l -Lysine Based Biodegradable Polyurethanes and Their Dual-Responsive Amphiphilic Nanocarriers for Drug Delivery to Cancer Cells. *ACS Appl Polym Mater* **2019**, *1* (7), 1866–1880. https://doi.org/10.1021/acsapm.9b00413.

(52) Saxena, S.; Jayakannan, M. Enzyme and PH Dual Responsive L-Amino Acid Based Biodegradable Polymer Nanocarrier for Multidrug Delivery to Cancer Cells. *J Polym Sci A Polym Chem* **2016**, *54* (20), 3279–3293. https://doi.org/10.1002/pola.28216.

(53) Aluri, R.; Saxena, S.; Joshi, D. C.; Jayakannan, M. Multistimuli-Responsive Amphiphilic Poly(Ester-Urethane) Nanoassemblies Based on l -Tyrosine for Intracellular Drug Delivery to Cancer Cells. *Biomacromolecules* **2018**, *19* (6), 2166–2181. https://doi.org/10.1021/acs.biomac.8b00334.

(54) Anantharaj, S.; Jayakannan, M. Melt Polycondensation Approach for Reduction Degradable Helical Polyester Based on L-Cystine. *J Polym Sci A Polym Chem* **2016**, *54* (18), 2864–2875. https://doi.org/10.1002/pola.28172.

(55) Saxena, S.; Jayakannan, M. π-Conjugate Fluorophore-Tagged and Enzyme-Responsive l -Amino Acid Polymer Nanocarrier and Their Color-Tunable Intracellular FRET Probe in Cancer Cells. *Biomacromolecules* **2017**, *18* (8), 2594–2609. https://doi.org/10.1021/acs.biomac.7b00710.

(56) Saxena, S.; Pradeep, A.; Jayakannan, M. Enzyme-Responsive Theranostic FRET Probe Based on l -Aspartic Amphiphilic Polyester Nanoassemblies for Intracellular Bioimaging in Cancer Cells. *ACS Appl Bio Mater* **2019**, *2* (12), 5245–5262. https://doi.org/10.1021/acsabm.9b00450.

(57) Anantharaj, S.; Jayakannan, M. Amyloid-Like Hierarchical Helical Fibrils and Conformational Reversibility in Functional Polyesters Based on l-Amino Acids. *Biomacromolecules* **2015**, *16* (3), 1009–1020. https://doi.org/10.1021/bm501903t.

(58) Saxena, S.; Jayakannan, M. Development of L-Amino-Acid-Based Hydroxyl Functionalized Biodegradable Amphiphilic Polyesters and Their Drug Delivery Capabilities to Cancer Cells. *Biomacromolecules* **2020**, *21* (1), 171–187. https://doi.org/10.1021/acs.biomac.9b01124.

Chapter 4

Development of L-Aspartic acid based Cationic Polyesters for Antimicrobial Application.

Abstract

In this chapter we have developed L-aspartic acid based cationic polyester for the antimicrobial applications. The L aspartic acid was converted in to a suitable monomer for the development polyester using melt polycondensation technique. The amine pendant of the monomer was protected as BOC group. The polymer was synthesized by the melt polycondensation strategy with diol of different spacer length, this polyester subsequently converted into the cationic polyester which are capable to undergo self-assembly in aqueous environment in the polymer nanoparticle. The cationic polyester formed nanoparticle with size below 150±10 nm diameter shows formation of spherical morphology with positive zeta potential value. The antimicrobial activity of the sample was determined as both solid and solution state. Different technique employed for determination of antibacterial activity study such as Resazurin assays, Colony suspension method, Spread plate method and Disc diffusion method. Each technique is unique in nature to determine antibacterial activity, the qualitative analysis by resazurin assay suggest minimum inhibitory concentration (MIC) close to 1mg/ml further it was traced by colony suspension method which suggested that the MIC_{90} found to be 0.8mg/ml in the solution state. In the solid-state antimicrobial activity found at the higher concentration such as 5mg/ml showed formation large zone of inhibition as compare to lower concentration 1mg/ml, it also suggested that at the solid-state antibacterial activity require much higher concentration as compare to solution state.The biocompatibility study of the polymer was performed using MTT assay with the normal cell line Wild type mouse embryonic fibroblast (WT MEF).

4.1 Introduction

The advent of antibiotics marked a pivotal moment in the field of medicine, revolutionizing our ability to combat bacterial infections. Alexander Fleming's discovery of penicillin in 1928 was a seminal moment in the history of antibacterial research. This serendipitous finding opened the doors to the development of various antibiotics, each with its own unique properties and mechanisms of action. Among the noteworthy antibiotics that emerged in subsequent years are ampicillin, ciprofloxacin, azithromycin, penicillin and more[1,2]. These set of antibiotics are is their relatively small molecular size, with molecular weights typically falling below 500 Daltons (Da). This modest size allows these drugs to penetrate bacterial cells efficiently, where they exert their antibacterial effect. Penicillin antibiotic class is known as beta-lactams. Penicillin specifically works by inhibiting the synthesis of the bacterial cell wall. Bacterial cells rely on a sturdy cell wall to maintain their structural integrity. Penicillin disrupts this process by interfering with the formation of cross-links in the peptidoglycan layer of the cell wall, leading to weakened cell walls and eventual cell lysis[3]. Ampicillin is also a beta-lactam antibiotic, similar to penicillin. It acts in a similar manner by interfering with bacterial cell wall synthesis. Ampicillin is effective against a broader spectrum of bacteria, making it a valuable tool in combating various infections[4]. Ciprofloxacin antibiotic belongs to the quinolone class. Its mechanism of action is different from beta-lactams. Ciprofloxacin targets bacterial DNA gyrase, an enzyme essential for DNA replication and repair. By inhibiting DNA gyrase, ciprofloxacin disrupts DNA synthesis and repair in bacteria, ultimately leading to their death[4]. Azithromycin, a member of the macrolide class of antibiotics, interferes with bacterial protein synthesis. It binds to the bacterial ribosome, specifically the 50S subunit, and inhibits the elongation of the protein chain. This disruption in protein synthesis impairs the bacteria's ability to thrive and reproduce. The intricate mechanisms of action described above showcase the diversity of approaches that antibiotics employ to combat bacterial infections. These antibiotics have played a crucial role in saving countless lives and continue to be essential tools in the fight against bacterial diseases[5]. A visual representation of mechanism of action of azythromycin is shown Figure 4.1

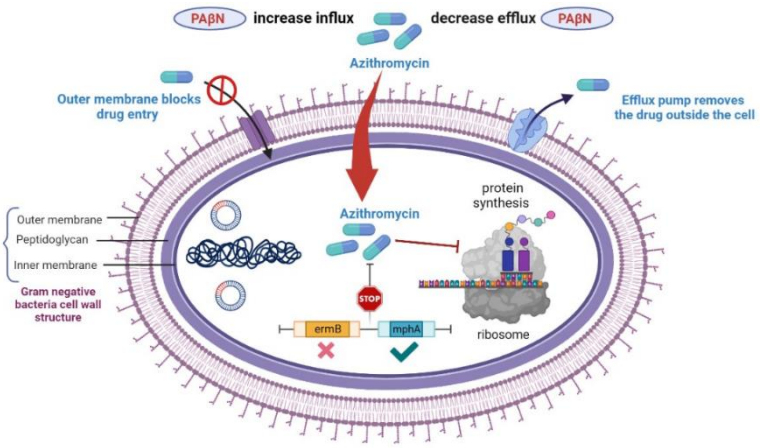

Figure 4.1 *Mechanism of action of the antibacterial drugs Azithromycin (Adapted from Int. J. Mol. Sci. 2023, 24(10), 8662).*

AMPs constitute another class of naturally occurring antibiotics that are integral to our innate immune system. Remarkably, they possess a broad spectrum of activity, capable of targeting and eliminating fungi, bacteria, viruses, and even cancer cells[6-9]. Cationic AMPs, a subset of antimicrobial peptides, are typically composed of 10 to 50 amino acids. They are characterized by having cationic and hydrophobic residues arranged on opposite sides within their three-dimensional structure.[10,11] These peptides are soluble in water due to their positive charge, typically ranging from +2mV to +9mV. Cationic AMPs adopt three fundamental secondary structures, first structure is Alpha-helix, notably, alpha-helical AMPs like magainin and LL37 lack a discernible secondary structure in aqueous environments but assume an alpha-helical conformation when interacting with non-polar environments, such as bacterial membranes. Thes second structure beta-sheet, in contrast, AMPs such as defensins and bactenecins possess a beta-sheet structure that is stabilized by disulfide bonds, rendering them effective against a variety of pathogens. While extended AMPs, A unique category of AMPs lacks a specific secondary structure. Instead, they are characterized by being rich in certain amino acids like histidine, arginine, glycine, or tryptophan. A notable example is indolicidin. The antimicrobial peptides adapt the different mechanism as compare to small molecules as discussed in earlier section, Due to their positive charge and hydrophobic nature it acts on the bacterial cell by disruption of cell walls[6]. It follows different kind of mode of action as shown in Figure 4.2.

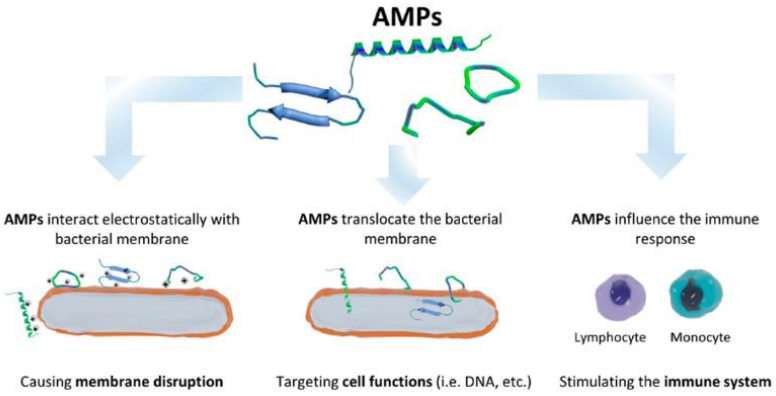

Figure 4.2 *Antimicrobial peptides and different modes of action. (Adapted from Biomacromolecules 2021, 22, 1, 57–75)*

These diverse structural arrangements contribute to the versatility and potency of AMPs in combating various microbial threats. AMPs represent a remarkable facet of our innate immunity and hold significant potential for therapeutic applications in the ongoing battle against infectious diseases and other health challenges[12,13]. Numerous antimicrobial peptides (AMPs), including polymyxin, colistin, daptomycin, and gramicidin, have undergone clinical trials, but their clinical success remains limited due to various challenges. These hurdles include in vivo toxicity, challenges in industrial scalability, and susceptibility to protease degradation. AMPs, with the exception of polymyxin, are more likely to cause nephrotoxicity and neurotoxicity when administered intravenously. Furthermore, the intricate synthesis of AMPs hinders their scalability for industrial production. Another common drawback of natural peptides is their vulnerability to proteases like chymotrypsin, which can lead to undesirable degradation and impact their pharmacokinetics. [14,15]

As time has progressed, bacteria and other microorganisms have evolved mechanisms to develop resistance against traditional antibiotics. This resistance can occur through various intricate processes, each contributing to the microorganisms' ability to thwart the effectiveness of available antibiotics. These mechanisms include, (i)Activation of Drug Efflux Pumps: Microorganisms can activate drug efflux pumps, specialized proteins embedded in their cell membranes, which actively pump antibiotics out of the cell. By expelling the drug, the microorganism reduces its intracellular concentration, rendering the antibiotic less effective or entirely ineffective[16,17]. (ii)Inactivation of Drugs by Bacterial Enzymes: Some microorganisms produce enzymes that can chemically modify and inactivate antibiotics. These enzymes, often referred to as

antibiotic-degrading enzymes, can alter the structure of the antibiotic molecule, rendering it powerless to combat the microorganism[16,17]. (iii)Alteration of Bacterial Cell Drug Targets: Bacteria can evolve changes in the molecular structures of their cellular drug targets. This transformation makes it more difficult for antibiotics to bind to and disrupt these targets, diminishing the drug's efficacy in combating the microorganism[16,17] (iv)Inhibition of Drug Uptake into the Cell: Microorganisms may develop mechanisms to hinder the entry of antibiotics into their cells. This can involve alterations in cell membrane permeability or the development of barriers that prevent antibiotics from reaching their intended targets within the microorganism[16,17].

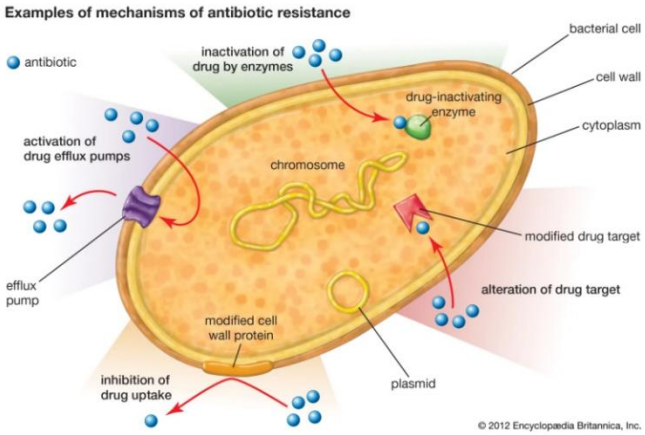

Figure 4.3 *Development of antibiotics resistance. (Adapted from https://www.britannica.com/science/drug-resistance).*

These processes are illustrated in Figure 4.3, emphasizing the sophisticated strategies that microorganisms employ to evade the effects of antibiotics. The emergence of antibiotic resistance is a significant global health concern, as it reduces the effectiveness of our existing arsenal of antibiotics. To address this issue, ongoing research and the development of new strategies to combat resistant microorganisms are essential in ensuring the continued efficacy of antibiotic treatments[105]. In this aspect it is very important for the for the development of new class of antibiotic material such as anti-bacterial polymers etc. Recent decade we have seen development of new antibiotics materials, these materials have property to kill or inhibit the bacterial cells by different mode of action.

Antibacterial Polymers This category encompasses artificial antimicrobial agents that undergo self-assembly into nanoparticles, typically falling within the size range of 10-200 nm. These nanoparticles exhibit a positive charge and comprise polymeric structures, with hydrophobic components responsible for their membrane-disrupting

capabilities. Their remarkable stability in aqueous environments is primarily attributed to their positive charge[18,19]. Junki Oh et al studied the antibacterial activity of the polymer having sulphonium ion in main chain. They synthesized poly(β-hydroxythioether)s, in the first step followed by alkylating to yield the cationic polymer. They varied the length of alkyl chain for antimicrobial application and found out that polymer with pentyl chain is biocompatible and showed effective antimicrobial action. Mechanistically these polymers disrupt the cells wall for killing the bacteria. In essence, this research enhances our understanding of polysulfonium salts and offers promising insights into their potential for combating resilient bacterial species[22]. Divakara et al synthesized poly(isobutylene-alt-N-alkyl maleimide) with property of side chain degradation, these polymer showed antibacterial property due to the presence of quaternary ammonium group, the hydrophobicity of the side chain varied because of the N-alkyl side chains. The synthesized polymer showed antibacterial activity without harming the mammalian cells [23].

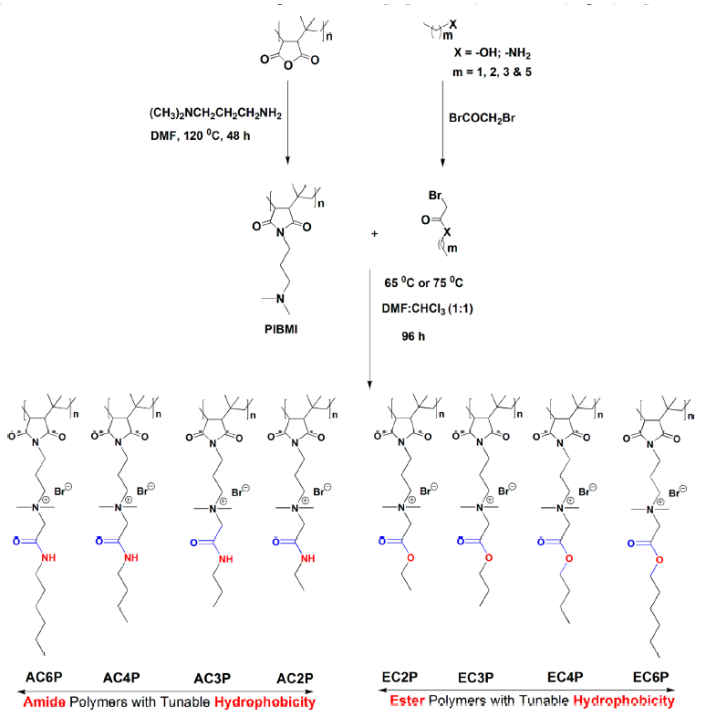

Figure 4.3 *Quaternary ammonium polymers for the antibacterial applications. (Adapted from Biomacromolecules 2016, 17, 3094−3102).*

Jinsol Yook et al designed and synthesized antibacterial polymers from biobased citronellol. The polymer poly(glycidyl methacrylate) was modified with side chain with different linker group such as was synthesised such thioether (S), sulfoxide (SO), ether (O) and sulfone (SO2) group which was attached to citronellol group. With different

linker groups the sulphoxide group attached to citronellol group showed maximum antibacterial activity. [24] Ishita Mukherjee et al developed the cationic polymer with side chain amino acids such as alanine, phenyl alanine and leucin group by RAFT polymerisation, the antibacterial activity was tested for both gram positive and gram negative bacteria i.e. *E. coli* and *B. subtilis* respectively. They shown the mechanism of action of the polymer on the bacterial surface using Electron microscopy (FESEM) analysis which reveals a marked transformation in bacterial cell morphology from rod-shaped to spherical during polymer treatment of *E. coli* cells. This effect was most pronounced with the leucine-based cationic homopolymer, while in case of *B. subtilis* cells did not exhibit significant morphological changes[25]. Masato Mizutani and colleagues synthesized a cationic polymer featuring primary amine groups in its side chain, demonstrating antibacterial properties against E. coli cells. They emphasized the significance of monomer structure, molecular weight, and composition in modulating its effectiveness. A model polymer with primary amine groups underwent self-degradation through intramolecular nucleophilic addition, amidation, and main-chain scission, resulting in reduced antibacterial and hemolytic activities. These polymers exhibited moderate antibacterial effects against E. coli and limited selectivity for red blood cells, indicating the need for further structural optimization and exploration of their performance under physiological conditions.[26] In our lab the caprolactone based cationic polyesters were developed using chlorine substituted polyester which on post polymerization modification produced quaternary amine functionalized polyester which demonstrated antimicrobial activity against gram negative E. Coli. The mechanism of antibacterial mechanism was further studied by employing fluorophore tagged cationic polyester which clearly suggested the membrane disruption mechanism[20,21].

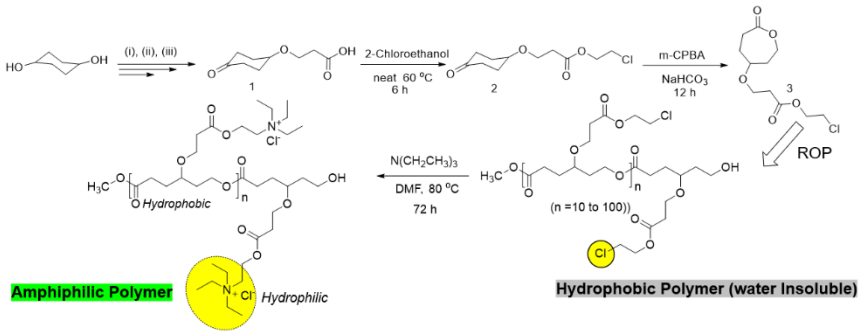

Figure 4.4 *Schematic representation of the synthesis caprolactone based cationic polyester for antibacterial applications. (Adapted from Biomacromolecules* 2020, 21, 7, 2896–2912*).*

This approach was further studied for the development of L-aspartic acid (natural resource) based cationic polyester for antibacterial application against gram negative *E. Coli* cells as shown in Figure 4.5.

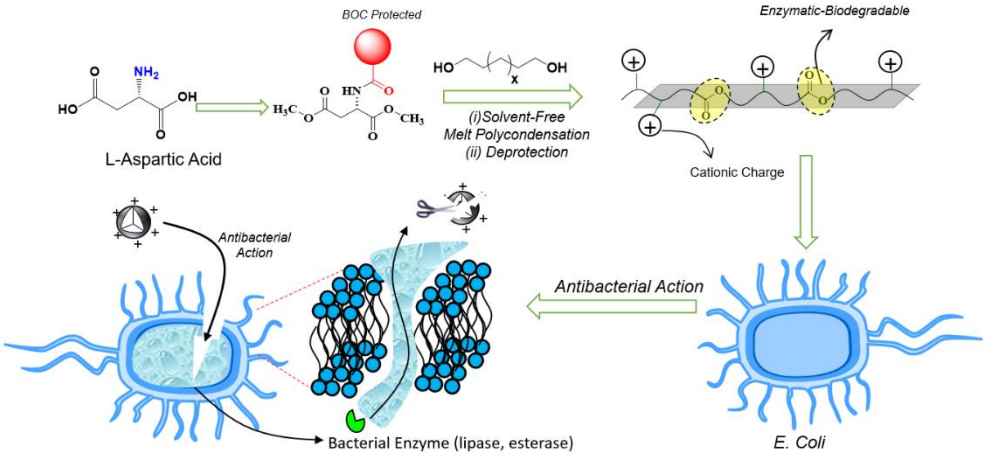

Figure 4.5 *Development of L-aspartic acid based cationic polyester of antimicrobial applications.*

In this chapter we have reported L-aspartic acid based cationic polyester for the antibacterial applications at both solid state and solution state. The L aspartic acid was converted dimethyl ester and amine group was protected as BOC group. The found to be stable at melt polymerization temperature. The polymer was synthesized using melt polycondensation strategy to produce BOC protected polyester, along with the monomer different spacer group diol was utilised using. The side BOC pendant was deprotected to produce cationic polyester primary ammonium salt. The cationic polymer was dispersible in water and form nanoparticle. The cationic polyester formed nanoparticle with size below 150±10 nm diameter shows formation of spherical morphology with positive zeta potential value. The antimicrobial activity of the sample was determined as both solid and solution state, Different technique employed for

antibacterial activity study such as Resazurin assays, Colony suspension method, Spread plate method and Disc diffusion method. Each technique is unique in nature to determine antibacterial activity, the qualitative analysis by resazurin assay suggest MIC close to 1mg/ml but MIC further traced to colony suspension method and MIC_{90} found to be 0.8mg/ml in the solution state. In the solid-state antimicrobial activity found at the higher concentration such as 5mg/mL showed formation large zone of inhibition as compare to lower concentration 1mg/mL. The polymer NPs encapsulated biomarker such as HPTS, polymer alone and polymer nanoparticles loaded both found to be biocompatible with the normal cell line WT MEF.

4.2 Experimental section

4.2.1 Materials and Methods

From Sigma Aldrich the following products were purchased, L-Aspartic acid, 1,12 dodecane diol, 1,6 hexanediol, 1, 10 decane diol, 1,8 Octane diol, Titanium tetra butoxide $Ti(OBu)_4$, and 8-hydroxypyrene-1,3,6-trisulfonic acid trisodium salt (HPTS). While Thionyl chloride, BOC anhydride, dichloromethane, methanol, and ethyl acetate, among other solvents, were locally sourced and subjected to purification prior to utilization. Other essential materials such as Nutrient agar, Luria Bertani Broth, 96 well plates, Resazurin, ampicillin, Tetrazolium salt, 3-(4,5-dimethylthiazol-2-yl)-2,5-diphenyltetrazolium bromide (MTT), paraformaldehyde, glycerol, and glutaraldehyde were procured from local vendors chemicals. Mice red blood cells were acquired from the C-57 B1/6 Mice at the IISER Animal House facility. Additionally, the Gram-negative bacterium E. coli (ATCC 25922) was obtained from the National Collection of Industrial Microorganisms (NCIM) in India. Lastly, the cell culture was maintained at 37 ºC with 5% CO_2 and 1% O_2.

4.2.2 Synthesis of L- aspartic dimethyl ester

L- aspartic acid (5g, 0.036mol) was taken in clean round bottomed flask to that dry methanol (100ml) was added under ice cold condition thionyl chloride (8ml 0.112 mol) was added to reaction mixture. After addition of thionyl chloride the reaction mixture becomes clear. The reaction mixture was refluxed for 12h for at 80 ºC. after completion of the reaction thionyl chloride was removed from the reaction mixture by vacuum distillation to get white crystalline solid. Yield = 6.5g (98%).

4.2.3 Synthesis of BOC monomer: M-Boc

Compound 1 (7g, 0.035mol) was taken in clean round bottomed flask in the reaction mixture saturated solution of sodium carbonate was added. Followed by that reaction was mixture was added with tetrahydrofuran and BOC anhydride (12.23mL 0.053mol) was added to reaction mixture dropwise under ice cold condition. The reaction was carried out for 12 h, the reaction for monitored using TLC. Tetrahydrofuran was removed by rotary evaporator and product was extracted in ethyl acetate the crude product was further purified by column chromatography with Pet ether: EtOAc 1:10 v/v. Yield = 5.3g (70%). ^{1}H NMR (400 MHz, CHLOROFORM-*d*) δ ppm 5.49 (d, *J*=7.58 Hz, 1 H) 4.47 - 4.68 (m, 1 H) 3.76 (s, 3 H) 3.70 (s, 3 H) 3.01 (dd, *J*=17.00, 4.28 Hz, 1 H) 2.83 (dd, *J*=17.12, 4.65 Hz, 1 H) 1.45 (s, 9 H). ^{13}C NMR (100 MHz, CDCl3) δ ppm: 171.66, 171.56, 155.49, 80.29, 52.85, 52.14, 50.03, 36.78 and 28.40. HRMS (ESI+): m/z [M+Na+] calcd. for C11H19NO6 Na[M+]: 284.1109; found: 284.1118.

4.2.4 Synthesis of P12 polymer

The typical melt polycondensation for the polyester is explained for synthesis of P12 i.e., polymer with 1,12 dodecane diol. M-Boc (0.6g, 0.0023mol) and 1, 12 Dodecane diol (0.46g, 0.0023mol) was taken in clean test tube shaped melt polymerisation tube. The polymerisation mixture was the subjected to melting at 120 ºC with N_2 purge. When the monomer and diol melted 1 mole % of the titanium tetrabutaoxide catalyst was added to the polymerisation mixture. The polymerisation mixture was subjected to nitrogen purge for 4h and followed by that the vacuum was applied to the polymerisation mixture 10^{-2} mbar for 2h. Polymer was purified by precipitation methanol. Yield= 1.0g (93%) ^{1}H NMR (400 MHz, CHLOROFORM-*d*) δ ppm 5.48 (br. s., 1 H) 4.55 (br. s., 1 H) 4.13 (s, 2 H) 4.07 (s, 2 H) 2.97 (br. s., 1 H) 2.82 (s, 1 H) 1.61 (br. s., 5 H) 1.45 (s, 9 H) 1.26 (br. s., 17 H). ^{13}C NMR (100 MHz, CDCl3) δ ppm: 172.23, 171.12, 155.50, 80.06, 65.95, 65.25, 63.10, 50.10, 36.87, 32.87, 29.64, 29.60, 29.31, 28.59, 28.55, 28.38, 25.94 and 25.87.

4.2.5 Synthesis of P10 polymer

The M-Boc (1.0g, 0.0038 moles) and 1, 12 dodecane diol (0.6g, 0.0038moles) was taken in polymerisation tube and the polymerisation was carried out by following the similar method as performed for **P12** polymer. Yield= 1.4g (95%) ^{1}H NMR (400 MHz,

CHLOROFORM-*d*) δ ppm 5.51 (br. s., 1 H) 4.56 (br. s., 1 H) 4.14 (s, 2 H) 4.08 (br. s., 2 H) 3.02 (br. s., 1 H) 2.84 (s, 1 H) 1.63 (br. s., 7 H) 1.45 (s, 9 H) 1.29 (br. s., 12 H). ^{13}C NMR (100 MHz, CDCl3) δ ppm: 170.94, 170.83, 155.21, 79.77, 65.63, 64.94, 49.82, 36.58, 29.22, 29.00, 28.98, 28.29, 28.25, 28.09, 25.64 and 25.56.

4.2.6 Synthesis of P8 polymer

The M-Boc (1.0g, 0.0038 moles) and diol (0.57, 0.0038 mole) was taken in polymerisation tube and the polymerisation was carried out by following the similar method as performed for **P12** polymer. Yield= 1.47g(97%). ^{1}H NMR (400 MHz, CHLOROFORM-*d*) δ ppm 5.49 (br. s., 1 H) 4.54 (br. s., 1 H) 4.14 (s, 2 H) 4.07 (s, 2 H) 2.96 (br. s., 1 H) 2.84 (s, 1 H) 1.64 (br. s., 6 H) 1.45 (s, 9 H) 1.37 (br. s., 4 H). ^{13}CNMR (100 MHz, CDCl3) δ ppm: 170.95, 170.83, 155.20, 79.78, 65.56, 64.88, 49.81, 36.56, 28.89, 28.86, 28.26, 28.22, 28.09, 25.58 and 25.50.

4.2.7 Synthesis of P6 polymer

The monomer (1.0g, 0.0038 moles) and diol (0.48, 0.0038 moles) was taken in polymerisation tube and the polymerisation was carried out by following the similar method as performed for **P12** polymer. Yield= 1.45g(96%). ^{1}H NMR (400 MHz, CHLOROFORM-*d*) δ ppm 5.50 (br. s., 1 H) 4.56 (br. s., 1 H) 4.14 (s, 2 H) 4.08 (s, 2 H) 2.97 (br. s., 1 H) 2.84 (s, 1 H) 1.65 (br. s., 6 H) 1.45 (s, 9 H) 1.31 (br. s., 8 H). ^{13}C NMR (100MHz, CDCl3) δ ppm: 171.58, 155.84, 80.46, 66.01, 65.34, 50.46, 37.17, 28.73 and 25.91.

Deprotection of pendant side BOC group:

4.2.8 Deprotection of P12 polymer

Deprotection of side chain BOC group from P12 polymer is explained in details. In as clean round bottomed flask polymer P12(0.40 g, 0.001 mol) was dessolved in dichloromethane (2.0 mL). To the reaction mixture at 0 °C trifluoro acetic acid (0.012 mol, 0.9 mL) was added dropwise. The reaction mixture stirred for 2h at room temperature. After completion of the reaction DCM solvent and TFA was removed from the reaction mixture using rotary evaporator. Yield = 0.38g (91%). ^{1}H NMR (400 MHz, DMSO-d_6) δ ppm 8.56 (br. s., 3 H) 4.36 (br. s., 2 H) 4.15 (br. s., 2 H) 4.05 (s, 2 H) 2.96 (br. s., 2 H) 1.57 (br. s., 4 H) 1.26 (br. s., 13 H) ^{13}C NMR (100 MHz, CD3OD)

δ ppm: 176.26, 172.87, 70.36, 68.75, 65.59, 52.04, 33.24, 33.04, 32.98, 32.34, 32.15, 29.65, 29.52 and 29.27.

4.2.9 Deprotection of P10 polymer

P10(0.40 g, 0.001 mol) was dissolved in dichloromethane (2.0 mL) and Trifluoro acetic acid (0.012 mol, 0.9 mL) was added dropwise in reaction mixture Similar procedure was followed for BOC deprotection from the polymer as explained for P12 polymer only concentration for the reagents and solvent were varied. Yield = 0.37 g (87%). ^{1}H NMR (400 MHz, DMSO-d_6) δ ppm 8.53 (br. s., 2 H) 4.37 (br. s., 1 H) 4.03 (br. s., 4 H) 2.96 (br. s., 2 H) 1.57 (br. s., 4 H) 1.38 (s, 2 H) 1.25 (br. s., 17 H) ^{13}C NMR (100 MHz, CD3OD) δ ppm: 176.26, 172.87, 70.36, 68.75, 65.59, 52.04, 33.24, 33.04, 32.98, 32.34, 32.15, 29.65, 29.52 and 29.27.

4.2.10 Deprotection of P8 polymer

P8(0.40 g, 0.001 mol) was dissolved in dichloromethane (2.0 mL) and Trifluoro acetic acid (0.012 mol, 0.9 mL) was added dropwise in reaction mixture Similar procedure was followed for BOC deprotection from the polymer as explained for P12 polymer only concentration for the reagents and solvent were varied. Yield = 0.37 g (88%). ^{1}H NMR (400 MHz, DMSO-d_6) δ ppm 8.58 (br. s., 3 H) 4.39 (br. s., 2 H) 4.14 (br. s., 2 H) 4.06 (br. s., 2 H) 2.95 (br. s., 2 H) 1.59 (br. s., 3 H) 1.32 (br. s., 4 H). ^{13}C NMR (100 MHz, CD3OD) δ ppm: 176.26, 172.87, 70.36, 68.75, 65.59, 52.04, 33.24, 33.04, 32.98, 32.34, 32.15, 29.65, 29.52 and 29.27.

4.2.11 Deprotection of P6 polymer

P6(0.40 g, 0.001 mol) was dissolved in dichloromethane (2.0 mL) and Trifluoro acetic acid (0.012 mol, 0.9 mL) was added dropwise in reaction mixture Similar procedure was followed for BOC deprotection from the polymer as explained for P12 polymer only concentration for the reagents and solvent were varied. Yield = 0.38 g (93%). ^{1}H NMR (400 MHz, DMSO-d_6) δ ppm 8.58 (br. s., 3 H) 4.39 (br. s., 2 H) 4.14 (br. s., 2 H) 4.06 (br. s., 2 H) 2.95 (br. s., 2 H) 1.59 (br. s., 3 H) 1.32 (br. s., 4 H). ^{13}C NMR (100 MHz, CD3OD) δ ppm: 176.26, 172.87, 70.36, 68.75, 65.59, 52.04, 33.24, 33.04, 32.98, 32.34, 32.15, 29.65, 29.52 and 29.27.

4.2.12 Resazurin assay

10^6 CFU of *E. Coli* was taken in 96 well-plates in each well along with 100 µl of LB media. These bacterial cells were incubated with different concentration of polymer ranging from 10^{-12} mg/mL to 2mg/mL. The sample plate was then incubated for 12h

at 37 ºC, after the completion of the incubation period sample plate was taken out of incubator and 5 µg of resazurin solution was added per well. The 96 well plate was again incubated for 4h and change in colour was monitored. The photograph of the 96 well plate was taken under white light illumination using the Syngene G: Box Chemi XX6 instrument.

4.2.13 Colony Suspension Method

To prepare the bacterial sample, several well-isolated E. coli colonies were suspended in LB broth until the suspension reached a final turbidity equivalent to the 0.5 McFarland standard. Subsequently, the bacterial suspension was further diluted to reach an optical density (OD) of 600 nm equal to 0.005, corresponding to a concentration of 1 X 10^6 CFU/mL. A volume of 100 µL from this bacterial suspension was dispensed into a 96-well plate. Additionally, 100 µL of polymeric stock solutions were serially diluted, ranging from 1 mg/mL to 0.1 mg/mL. These diluted polymeric solutions, along with a positive control (lacking polymer) and a negative control (containing Azithromycin at 50 µg/mL), were combined with the E. coli cell suspension. Bacterial turbidity was continuously monitored at an excitation wavelength (λexc) of 600 nm over an 18-hour period using the Perkin Elmer Enspire Multimode Plate Reader.

4.2.14 Spread Plate method

A single colony derived from an E. coli-streaked plate was selected and cultured in 3 mL of LB broth for a duration of 4 hours. The experimental procedure was carried out in duplicate to ensure reproducibility. The concentration of E. coli was subsequently adjusted to 1 X 10^6 CFU/mL. For further investigation, 100 µL of the E. coli suspension was co-incubated with 100 µL of a cationic polymeric sample, both at a concentration of 1 X MIC, at various time points. These incubations were performed within 1.5 mL Eppendorf tubes equipped with ventilation pores in their caps. The incubation conditions involved shaking at 37°C. Following the designated incubation period, the samples were subjected to a 10-fold dilution, and 100 µL of each diluted sample was evenly spread onto LB agar plates, allowing them to air dry for 30 minutes. Subsequently, these plates were placed in an incubator set at 37°C for a duration of 18 hours.

4.2.15 Disc Diffusion method

In this study, LB agar was poured onto a polystyrene petri dish with dimensions of 100 mm in diameter and 20 mm in depth, followed by cooling it to solidify. A single colony of Escherichia coli (E. coli) was selected and subjected to incubation at 37°C for a duration of 6 hours. Subsequently, the E. coli cell suspension was appropriately diluted to achieve an optical density (O.D.) of 0.1 at 600 nm. A 100 µL volume of this final inoculum was uniformly spread across the LB agar plate and allowed to air dry. The 20 µL of various samples, including a 1 mg/mL concentration of the polymer alone, a 25 µg/mL concentration of azithromycin alone, and a 1 mg/mL concentration of azithromycin-loaded polymer, were dispensed onto 6 mm diameter Whatman filter paper disks, where they were permitted to dry for 2 hours under a medium airflow within a hood. Following drying, these disks were meticulously positioned onto the LB agar plate and then maintained at a temperature of 37°C for a period of 18 hours. Subsequently, images of the inhibition zones were captured under white light illumination using the Syngene G: Box Chemi XX6 instrument.

For the calculation of the inhibition zone area, the formula used was:

Area of zone of inhibition = $\prod (R^2-r^2)$

R- radius of zone of inhibition

r- radius of paper disc.

4.2.16 Cell viability assay

Biocompatibility of the cationic polyester was determined using MTT assay. The biocompatibility of the polyester was checked in normal cell lines i.e., WT MEF. 10^3 cells per well seeded in 94 well plate, and it was grown for 18h. Followed by that media was aspirated and complete media along with the polymer was added per well and incubated for 72h. The concentration of the polymer was varied from 1µg/mL to 100 µg/mL. After 72h media was aspirated and 0.5mg/mL MTT solution was added per well and plate was incubated for 4h. followed by that media was removed gently from the well so that it does not disturb the formazan crystals. 100µL of the dimethyl sulphoxide was added to each well and using microplate reader at λmax=570nm

4.3 Result and Discussion:

4.3.1 Synthesis of monomer

Synthesis of L-aspartic acid based cationic polyester was achieved by following method. L aspartic acid was converted to dimethoxy ester of L-aspartic acid as discussed in previous chapters. L-aspartic acid was suspended in AR grade methanol and reacted with thionyl chloride to produce desired product. Amine group of compounds 1 was converted into urethane group by reacting it with BOC anhydride. The resulting monomer was referred as M-BOC, Synthetic scheme of the monomer was shown in Scheme 4.1.

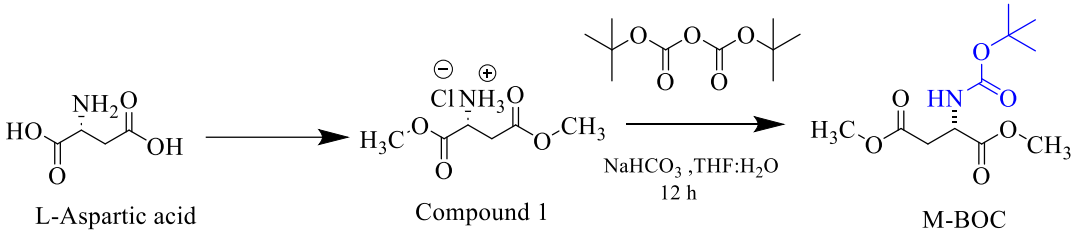

Scheme 4.1 *Synthetic scheme of the monomer-BOC, first step involves synthesis of dimethyl ester followed by protection of amine group as BOC.*

The Chemical structure of the M-BOC monomer was confirmed by ^{1}H and ^{13}C NMR spectra, the successfully protection of the BOC group was confirmed by peak of Ter. butyl group at 1.47ppm with integration for nine proton. The methyl ester peak appeared at 3.76ppm and 3.70 ppm due to non-symmetrical nature of the monomer. While amide a peak at 5.48 further confirms successful formation of the monomer.

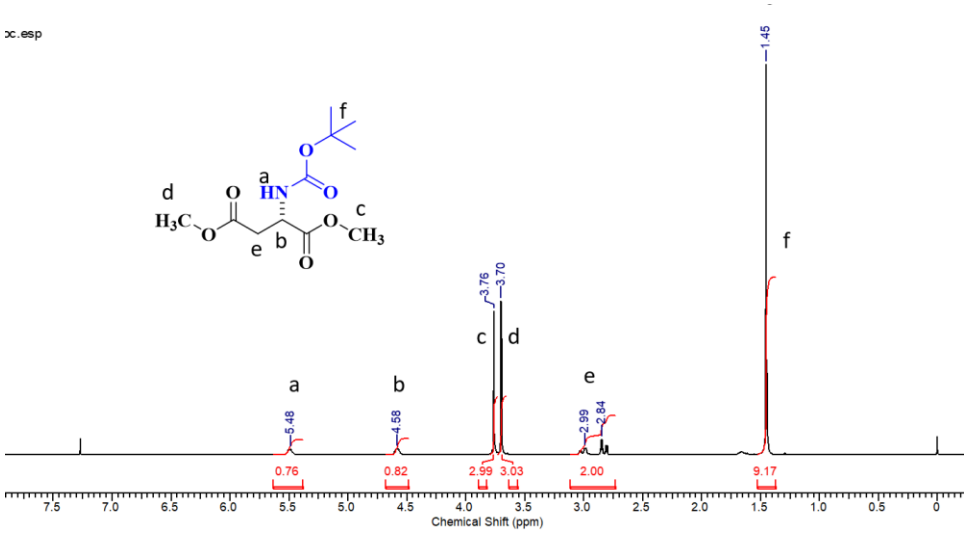

Figure 4.6 *Chemical structure of M-BOC monomer and ^{1}H NMR Spectra of M-BOC monomer.*

The chemical structure and ^{1}H NMR spectra of the monomer is shown as Figure 4.6. The peaks of the spectra of are assigned alphabetically. Thermal stability of M-BOC was measured by thermogravimetric analysis (TGA), The monomer M-BOC was found to be stable under melt polymerisation condition with thermal stability for M-BOC is stable up to 250 ºC which similar as compare to other monomers synthesized in earlier chapter. (See Figure 4.7)

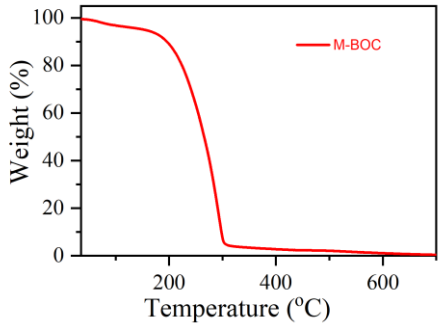

Figure 4.7 *TGA thermogram of M-BOC monomer.*

4.3.2 Synthesis of P-BOC polymer

After testing the thermal stability of the synthesized monomer, it was then polymerised by using melt polycondensation strategy. The M-BOC monomer and 1, 12 dodecane diol added to the polymerisation tube along $Ti(OBu)_4$ as a catalyst and polymerised with melt polycondensation as above-mentioned chapters. The polymerization was carried out at 120 ºC as the monomer unit is unstable above 130 ºC. The monomer known to undergo thermo-selective polymerisation under melt polycondensation at or below 120 ºC it exclusively undergoes transesterification reaction while of polymerisation above it, the polymer chains found to undergo cross linking due to the participation of side chain urethane group in the monomer[27]. There is probability of ester group to undergo faster reaction as compare to urethane because the fact that lone pair of the nitrogen in urethane group participate the conjugation which makes it less nucleophilic as compare to ester group[28]. The polymerisation mixture was then subjected to 120 ºC with continues nitrogen purge and after 10 min 1 mol % catalyst was added.

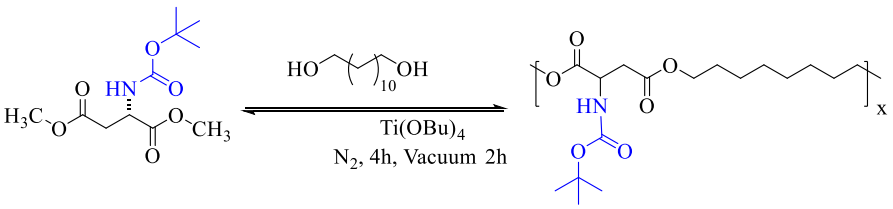

Scheme 4.2 *Synthesis of P-BOC polymer using melt polycondensation strategy.*

The melt polycondensation was carried out in two steps in first step the polymerisation mixture was heated at 120 ºC with continue N_2 purge for 4h followed by that in next step vacuum up to 10^{-2} mbar was applied for 2h to produce polyester as shown in Scheme 2. This synthesized polyester was referred as P-BOC. The polymerisation was confirmed using ^{1}H and ^{13}C NMR spectra in as Figure 8 ^{1}H NMR spectra of monomer M-BOC and P-BOC is compared.

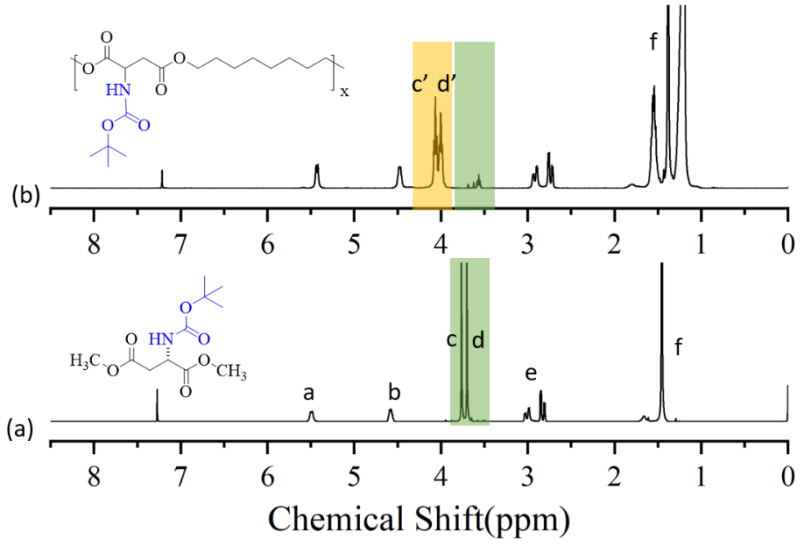

Figure 4.8 *Stalk of ^{1}H NMR spectra of monomer M-BOC(a) and polymer P-BOC (b)*

The NMR spectra was assigned alphabetically, after the polymerisation the all the monomer peaks found to be intact only dimethyl ester peaks of the monomer at 3.4-3.7 range undergo polymerization as shown in Figure 4.8a the peak c and d undergo transesterification with diol and get vanished in the polymer spectra Figure 4.8b. The presence of diester corresponding to the backbone CH_2 groups appeared at 4.4 ppm which are labelled as c' and d'. The polymerisation process was also confirmed by ^{13}C NMR methyl ester peak appeared in the range of 50.00 ppm to 54.00 ppm which upon polymerisation gets vanished and new polyester peak appeared at 62 and 64 ppm range. The no of repeating units (X_n) of the polymers were determined from ^{1}H NMR spectra by comparing the integration of end group peak at 3.88 and 3.88 ppm with integration of the new appeared peak 4.2 and 4.3 ppm. Using the Carothers's formula percentage of polymerisation was calculated and it was found that polymerisation has gone to 97-99 %. Number average molecular weight M_n of the polymer was calculated using

formula $M_n=X_n* M_o$. The molecular weight was found to be in less than 24000 g/mol. The M-BOC monomer was polymerised with different series of diols with different spacer length such hexanediol, octanediol, decanediol and dodecanediol to produce polymer. These polymers are referred with the P6, P8, P10 and P12 depending upon diol utilised during the polymerisation. These synthesized polyesters were then subjected to size exclusion chromatography (SEC) in tetrahydrofuran (THF) as eluent and polystyrene as standard. SEC chromatogram shown as Figure 4.9 shows monomodal distribution, the number average molecular weight (M_n) was found to be in range of 6000-14800 g/mol while weight average molecular weight (M_w) of the polyester 15700-35000 g/mol with polydispersity index closes to 2 summarized in the form of Table 4.1.

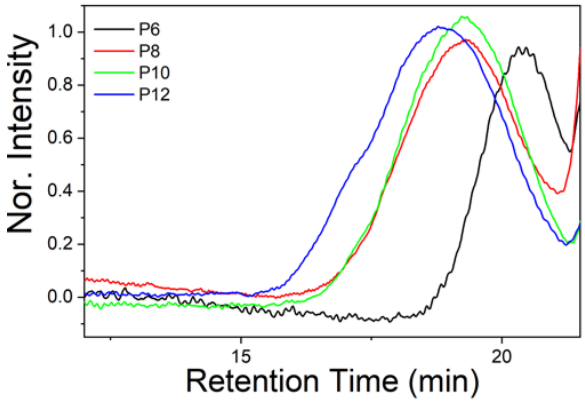

Figure 4.9 SEC Chromatogram of the synthesized polymers

Table 4.1 *SEC data of the polymers with THF as eluent.*

Polymer	Diols	Mn (g/mol)	Mw (g/mol)	Dispersity
P6	1,6 hexanediol	6300	15700	2.5
P8	1,8 octanediol	10300	27100	2.7
P10	1,10 decanediol	10300	27300	2.7
P12	1,12 dodecanediol	14,800	35000	2.3

Then the polyesters were then subjected to thermal characterisation by thermogravimetric analysis (TGA) and differential scanning calorimetry (DSC) as Figure 4.10. The polymers show bimodal decomposition pattern due to presence of two different groups the first decomposition hump is due to unstable side chain BOC pendant which decomposed at 125 ºC while the polymer hump corresponds to

degradation of the polyester backbone at 350 ºC. This is due to the fact that at lower temperature BOC side chain get decomposed while the polyester backbone decomposes at 280 ºC. All polyesters synthesized with different spacer diol were found to be amorphous in nature with glass transition temperature (T_g) value close to 0 ºC. (See Figure 4.10b.

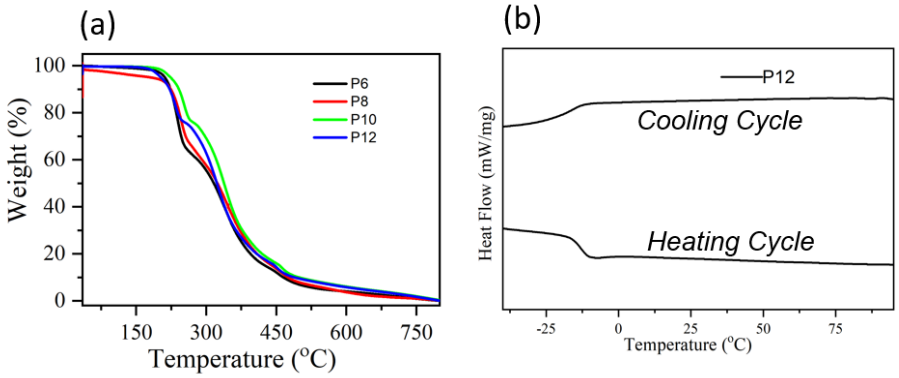

Figure 4.10 (a)TGA Thermogram of the synthesized polymers (b) DSC thermogram for P12.

4.3.3 Synthesis of amine functionalised polyester

In the polymer P-BOC the pendant side chain BOC group which is susceptible to the acidic condition and was selectively deprotected under acidic condition with trifluoracetic acid without disturbing the polyester backbone to produce amines functionalised polyester composed of positively charged species with trifluoracetic acid as counter ion.

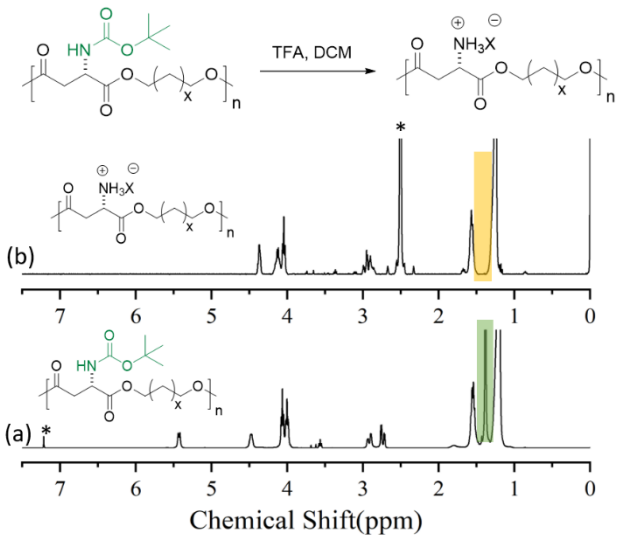

Figure 4.11 *(a)^{1}H NMR spectra of the P-BOC in $CDCl_3$(b) ^{1}H NMR spectra of the P-AM in DMSO-d_6 astaric mark represent solvent peak in spectra*

The polymer was referred as P-AM**.** The conversion of amine from the BOC was confirmed by disappearance for BOC peak from the polymer as shown in Figure 4.11 (a) using ^{1}H NMR spectra the peak at 1.47 ppm corresponds to the BOC peak of 9 protons in the P-BOC NMR spectra marked as green peak. After deprotection the polymer was dissolved in DMSO d_6 and ^{1}H spectra were recorded as shown as Figure 4.11b in the area marked with orange colour is does not show any peak which shows the successful deprotection of the BOC group of side pendant in polymer chain. Similarly, the structure of all the four deprotected polymers were characterised by NMR.

4.3.4 Self-assembly of polyester

The polymer P-BOC was found to be insoluble in water but after completed deprotection of BOC group from the polymer chain, the polymer became water soluble. The P-AM polymer composed of two different segments the polyester backbone contributes for the hydrophobicity while side chain pendant acts and hydrophilic in nature. This hydrophobic and hydrophilic balance in the polymer chain make the polymer amphiphilic in nature. In water polymer undergo phase segregation to produce segregated species as show in Figure 4.12a which undergo self-assembly to produce spherical nanoparticle in water, as shown in Figure 4.12a the polymeric nanoparticle was the subjected to study the size using dynamic light scattering (DLS) measurement. The polymer produces the nanoparticle of 100nm in diameter (See Figure 4.12b). Surface charge of the nanoparticle was studied using zeta potential. It was found that the polymer undergoes self-assembly to produce cationic nanoparticle. The self-assembly of all the polymers was studied and was it was found to be positive as shown in Figure 4.12c.

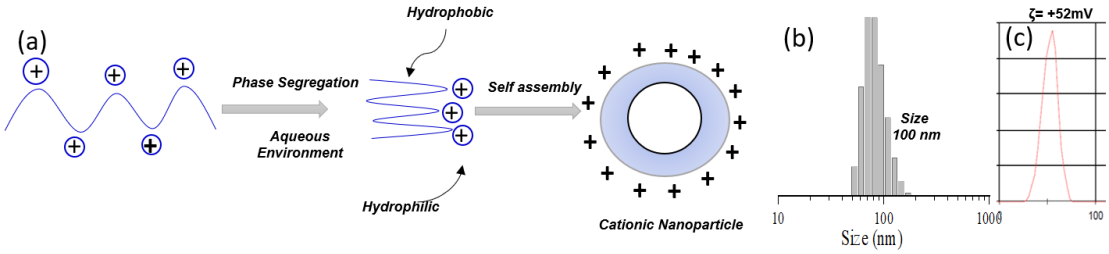

Figure 4.12 *(a) Schematic representation of self-assembly of cationic polymer in aqueous medium (b) DLS histogram of cationic nanoparticle(c) Zeta potential measurement of cationic nanoparticle.*

Table 4.2 *Table showing the polymer nano-assembly size obtained from the DLS and Zeta potential.*

Polymer	Size(nm)	Zeta Potential
P6	95	+11.9mV
P8	120	+52.1mV
P10	100	+51.5mV
P12	150	+78.3mV

The size and zeta potential of the cationic polymeric nanoparticle is summarised in the form of Table 4.2. It can be observed that as the spacer length of diol used for the polymer synthesis the zeta potential of the cationic nanoparticle increases while the size of the nanoparticle does not show any drastic change with change in the spacer length as the polymer with P12 has the highest positive zeta potential value. The nascent polymer was solubilised in water and tested for antibacterial activity.

4.3.5 Antibacterial activity the polymeric nanoparticle with appropriate amphiphilicity and cationic charge is required for the antibacterial activity. As the polymer possess requirements, the antibacterial activity was checked in solid as solution state. The antibacterial activity of the polymer was determined using resazurin assay.

4.3.5.1 Resazurin assay

Resazurin assay works on the principle that live cell converts resazurin (a blue coloured dye) to resorufin (a pink coloured dye) by the action of mitochondrial reductase enzyme of the live cell as shown in scheme in Figure 4.13a. To study the antibacterial activity gram negative bacteria *Escherichia Coliform (E. Coli)* was chosen. The experimental protocol is as follows, the experiment was performed in duplicate by taking two different variant of *E. Coli* referred as Wild type 1 (WT-1) and Wild type 2 (WT-2) and the experiment was carried out by colony suspension method. 10^6 *E. Coli* cells were seeded per well in 96 well plate with LB broth media these cells were incubated for 18 h along with different concentration of the polymer solution. The concentration of the polymer screened for antibacterial activity ranges from 10^{-12} mg/mL to 2 mg/mL, these bacteria along with the polymer solution were grown for 18h by incubating at 37 ºC.

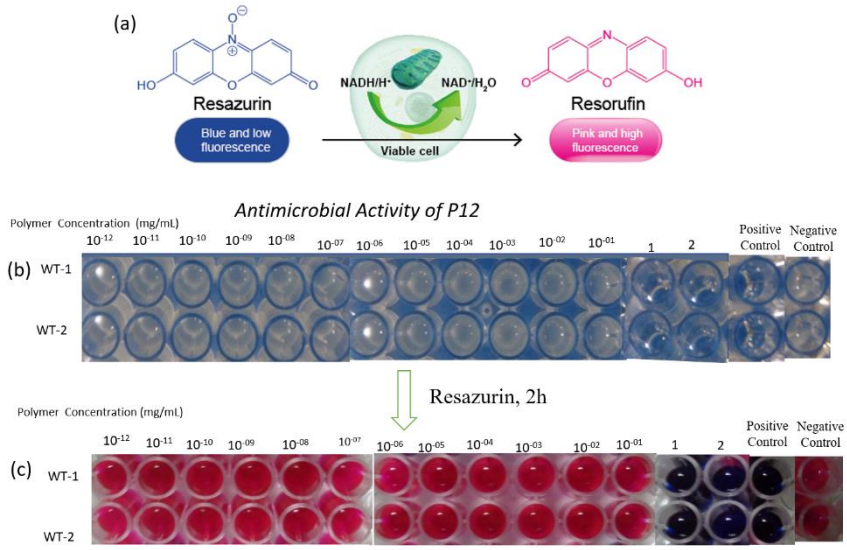

Figure 4.13 *(a) Mechanism of the resazurin assay (b) Photograph of 96 well plate the E. Coli incubated for 18h with different concentration of polymer solution (c) Photograph of 96 well plate after incubation with resazurin for 2h.*

In this experiment antibiotic ampicillin was employed as the positive control while *E. coli* without any antibacterial agent was considered as negative control. Figure 4.13b shows that up to the concentration of 0.1 mg/mL there is growth of bacterial observed in the form of turbidity while at the concentration of 1 mg/mL clear solution account for antibacterial activity which can be confirmed by comparison with the positive and negative control After completion of incubation of 18h, the 96 well plate was taken out and 5µ/mL of the resazurin solution was added in each well and the plates were again incubated for 2h. The result of the experiment is shown as in Figure 4.13c. Minimum Inhibitory Concentration (MIC) of the polymer was found to be 1 mg/mL as confirmed by turbidity after 18h. Blue colour at the 1 mg/mL and 2 mg/mL can be compared with the positive control ampicillin, while negative control showed the growth of bacteria development of the pink coloured.

4.3.5.2 Colony Suspension Method

The antibacterial activity of the polymer in the solution state was further confirmed by the colony suspension method. Similar protocol was as above the polymer was incubated with the bacteria in their log phase growth. In 96 well plate 10^6 CFU per mL cells were grown along with the polymer and continuously monitored for their turbidity at 600nm as a measure their growth in vario-scan instrument for 12h. The experiment was performed in triplicate, the polymer concentration traced in the range of 0.1 mg/mL

to 1 mg/mL. The ampicillin was used as positive control at its minimum inhibitory concentration 64 µg/mL and bacterial suspension without any antibacterial agent used as the negative control.

s

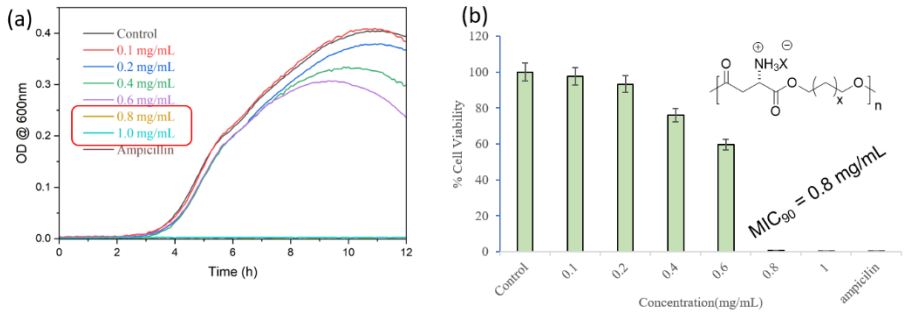

Figure 4.14 *(a) Antibacterial activity of the P12 by colony suspension method (b) Viability of the bacterial cells at different concentration of the polymer.*

The report of the experiment is shown as the Figure 4.14a, such suggest that polymer is effective at the concentration of 0.8 mg/mL. The cell viability of the bacterial was studied and it was found that the polymer is effective from the concentration 0.6 mg/mL onwards, and shows the MIC_{90} at 0.8 mg/mL. This MIC data can be compared with ampicillin (See Figure 4.14b).

4.3.5.3 Spread plate method

The antibacterial activity of the polymer was further detected in the solid state by using spread plate method. In this method, the bacterial along with the different concentration of the polymer was incubated for 12h time with continues shaking in an Eppendorf in the Lauria Broth (LB), after the completion of incubation the Eppendorf was taken out and streaked on the nutrient agar plate. This streaked plate was the incubated at 37 ºC for 12h allow the survived bacteria to grow. The photograph of the experiment is shown in the Figure 4.15.

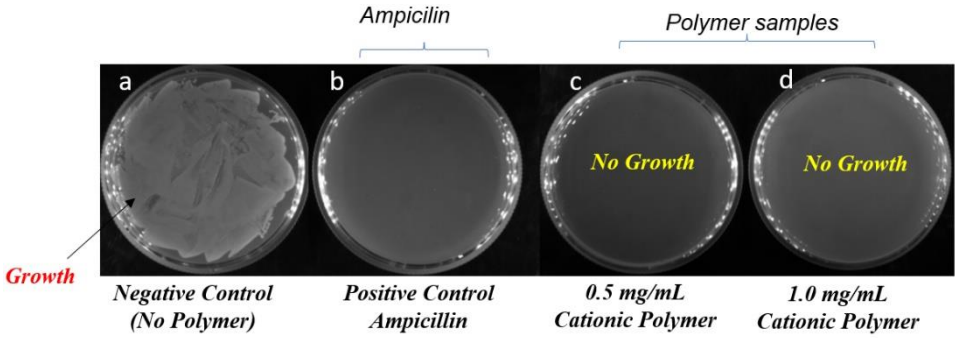

Figure 4.15 *Antibacterial activity of the P12 by spread plate method. (a) negative control (b)positive control. Plate with the polymer concentration of 0.5 mg/mL(c) and 1.0 mg/mL(d).*

In the Figure plate a and b corresponds to negative and positive control, the control experiment kept same as earlier for bacterial culture and ampicillin respectively. The negative control is shown as Figure 4.15a were there was no antibacterial agent to inhibit growth of the bacteria, the plate shows full growth of the bacterial colony. Where as in positive control in the plate Figure 4.15b there is a complete inhibition of the bacterial growth due effect of antibiotic i.e., ampicillin. When the bacterial culture incubated with two different concentrations of the polymer i.e., 0.5 mg/mL and 1.0 mg/mL. The polymer at these two concentrations showed the complete inhibition in the bacterial growth as shown in Figure 4.15c and 4.15d.

4.3.5.4 Disc Diffusion method

Disc diffusion method of testing antibacterial activity of the polymer is widely utilised of testing the wide variety of the antibacterial material testing. This method was first discovered by Alexander Flemming in 1950 with the discovery of penicillin antibiotic, this method was further refined by W. Kirby and A. Bauer later. This method is based on the fact that the antibacterial agent inhibits the growth of bacterial around it forming a zone of inhibition.

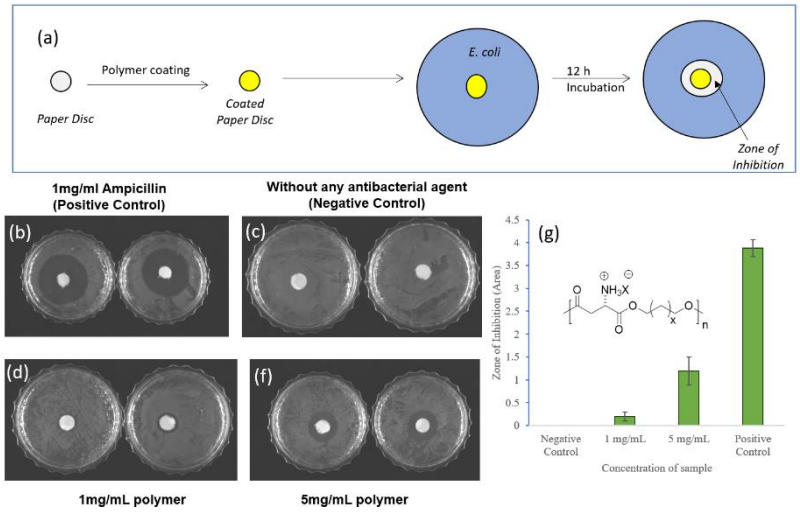

Figure 4.16 *Schematic representation of disc diffusion method step wise (a) Positive control (b) Negative control (c) plate with polymer concentration of 1.0 mg/mL (d) and 5.0 mg/mL(f).*

The protocol of the disc diffusion method is shown by schematic representation in Figure 4.16a. Paper disc of Whatman's filter paper prepared as shown, this filter paper was then treated with polymer coating by preparing the solution of the polymer of 1.0 mg/mL and 5.0 mg/mL. After the treatment the polymer solution was dried for

2h under aseptic condition in order to coat the surface of the with the polymer. In the Petri plate containing nutrient agar was streaked with 10^8 CFU of bacterial cell. Once the disc is dried it was then placed at the top of nutrient agar plate. These plates were then incubated with 37 ºC for 12 hrs. Plate considered as positive control when the paper disc was treated with ampicillin solution while the untreated paper was considered as negative control. Then after completion of period of incubation the plates were observed and photographs were captured. Figure 4.16b shows the plates treated with ampicillin, it shows the formation of large zone of inhibition. While the negative control does not show any zone of inhibition around the paper Figure 4.16c. The paper disc treated with the polymer samples is shown in the Figure 4.16 d and 4.16e where the 1.0 mg/mL sample showed the formation of small zone of inhibition while at the higher concentration of the polymer 5.0 mg/mL there is formation of large zone of inhibition. This zone of inhibition was calculated in each case and it is plotted with respect to concentration of the polymers as shown in Figure 4.16g. Th area of zone of inhibition was calculated using Image J software, calculating the diameter of circle.

Area of zone of inhibition = $\prod (R^2-r^2)$

R- radius of zone of inhibition

r- radius of paper disc.

4.3.6 Cell viability studies

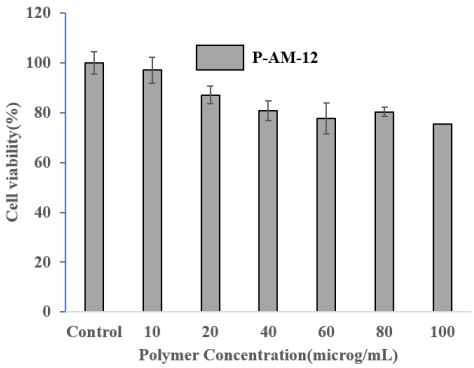

Figure 4.17 *MTT assay for the cationic polyester in WT MEF cell lines from 1 to 100 µg/mL.*

The biocompatibility of the cationic polymers was determined using MTT assay. Similar protocol was followed as explained earlier chapters using normal cell lines WT MEF. In a 96 well plate 1000 cell per well seeded along with complete media, Cells were grown for 16h and followed by it medium was removed and fresh media

was added in the well along with the different concentration of the polymer. The concentration of the polymer varied from 1μg/mL to 100μg/mL after incubating the plate for 72h, media was aspirated and MTT solution was added per well followed by incubating it with 4h. If the cells were alive MTT solution added get converted into formazan crystal. These formazan crystals then dissolve in 100 μL of the DMSO and absorbance recorded in the varioscan at 570nm laser and by comparing the absorbance intensity of the formazan in control and sample cell viability was calculated. The prepared cationic polymer was found to be biocompatible with WT MEF up to the concentration of 100μg/mL as shown in Figure 4.17.

4.4 Conclusion

L aspartic acid based cationic polyester was synthesized in two steps. In the first steps melt polymerizable unit form L aspartic acid was prepared which was polymerised by polycondensation to produce BOC functionalised polyester. In the second step the pendant BOC group was deprotected in presence of the basic condition to get cationic polyester. All the polymer with different spacer length was found to produce moderate polymer molecular weight. P-BOC polymer found to show that good thermal stability with amorphous in nature, which can be good candidate for thermoplastic application. Once the polymer becomes cationic in nature it becomes water soluble. The cationic polymer found to be produced polymer nanoparticle in aqueous environment, with size range in below 150±10nm range and zeta potential studies further confirmed the positively charge on the nanoparticle. The antibacterial study of the studies of the polymer was confirmed at both solid state and the solution state, the qualitative analysis experiment resazurin assay the polymer showed MIC close to 1mg/ml. Antibacterial studies by colony suspension method shows the MIC_{90} of 0.8mg/ml. Cell viability assay of WT MEF of polymer suggest that the cationic polymer was biocompatible.

4.5 References

(1) Kapoor, G.; Saigal, S.; Elongavan, A. Action and Resistance Mechanisms of Antibiotics: A Guide for Clinicians. *Journal of Anaesthesiology Clinical Pharmacology*. Medknow Publications July 1, 2017, pp 300–305. https://doi.org/10.4103/joacp.JOACP_349_15.

(2) Bell, B. G.; Schellevis, F.; Stobberingh, E.; Goossens, H.; Pringle, M. *A Systematic Review and Meta-Analysis of the Effects of Antibiotic Consumption on Antibiotic Resistance*; 2014. http://www.biomedcentral.com/1471-2334/14/13.

(3) Corcione, S.; Lupia, T.; De Rosa, F. G. Novel Cephalosporins in Septic Subjects and Severe Infections: Present Findings and Future Perspective. *Front Med (Lausanne)* **2021**, *8*. https://doi.org/10.3389/fmed.2021.617378.

(4) Aldred, K. J.; Kerns, R. J.; Osheroff, N. Mechanism of Quinolone Action and Resistance. *Biochemistry*. American Chemical Society March 18, 2014, pp 1565–1574. https://doi.org/10.1021/bi5000564.

(5) Oelmann, S.; Travanut, A.; Barther, D.; Romero, M.; Howdle, S. M.; Alexander, C.; Meier, M. A. R. Biocompatible Unimolecular Micelles Obtained via the Passerini Reaction as Versatile Nanocarriers for Potential Medical Applications. *Biomacromolecules* **2019**, *20* (1), 90–101. https://doi.org/10.1021/acs.biomac.8b00592.

(6) Zasloff, M. *Antimicrobial Peptides of Multicellular Organisms*; 2002; Vol. 415. www.nature.com.

(7) Rll<y, I. H. J.; Woo, W. N. K. •; Old, R. L. J. W. P.; Steiner, H.; Hultmark, D.; Engstromt, A.; Bennicht, H.; Boman, H. G. *5. Ro Mmel.Ere*; 1977; Vol. 279.

(8) Simmaco, M.; Mignogna, G.; Barra, D. Antimicrobial Peptides from Amphibian Skin: What Do They Tell Us? *Biopolymers* **1998**, *47* (6), 435–450. https://doi.org/10.1002/(SICI)1097-0282(1998)47:6<435::AID-BIP3>3.0.CO;2-8.

(9) Shai, Y. *Mechanism of the Binding, Insertion and Destabilization of Phospholipid Bilayer Membranes by K-Helical Antimicrobial and Cell Non-Selective Membrane-Lytic Peptides*. www.elsevier.com/locate/bba.

(10) Burkhard Bechinger, Zasloff, M.; Opella', S. J. *Structure and Orientation of the Antibiotic Peptide Magainin in Membranes by Solid-State Nuclear Magnetic Resonance Spectroscopy*; Cambridge University Press, 1993; Vol. 2.

(11) Zasloff, M. *Magainins, a Class of Antimicrobial Peptides from Xenopus Skin: Isolation, Characterization of Two Active Forms, and Partial CDNA Sequence of a Precursor (Vertebrate Peptide Antibiotics)*; 1987; Vol. 84. https://www.pnas.org.

(12) Hancock, R. E. W.; Sahl, H. G. Antimicrobial and Host-Defense Peptides as New Anti-Infective Therapeutic Strategies. *Nature Biotechnology*. December 2006, pp 1551–1557. https://doi.org/10.1038/nbt1267.

(13) Meng, H.; Kumar, K. Antimicrobial Activity and Protease Stability of Peptides Containing Fluorinated Amino Acids. *J Am Chem Soc* **2007**, *129* (50), 15615–15622. https://doi.org/10.1021/ja075373f.

(14) Ghosh, C.; Sarkar, P.; Issa, R.; Haldar, J. Alternatives to Conventional Antibiotics in the Era of Antimicrobial Resistance. *Trends in Microbiology*. Elsevier Ltd April 1, 2019, pp 323–338. https://doi.org/10.1016/j.tim.2018.12.010.

(15) Mahlapuu, M.; Håkansson, J.; Ringstad, L.; Björn, C. Antimicrobial Peptides: An Emerging Category of Therapeutic Agents. *Frontiers in Cellular and Infection Microbiology*. Frontiers Media S.A. 2016. https://doi.org/10.3389/fcimb.2016.00194.

(16) C Reygaert, W. An Overview of the Antimicrobial Resistance Mechanisms of Bacteria. *AIMS Microbiol* **2018**, *4* (3), 482–501. https://doi.org/10.3934/microbiol.2018.3.482.

(17) Munita, J. M.; Arias, C. A. Mechanisms of Antibiotic Resistance. *Microbiol Spectr* **2016**, *4* (2). https://doi.org/10.1128/microbiolspec.VMBF-0016-2015.

(18) Zhong, Y.; Xiao, H.; Seidi, F.; Jin, Y. Natural Polymer-Based Antimicrobial Hydrogels without Synthetic Antibiotics as Wound Dressings. *Biomacromolecules* **2020**, *21* (8), 2983–3006. https://doi.org/10.1021/acs.biomac.0c00760.

(19) Salas-Ambrosio, P.; Tronnet, A.; Verhaeghe, P.; Bonduelle, C. Synthetic Polypeptide Polymers as Simplified Analogues of Antimicrobial Peptides. *Biomacromolecules* **2021**, *22* (1), 57–75. https://doi.org/10.1021/acs.biomac.0c00797.

(20) Ghosh, R.; Malhotra, M.; Madhuri Sathe, R. R.; Jayakannan, M. Biodegradable Polymer Theranostic Fluorescent Nanoprobe for Direct Visualization and Quantitative Determination of Antimicrobial Activity. *Biomacromolecules* **2020**, *21* (7), 2896–2912. https://doi.org/10.1021/acs.biomac.0c00653.

(21) Ghosh, R.; Jayakannan, M. Theranostic FRET Gate to Visualize and Quantify Bacterial Membrane Breaching. *Biomacromolecules* **2023**, *24* (2), 739–755. https://doi.org/10.1021/acs.biomac.2c01202.

(22) Oh, J.; Khan, A. Main-Chain Polysulfonium Salts: Development of Non-Ammonium Antibacterial Polymers Similar in Their Activity to Antibiotic Drugs Vancomycin and Kanamycin. *Biomacromolecules* **2021**, *22* (8), 3534–3542. https://doi.org/10.1021/acs.biomac.1c00627.

(23) Uppu, D. S. S. M.; Samaddar, S.; Hoque, J.; Konai, M. M.; Krishnamoorthy, P.; Shome, B. R.; Haldar, J. Side Chain Degradable Cationic-Amphiphilic Polymers with Tunable Hydrophobicity Show in Vivo Activity. *Biomacromolecules* **2016**, *17* (9), 3094–3102. https://doi.org/10.1021/acs.biomac.6b01057.

(24) Yook, J.; Jeong, D.; Lee, J. C. Synthesis of Citronellol-Derived Antibacterial Polymers and Effect of Thioether, Sulfoxide, Sulfone, and Ether Functional Groups on Their Bactericidal Activity. *Macromolecules* **2023**, *56* (9), 3406–3420. https://doi.org/10.1021/acs.macromol.2c02518.

(25) Mukherjee, I.; Ghosh, A.; Bhadury, P.; De, P. Side-Chain Amino Acid-Based Cationic Antibacterial Polymers: Investigating the Morphological Switching of a Polymer-

Treated Bacterial Cell. *ACS Omega* **2017**, *2* (4), 1633–1644. https://doi.org/10.1021/acsomega.7b00181.

(26) Mizutani, M.; Palermo, E. F.; Thomas, L. M.; Satoh, K.; Kamigaito, M.; Kuroda, K. Design and Synthesis of Self-Degradable Antibacterial Polymers by Simultaneous Chain- and Step-Growth Radical Copolymerization. *Biomacromolecules* **2012**, *13* (5), 1554–1563. https://doi.org/10.1021/bm300254s.

(27) Anantharaj, S.; Jayakannan, M. Polymers from Amino Acids: Development of Dual Ester-Urethane Melt Condensation Approach and Mechanistic Aspects. *Biomacromolecules* **2012**, *13* (8), 2446–2455. https://doi.org/10.1021/bm300697h.

(28) Anantharaj, S.; Jayakannan, M. Catalysts and Temperature Driven Melt Polycondensation Reaction for Helical Poly(Ester-Urethane)s Based on Natural L-Amino Acids. *J Polym Sci A Polym Chem* **2016**, *54* (8), 1065–1077. https://doi.org/10.1002/pola.27970.

Overall Conclusion

The work can be concluded from the thesis titled "L-Aspartic Acid Based Functional Polyesters for Drug Delivery and Antimicrobial Applications" that the development of the polymer from the renewable resource, i.e., amino acid, to replace existing petroleum-based polymers is dealt with. With excellent structural tunability and biodegradability, the polymer is created.

In Chapter 2, the utilization of L-aspartic acid as a fundamental building block for the development of amide-functionalized polyesters through a melt polycondensation approach is centered upon. The versatility of L-aspartic acid as a precursor is explored, wherein various amide-functionalized di-ester monomers are synthesized by conjugating different aromatic and aliphatic acids. These monomers are subsequently polymerized with 1,12-dodecanediol, yielding high molecular weight polyesters. Notably, the catalyst choice plays a crucial role in achieving the desired molecular weight, with titanium tetrabutoxide ($Ti(OBu)_4$) being proven to be the most effective in this regard. The resulting polyesters exhibit excellent thermal stability and, for the most part, an amorphous nature. The one exception to this amorphous characteristic is observed in a polymer with long pendant chains, such as stearate and pentadecyl phenol as side chains. To enhance the water solubility of these polymers, a P-PEG-functionalized polymer is engineered. This P-PEG-functionalized polymer is designed to self-assemble into spherical nanoparticles in aqueous environments, enabling their potential application in drug delivery. The nanoparticles demonstrate a capacity to load various substances, including drugs and biomarkers, and their biodegradable nature is indirectly confirmed through in vitro drug release kinetics. Furthermore, these nanoparticles prove to be biocompatible with both normal and cancer cell lines, while drug-loaded nanoparticles exhibit inhibitory effects on cancer cell growth. The potential of amide-functionalized polyesters derived from L-aspartic acid as effective drug delivery carriers is underscored by this chapter's findings, supported by confocal microscopy.

In Chapter 3, the research is dedicated to the development of a novel fluorescently tagged polyester derived from L-aspartic acid, representing an innovative approach to biomedical applications. New monomers based on L-aspartic acid are designed, which are subsequently polymerized using a melt polycondensation technique, resulting in the creation of copolymers with specific compositions. The structural properties of the copolymers are extensively characterized, with the precision of the method validated through ^1H NMR studies, and moderate molecular weights

confirmed by SEC chromatography. The transformation of the copolymer involves the deprotection of acetal groups to obtain a hydroxyl-functionalized TPE-tagged polymer, known for its thermal stability up to 300 ºC. Unique insights into the polymer's behavior are revealed through differential scanning calorimetry (DSC), highlighting semicrystalline characteristics brought about by π-π interactions within the polymer chains. This semicrystallinity is further intensified through the synergistic effects of π-π interactions and hydrogen bonding. The polymer also displays the intriguing property of aggregation-induced emission (AIE) in solution state studies, allowing for the determination of the critical aggregation concentration (CAC), and subsequently, the formation of nano-assemblies in aqueous environments capable of encapsulating a wide range of dyes, both hydrophilic and hydrophobic. Detailed characterization using FEEM and HR-TEM confirms the nano-assemblies possess spherical morphology with dimensions in the sub-nanometer range. The investigation extends to the photophysical properties of the polymer nanoparticles, including emission spectra and lifetime measurements, revealing the presence of Förster resonance energy transfer (FRET) within the nanocavities of the nanoparticles. Importantly, the biocompatibility of the polymer is established, demonstrating its potential as an efficient drug delivery carrier for both normal and cancer cells. The interaction between the polymer chain and the loaded cargo is also explored, shedding light on FRET at the cellular level. Finally, in vivo biodistribution studies in Bulb C mice, employing an IVIS imaging setup, provide concrete evidence supporting the utility of the polymer-based nanocarrier for efficient cargo delivery, marking a significant step forward in the realm of biomedical applications.

Chapter 4 of the study delves into the synthesis of a cationic polyester based on L-aspartic acid in a two-step process. In the first step, a melt-polymerizable unit derived from L-aspartic acid is prepared, and this unit is subsequently polymerized via polycondensation to yield a BOC-functionalized polyester. In the second step, the pendant BOC groups are deprotected under basic conditions, resulting in the formation of a cationic polyester. These cationic polyesters, with varying spacer lengths, consistently exhibit moderate molecular weights. The P-BOC polymer is particularly noteworthy for its excellent thermal stability and amorphous nature, making it a promising candidate for thermoplastic applications. Upon acquiring a cationic nature, these polymers become water-soluble. They have the capability to form polymer nanoparticles in aqueous environments, with particle sizes falling within the range of

approximately 150±10nm, and zeta potential studies affirm the positively charged nature of these nanoparticles. The antimicrobial properties of the polymers are explored in both solid and solution states, revealing their effectiveness. Qualitative analyses, including the resazurin assay, indicate minimal inhibitory concentrations (MICs) close to 1mg/ml, and further antibacterial studies employing the colony suspension method establish a MIC90 of 0.8mg/ml. Additionally, cell viability assays conducted on WT MEF cells demonstrate the biocompatibility of these cationic polymers, which hold promise for a range of biomedical applications, particularly in the realm of antimicrobial treatments.

Future Directions

This thesis deals with the development of functional polyester with different side chain pendant of the polymer backbone such as PEG 350, Hydroxyl group and amine functionalised polyester. The scope of this research work can be expanded by developing the polyester with different side chain functional group such as carboxylic acid, Sulfhydryl etc. The suitable monomer can be designed with aim to attached the drug to the polymer to make polymer-based prodrug for both anticancer and antibacterial applications. Development of stimuli responsive polymer can be achieved by attaching the suitable ligand to the polymer for the targeted attack to the site of cancer tumour.

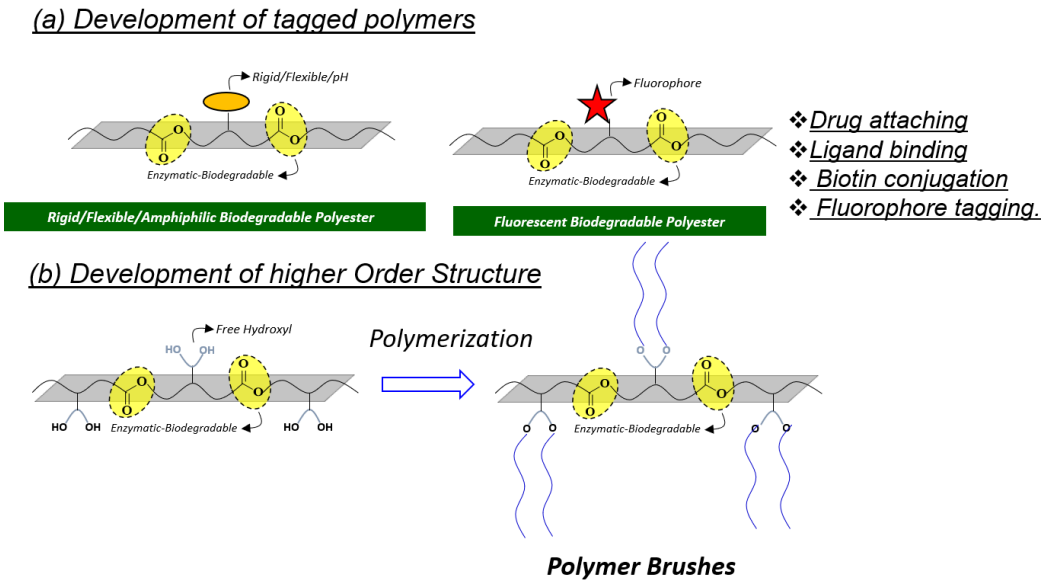

Figure 5.1 *(a) Development of the stimuli responsive polymer (b) L-aspartic acid based higher order structure.*

pH responsive polymer can be created by attaching carboxylic group as pendant to polyester chain, which can undergo protonation and deprotonation depending upon the pH of the media. In addition to the above the carboxylic acid group in the polymer can be further conjugate with drug. The chapter 3 deals hydroxyl functionalised polyester which can be utilised for the development of brush type polymer by employing the pendant hydroxyl group on the polymer as macroinitiator for the ring opening polymerisation for polylactide, substituted caprolactone etc which can be subsequently utilised for polymer for drug delivery application. The cationic polymer developed in 4 chapter possess positive charge on the polymer can be used for the development of polyplexes for gene delivery in cancer treatment.

List of Publications

1. **Mohammed Khuddus** and Manickam Jayakannan, Melt Polycondensation Strategy for Amide-Functionalized L-Aspartic Acid Amphiphilic Polyester Nano-assemblies and Enzyme-Responsive Drug Delivery in Cancer Cells, **Biomacromolecules *2023*, 24**, 2643-2660.

2. **Mohammed Khuddus,** Utreshwar Gavhane, Sonashree Saxena and Manickam Jayakannan Fluorescent Biodegradable Polyester from L-Aspartic Acid for Therapeutics in Cancer Cells. (Manuscript under preparation).

3. **Mohammed Khuddus,** Ruma Ghosh and Manickam Jayakannan Development of L-Aspartic acid based cationic polyester for antimicrobial applications (Manuscript under preparation).

4. **Mohammed Khuddus,** Utreshwar Gavhane and Manickam Jayakannan. Post polymerization click approach for the developed of nanocarriers for drug delivery in cancer cells. (Manuscript under preparation)

pubs.acs.org/Biomac

Article

Melt Polycondensation Strategy for Amide-Functionalized L-Aspartic Acid Amphiphilic Polyester Nano-assemblies and Enzyme-Responsive Drug Delivery in Cancer Cells

Mohammed Khuddus and Manickam Jayakannan*

Cite This: *Biomacromolecules* 2023, 24, 2643−2660

Read Online

ACCESS | Metrics & More | Article Recommendations | Supporting Information

ABSTRACT: Aliphatic polyesters are intrinsically enzymatic-biodegradable, and there is ever-increasing demand for safe and smart next-generation biomaterials including drug delivery nano-vectors in cancer research. Using bioresource-based biodegradable polyesters is one of the elegant strategies to meet this requirement; here, we report an L-amino acid-based amide-functionalized polyester platform and explore their lysosomal enzymatic biodegradation aspects to administrate anticancer drugs in cancer cells. L-Aspartic acid was chosen and different amide-side chain-functionalized di-ester monomers were tailor-made having aromatic, aliphatic, and bio-source pendant units. Under solvent-free melt polycondensation methodology; these monomers underwent polymerization to yield high molecular weight polyesters with tunable thermal properties. PEGylated L-aspartic monomer was designed to make thermo-responsive amphiphilic polyesters. This amphiphilic polyester was self-assembled into a 140 ± 10 nm-sized spherical nanoparticle in aqueous medium, which exhibited lower critical solution temperature at 40−42 °C. The polyester nano-assemblies showed excellent encapsulation capabilities for anticancer drug doxorubicin (DOX), anti-inflammatory drug curcumin, biomarkers such as rose bengal (RB), and 8-hydroxypyrene-1,3,6-trisulfonic acid trisodium salt. The amphiphilic polyester NP was found to be very stable under extracellular conditions and underwent degradation upon exposure to horse liver esterase enzyme in phosphate-buffered saline at 37 °C to release 90% of the loaded cargoes. Cytotoxicity studies in breast cancer MCF 7 and wild-type mouse embryonic fibroblasts cell lines revealed that the amphiphilic polyester was non-toxic to cell lines up to 100 μg/mL, while their drug-loaded polyester nanoparticles were able to inhibit the cancerous cell growth. Temperature-dependent cellular uptake studies further confirmed the energy-dependent endocytosis of polymer NPs across the cellular membranes. Confocal laser scanning microscopy assisted time-dependent cellular uptake analysis directly evident for the endocytosis of DOX loaded polymer NP and their internalization for biodegradation. In a nutshell, the present investigation opens up an avenue for the L-amino acid-based biodegradable polyesters from L-aspartic acids, and the proof of concept is demonstrated for drug delivery in the cancer cell line.

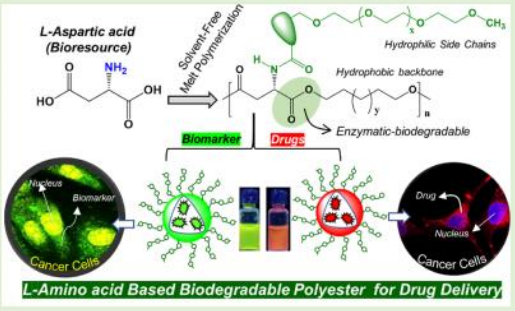

INTRODUCTION

Biodegradable polymers are emerging as important components in tissue engineering,[1] bone repair,[2] nano-vehicles for therapeutics drugs and genes in cancer treatment, and so forth.[3−5] Among various chemical linkages that are readily susceptible to biodegradation under physiological conditions, aliphatic polyesters are very special due to their unique ability to degrade by lysosomal enzyme stimuli at the intracellular compartments.[6−8] Aliphatic polyesters are typically synthesized either by ring opening polymerization (ROP) of cyclic monomers[9,10] or direct polycondensation of dicarboxylic acids and diols.[11,12] The ROP strategy has been used industrially for the production of polycaprolactone (PCL),[13−15] poly(L-lactic acid) and poly(D,L-lactic-*co*-glycolic acid), and their di- and tri-block copolymers.[16,17] In the last decade, significant efforts have been taken to enhance the hydrolytic and environmental stability of the PLLA.[18] Attempts have also been made to overcome the slow enzymatic biodegradation of PCL chains by functionalization of various side chains[19] for drug delivery in cancer[20−22] and antimicrobial agents.[23,24] On the contrary, the polycondensation approach for aliphatic polyesters has had limited success in commercial exploration due to poor mechanical properties, low molecular weights, limited enzymatic or microbial biodegradation, and so forth.[25] 1,4-Cyclohexane dicarboxylic acid (from DuPont)-,[26]

Received: February 6, 2023
Revised: April 23, 2023
Published: May 15, 2023

Melt Polycondensation Strategy for Amide-Functionalized l-Aspartic Acid Amphiphilic Polyester Nano-assemblies and Enzyme-Responsive Drug Delivery in Cancer Cells

Author: Mohammed Khuddus, Manickam Jayakannan

Publication: Biomacromolecules

Publisher: American Chemical Society

Date: May 1, 2023

PERMISSION/LICENSE IS GRANTED FOR YOUR ORDER AT NO CHARGE

This type of permission/license, instead of the standard Terms and Conditions, is sent to you because no fee is being charged for your order. Please note the following:

- Permission is granted for your request in both print and electronic formats, and translations.
- If figures and/or tables were requested, they may be adapted or used in part.
- Please print this page for your records and send a copy of it to your publisher/graduate school.
- Appropriate credit for the requested material should be given as follows: "Reprinted (adapted) with permission from {COMPLETE REFERENCE CITATION}. Copyright {YEAR} American Chemical Society." Insert appropriate information in place of the capitalized words.
- One-time permission is granted only for the use specified in your RightsLink request. No additional uses are granted (such as derivative works or other editions). For any uses, please submit a new request.

If credit is given to another source for the material you requested from RightsLink, permission must be obtained from that source.

BACK CLOSE WINDOW

Indian Institute of Science Education and Research
(IISER – PUNE)

Dr. Homi Bhabha Road, Pashan, Pune 411 008.

Certificate

This is to certify that the project **"Amino Acid and Sugar Based Biodegradable Polymers for Anticancer Drug Delivery" (IISER_Pune/ IAEC/2022_01/16)** from **Prof. M. Jayakannan** has been approved by the IAEC.

Authorized by	Name	Signature	Date
Chairman:	Dr. Nixon Abraham		04 Mar 2022
Member Secretary:	Dr. Suraj Ingle		04 Mar 2022
Main Nominee of CPCSEA:	Dr. Shital Suryavanshi	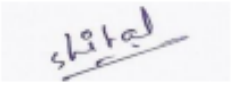	04 Mar 2022

Appendix

Chapter 2

(a)

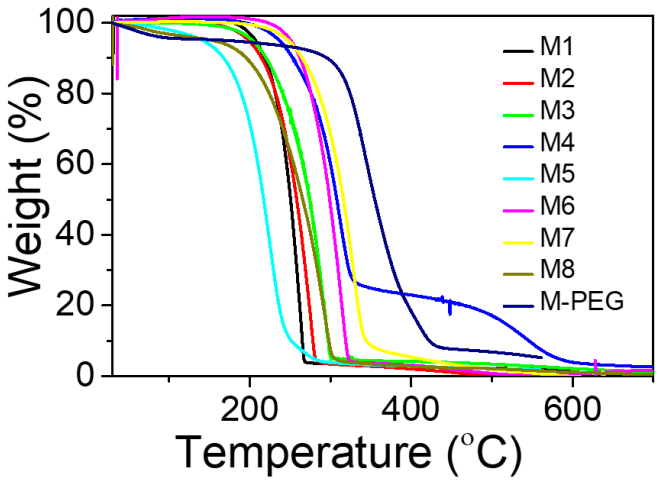

(b)

Monomer	TGA (°C)
M1	190
M2	200
M3	210
M4	240
M5	170
M6	260
M7	260
M8	160
M-PEG	210

Appendix Figure S1 *(a) TGA thermograms of L-aspartic acid based diester monomers at 10 °/min under N_2 atmosphere. (b) Table containing the thermal stability of monomers.*

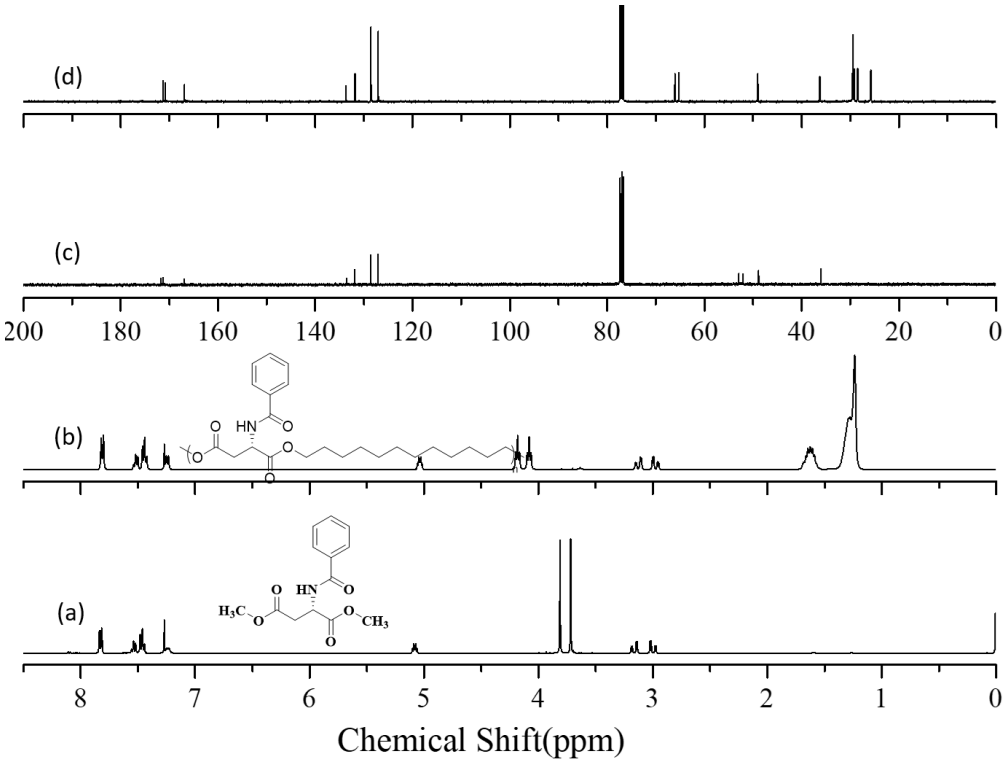

Appendix Figure S2 *^{1}H NMR spectra of monomer M1 (a) and its polymer P1 (b). ^{13}C NMR spectra of monomer M1 (c) and its polymer P1 (d). The spectra were recorded in $CDCl_3$*

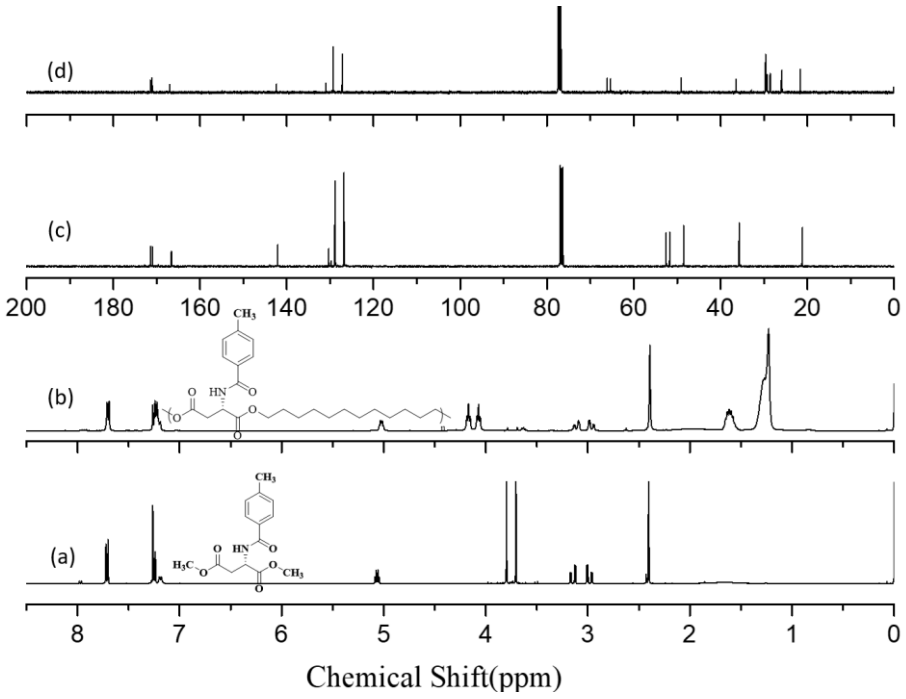

Appendix Figure S3 *^{1}H NMR spectra of monomer M2 (a) and its polymer P2 (b). ^{13}C NMR spectra of monomer M2 (c) and its polymer P2 (d). The spectra were recorded in $CDCl_3$*

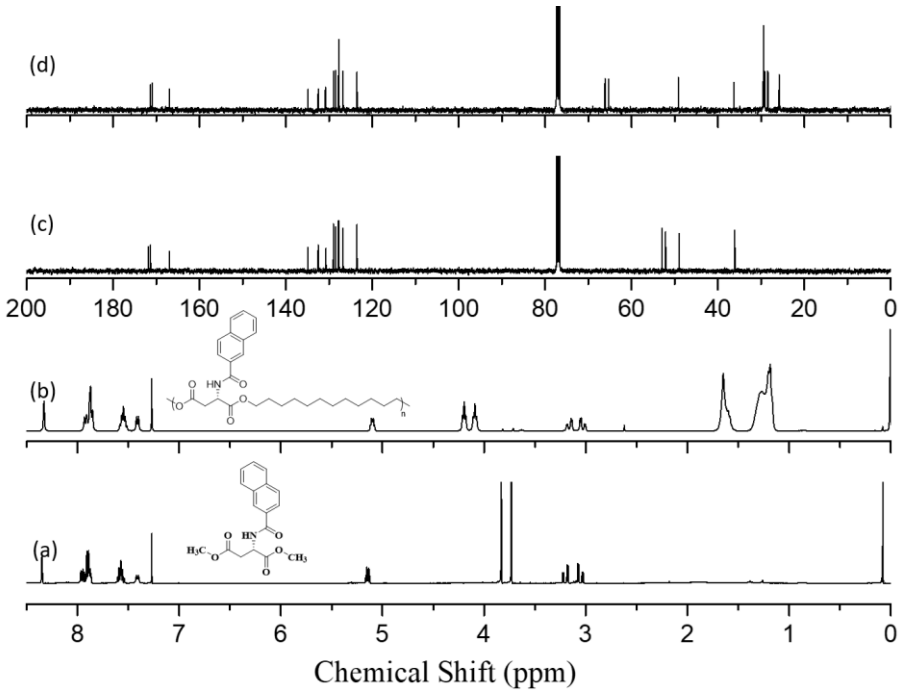

Appendix Figure S4 *^{1}H NMR spectra of monomer M4 (a) and its polymer P4 (b). ^{13}C NMR spectra of monomer M4 (c) and its polymer P4 (d). The spectra were recorded in $CDCl_3$*

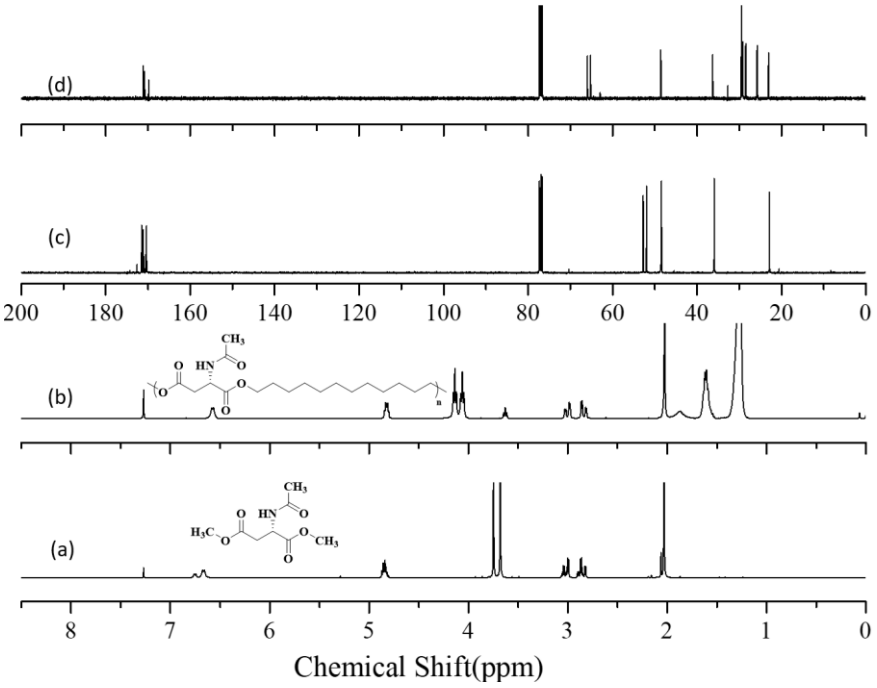

Appendix Figure S5 *^{1}H NMR spectra of monomer M5 (a) and its polymer P5 (b). ^{13}C NMR spectra of monomer M5 (c) and its polymer P5 (d). The spectra were recorded in $CDCl_3$*

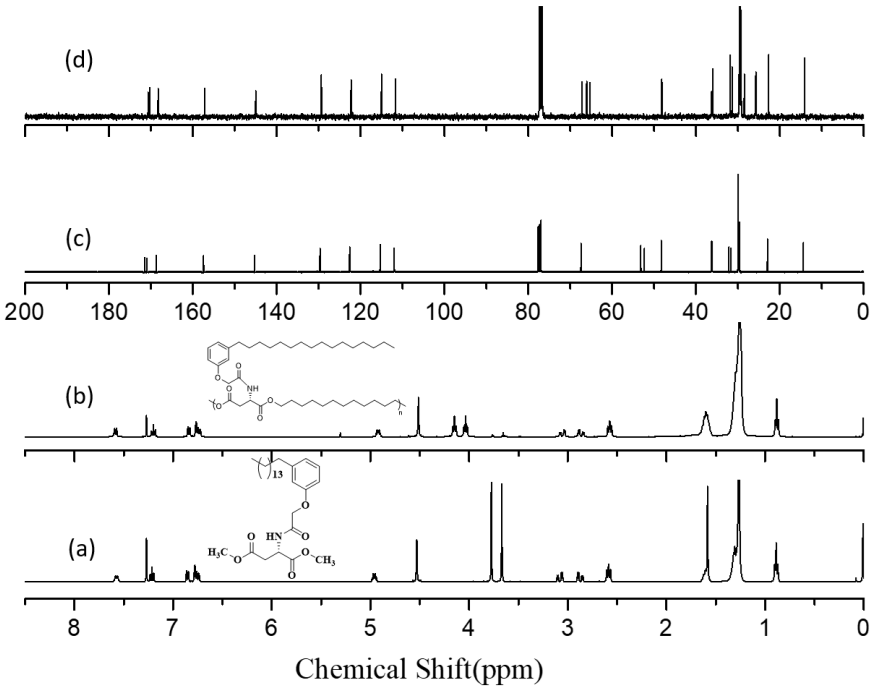

Appendix Figure S6 *^{1}H NMR spectra of monomer M6 (a) and its polymer P6 (b). ^{13}C NMR spectra of monomer M6 (c) and its polymer P6 (d). The spectra were recorded in $CDCl_3$*

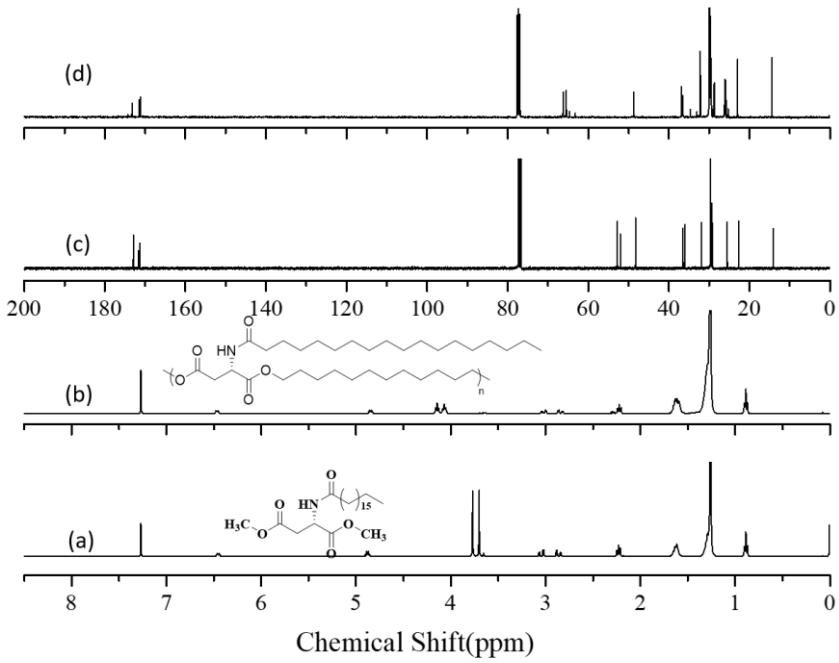

Appendix Figure S7 *^{1}H NMR spectra of monomer M7 (a) and its polymer P7 (b). ^{13}C NMR spectra of monomer M7 (c) and its polymer P7 (d). The spectra were recorded in $CDCl_3$*

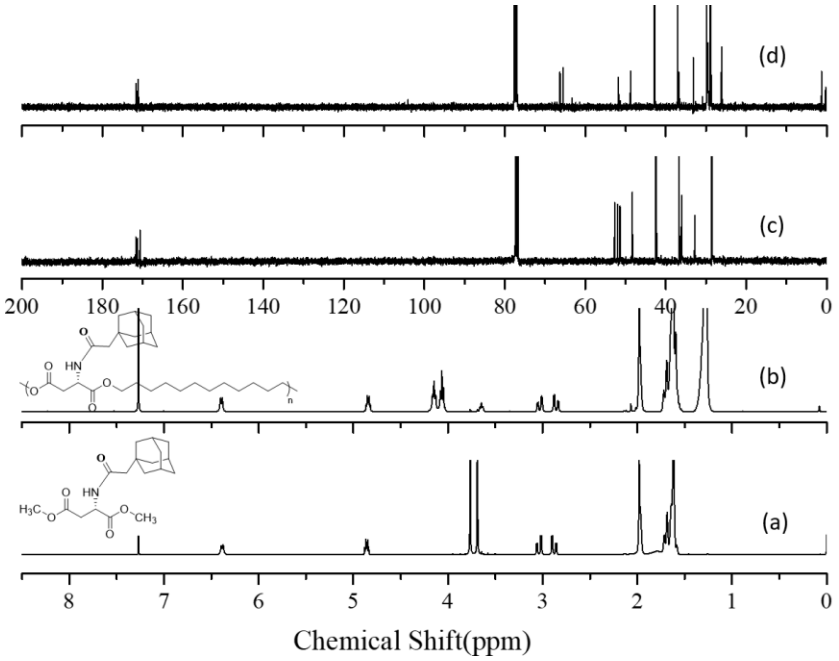

Appendix Figure S8 *^{1}H NMR spectra of monomer M8 (a) and its polymer P8 (b). ^{13}C NMR spectra of monomer M8 (c) and its polymer P8 (d). The spectra were recorded in $CDCl_3$*

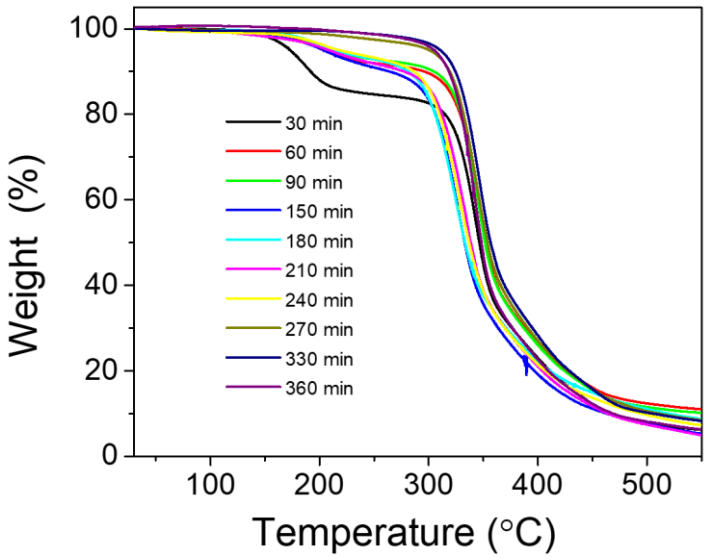

Appendix Figure S9 *TGA of aliquots of the kinetics of polymerisation of P-3. TGA was performed at 10 °/min under N_2 atmosphere.*

Chapter 3

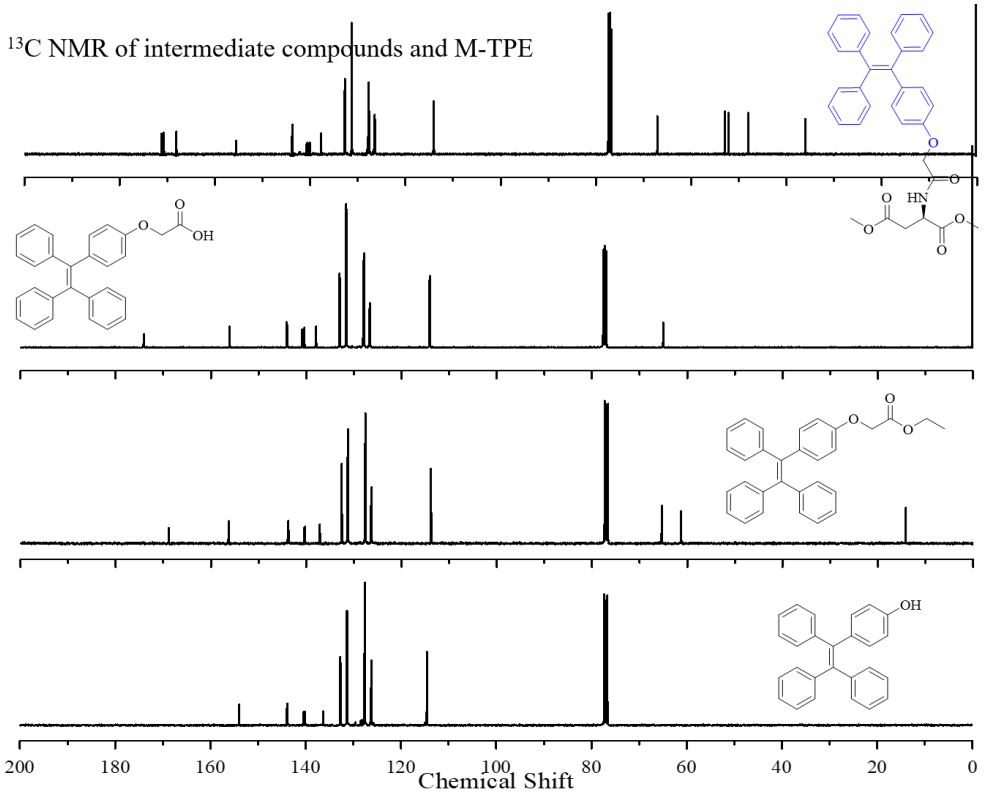

Appendix Figure S10 ^{13}C NMR spectra of M-TPE and intermediate compounds.

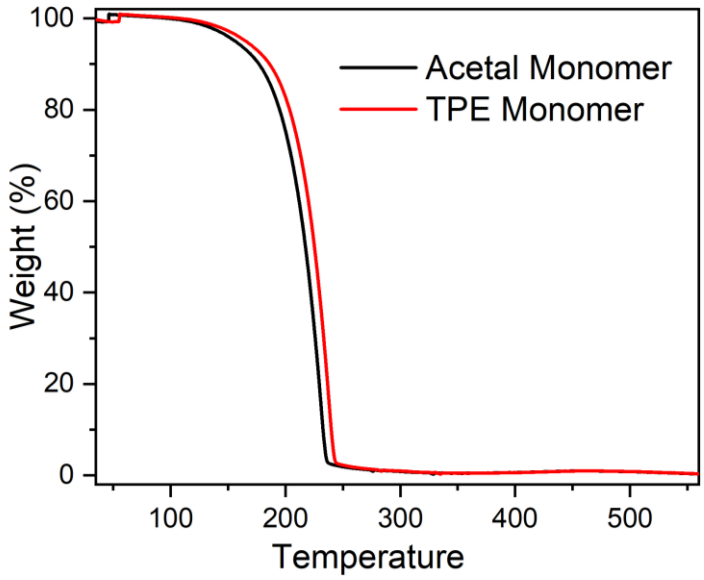

Appendix Figure S11 TGA of monomers and TPE diol.

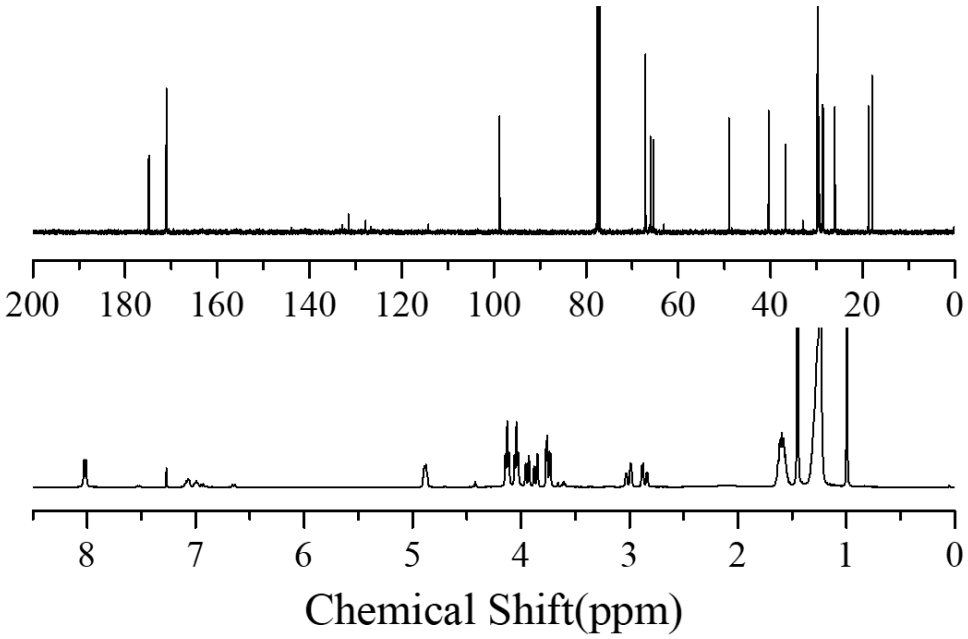

Appendix Figure S12 ^{1}H and ^{13}C NMR spectra of $PTPE_4$.

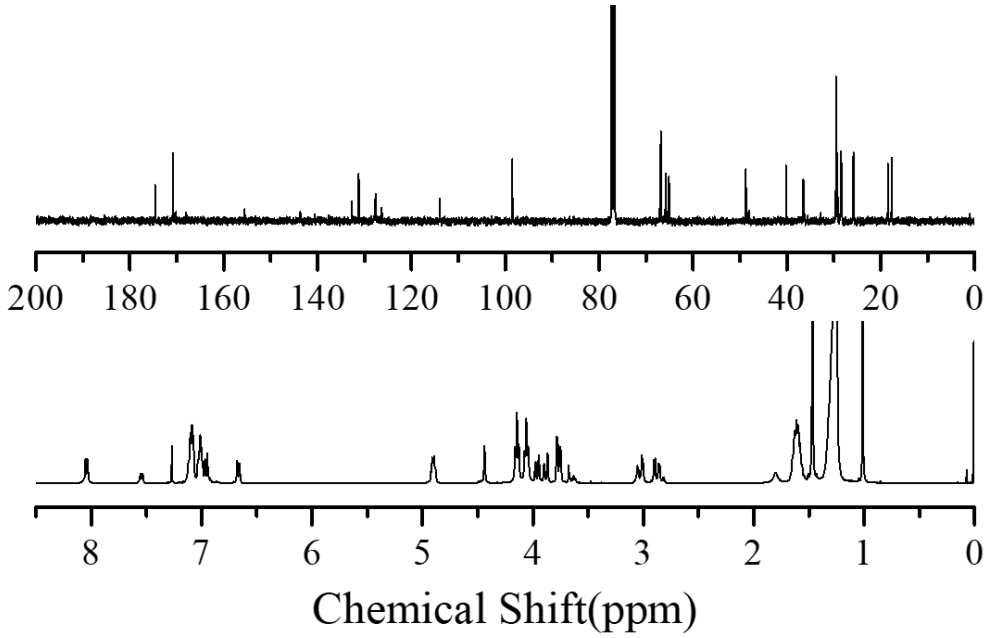

Appendix Figure S13 ^{1}H and ^{13}C NMR spectra of $PTPE_9$.

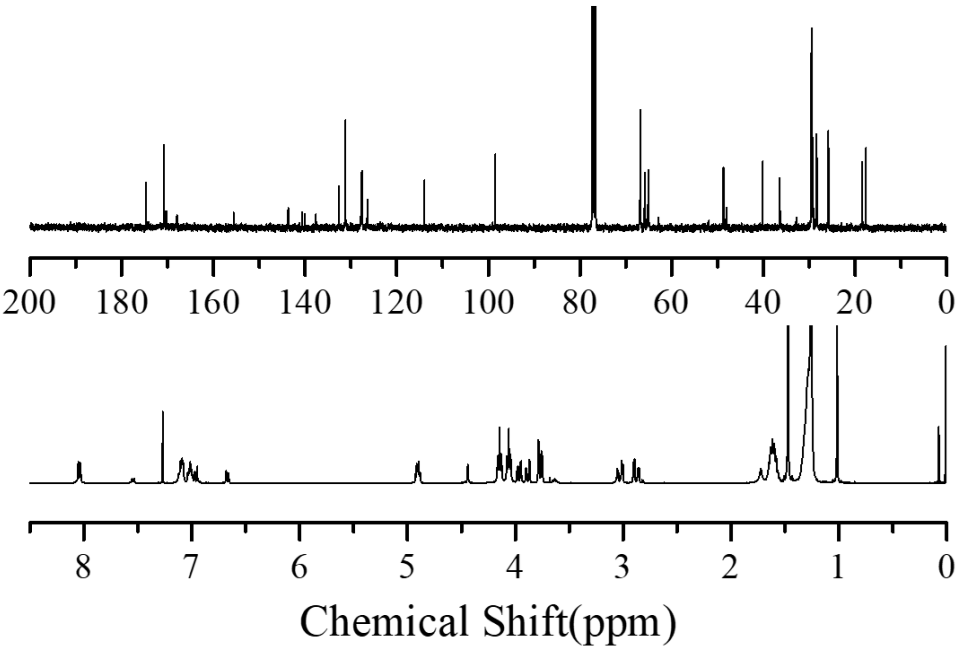

Appendix Figure S14 ^{1}H and ^{13}C NMR spectra of $PTPE_{18}$.

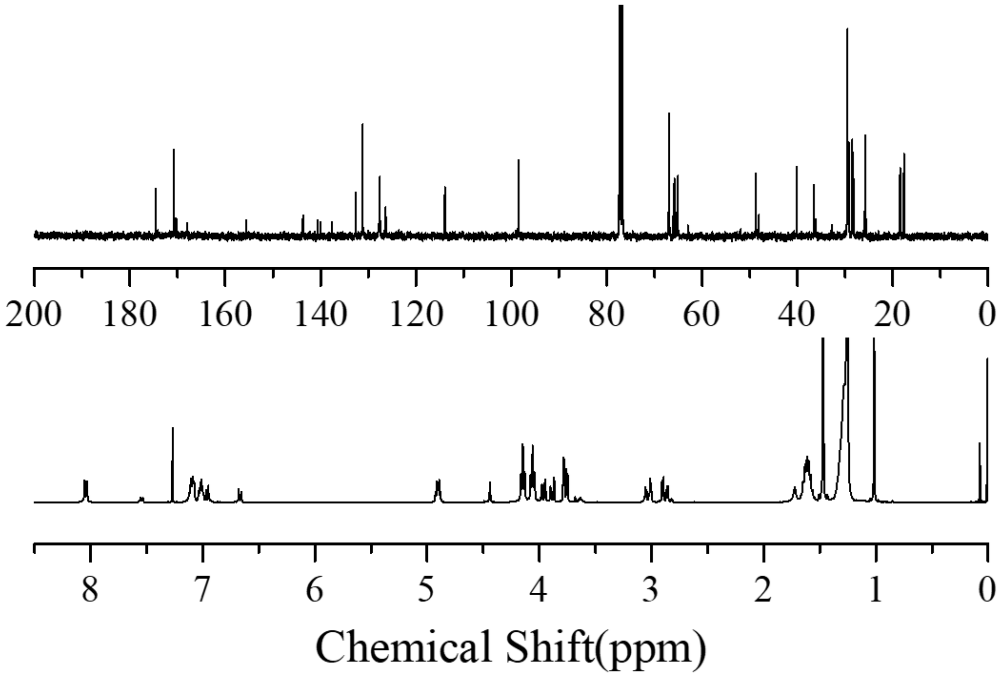

Appendix Figure S15 ^{1}H and ^{13}C NMR spectra of $PTPE^{27}$.

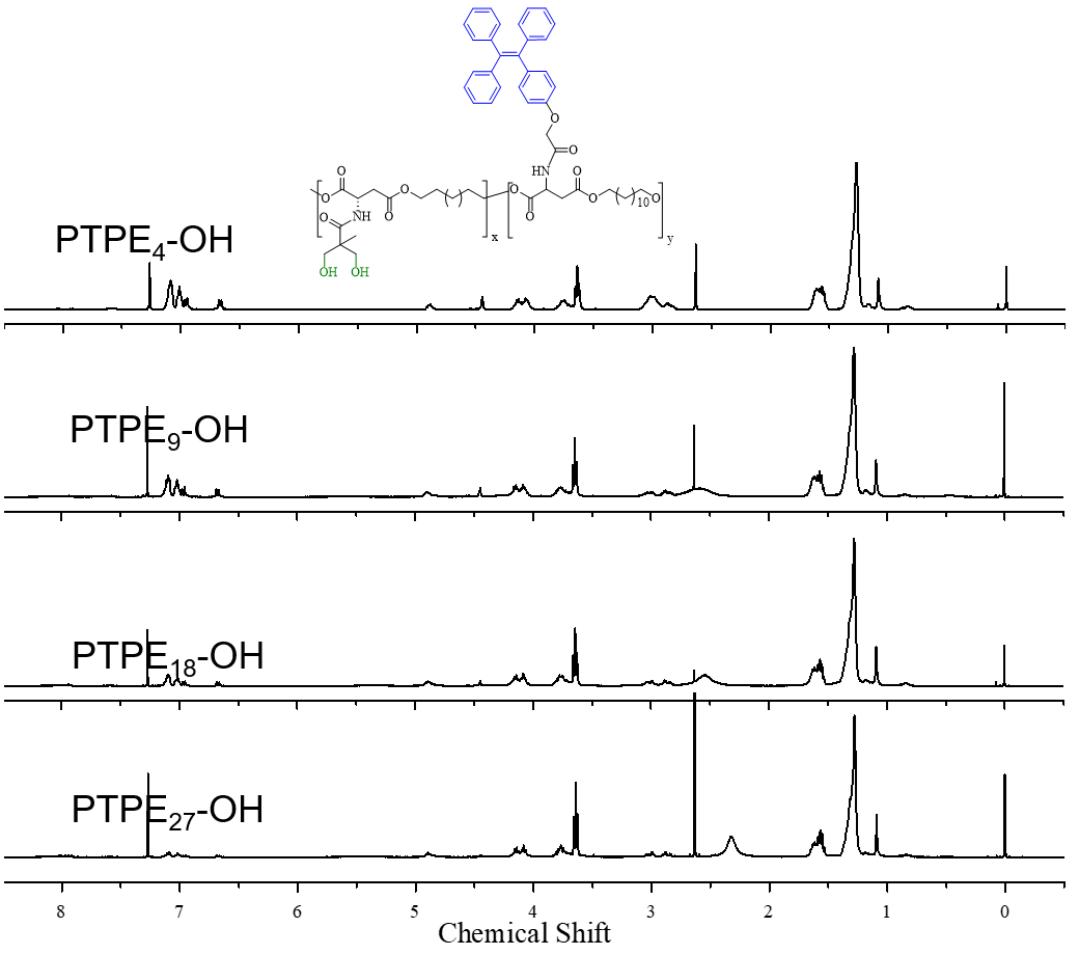

Appendix Figure S16 Deprotection of acetal group to form PTPE-OH polymer

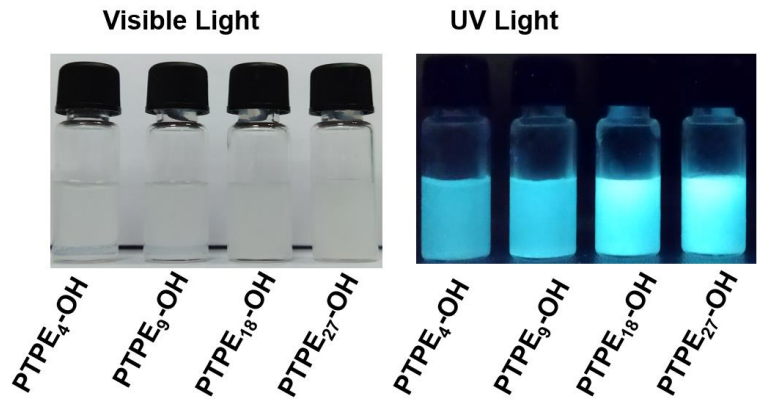

Appendix Figure S17 Photograph vial containing different polymer solution under normal and UV light.

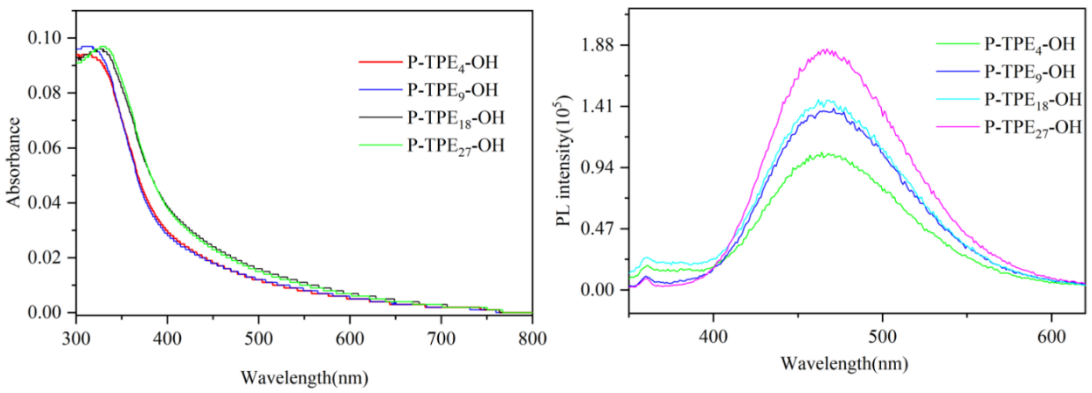

Appendix Figure S18 Photophysical characterisation of the copolymer (a) Absorbance spectra. (b) Emission Spectra

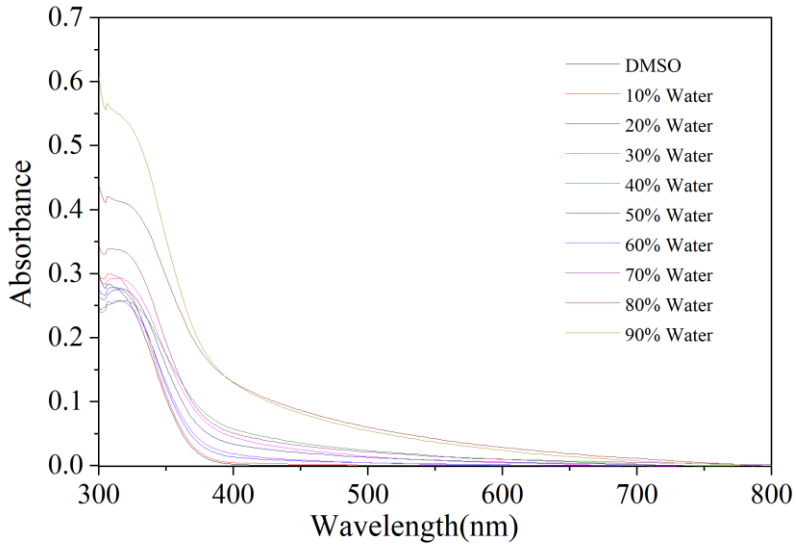

Appendix Figure S19 (a) absorbance spectra of the sample for solution dependent aggregation.

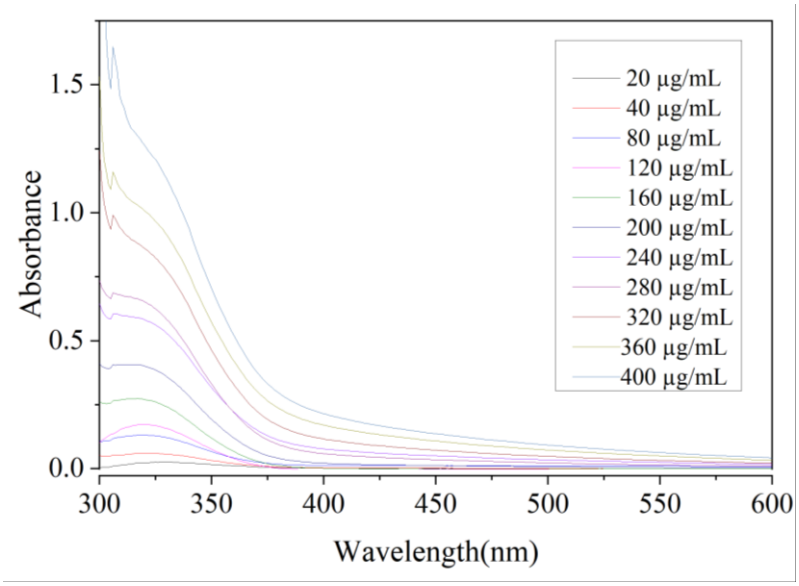

Appendix Figure S20 (a) absorbance spectra (b) Emission spectra (c) Plot for the CAC experiments.

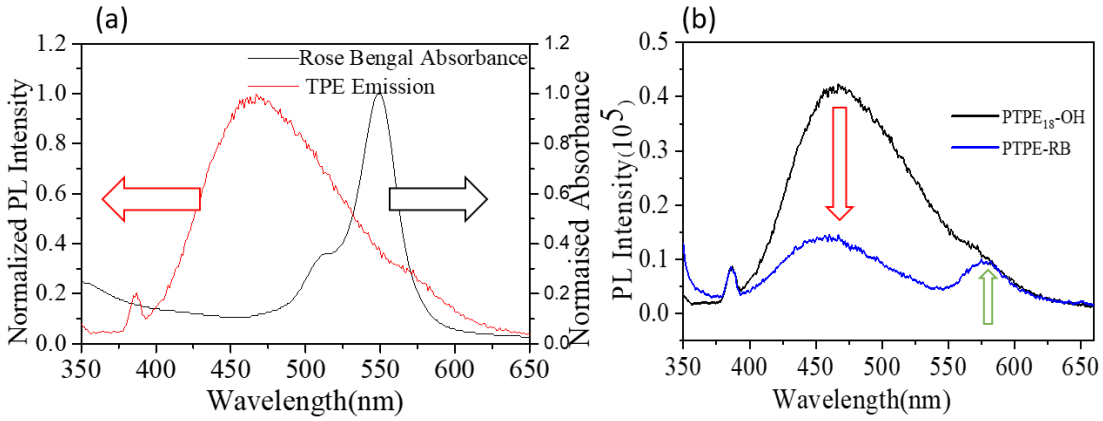

Appendix Figure S21 (a) absorbance spectra (b) Emission spectra (c) Plot for the CAC experiments.

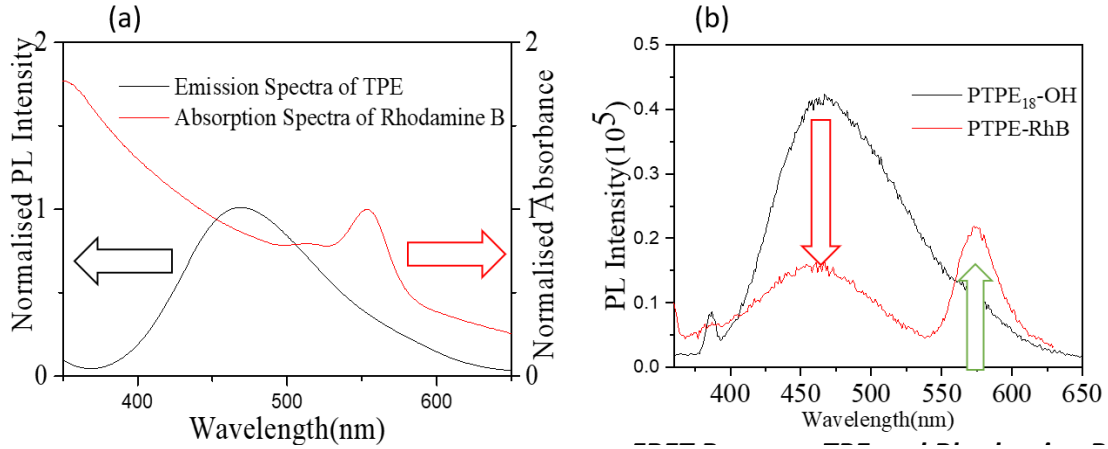

Appendix Figure S22 (a) absorbance spectra (b) Emission spectra (c) Plot for the CAC experiments.

Energy Transfer and FRET Distance

FRET is a distance dependent process and depends upon the intermolecular distance between donor and acceptor and the distance at which the FRET is 50% efficient is called Förster distance (R_0).[6] and determined by equation:

$$R_0 = [8.79 \times 10^{-5} (\kappa^2 \eta^{-4} Q_D J(\lambda))]^{1/6}$$

where κ^2 is the angle between the dipole moments of donor and acceptor, Q_D is the quantum yield of donor, η is refractive index of the medium and J (λ), the overlap integral form the emission spectrum of donor with the absorption spectrum of acceptor is given as;[6]

$$J(\lambda) = \int_0^\infty F_D(\lambda) \mathcal{E}_A(\lambda)\, \lambda^4\, d\lambda$$

where F_D is the corrected fluorescence intensity of donor and $\mathcal{E}_A(\lambda)$ is the molar extinction coefficient of the acceptor.

The FRET efficiency can be determined from the equation:

$$E_{FRET} = (R_0^6) / [R_0^6 + R^6]$$

where R is the distance between donor and acceptor molecules. The parameter R_0 is also dependent on the J(λ), the overlap integral of the emission spectrum of donor and absorption spectrum of acceptor. E_{FRET} is determined from the fluorescence life of donor molecule as follows:[6]

$$E = 1-[\tau_{DA}/\tau_D]$$

where τ_D is the average fluorescence lifetime of donor in absence of acceptor and τ_{DA} is the average fluorescence lifetime of donor in presence of acceptor. The values of $J(\lambda)$ and R_0 determined as above were computationally determined using the programme as per the literature report.